AN INVESTIGATION OF STRUCTURE AND PROPERTIES IN A MODEL SET OF DIBLOCK COPOLYMER-HOMOPOLYMER BLENDS

by

FRANK STEVEN BATES

B.S., State University of New York at Albany
(1976)

S.M., Massachusetts Institute of Technology
(1979)

SUBMITTED TO THE DEPARTMENT OF
CHEMICAL ENGINEERING IN PARTIAL
FULFILLMENT OF THE
REQUIREMENTS FOR THE
DEGREE OF

DOCTOR OF SCIENCE

at the

MASSACHUSETTS INSTITUTE OF TECHNOLOGY

January, 1982

Signature redacted

Signature of Author _____
Department of Chemical Engineering
January 5, 1982

Signature redacted

Certified by _____
Robert E. Cohen
Thesis Supervisor

Signature redacted

Accepted by _____
Glenn C. Williams
Chairman, Department Committee

AN INVESTIGATION OF STRUCTURE AND PROPERTIES IN A MODEL SET OF DIBLOCK COPOLYMER-HOMOPOLYMER BLENDS

by

FRANK STEVEN BATES

Submitted to the Department of Chemical Engineering
on January 5, 1982 in partial fulfillment of the
requirements for the Degree of Doctor of Science in
Chemical Engineering

ABSTRACT

The structure and dynamic mechanical behavior of the rubber inclusions and phase boundaries in a rubber modified glassy polymer have been investigated. A model set of well-characterized, anionically polymerized, diblock copolymer-homopolymer blends was prepared from styrene and butadiene containing microspherical polybutadiene domains. Phase boundary thickness, domain size and domain ordering were determined by small angle neutron scattering and electron microscopy. The interfacial thickness equals that predicted from theory while microsphere size and order deviate from the predicted bulk equilibrium states in all but the lowest molecular weight samples as a result of solvent casting. Dynamic mechanical properties were determined in a tensile mode at 3.5 Hz between -140 and 110°C. Increasing the volume fraction of interfacial material in these composites produces no change in the storage modulus and a small increase in the level of viscoelastic loss between component glass transition temperatures. Inclusion of high molecular weight polybutadiene in a glassy polystyrene matrix results in a predictable lowering of the rubber glass transition temperature, T_g^B, due to negative triaxial stresses. Low molecular weight polybutadiene exhibits a higher T_g^B, indicating rubber failure, which is believed to be dependent on the polybutadiene fractional free volume.

Thesis Supervisor: Dr. Robert E. Cohen
Title: Associate Professor of Chemical Engineering

ACKNOWLEDGEMENTS

I am grateful to my advisor, Professor Robert Cohen, for providing intellectual and financial support throughout the course of this work. I would also like to acknowledge Dr. Charles Berney for introducing me to the field of SANS.

Thanks to my friend Bob DiGiacomo who spent many hours skillfully glass blowing my synthesis equipment.

Chris Schwier, Glenn Hong, Martin Suenson and Janis Piersall have been the closest of friends over the past several years, for which I am deeply grateful. Chris has worked closely with me in much of this study, particularly in the synthesis stage. He and Martin have furnished a significant fraction of the computer software along with providing a stimulating environment for formulating and discussing problems and ideas. Jan has been a constant source of love and support. She has also edited and typed this document which speaks for itself.

It is my privilege to dedicate this thesis to my family in appreciation of twenty-seven years of devotion.

TABLE OF CONTENTS

LIST OF TABLES

LIST OF FIGURES

CHAPTER 1: Introduction

1.1 MULTICOMPONENT POLYMER BLENDS

The past several decades have seen a tremendous increase in the production and applications of polymers. At the same time, the number of individual monomeric precursors, constituting the bulk of the industry, have remained essentially unchanged. These trends are expected to continue in the forseeable future. Therefore, new and improved polymer properties have in the past, and will in the future, be obtained by suitably blending existing pure component materials. A general treatment of the subject of polymer blends can be found in Reference (1).

Multicomponent polymer blends can be formulated in a variety of ways, the most obvious being a simple mixture of homopolymers. A synergistic effect on properties can sometimes be obtained by blending miscible polymers. An important example is the highly successful product NORYL (General Electric Co.), a blend of polyphenyleneoxide and polystyrene. Homogeneous mixing of polymers is uncommon and, under conditions leading to phase separation, blending often does not result in an improvement of properties. Hence, most present-day polymer composites are developed at a molecular level. Numerous synthetic elastomers, such as SBR, are obtained by free-radical copolymerization of a mixture of different monomers, i.e. styrene and butadiene. Many condensation polymers, such as nylons and polyurethanes, are also produced from a blend of monomers. More recently, methods such as graft

and block copolymerization have been developed whereby polymeric molecules can be synthesized containing individual sections or "blocks" of a single component. Upon phase separation these materials exhibit structures and properties which are unattainable in blends of homopolymers. Rubber-modified thermoplastics, such as high impact polystyrene (HIPS) and acrylonitrile-butadiene-styrene resin (ABS) are examples of blends which are manufactured by graft copolymerization techniques. In all composites the phase structure is strongly influenced by the synthetic history.

Of the numerous poorly understood topics concerning multiphase polymer composites, one can be identified which is common to all such materials: phase boundaries. Helfand (2,3) has provided theoretical predictions as to the structure of polymer-polymer domain boundaries, yet very little data is available concerning this parameter. The influence of an interface on mechanical properties is also not well understood. All experiments which have addressed the issue of interfacial contributions to mechanical behavior have been conducted on rubbery continuous block copolymers of styrene and butadiene or isoprene (4-7). Examination of glassy continuous composites has focused mainly on HIPS and ABS (8,9) which contain several orders of magnitude less interfacial surface area per unit volume than do block copolymers. This mitigates the ability to investigate the influence of domain boundaries on the toughening mechanisms of these materials. It has recently been speculated that polymer-polymer interfaces play an important role in the crazing behavior (a primary means of energy absorption upon deformation) of rubber modified glasses (10).

Block copolymers presently represent the most versatile class of multicomponent polymers for studying the influence of phase structure on properties. Their method of preparation, anionic polymerization, affords control over block length, block geometry, microstructure and overall composition, each of which can influence phase structure and mechanical behavior. A wide variety of monomers can be block copolymerized, although in practice the synthesis procedures are quite tedious (11). Nevertheless, these materials have gained wide popularity in the research laboratory and to a limited extent commercially.

1.2 BLOCK COPOLYMERS AND BLENDS

The most striking structural feature of block copolymers, and blends with their respective homopolymers, is the regularity and size of the phase separated domains. These microdomain characteristics are brought about by the monodisperse nature of the block components; a recent theoretical treatment of this phenomena can be found in Ref. (12). Exploiting the molecular control afforded by anionic polymerization provides for some dramatic microstructural engineering. Increasing block molecular weight will systematically increase phase dimensions, while varying composition results in predictable changes in phase structure. Understanding these molecular-structural relationships allows one to optimize on phase morphology during polymer synthesis. In the case of rubbery continuous and co-continuous diblock and triblock copolymers of styrene and butadiene or isoprene, the predictions of Helfand (12) are in excellent agreement with experimental findings. On the other hand, the domain dimensions of glassy continuous

polystyrene-polydiene block copolymers containing spherical rubber particles, are systematically half that predicted from theory (13).

Not surprisingly the mechanical properties of block copolymers and blends are dramatically affected by microdomain type, order and possibly size. Due primarily to their commercial availability, extensive studies have been made of rubber continuous triblock copolymers of styrene and butadiene (SBS) which are marketed under the tradenames KRATON (Shell Chemical Co.) and SOLPRENE (Phillips Petroleum Co.). As previously mentioned, nearly all interfacial property investigations have relied on this type of material. With one exception (7), these studies have neglected structural considerations when deducing interfacial contributions to mechanical properties. To date, there have been no such examinations of glassy continuous materials.

The ability to generate composites containing a very large surface-to-volume ratio makes glassy continuous, rubber containing block copolymers extremely attractive for investigating the structure related characteristics of rubber modified glassy polymers in general. Furthermore, the ability to control particle shape, size and volume fraction permits a systematic parametric study, otherwise extremely difficult or impossible, e.g. using materials such as HIPS or ABS. Only by controlling structure, through molecular engineering, can fundamental structure-property relationships in multicomponent polymer blends be identified. Anionic polymerization of block copolymers and homopolymers provides a powerful method of accomplishing this task.

1.3 OVERVIEW

1.3.1 Motivation: The motivation for this work originated with a desire to investigate the structural and mechanical characteristics of polymer-polymer domain boundaries. Block copolymers provide the most effective method of controlling the amount of interface in a composite by regulating the phase structure and size via block molecular weight and composition. This study has focused on glassy continuous block copolymers and blends with homopolymers of styrene and butadiene for several reasons. It was not clearly understood why spherical microdomains in these materials exhibit such large dimensional deviations from theory. A systematic investigation of the interface required a concurrent manipulation of structure, which provided an enticing opportunity to also address the question of equilibrium domain dimensions in these block copolymers.

The strongest motivation for directing this investigation of interfaces towards a system involving rubber modified polystyrene was the establishment of a parallel project aimed at probing the craze behavior of such materials. The presently reported work has been directed at establishing the means of synthesizing and producing tailored block copolymers and quantifying the resulting structural features as a function of molecular architecture. An ability to manipulate structure has provided the mechanism for interpreting dynamic mechanical properties. The results obtained from this project are presently being utilized in exploring the crazing phenomena of the same composites.

1.3.2 Outline: The following document condenses a research effort

which has involved three distinct, but interdependent, disciplines of polymer science and engineering: synthesis and characterization, small angle scattering and electron microscopy, and dynamic mechanical analysis. In order to more effectively treat these topics, each has been individually reviewed in the appropriate chapters rather than in a general review.

Initiation of this project necessitated the establishment of an anionic polymerization facility capable of producing sizeable batches (~50g) of block copolymers of specified geometry. Initial efforts at achieving this goal by means of conventional methods met with little success. The development of the polyvinyl "living" gels, as detailed in Appendix A, proved to be the key step in synthesizing the desired materials. Chapter 2 deals with the anionic polymerization of the diblock copolymers and homopolymers used throughout this study and their molecular characterization is reported in Chapter 3.

Chapter 4 has been devoted to discussing the phase behavior and experimental methods of structural analysis in block copolymers and blends. Both electron microscopy (EM) and small angle neutron scattering (SANS) have been extensively used for the purpose of structural analysis in this work. SANS results are presented in Chapter 5 while those from EM can be found in Chapters 4, 5 and 7.

The results of the dynamic mechanical testing of the polystyrene-polybutadiene composites are contained in Chapter 6.

An overall analysis of the structure and properties presented in the previous chapters is undertaken in Chapter 7. The combined three-pronged research effort was successful in both addressing the initially

posed questions and resolving several that unexpectedly developed.

Finally, this work is summarized and recommendations for future investigations are presented in Chapter 8.

References

1 D.R. Paul and S. Newman, eds., Polymer Blends, vols. 1 and 2, Academic Press, New York (1978).

2 E. Helfand, J. Chem. Phys., 62, 999 (1975).

3 E. Helfand and A.M. Sapse, J. Chem. Phys., 62, 1327 (1975).

4 J. Diamant, D.S. Soong and M.C. Williams, to appear in Contemporary Topics in Polymer Sci., vol. 4, ed. W.J. Bailey, Plenum Press, N.Y. (1981).

5 R.E. Cohen and N.W. Tschoegl, Trans. Soc. Rheology, 20, 1, 153 (1976).

6 A. Beamish, R.A. Goldberg and D.J. Harriston, Polymer, 18, 49 (1977).

7 G. Kraus and K.W. Rollmann, J. Polymer Sci. Phys. Ed., 14, 1133 (1976).

8 F. Ramsteiner, Polymer, 20, 839 (1979).

9 A.M. Donald and E.J. Kramer, submitted to J. Mat. Sci. (1981).

10 A.S. Argon, R.E. Cohen, B.Z. Jang and J.B. VanderSande, J. Polymer Sci. Phys. Ed., 19, 2, 253 (1981).

11 M. Szwarc, Carbanions, Living Polymers and Electron Transfer Processes, Interscience (1968).

12 E. Helfand and Z.R. Wasserman, to appear in Developments in Block Copolymers, ed. I. Goodman, Applied Sciences Publishers Ltd.

13 T. Hashimoto, M. Fujimura and H. Kawai, Macromolecules, 13, 1660 (1980).

CHAPTER 2: Synthesis

2.1 ANIONIC POLYMERIZATION

2.1.1 Development: Many years ago it was recognized by Flory (1) that in the absence of termination or chain transfer a linear chain polymerization would ideally lead to a Poisson distribution in sizes amongst the polymer molecules,

$$N_x = e^{-\nu}\nu^{x-1}/(x-1)! \qquad 2\text{-}1$$

provided all species are initiated and grow simultaneously. N_x is the fraction of molecules containing x monomer units, ν is the overall number of monomer units reacted per chain, and the initiator is treated as a monomer unit. A slightly modified Poisson distribution defines the weight fraction distribution (1).

$$w_x = [\nu/(\nu+1)]xe^{-\nu}\nu^{x-2}/(x-1)! \qquad 2\text{-}2$$

From these, the number average and weight average molecular weights can be shown to be

$$M_n = M_o(\nu+1) \qquad 2\text{-}3$$

and

$$M_w = M_o(\nu^2+3\nu+1)/(\nu+1) \qquad 2\text{-}4$$

respectively, where M_o is the molecular weight of a monomer unit. Polymer size distribution is generally expressed as a polydispersity index defined as:

$$M_w/M_n = 1+\nu/(\nu+1)^2 \qquad 2\text{-}5$$

Pioneering work by Szwarc and his associates (2,3) proved the termination free or "living" nature of anions of various vinyl monomers, and clearly demonstrated the possibilities for such systems. Later workers (4,5) achieved the goal of synthesizing polymers having a narrow molecular weight distribution using the anionic polymerization technique, although a strictly Poisson distribution has never been obtained. Factors causing deviation from equations 2-1 to 2-5 have been dealt with in detail by Szwarc (6) and include the effects of spurious impurities, carbanion instability, inefficient mixing, slow initiation and depropagation.

Given sufficient time, monodisperse "living" polymer will redistribute its molecular weight distribution to a value of 2 (6) due to the establishment of equilibrium between residual monomer and "living" polymer. Fortunately, in most cases the rate of depropagation is so slow that termination long preceeds such an event; more than a century is required for final equilibration of a "living" styrene polymerization (6). Instability of polystyrene and polybutadiene carbanions does not represent a problem under normally employed conditions. The topic of initiation rate will be addressed in Section 2.2.1. By far the greatest limitation to the practical exploitation of anionic polymerization is the elimination of impurities capable of reacting with carbanions in solution. These include oxygen, water, acids, alcohols, and any other compounds which appear acidic to the basic nucleophilic site. Polymerization of high molecular weight polymers ($>10^5$ g/mol) places particularly stringent demands

on the purity of monomers, solvent and reaction equipment since the anion concentration may be as low as 10^{-5} mol/l.

2.1.2 Block Copolymers: Absence of termination in a growing polymer provides for some dramatic molecular engineering. Szwarc (2) originally pointed out the possibility of reacting a second monomer with the "living" end of a completed polymer resulting in the production of a block copolymer. Omoto et al. (7) have demonstrated that a synthesis of this type leads to random coupling of blocks which can be shown to possess a diblock polydispersity of (8),

$$M_w/M_n = x^2(M_w/M_n)_A+(1-x)^2(M_w/M_n)_B+2x(1-x) \qquad 2\text{-}6$$

x being the weight fraction of block A.

The ability to cross react carbanion A with monomer B is determined by the relative nucleophilicity of A and electroaffinity of B. For example, anionically growing polystyrene will initiate the polymerization of methyl methacrylate but "living" anionic polymethyl methacrylate will not initiate polymerization of styrene (9). In the case at hand, either anionic polystyrene or polybutadiene will add to both monomeric counterparts although the cross reaction rates are significantly different for each (Section 2.2.4).

Anionic diblock polymerization techniques have been extended to the synthesis of a wide variety of tailored macromolecules. Linear multiblock, multiarm star block copolymers and model networks can be produced by the same or slightly modified methods used in the synthesis of diblock polymers (10,11).

2.1.3 Reaction Variables: Although not imperative, anionic

polymerizations are generally conducted in a homogeneous solution. Solvents and monomers must contain no sites which can terminate the "living" polymer chain. Aside from these restrictions, a great deal of flexibility exists in the choice of initiator, solvent, monomer and reaction temperature, all of which may strongly affect the molecular characteristics of the product.

Initiators can be divided into two main classes: those which add onto a monomer, such as butyllithium, and those which react by electron transfer, such as sodium naphthalene. In both cases the counterion is an alkali earth metal. Initiator functionality and cation type both influence the molecular characteristics of the resulting "living" polymer. Use of a bifunctional initiator, such as sodium naphthalene, results in a polymer which grows from both ends allowing for a two-step triblock synthesis. Variation in metal counterion can influence the rate of polymerization (6) and resulting tacticity (12) and microstructure. The latter of these is particularly important to the present work. Lithium catalyzed polymerization of butadiene in a suitable solvent will lead to the production of predominantly 1,4 polybutadiene, while other cations induce a significant degree of 1,2 addition (6).

Solvents are generally categorized according to their ability to solvate ion pairs and agglomerates in solution. Non-polar hydrocarbons, such as hexane and benzene, have little solvating power while basic solvents, like tetrahydrofuran and dimethoxyethane, are capable of significantly dissociating ion pairs. This behavior dramatically affects polymerization rate and molecular structure. 1,4 polybutadiene can only be obtained using a lithium counterion

in a non-polar solvent.

Propagation and depropagation reaction rates are strongly dependent on temperature. Depropagation can be neglected provided the polymerization is operated well below the system ceiling temperature (6). Such is the case for styrene and butadiene under temperatures presently employed, the kinetics of which are dealt with in Section 2.2. Reaction temperature can also influence carbanion stability, reactivity towards solvents and monomer side groups, and product tacticity and microstructure. For example, above -40°C polystyryl and polybutadienyllithium will react with tetrahydrofuran terminating polymerization. No such difficulties are encountered when using hydrocarbon solvents, even at elevated temperatures. With regards to structure, Uranek (13) has shown that the microstructure of polybutadienyllithium in cyclohexane is nearly independent of temperature between -19°C and 100°C, and this is assumed to be the case in benzene.

2.1.4 Polymerization Conditions: Butyllithium and benzene were chosen as initiator and solvent respectively for the synthesis of diblock copolymers of styrene and butadiene. Benzene is a suitable medium for the polymerization of both blocks, a good solvent for each and a non-polar hydrocarbon for the production of predominantly 1,4 polybutadiene. It should be noted that although toluene is seemingly an attractive alternative to benzene as a solvent, it will act as a carbanion chain transfer agent (14) rendering it unacceptable for these polymerizations. Reactions were conducted in a 5% solution at a temperature of 40°C for styrene and 50°C for butadiene whereby quantitative conversion is obtained in several hours (see Section 2.2).

2.2 KINETICS

2.2.1 Initiation: The previously described Poisson distribution in molecular weight as developed by Flory (1) was based upon the assumption of instantaneous initiation of all growing species. In practice, the initiation of organic monomers by organo-metallic compounds proceeds at a finite rate k_i which must be compared to the subsequent rate of polymerization k_p. Gold (15) and later Nanda and Jain (16) derived expressions relating molecular weight and polydispersity to monomer conversion and k_p/k_i. In the limit of very slow initiation relative to polymerization the product molecular weight becomes very high and polydispersity index approaches 1.33. Experimentally this leads to an inability to control molecular weight due to inefficient use of initiator.

The problem of slow initiation becomes critical when alkyllithium compounds are used to promote anionic polymerization in hydrocarbon solvents. These compounds are known to exist as associated agglomerates in an aliphatic or aromatic medium. The rate of initiation is governed by both the dissociation constant of the agglomerates and intrinsic rate constant of the monomeric alkyllithium which is the active initiator (6). While n-butyllithium (a primary carbanion) is intrinsically more reactive than sec-butyllithium (a secondary carbanion) the latter exhibits a significantly greater reactivity towards styrene in benzene (17,18). This result can be understood in terms of the hexameric nature of n-butyllithium in non-polar solvents. Worsfold and Bywater (19) have shown that such association leads to an initiation rate which is 1/6 order in initiator. In a similar

fashion sec-butyllithium exhibits 4 fold association and an initiation rate which is 1/4 order in initiator (20,21).

Although the above discussion strongly suggests employing sec-butyllithium in anionic polymerizations conducted in non-polar solvents, there are several drawbacks to its use. It is considerably less stable than n-butyllithium and will slowly decompose to lithium hydride and butene. Commercially available sec-butyllithium was always found to contain precipitated impurities assumed to be lithium hydride and/or lithium alkoxides (22). The latter are known to affect both the rate of initiation and polymerization of styrene and isoprene (23,24). Although sec-butyllithium can be purified by distillation (23) the procedure is inconvenient and time consuming. Therefore, monomer initiation must be accomplished using n-butyllithium. An acceptable initiation rate can also be achieved with this primary alkyllithium in benzene by adding anisole at a 5-10 fold greater concentration than initiator. Geerts et al. (25) reported a substantial increase in the rate of styrene initiation with no change in polystyryllithium reactivity and Morton et al. (26) have shown that the microstructure of polydienes prepared in the presence of this small amount of the aromatic ether remain unaffected. Presumably anisole acts to inhibit the higher order association found in n-butyllithium but does not influence the mechanism of monomer addition to carbanions of styrene or dienes. This is in sharp contrast to the effect of aliphatic ethers such as tetrahydrofuran and 1,2 dimethoxyethane which favorably influences k_p/k_i but dramatically modifies resulting polydiene microstructure (6) rendering them unacceptable for use as initiation accel-

erators in this work. Although lacking kinetic data, initiation by n-butyllithium/anisole in benzene can be assumed to be rapid and efficient as confirmed by subsequent product characterization (Chapter 3).

2.2.2 Styrene: As with alkyllithium initiators, addition of styrene to polystyryllithium is strongly influenced by the association of ion pairs in non-polar solvents. In the original study of the kinetics of propagation of polystyryllithium in benzene, Worsfold and Bywater (19) showed the reaction to be 1/2 order in "living" polystyrene and proposed the following mechanism,

$$(\sim\sim\sim\sim S^-,Li^+)_2 \rightleftarrows 2\sim\sim\sim\sim S^-,Li^+ \qquad K_{diss}$$

$$\sim\sim\sim\sim S^-,Li^+ + S \rightarrow \sim\sim\sim\sim SS^-,Li^+ \qquad k_p$$

where most species exist in the associated dimeric form and only monomeric ion pairs are reactive. The rate of monomer (S) consumption is then expressed as,

$$\frac{-d[S]}{dt} = \frac{k_p K_{diss}^{1/2}}{\sqrt{2}} [S][\sim\sim\sim\sim S^-,Li^+]^{1/2} \qquad 2\text{-}7$$

where $[\sim\sim\sim\sim S,^-Li^+]$ represents the total concentration of "living" polymer. This expression has been verified by other workers in a variety of hydrocarbon solvents over a concentration range of 10^{-3} to 10^{-5}M in polystyryllithium (27,28), confirming the dimeric nature of growing ion pairs.

Separation of global reaction rate data into K_{diss} and k_p has

met with limited success. Fortunately the product $k_p K_{diss}^{1/2}$ suffices in determining reaction times for a given conversion at a specified temperature. Using data reported by Worsfold and Bywater (19) the following Arrhenius expression has been obtained for the global reaction rate constant of styrene addition to polystyryllithium in benzene:

$$k_S = \frac{k_p K_{diss}^{1/2}}{\sqrt{2}} = 5.03 \cdot 10^8 \exp(-14{,}550/RT) \qquad 2\text{-}8$$

It should be noted that Fetters and Young (29) have recently contested the dissociation controlled mechanism of polystyryllithium propagation. They have found no direct relationship between association states and polymerization reaction order which remains constant at half-order in polystyryllithium. Therefore, although the assumptions in developing equation 2-7 may be incorrect, the form of the rate expression remains valid. This working kinetic expression is necessary to insure a desired monomer conversion prior to subsequent monomer addition or termination.

2.2.3 Butadiene: Polybutadienyllithium has also been found to associate in non-polar solvents accompanied by reaction rates of fractional order in "living" polymer. In cyclohexane and heptane the order is 1/6 (27) while in benzene it is expected to be 1/2 (30). Rate expressions for the propagation of butadiene have been derived in a form similar to equation 2-7 although actual rate data for polybutadienyllithium and butadiene in benzene was not found. Fetters (31) has claimed that in benzene the lithium catalyzed rate

of polymerization of isoprene is only slightly greater than that of butadiene. Therefore, a rate expression developed for polyisoprenyllithium (30) is adapted to polybutadienyllithium in benzene. The rate of butadiene consumption is expressed as,

$$\frac{-d[B]}{dt} = k_B[B][\sim\sim\sim\sim B^-,Li^+]^{1/2} \qquad 2\text{-}9$$

where $[\sim\sim\sim\sim B^-,Li^+]$ represents the total concentration of "living" polymer. Cramond et al. (30) have experimentally verified the first and half-order dependance on monomer and active chain concentration respectively along with determining the Arrhenius constants for k_B.

$$k_B = 10^9 \exp(-13{,}300/RT) \qquad 2\text{-}10$$

Since butadiene will be polymerized in the presence of anisole (Section 2.2.1) the actual rate of reaction may be somewhat higher than predicted. Szwarc (6) has drawn an analogy between the coordinating behavior of polybutadienyllithium and that of n-butyllithium, known to be influenced by the presence of anisole (Section 2.2.1). The effect will be to increase conversion for a given time. This is acceptable in the present work since in all cases conversions of 99 percent or greater are desired.

2.2.4 Cross Reaction: The homogeneity of each block in a diblock copolymer is strongly dependent upon its synthetic history. It is necessary in the present work to insure a step change in composition between polystyrene and polybutadiene blocks. This can be accomplished by properly choosing the sequence of polymerization of styrene and

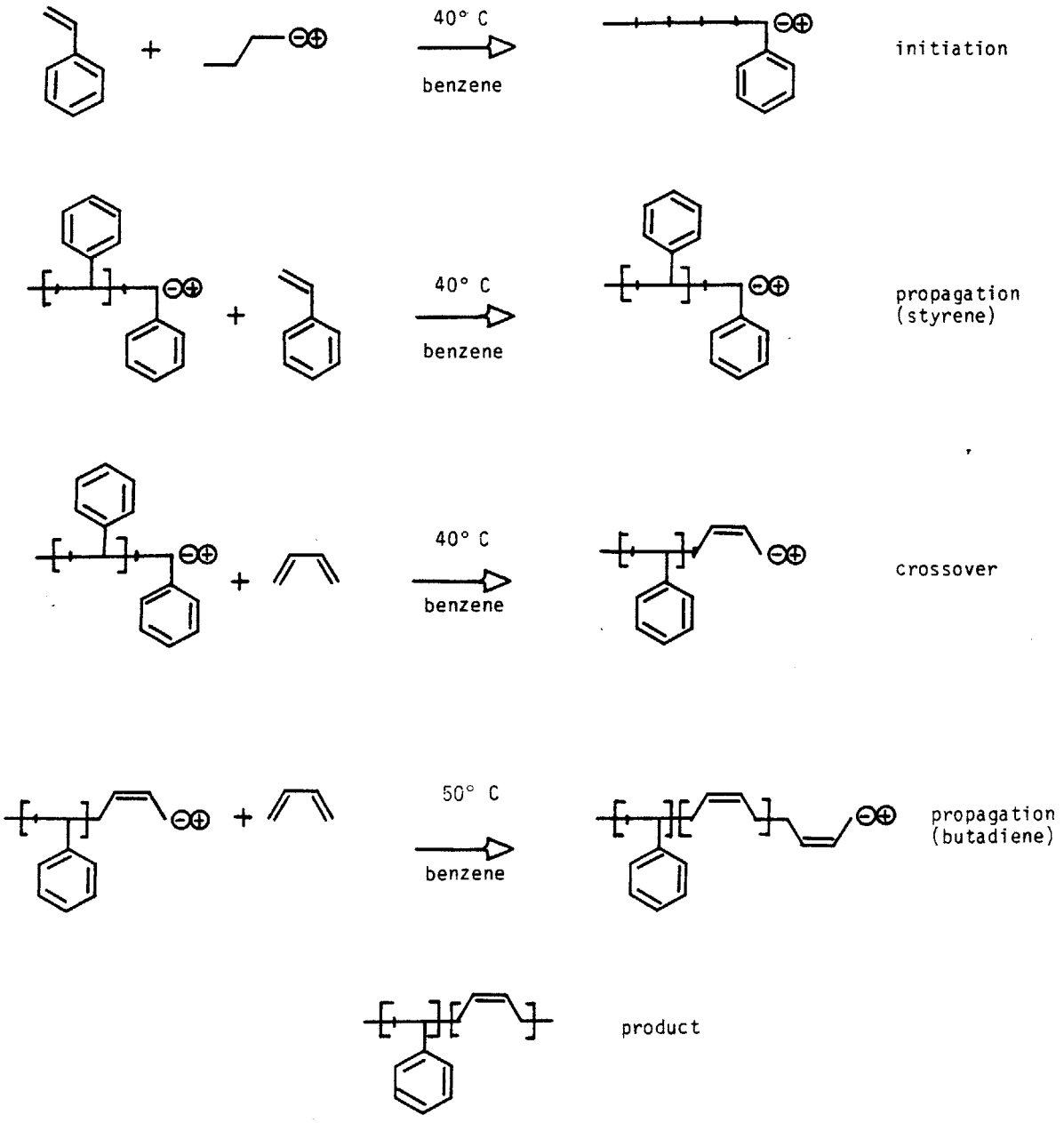

Figure 2-1 Reaction scheme for synthesizing a diblock copolymer of styrene and butadiene

butadiene. The reactivity ratios of styrene and butadiene with either styryllithium or butadienyllithium in benzene at 29°C have been reported as (32),

$$k_{SS}/k_{SB} = 0.08\text{-}0.41$$

$$k_{BB}/k_{BS} = 4.5$$

where k_{SB} is the rate constant for addition of butadiene to polystyryllithium. These reactivity ratios strongly suggest the initial polymerization of styrene followed by the addition of butadiene. Carrying the styrene polymerization to high conversion in conjunction with the favorable reactivity ratio between styrene and butadiene insures a sharp junction between polystyrene and polybutadiene blocks.

Upon reaching a desired conversion "living" polymers are reacted with methanol thereby end-capping with hydrogen. The overall reaction scheme is depicted in Figure 2-1.

2.3 EQUIPMENT

2.3.1 Inert Gas System: The development of a successful anionic polymerization facility revolves around eliminating all deleterious impurities from reaction equipment and reagents. Since oxygen and water will irreversibly react with both polystyryllithium and polybutadienyllithium terminating polymerization, the reaction medium must be isolated from the environment. This has conventionally been

achieved by sealing all reagents under glass which is then evacuated to high vacuum (6). This method has the advantage of providing and maintaining an absolute level of purity. Unfortunately, polymerization of larger quantities of polymer (>10g) becomes cumbersome with this high vacuum technique.

A second method of isolating a polymerization system from the environment is to blanket all reagents with an inert gas, such as argon. This inert gas technique is not size limited although attaining a purity level comparable to a high vacuum system is very difficult. In light of the numbers and quantity of polymer to be synthesized for this work, an inert gas system was chosen for the anionic polymerizations.

Ultra-high purity (99.999%) argon gas purchased from Matheson Gas Products was further purified utilizing an Ace-Burlitch Inert Atmosphere System sold by Ace Glass, Inc. (Figure 2-2). Argon gas enters through a double-bubbler trap containing Dow Corning 550 silicon oil, passes over a deoxifying BASF copper-based catalyst followed by drying over Linde 4X molecular sieves. A double manifold is connected to both the purified gas stream and a vacuum line (mechanically pumped) permitting alternate evacuation and gas flushing through each of four lines. System overpressure is regulated up to 20 cm Hg using an immersed capillary tube and a variable height mercury reservoir. High density polyethylene lines (3/8" o.d.) connect manifold valves with target vessels via 3/8" cajon Ultra-Torr fittings.

2.3.2 High Vacuum System: A 32 mm o.d. pyrex manifold was

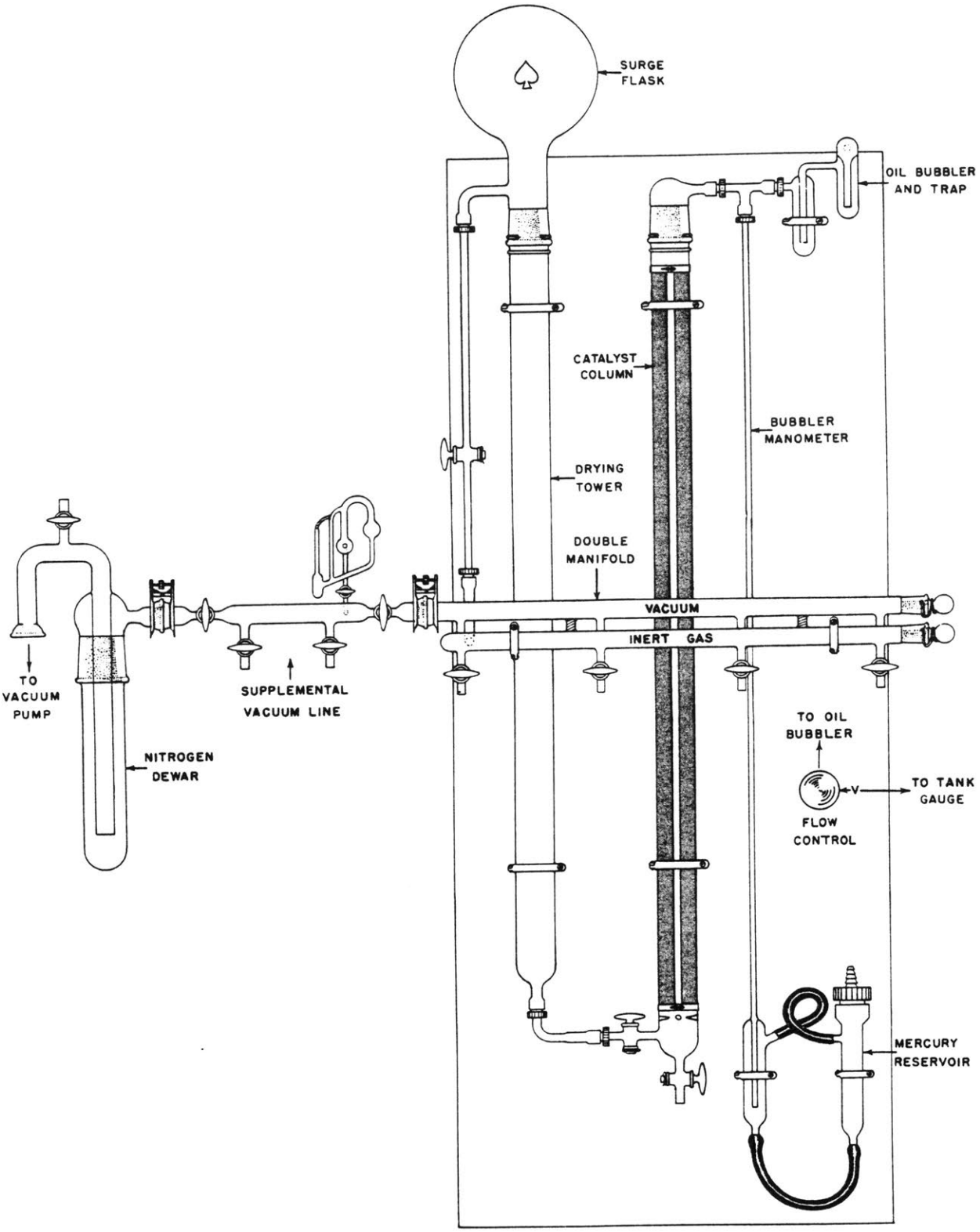

Figure 2-2 Argon gas purification and delivery system. Reproduced from Ace No-Air Glassware instructions, Ace Glass, Inc.

equipped with four teflon/O-ring vacuum valves (Ace Glass, Inc.) and connected through a 10 mm high-vacuum pyrex valve and cold trap to a single stage oil diffusion pump charged with Dow Corning 704 diffusion pump oil. Each valve was fitted with a 24/40 ground glass joint. System pressure was monitored using an NRC Equipment Corporation thermocouple gauge and ion emission gauge. This system was capable of maintaining a vacuum of 10^{-5} torr.

A butadiene gas purification line was designed for operation in conjunction with the high vacuum system. The monomer gas cylinder is connected to a fritted-glass bottom gas washing bottle with polyethylene tubing furnished with cajon Ultra-Torr fittings. This is followed by a teflon/O-ring valve, a 3.8 X 50 cm column of NaOH pellets and a 3.8 X 50 cm column of 4X Linde molecular sieves, each connected by cajon unions and ending in a teflon/O-ring valve. Monomer is delivered via polyethylene tubing, containing cajon Ultra-Torr fittings, to a 500 ml flask through a teflon/O-ring valved side arm. The flask is attached to the high vacuum manifold. Polyethylene tubing is a thick-walled 3/8" o.d. variety, cajon fittings are 3/8" diameter and all O-rings are made of viton rubber. This system allows for the deinhibiting, drying and collection of butadiene for later purification on the high vacuum manifold. The overall system is illustrated in Figure 2-3.

2.3.3 Distillation Equipment: Solvent distillations were performed on a 250 mm vacuum jacketed and silvered hempel column packed with 6 mm o.d. glass Raschig rings. A vacuum type distillation head with teflon reflux valve permitted connection of the distillation

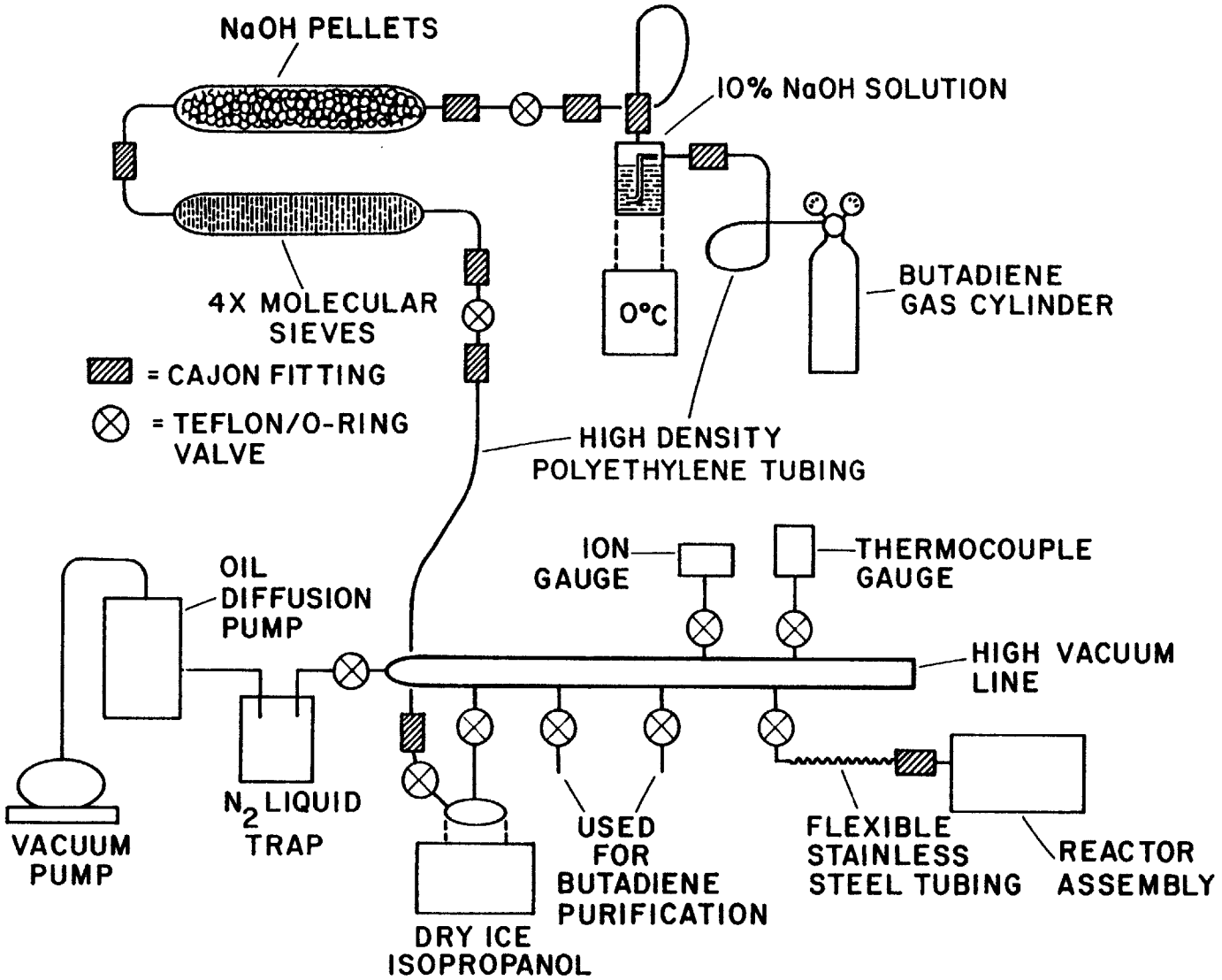

Figure 2-3 Butadiene purification equipment

unit to the gas purification system. All solvent distillations were performed under purified argon.

A separate vacuum distillation unit was required for the purification of styrene monomer. A 170 mm Vigreux distillation column was operated in connection with a 250 mm Liebig condensor containing a modified drip tip for use with a three-membered distilling receiver which rotates on the condensor. One of the members of the distilling receiver was replaced with a drip tube and 13 mm glass sleeve. This provides for the attachment of receiving vessel via a #15 Ace-Thred threaded O-ring connector. The modified condensor drip tip and distilling receiver insure that once the distillate reaches the condensor there will be no contact with vacuum grease, known to be deleterious to an anionic polymerization (6). The still is attached with thick walled vacuum tubing to a mercury monometer and dry ice/isopropanol trap followed by connection to the inert gas system. A metering valve is placed in line between the trap and inert gas system and is itself connected to the gas/vacuum manifold. This arrangement permits the operation of the distillation unit at less than atmospheric pressure while under argon. Prior to heating, the still and contents can be cyclically degassed by alternately applying gas and vacuum. During operation the system pressure (temperature) can be fixed by metering a given quantity of argon to the distillation unit.

2.3.4 Reaction Equipment: The most critical criterion in designing anionic polymerization equipment is the exclusion of all impurities which might react with the "living" polymer. Earlier work utilized reaction equipment fitted with ground glass joints (33). Unfortunately,

solvents and monomers (in particular dienes) readily dissolve the polydimethylsiloxane based grease used to seal these joints. Therefore, a new type of connector was incorporated in all reaction equipment. Ace-Thred threaded connectors consist of an internally threaded glass base which receives an appropriate diameter glass tube containing an O-ring. A nylon bushing provides positive pressure on the O-ring creating a seal (Figure 2-4). Use of these connectors eliminates the need for grease and yields a flexible joint.

The reactor is a 2000 ml flask modified with five #15 Ace-Thred connectors and two Ace thermometer adaptors. A 9 cm diameter flat circular area makes up the base of the reactor. This allows for facile stirring by an 8 cm long glass covered magnetic stirrer. A 360°C thermometer and neoprene septum (Supelco, Inc. #3-3247) occupy the thermometer adapters. The gas/vacuum and monometer tube are connected to a three-way valve which is connected to the reactor at a 45° angle, thereby insuring that grease from the valve remains isolated from the vessel.

The single ended butadiene burets (20 and 100 ml) contain Ace teflon stopcocks (3 and 5 mm) fitted to a 24/40 ground glass fitting through which runs a length of 13 mm tubing (Figure 2-4). The 24/40 joint permits attachment to the high vacuum manifold while the 13 mm tubing allows connection to the reactor with a bushing. Since the vapor pressure of butadiene exceeds two atmospheres at room temperature, it is necessary to keep the liquid cool while under glass. An insulated 1/4" copper coil jacket operated in series with copper coil immersed in an ice bath and driven by a peristaltic pump maintains the

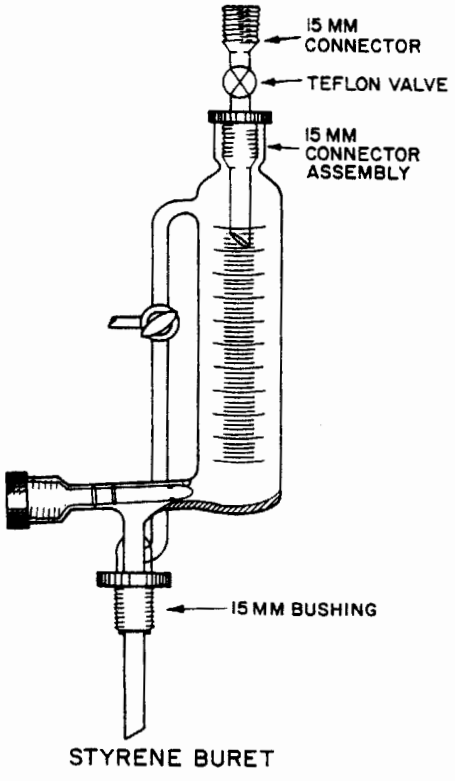

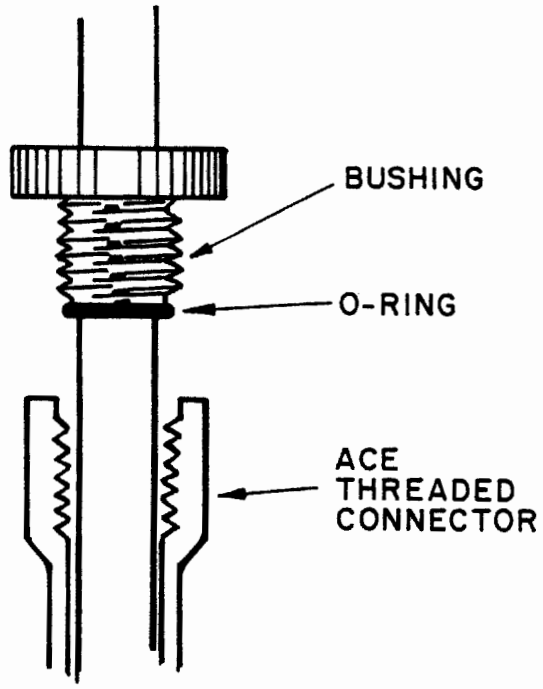

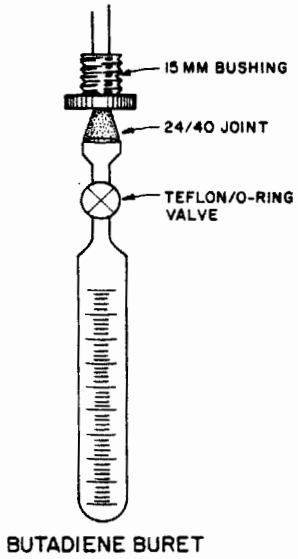

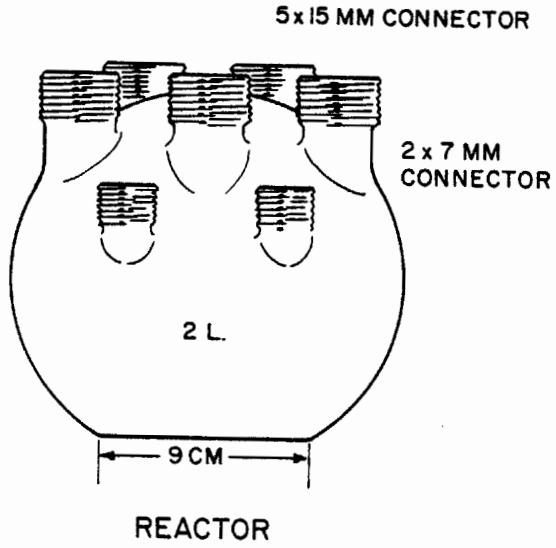

Figure 2-4 Reaction equipment

buret at less than 5°C while filled with butadiene.

Styrene burets (100 and 250 ml) contain a #15 connector at the top and a teflon valve (rotaflow TF6/13) at the base. An equalizing arm fitted with a three-way 2 mm pyrex valve connects the buret body with a 13 mm tube extending from the base and surrounding a drip tube (Figure 2-4). Therefore, the base can be fitted to the reactor with a bushing and O-ring. The top connector is fastened with a 3 mm Ace teflon stopcock which attaches to the styrene still.

The solvent reservoirs are 3000 ml round bottom flasks modified with two #15 and one #25 connectors. A teflon valve (rotaflow TF6/13) is attached to a fritted glass filter via a glass tube which extends to the bottom of the flask. This assembly is attached to the flask via a #15 connector with an O-ring and bushing. A 2 mm pyrex teflon valve is attached in the same manner to the second #15 connector. The #25 connector holds a glass rod from which suspends a nichrome wire basket, the use of which is addressed in the next section. A teflon valve (rotaflow TF6/13) is connected to the reactor via bushing and O-ring and to the solvent reservoir with a 1/4" cajon union. The solvent assembly is illustrated in Figure 2-5.

Initiator transferal was accomplished using Hamilton glass luer-tip gas tight syringes furnished with 20 ga stainless steel needles. An initiator dilution vessel was constructed from a calibrated erlenmeyer flask fitted with a 2 mm pyrex valve and septum holder. Dilution from stock bottles was performed using stainless steel cannulae and an argon overpressure.

2.4 MATERIALS

2.4.1 Styrene: Styrene monomer was received from Aldrich Chemical Co. inhibited with 10-15 ppm p-tert-butylcatechol. The inhibitor was extracted using a 10% solution of sodium hydroxide and the monomer subsequently washed generously with distilled water. The deinhibited styrene was initially dried for two hours over Linde 4X molecular sieves, then placed over calcium hydride and stored at 0°C. One to two days prior to a polymerization the styrene was distilled from the calcium hydride at 50°C with a middle fraction being isolated and stored at -20°C in a distillation flask. The day of a polymerization the styrene-containing flask was attached to the vacuum/argon distillation unit and the styrene was degassed by alternately evacuating and flushing the system with argon. Fresh sodium wire was then added to the styrene and the system repurged with argon. A middle fraction of monomer was then distilled at 50°C directly into the delivery buret.

It should be noted that deinhibited styrene should be used within one to two weeks. Aside from spontaneous polymerization, oxidation of monomer was found to lead to extensive complications in later polymerizations. Gas chromatographic analysis revealed that deinhibited styrene left standing more than a month (at 0°C) developed trace amounts of benzaldehyde which was not removed by the described separation scheme. Benzaldehyde will react with butyllithium, styryllithium and dienyllithium and therefore must be avoided.

2.4.2 Butadiene: Instrument purity 1,3 butadiene was obtained from Matheson containing 115 ppm p-tert-butylcatechol. The monomer

was deinhibited with a 10% sodium hydroxide solution contained in a gas-washing bottle maintained at 0°C. Deinhibited monomer was then passed over sodium hydroxide pellets and 4X molecular sieves and precipitated in a flask containing calcium hydride using a dry ice/isopropanol bath (-78°C). Following 24 hours of stirring over calcium hydride at 0°C, the monomer was transferred by distillation to a teflon/O-ring valved flask and stored at 0°C.

Several days prior to a polymerization the butadiene storage vessel was attached to the high vacuum line and an aliquot of butadiene was distilled into an evacuated flask. Further purification was achieved by successively distilling the monomer into flasks containing freshly prepared sodium mirrors. Since metallic sodium will slowly initiate the anionic polymerization of butadiene, the development of a polymer film on the inside of a mirrored flask is an indication of monomer purity. Caution should be exercised as the rate of polymerization greatly exceeds the rate of initiation. Generally three or four mirrors, each given 12 to 24 hours at 0°C, resulted in purified monomer. The butadiene was then transferred into a delivery buret and frozen with liquid nitrogen.

2.4.3 Butadiene-d_6: Perdeuterated 1,3 butadiene was obtained from Mercke, Sharp and Dohme, Canada, Ltd., in an uninhibited gaseous form. The shipping vessels were connected directly to the high vacuum system with Ultra-Torr fittings and monomer precipitated over calcium hydride. Following stirring for 24 hours at 0°C, the butadiene was distilled on to fresh sodium mirrors, each for 24 hours, until a thin polymer film developed on the flask. The monomer was then transferred to a tared

delivery buret, weighed and frozen with liquid nitrogen. At the completion of one of the purifications, a sample was removed and analyzed on a Varion MAT44 mass spectrometer and the spectrum was compared with published results for hydrogenated 1,3 butadiene (34). The results verified a 98 atom % deuterium level and a high degree of purity.

2.4.4 Solvent: Reagent grade benzene, purchased from J.T. Baker Co., was used for all the polymerizations. The solvent was initially dried by fractional distillation under argon, discarding the first 20% of the distillate. A second distillation under argon was performed in the presence of several milliliters of n-butyllithium. A middle fraction was recovered and isolated under argon.

The double distilled benzene is further purified using a "living" gels technique. Several grams of homogeneous divinylbenzene gels (Appendix A), swollen in benzene and cut into 0.2 - 1.0 cm^3 particles, are suspended over the solvent in a nichrome wire basket. A sufficient amount of anisole (Fischer Scientific Company) is injected into the solvent via the valved injection port (Figure 2-5) such that a molar ratio of 5-10 to 1 between anisole and initiator will be present during a later polymerization. Ample n-butyllithium is added to the solvent in order to neutralize all species deleterious to an anionic polymerization. It was found that 100 to 200 microliters of 2.4 M n-butyllithium per liter of solvent was sufficient using the above scheme. The basket of gels is then lowered halfway into the solvent and the system is left under moderate stirring for several days. The appearance of a reddish-brown color on the previously colorless gels is evidence of pure solvent. This

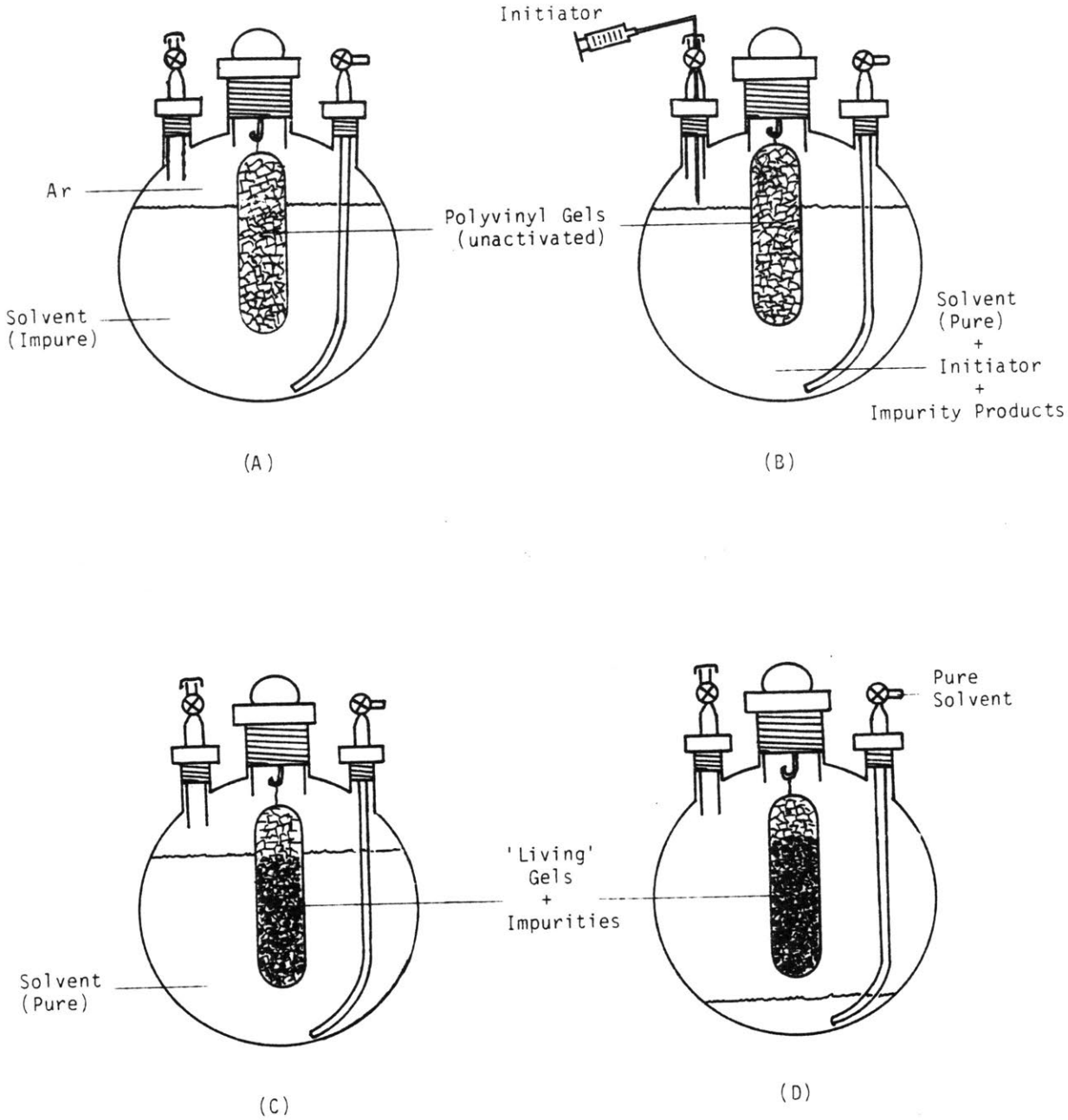

Figure 2-5 Purification of solvent using polyvinyl gels. See Appendix A for details concerning gel preparation.

color reflects the initiation of pendant vinyl groups attached to the gel backbone. Partially lowering the gel basket provides fresh gel material for initiator removal. Once the newly immersed gel remains colorless the solvent is both pure and initiator free. Purified solvent remains useful indefinitely, provided the gel remains colored (nucleophilic). The "living" gel procedure is illustrated in Figure 2-5.

2.4.5 Initiator: n-butyllithium was obtained from Alfa Products as a 2.4 molar solution in n-hexane. The initiator was either used as received, or diluted with cyclohexane in a separate dilution vessel. Initiator concentration was determined prior to a polymerization using a modified method of Eppley and Dixon (35). The indicator solution consists of 20% by volume dimethoxyethane, 80% dimethylsulphoxide and 0.1 g/l triphenylmethane. 10 ml of this solution are titrated under argon with initiator until a red color persists. An aliquot of benzoic acid in dried benzene of known concentration is added and back titrated with initiator. The procedure is repeated until consistent results are obtained from which the initiator concentration is determined.

Initiator efficiency was found to be slightly less than quantitative, becoming more apparent during high molecular weight polymerizations. This predictable loss of initiator was empirically found to be related to the quantity of styrene added to the reactor. Therefore, the concentration of added initiator was corrected for losses due to 6.8×10^{-4} moles of impurity per liter of styrene.

2.5 POLYMERIZATIONS

2.5.1 Polystyrene: The assembled reactor, containing glass stirrer, thermometer, styrene buret and solvent entry valve, is attached to the high vacuum system and inert gas system via the three-way valve assembly. The remaining parts are sealed with glass plugs. Reactor and buret are pumped down using the inert gas system roughing pump and then isolated on the high vacuum line. The reactor is then fitted with a heating mantle and baked out for 24 hours at 300°C. This high temperature insures desorption of surface water (120°C) and dehydroxylation of surface siloxyl groups (180°C) (36). After bake out, reactor and buret are isolated and filled with purified argon followed by attachment to the vacuum distillation unit through the connector/valve assembly atop the styrene buret. A middle fraction of styrene monomer is distilled directly into the isolated buret and the vacuum distillation unit is disassembled and removed. A monometer line, argon gas line and solvent unit are attached to the reactor. After pressurizing the reactor with argon, a septum is inserted and secured with a nylon bushing. Several cycles of gas and vacuum are followed by filling with argon to one-half atmosphere pressure. 1-1.5 liters of solvent are driven into the reactor using an overpressure of argon. The temperature is maintained at 40°C using an external temperature bath and a predetermined amount of initiator is injected into the vigorously stirred solvent. Addition of a metered amount of styrene leads to the rapid development of a yellow-orange color indicating the presence of polystyryllithium anions. The solution is stirred until 99% theoretical conversion, as predicted by equations 2-7,8,

and the reaction is terminated by injection of one ml of methanol. Polystyrene is recovered from solution by precipitation in methanol followed by vacuum drying at room temperature for several days and at 100°C for 24 hours. The product is then stored in a sealed container at -20°C. Polystyrene synthesis results are listed in Table 2-1.

2.5.2 Polybutadiene: The reactor is assembled as in the case of polystyrene, replacing the styrene buret with a butadiene buret(s). After baking out under vacuum, butadiene is distilled through the reactor into the buret(s), isolated and frozen with liquid nitrogen. Using a Gunn and Yamada method (37) the density of butadiene at -78°C and 0°C can be estimated and the quantity of butadiene in the volumetric buret determined. Following filling, the butadiene buret(s) is fitted with a cooling jacket operated at 0°C and the septum and solvent reservoir attached to the reactor. Solvent and initiator are added and the stirred solution is brought to 50°C followed by slow addition of butadiene. Polymerization of butadiene is evidenced by the monatomic drop in system pressure. The polybutadienyllithium solution is terminated at 99% conversion, as determined by equations 2-9,10, with one ml of methanol. Polybutadiene is recovered by precipitation in methanol followed by vacuum drying at room temperature for several days. The product is stored in the dark at -20°C in a sealed container. Polybutadiene synthesis results are listed in Table 2-1.

2.5.3 Poly(styrene-b-butadiene): Preparation of monomers and reactor are the same as in the case of each homopolymer with the exception that butadiene monomer is received in a tared buret and weighed

TABLE 2-1

Polymer Synthesis Results

Sample	Styrene (g)	Butadiene (g)	Initiator[c] (moles X 10^4)	Conversion[a] (%)	M_n[e] (kg/mol)
SB1	44.	6.2	5.2	100.	85-12
SB2	76.	22.8	9.5	97.5	80-24
SB3	34.	17.5	4.0	101.	85-44
SB4	76.5	10.7	4.9	100.	155-22
SB5	38.	11.4	2.25	101.	170-50
SB6	33.	16.5	1.95	100.	170-84
SB7	74.5	8.3	1.4	95.	530-59
SB8	41.	12.2	0.95	97.5	440-130
SB9	46.5	23.0	1.05	96.	440-220
SB_d1	47.	7.8[b]	5.9	100.	79-13
SB_d2	11.5	6.4[b]	1.35	99.	85-47
SB_d3	54.5	6.8[b]	1.35	98.5	400-50
S1	95.		14.0		68
S2	95.		7.5		125
S3	68.		1.8		380
B1		53	27.3[d]		19
B2		108	25.0[d]		43

[a]theoretical conversion is 99% [b]perdeuterated butadiene [c]corrected for residual impurities (6.8×10^{-4} mol/l of styrene) [d]no correction on initiator concentration [e]predicted from stoichiometry

prior to attachment to the reactor. The smaller quantity of butadiene precludes accurate volumetric determination of charge. Following attachment to the reactor the butadiene is frozen with liquid nitrogen until the styrene distillation sequence is begun. During styrene distillation and polymerization butadiene monomer is maintained below 5°C with the cooling jacket operated at 0°C.

Styrene is initiated with n-BuLi in benzene in the presence of anisole at 40°C and vigorously stirred until 99% conversion as determined by equations 2-7,8. A one ml aliquot of styryllithium solution is then extracted using a 2 ml Hamilton gas-tight syringe fitted with a 6", 20 ga stainless steel needle; the assembled syringe has been previously flushed with excess argon. The aliquot of "living" polymer solution is terminated and precipitated by injection into methanol and recovered and dried for later analysis. Butadiene is slowly added to the solution and the temperature increased to 50°C with the overall transient lasting approximately 10 minutes. A rapid crossover reaction between polystyryllithium and butadiene is evidenced by a color transition from yellow-orange to clear several seconds following butadiene addition. At 99% butadiene conversion, as determined by equations 2-9,10, the reaction is terminated by injection of one ml methanol.

Diblock copolymers were recovered by precipitation in methanol followed by vacuum drying for several days at room temperature and 24 hours at 100°C. The products were stored at -20°C in the dark in a sealed container. Poly(styrene-b-butadiene) synthesis results are listed in Table 2-1.

2.5.4 Poly(styrene-b-butadiene d_6): Polymerization of a diblock copolymer of styrene and perdeuterated butadiene is identical to the hydrogenated counterpart. Reaction parameters are as listed in Section 2.5.3 with the exception of one perdeuterated diblock containing 36% by weight butadiene d_6. In the latter case the reaction was not terminated at a theoretical yield of 99% but permitted to react overnight (14 hours) after which one ml of alcohol was added. Theoretically, it is not necessary to terminate a "living" diblock at 99% conversion since the termination free nature of the carbanion allows it to remain in solution nearly indefinitely. The butadiene d_6 reaction time was extended to insure complete utilization of the monomer. As will be discussed in the following chapter, a spurious side reaction becomes apparent under such conditions and therefore, the practice was not repeated. Poly(styrene-b-butadiene d_6) diblocks were recovered and stored as in Section 2.5.3 and the results are reported in Table 2-1.

References

1 P.J. Flory, Principles of Polymer Chemistry, Cornell University Press (1953).

2 M. Szwarc, Nature, 178, 1168 (1956).

3 M. Szwarc, M. Levy and R. Milkovich, J. Am. Chem. Soc., 78, 2656 (1956).

4 A.F. Sirrianni, D.J. Worsfold and S. Bywater, Trans. Faraday Soc., 55, 2124 (1959).

5 F. M. Brower and M.W. McCormick, J. Polymer Sci., A, 1, 1749 (1963).

6 M. Szwarc, Carbanions, Living Polymers and Electron Transfer Processes, Interscience (1968).

7 M. Omoto, T. Tanaka, S. Kadokura and H. Inagaki, Polymer, 20, 129 (1979).

8 T. Kotaka, N. Donkai and T.I. Min, Bull. Inst. Chem. Res., Kyoto University, 52, 2, 332 (1974).

9 P. Rempp, Polymer Preprints, 7, 141 (1966).

10 M. Morton, Polymer Preprints, 21, 1, 26 (1980).

11 P. Rempp, E. Franta and J. Herz, Polymer Preprints, 21, 1, 28 (1980).

12 J. Junquera, N. Cardona and J.E. Figueruelo, Makromol. Chem., 160, 159 (1972).

13 C.A. Uraneck, J. Polymer Sci., A-1, 9, 2273 (1971).

14 A.L. Gatzke, J. Polymer Sci., A-1, 7, 2281 (1969).

15 L. Gold, J. Chem. Phys., 28, 91, (1958).

16 V.S. Nanda and R.K. Jain, J. Polymer Sci., A, 2, 4583 (1964).

17 G. Holden and R. Milkovich, U.S. Pat. 3,231,635 (1966).

18 F. Kuntz, J. Polymer Sci. A, 2, 2827 (1964).

19 D.J. Worsfold and S. Bywater, Can. J. Chem., 38, 1891 (1960).

20 H.L. Hsieh, J. Polymer Sci., A, 3, 163 (1965).

21 S. Bywater and D.J. Worsfold, J. Organomet. Chem., 10, 1 (1967).

22 L.J. Fetters, personal communication (1979).

23 S. Bywater and D.J. Worsfold, J. Organomet. Chem., 9, 1 (1967).

24 J.E.L. Roovers and S. Bywater, Trans. Faraday Soc., 62, 1876 (1966).

25 J. Geerts, M. Van Beylen and G. Smets, J. Polymer Sci., A-1, 7, 2805 (1969).

26 M. Morton, J.E. McGrath and P.J. Juliano, J. Polymer Sci., C, 26, 99 (1969).

27 A.F. Johnson and D.J. Worsfold, J. Polymer Sci., A, 3, 449 (1965).

28 M. Morton, E.E. Bostik and R. Livigni, Rubber Plastic Age, 42, 397 (1961).

29 L.J. Fetters and R.N. Young, Polymer Preprints, 21, 1, 34 (1980).

30 D.N. Cramond, P.S. Lawry and J.R. Urwin, European Polymer J., 2, 107, (1966).

31 R.J. Ceresa, ed., Block and Graft Copolymerization, vol. 1, J. Wiley and Sons (1973).

32 M. Morton and F.R. Ells, J. Polymer Sci., 61, 25 (1962).

33 F.S. Bates, S.M. thesis, Massachusetts Institute of Technology (1979).

34 Eight Peak Index of Mass Spectra, vol. 1, first edition, Mass Spectrometry Data Centre U.K. (1970).

35 R.L. Eppley and J.A. Dixon, J. Organometallic Chem., 8, 176 (1967).

36 R.K. Iler, The Chemistry of Silica, John Wiley and Sons (1979).

37 R.C. Reid, J.M. Prausnitz and T.K. Sherwood, The Properties of Liquids and Gases, third edition, McGraw-Hill, (1977).

CHAPTER 3: Molecular Characterization

3.1 NMR SPECTROSCOPY

Proton nuclear magnetic resonance spectroscopy was utilized for determining polybutadiene microstructure. Polymer samples were dissolved in carbon tetrachloride at 10% concentration and placed in 5 mm NMR tubes. Measurements were taken on an Hitachi Perkin-Elmer R-24B 60 MHz high resolution spectrometer operated between 0 and 10 ppm at a sweep time of 300 seconds and standardized with TMS (0 ppm). NMR spectra for samples SB4 and B2 are presented in Figure 3-1. Peaks appearing in Figure 3-1 have been attributed to the following hydrogen species (1),

Peak (ppm)	Hydrogen type
6.9-7.0	p,m aromatic
6.4-6.5	o aromatic
5.3-5.4	non-terminal olefinic
4.9-5.0	terminal olefinic

From these designations and the relative areas due to terminal and non-terminal olefinic hydrogen atoms, the percentage of 1,4 versus 1,2 additions present in the polybutadiene can be calculated. Since sample B2 can be measured with the greatest degree of accuracy, the reported value of 87% 1,4 is based upon this homopolymer although the diblock copolymers exhibit the same olefinic peaks as illustrated in Figure 3-1. This is expected based upon their identical synthetic histories.

Since the microstructure of perdeuterated polybutadiene cannot

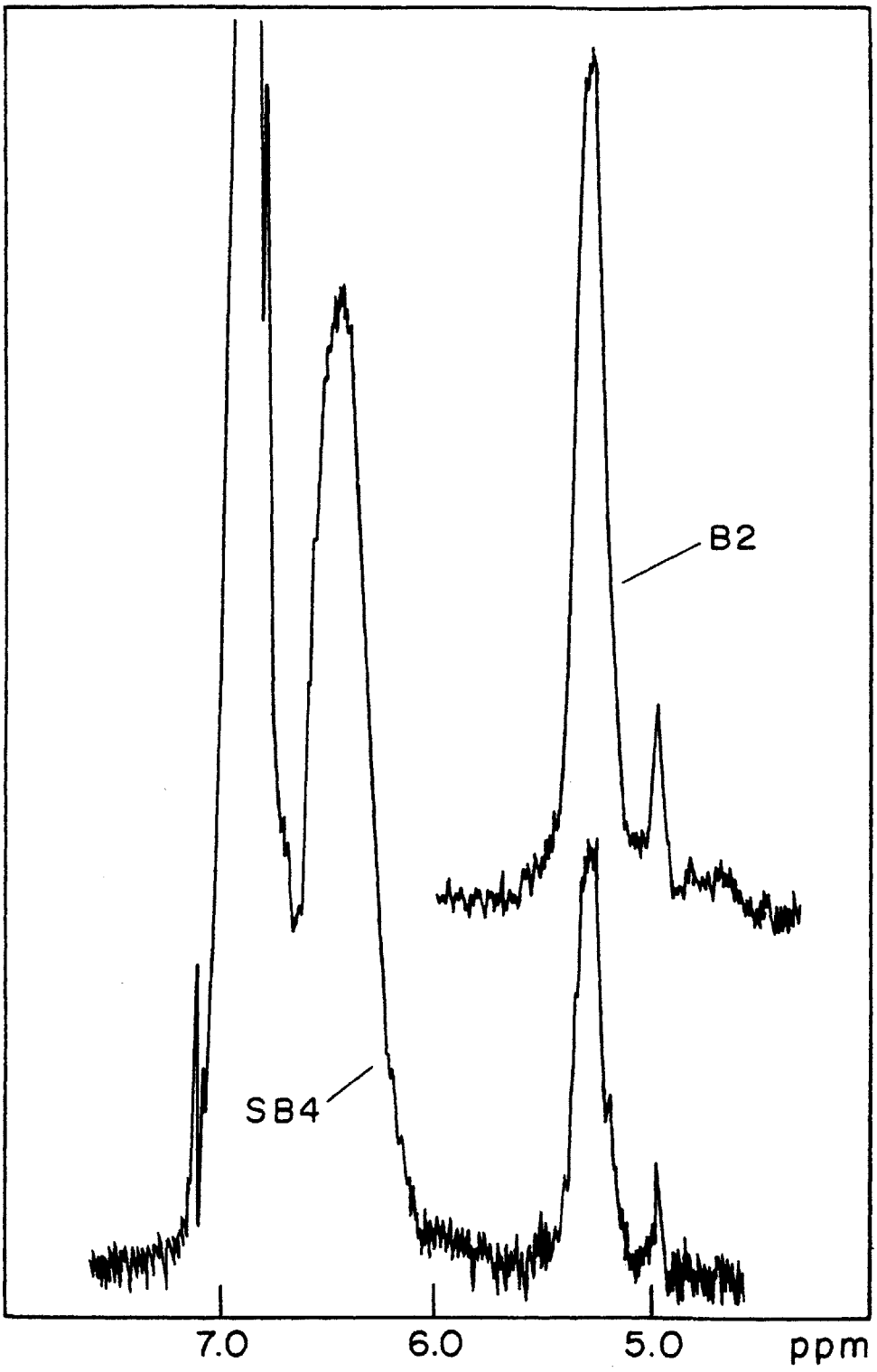

Figure 3-1 NMR spectra for polybutadiene and polystyrene-b-polybutadiene diblock copolymer. B2 spectrum has been shifted vertically.

be determined by proton NMR, samples SB_d1 and SB_d2 were dissolved in perdeuterated chloroform (10% solution) and analyzed on a Bruker 250 ^{13}carbon NMR. The resulting spectra did not yield quantitative information concerning the percentage of 1,4 versus 1,2 repeat units in the perdeuterated polybutadiene. Nevertheless, based upon an identical synthetic history, the perdeuterated polybutadiene can be assumed to contain the same microstructure as the hydrogenated polybutadiene. As will be shown in Chapter 6, both types of polybutadiene exhibit the same glass transition temperature, thereby supporting this assumption.

3.2 UV ABSORPTION SPECTROSCOPY

The composition of each diblock copolymer sample was determined by ultraviolet (UV) absorption spectroscopy. At a wavelength of 262 mm polystyrene exhibits a maximum in UV absorption while polybutadiene is virtually transparent. Therefore, comparing the 262 mm UV absorbance of a solution of poly(styrene-b-butadiene) with that of polystyrene, each of known concentration, will directly yield the weight percent of polystyrene in the diblock copolymer.

Polymer specimens were dissolved in reagent grade chloroform (Mallinckrodt, Inc.) taken from a single bottle at concentrations ranging from 0.24 to 0.27 g/l. Absorption measurements were taken on a Bausch and Lomb Spectronic 2000 Spectrophotometer set at a 262 mm emission wavelength. Sample solution and reference solvent were contained in quartz Spectrosil (VWR Scientific, Inc.) spectrophotometer cells providing a light path of one cm. Reference and sample cells were matched by the instrument prior to absorption measurements.

TABLE 3-1

Diblock Copolymer Composition

	weight fraction polybutadiene	
Sample	Stoichiometry	UV Absorption
SB1	0.12	0.120
SB2	0.23	0.217
SB3	0.34	0.317
SB4	0.12	0.118
SB5	0.23	0.242
SB6	0.33	0.329
SB7	0.10	0.096
SB8	0.23	0.214
SB9	0.33	0.328
SB_d1	0.14	0.136
SB_d2	0.36	0.362
SB_d3	0.11	0.106

The above concentrations were chosen so that absorbance measurements ranged from 0.34 to 0.53, thereby minimizing the effect of inaccuracies in concentration (2). Optimal accuracy occurs at an absorbance of 0.43 (2). Table 3-1 lists the diblock copolymer compositions obtained by UV absorption along with percentages predicted by synthesis stoichiometry.

3.3 HPSEC

3.3.1 Size Exclusion Chromatography: As the title implies, size exclusion chromatography involves the separation of compounds according to their molecular dimensions. In the case of polymers, this dimension is dictated by the hydrodynamic volume in solution which is directly related to the molecular weight and polymer-solvent interaction parameter. Therefore, in a given solvent, polymer species can be separated by molecular weight when passed over a suitable porous medium. Molecules of large hydrodynamic volume tend to be excluded and therefore eluted prior to smaller, more permeable molecules. This principle has been exploited in the development of gel permeation columns (GPC) and more recently, high pressure size exclusion columns (HPSEC) used in separating polymer molecules in solution by molecular weight. Yau et al. (3) have extensively reviewed this powerful method of polymer characterization; further discussion will be restricted to topics related to the present work.

3.3.2 Equipment: A High Pressure Size Exclusion Chromatograph (HPSEC) was assembled from the following components. An Altex model 100A solvent metering pump was utilized for solvent delivery. This

unit is a dual reciprocating piston pump capable of delivering a constant, virtually pulseless, flow rate with better than 1% accuracy. The sample injector is a Rheodyne, Inc. model 7125 rotary valve syringe injector fitted with a 100 µl injection loop. Injection volume may vary up to complete filling of the sample loop. At the heart of the HPSEC unit is a set of Dupont Zorbax PSM Bimodal HPSEC polymer fractionating columns (4). These columns have been substituted for the more conventional gel permeation columns (GPC) since their range of operation, durability, resolution, thermal stability and response time are superior to the latter. Eluted polymer samples in solution are monitored with a Waters Assoc. model R401 differential refractometer wired to a Fisher series 5000 chart recorder.

Injector, columns and detector are connected in series with short lengths of 0.009" i.d. thick-walled stainless steel tubing and zero volume Swagelok fittings to minimize system dead volume and associated sample spreading during use. All other tubing is 0.040" i.d. stainless steel connected with standard Swagelok fittings.

The HPSEC system was operated with toluene at room temperature using a flow rate of 1.0 ml per minute at a corresponding pressure of 70 bar. Solvent was filtered through a 1.0 µm millipore filter (Millipore Corp.) prior to introduction into the instrument.

3.3.3 Calibration: The HPSEC was calibrated with nine monodisperse polystyrene standards of known molecular weight (3.5×10^4 - 2.0×10^6 g/mol) obtained from Polysciences, Inc. Solutions of polystyrene in toluene ranging in concentration from 0.25 to 1.0 g/l (dependent on molecular weight) were twice filtered through a 1.0 µm

millipore filter prior to injection into the HPSEC. Injection volume was 50 µl.

A calibration curve is usually established by relating the peak retention volume (V) to molecular weight (M) of a series of narrow molecular weight distribution samples (3) yielding the linear relationship:

$$M(V) = D_1 \exp(-D_2 V) \qquad 3\text{-}1$$

This peak position calibration technique was found to lead to consistent deviations between the calculated molecular weight of the polystyrene standards and that reported by the manufacturer. Therefore, a modified Hamielec method (5) was employed whereby D_1 and D_2 are iteratively varied until calculated values of molecular weight are consistent with those reported by Polysciences, Inc. Figure 3-2 illustrates the peak position calibration curve and final working curve along with a representative chromatograph.

Several methods exist for characterizing the degree of sample spreading and skewing induced in a chromatograph by the instrument (6,7). One such method (7) involves comparison of the polydispersity index as measured in the instrument versus the value obtained by osmometry and light scattering. Such a comparison on the HPSEC used in the present work revealed a negligible difference between the measured and reported (Polysciences by osmometry and light scattering) values of M_w/M_n for the polystyrene calibration standards; this ideally can be attributed to the monodispersity in pore size in the column packing material and negligible dead volume in the system. Therefore, all polydispersity indices are reported as measured on

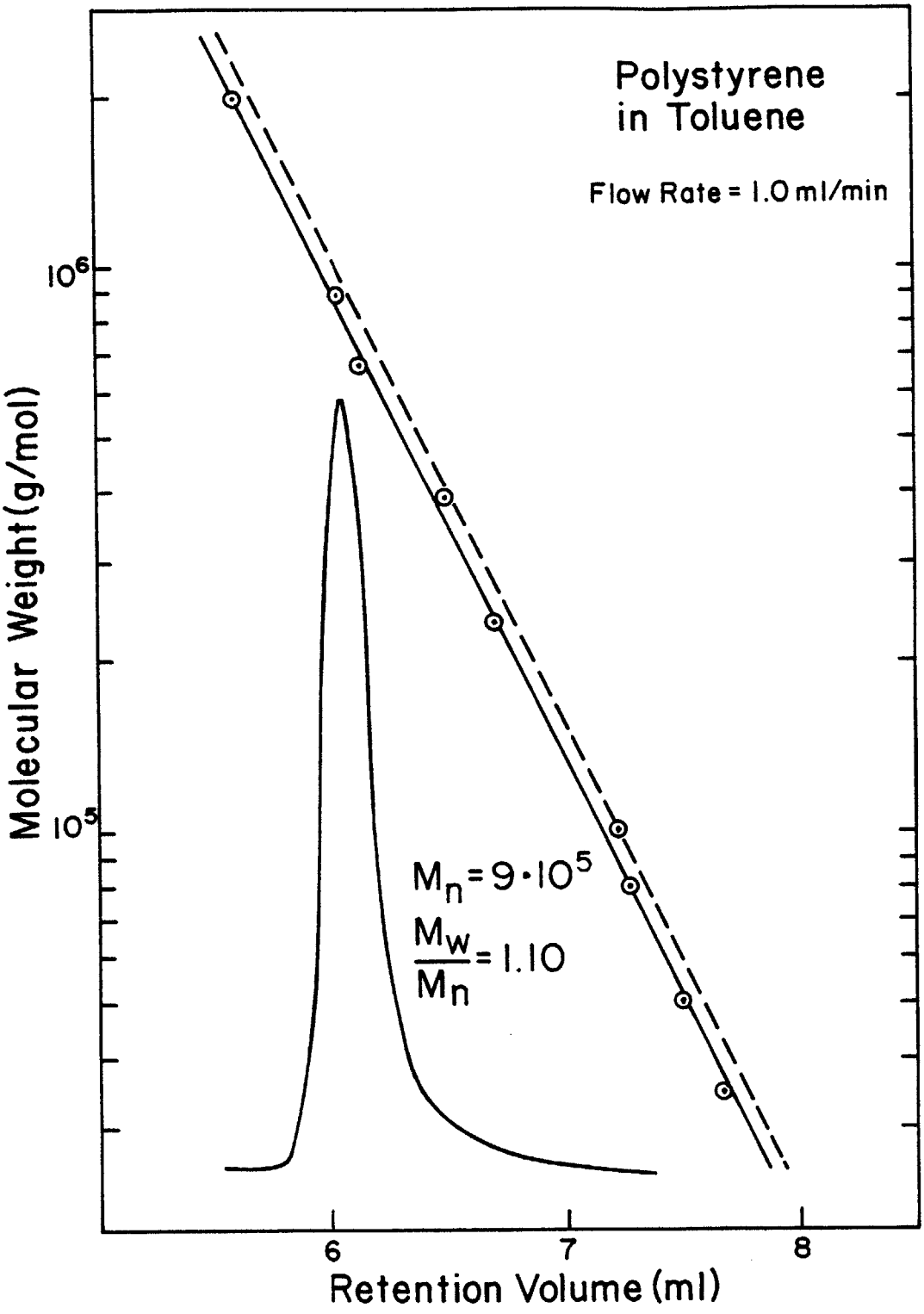

Figure 3-2 HPSEC calibration curve. Solid line is given by polystyrene standard peak locations, dashed line is actual calibration curve.

the instrument without using corrections for axial spreading of the injected sample.

3.3.4 Homopolymers: A high pressure size exclusion chromatograph was obtained on all homopolymers, including first block polystyrene samples removed from the reactor prior to second block addition. Chromatograph samples were dissolved in toluene at a concentration of 0.25 to 1.0 g/l (dependant on molecular weight), twice filtered with a 1.0 μm millipore filter and injected in 50 μl batches into the HPSEC. Resulting chromatographic traces were baseline corrected using pre- and post-peak response levels which in all cases were identical.

Analysis of polystyrene HPSEC traces was accomplished by conventional methods (3), making direct use of the calibration curve shown in Figure 3-2. Ordinate values of chromatographs are proportional to $N_i M_i$, the number of species of molecular weight i times the molecular weight, while the abscissa values, retention volume, can be converted to M_i using equation 3-1. From this information M_n, M_w and M_w/M_n were determined.

Polybutadiene chromatographs cannot be interpreted directly. Instead, a universal calibration technique (8) must be employed, making use of the empirical Mark-Houwink equation,

$$[\eta] = KM^a \qquad 3\text{-}2$$

where $[\eta]$ is the intrinsic viscosity and K and a vary with polymer type, temperature and viscosity. Benoit and coworkers (8) have shown that for a given solvent and temperature a plot of log $[\eta]M$ versus

retention volume yields a single curve for all polymeric species. Therefore, we can determine the actual molecular weight of polybutadiene, M_B, from the molecular weight determined by equation 3-1, M_S, using the relationship:

$$\log M_B = \frac{1+a_S}{1+a_B} \log M_S + \frac{1}{1+a_B} \log (K_S/K_B) \qquad 3\text{-}3$$

The following Mark-Houwink constants appearing in equation 3-3 have been obtained for toluene from the literature (9).

$$a_S = 0.73 \qquad K_S = 9.77 \times 10^{-3} \text{ ml/g}$$
$$a_B = 0.713 \qquad K_B = 39 \times 10^{-3}$$

Table 3-2 lists the results of homopolymer analysis and actual HPSEC traces are compiled in Appendix B.

3.3.5 Diblock Copolymers: Solutions of diblock copolymers were prepared and run on the HPSEC by the same procedure as homopolymers. Three pairs of chromatographs are presented in Figure 3-3 representing samples SB_d1, SB_d2 and SB_d3. In each case the first chromatograph is the polystyrene sample extracted prior to butadiene addition and the second is the completed diblock.

Analysis of the diblock copolymer chromatographs is complicated by the fact that the hydrodynamic volume of these samples is determined by individual contributions from each block. Several authors have examined block copolymers by GPC and found that they conform to a "universal" calibration curve (10-12). However, accurate application of HPSEC (or GPC) to diblock copolymers requires a knowledge

of the relationship between composition, molecular weight and elution volume. Tung (12) has successfully applied the following equation (13) to the analysis of poly(styrene-b-diene) block polymers,

$$\log M_c = x_S \log M_S + (1-x_S) \log M_B \qquad 3\text{-}4$$

where M_c is the molecular weight of the copolymer and M_S and M_B are the molecular weights of component homopolymers having the same HPSEC elution volume. x_S represents the weight fraction of block S in the diblock. M_B, in this case polybutadiene, can be calculated using equation 3-2 and the associated Mark-Houwink parameters.

Equation 3-4 neglects heterocontact contributions to the hydrodynamic volume of a block copolymer in dilute solution. Ho-Duc and Prud'homme (11) have empirically developed an alternative expression which takes these segmental interactions into account:

$$[\eta_{S-B}]^{2/3} = x_S[\eta_S]^{2/3} + (1-x_S)[\eta_B]^{2/3} \qquad 3\text{-}5$$

Therefore, the intrinsic viscosity of a copolymer can be determined from the intrinsic viscosity of homopolymers of equal molecular weight. Equations 3-3 and 3-5, together with the appropriate Mark-Houwink parameters, can be iteratively solved in conjunction with the universal calibration curve to yield the block copolymer molecular weight.

Polydispersity indices were obtained directly from the HPSEC chromatographs for diblock copolymers. Since this parameter is sensitive to changes in retention volume arising from compositional variations in copolymer samples, true polydispersity indices may be somewhat different than the measured values.

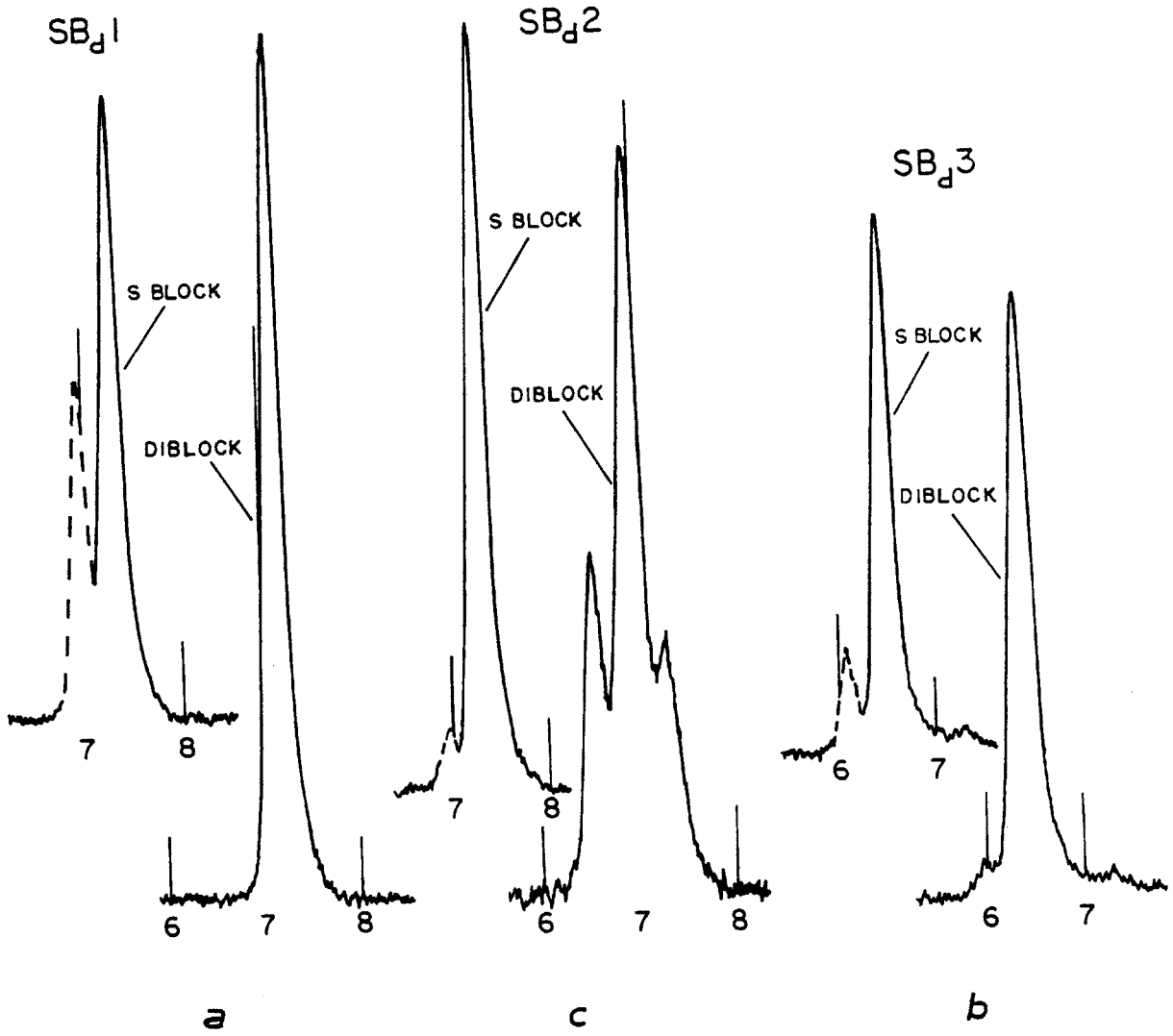

Figure 3-3 HPSEC chromatographs from the diblock copolymers containing perdeuterobutadiene. S-block chromatographs are from the polystyrene extracted from the reactor prior to butadiene addition. the dashed sections are artifacts of sampling (see Appendix B) and the numbered markers indicate retention vol. (ml)

HPSEC provides an effective method of determining the purity of a block copolymer specimen as illustrated in Figure 3-3. Figures 3-3a and 3-3b exhibit single Poisson peaks in the case of polystyrene and poly(styrene-b-butadiene). This is indicative of a termination free polymerization (14). On the other hand, several peaks are evident in the copolymer curve in Figure 3-3c. The main central peak is due to diblock copolymer while the low molecular weight peak is that of polystyrene. This indicates a partial loss of polystyryl-lithium anions prior to butadiene addition. The area under each of these peaks is proportional to the weight fraction of polymer in the sample. Using the first block homopolystyrene chromatograph as a template, the area attributable to terminated polystyrene in the composite trace can be subtracted. Since the overall composition of the sample is known (Table 3-1) the resulting area can be corrected for refractive index differences between polystyrene and polybutadiene and then compared to the area due to homopolystyrene. In this manner, sample SB_d3 was determined to contain 11% by weight homopolystyrene. Small amounts (less than 10% by weight) of homopolystyrene were also found present in four of the other samples and their chromatographs were corrected accordingly.

The third peak seen in the copolymer trace of Figure 3-3c appears at twice the molecular weight of the main peak and is attributed to coupled diblock copolymer. Apparently, "living" polybutadiene slowly dimerizes under the reaction conditions employed, although the mechanism of such a reaction remains obscure. This problem was eliminated by adhering to the kinetics developed in section 2.2.3, whereby "living"

TABLE 3-2

Characterization Results

	[a] Homopolymers		Diblock Copolymers			
Sample	[b] M_n	M_w/M_n	[b,c] M_n(S-B)			M_w/M_n
			d	eq. 3-4	eq.3-5	
SB1	79	1.06	79-11	74-10	71-10	1.06
SB2	77	1.06	77-21	76-21	72-20	1.06
SB3	85	1.06	85-45	75-40	71-37	1.07
SB4	149	1.05	149-20	150-20	146-19	1.07
SB5	126	1.06	126-46	134-49	127-46	1.06
SB6	122	1.07	122-66	133-71	125-67	1.07
SB7	560	1.08	560-59	480-51	470-50	1.11
SB8	450	1.08	450-123	390-106	370-101	1.15
SB9	420	1.07	420-230	410-230	390-210	1.12
SB_d1	80	1.06	80-13	84-13	81-13	1.07
SB_d2	78	1.06	78-54	70-48	66-45	1.10
SB_d3	380	1.07	380-46	380-46	370-44	1.10
S1	64	1.06				
S2	116	1.05				
S3	390	1.05				
B1	20	1.04				
B2	44	1.04				

[a] polystyrene block in the case of diblock copolymers [b] kg/mol
[c] based on compositions given in Table 3-1 [d] these values are quoted in the text and were determined from HPSEC block polystyrene M_n

polymer is terminated before such dimerization becomes noticeable.

Diblock copolymer molecular weights have been determined by three methods and are presented in Table 3-2. The first method relies upon the molecular weight of the polystyrene block as determined by HPSEC while equations 3-4 and 3-5 are employed in the second two cases. In all cases the compositions are taken from Table 3-2. Since the first technique is the most direct, requiring no solubility parameters or empirical formulas, diblock copolymer molecular weights will be reported as obtained by this method, although all three techniques show good agreement. With the exception of two samples, calculated molecular weights are in excellent agreement with those predicted from synthesis stoichiometry (Table 2-1). Values somewhat lower than expected were obtained for samples SB5 and SB6, later found to be the result of faulty initiator titration. Diblock copolymer HPSEC traces are given in Appendix B.

References

1 W.C. Senn, Analytica Chimica Acta, 29, 505 (1963).

2 D.G. Peters, J.M. Hayes and G.M. Hieftje, Chemical Separations and Measurements, W.B. Saunders Co. (1974).

3 W.W. Yau, J.J. Kirkland, D.D. Bly, Modern Size Exclusion Liquid Chromatography, J. Wiley and Sons (1979).

4 W.W. Yau, C.R. Ginnard and J.J. Kirkland, J. Chromatogr., 149, 465 (1978).

5 S.T. Balke, A.E. Hamielec, B.P. LeClair and S.L. Pearce, Ind. Eng. Chem., Prod. Res. Div., 8, 54 (1969).

6 K.S. Chang and R.Y.M. Huang, J. Appl. Polym. Sci., 13, 1459 (1969).

7 S.T. Balke and A.E. Hamielec, J. Appl. Polym. Sci., 13, 1381 (1969).

8 Z. Grubistic, P. Rempp and H. Benoit, J. Polymer Sci., B, 5, 753 (1967).

9 J. Brandrup and E.H. Immergut, eds., Polymer Handbook, second edition, (1975).

10 A. Dondos, P. Rempp and H. Benoit, Die Makromoleculare Chimie, 175, 1659 (1974).

11 N. Ho-Duc and J. Prud'Homme, Macromolecules, 6, 472 (1973).

12 L.H. Tung, J. Appl. Polymer Sci., 24, 953 (1979).

13 J.R. Runyon, D.E. Barnes, J.F. Rudd and L.H. Tung, J. Appl. Polymer Sci., 13, 2359 (1969).

14 P.J. Flory, Principles of Polymer Chemistry, Cornell University Press (1953).

CHAPTER 4: Structure

4.1 PHASE BEHAVIOR OF BLOCK COPOLYMERS AND BLENDS

4.1.1 Phase Separation: Multicomponent polymeric systems can be qualitatively divided into two categories, single phase and multiphase. Although at times subjective, identification of phase structure by electron microscopy or small angle scattering is indicative of a multiphase blend. Phase behavior may also be determined by investigating the physical properties of a blend such as its thermal (Tg, Tm) and mechanical characteristics (1).

Homopolymer-homopolymer miscibility has been the subject of enormous study in the past several decades. Flory (2) originally demonstrated the unusual behavior of polymer-polymer systems relative to low molecular weight mixtures. The conventional expression for the free energy of mixing is,

$$\Delta G_M = \Delta H_M - T\Delta S_M \qquad 4\text{-}1$$

where the heat of mixing ΔH_M is proportional to the segment-segment interaction energy χ (2), and ΔS_M is the entropy of mixing derived by Flory (2) using a liquid-lattice model. Due to the large number of segments per molecule, ΔS_M in polymer mixtures is very small and correspondingly, miscibility should only occur if χ is extremely small or negative. Therefore, in most hydrocarbon polymer-polymer blends immiscibility is the expected rule.

More recently, McMaster (3) and Sanchez and Lacombe (4,5) have

refined the original treatment by Flory and their theoretical findings are in reasonable agreement with experimental results on miscibility. Under all practical conditions, styrene and butadiene polymer mixtures phase separate due to a large positive value of χ (6); according to Flory (2) the critical blend molecular weight for demixing at room temperature is $\sim 2 \cdot 10^3$ g/mol. In blends of similar polymers such as dienes the critical molecular weight is found to be much higher (1,7).

Block copolymers exhibit significant differences in their manner of phase separation from that of the corresponding homopolymers. The covalent bond linking blocks severely restricts the possible locations of each block in a liquid lattice leading to a lower value of ΔS_M. This results in a phase diagram in which the equilibrium and stability curves deviate from those of the corresponding homopolymers. Meier (8) and later Helfand et al. (9) and Leibler (10) have addressed this issue and all conclude that the critical point for a block copolymer at a specified temperature is governed by the overall number average degree of polymerization x, and χ. The value of x at the critical point in a block copolymer is calculated to be 2.5 to 5.5 times greater than x critical for the corresponding homopolymer blend. Helfand's theory (9) for microphase separation in block copolymers indicates that polystyrene-polybutadiene diblock copolymers (50 wt % polystyrene) will be heterogeneous above a molecular weight of $\sim 12 \cdot 10^3$ g/mol. Several authors have shown these conclusions to be either qualitatively or quantitatively correct. Kraus et al. (11) studied block copolymers and homopolymers of styrene and α-methyl styrene while Ramos (1) investigated blends of polyisoprene, polybutadiene and diblock copolymers of

each. The data of Ramos has been replotted to reveal the phase separation behavior of this three component system and is presented in Appendix D. Values calculated for the point of phase transition in polystyrene-polybutadiene block copolymers (9) are in excellent agreement with experimental findings (12,13).

Upon phase separation block copolymers exhibit a variety of microphase structures not found in their homopolymer analogs. This phenomena, originally investigated by Skoulios et al. (14), can also be attributed to the covalent bond linking dissimilar phase separated block species. Since all block junctions are constrained to the phase boundaries, the requirement of constant phase density restricts phase size to molecular dimensions. Five distinct phase structures have been identified (15,16),

spheres of S in a matrix of B
cylinders of S in a matrix of B
lamellae of S with lamellae of B
matrix of S with cylinders of B
matrix of S with spheres of B

where in the present work S and B represent polystyrene and polybutadiene. Numerous authors (8-10,17) have explained these structures as minimum free energy states of the system, controlled predominately by the overall composition.

Figure 4-1 is a phase diagram showing the regions of lowest free energy for diblock copolymers of styrene and butadiene as calculated from the theory of Helfand and Wasserman (9) at 90°C. Values for diblock copolymers reported in Chapter 3 are coplotted in Figure 4-1. Electron micrographs (see Section 4.3.1) of samples SB4, SB5 and SB6 cast from toluene are presented in Figure 4-2. They confirm the

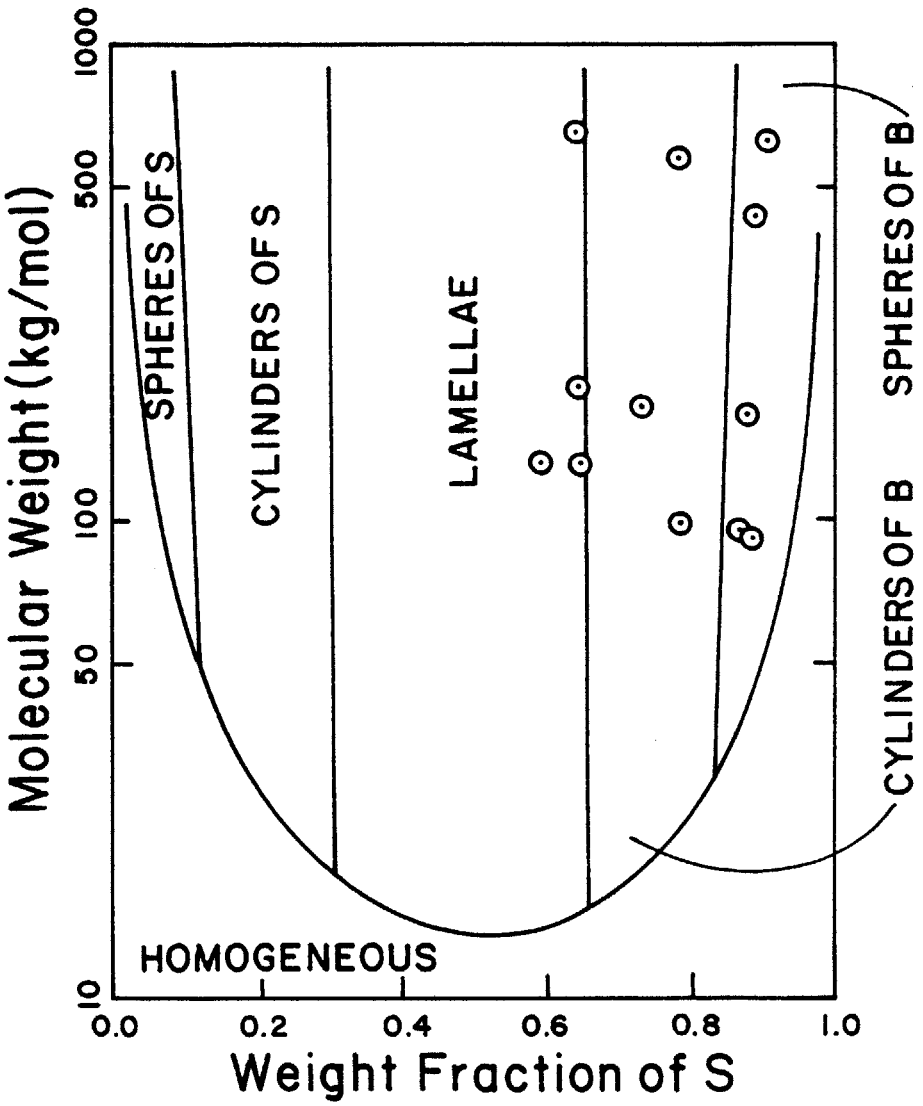

Figure 4-1 Phase diagram at 90°C for polystyrene-b-butadiene diblock copolymer according to Helfand and Wasserman (9). Location of samples appearing in Table 3-2 are indicated by circles.

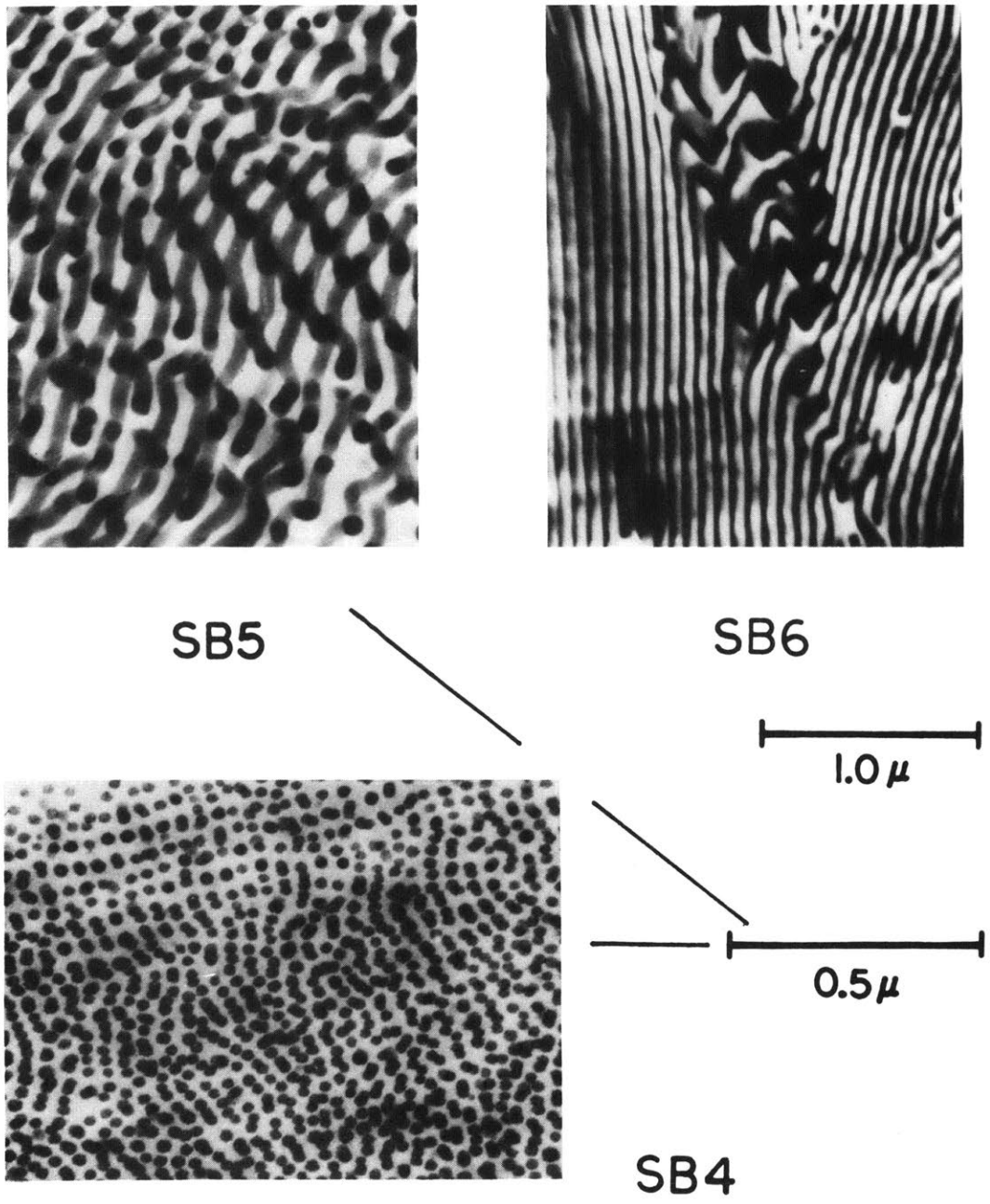

Figure 4-2 Electron micrographs of samples solvent cast from toluene at 80°C. Dark regions are osmium stained polybutadiene.

predicted microphase separation behavior of these block copolymers.

4.1.2 Microdomain Order: Phase separated microdomains of block copolymers exhibit regularity on several levels. Long range liquid crystalline structures brought about by the ordering of microdomains have been extensively studied for more than a decade (18,19). Electron microscopic and small angle x-ray (SAXS) analyses have provided information regarding the domain packing order in lamellar, cylindrical and spherical morphologies. Lamellar microdomains can take on only one basic structure, although the degree of order is strongly dependent upon processing conditions. Cylindrical domains have been conclusively shown to organize into a hexagonal close-packed array (18) consistent with the theoretical findings of Leibler (10). Spherical morphologies may in theory take on a variety of packing arrangements. Helfand and Wasserman (20) assume a hexagonally close-packed structure in their analysis of microphase separated spheres while Leibler (10) has calculated a body centered cubic (bcc) ordering. Pedemonte et al. (21) and Gallot et al. (22) have inferred a bcc structure for micropheres in polystyrene-polybutadiene-polystyrene (SBS) triblock copolymer by electron microscopy. SAXS experiments by Hashimoto et al. (23) revealed a cubic structure in polystyrene-polyisoprene (SI) diblocks containing a spherical morphology, although they could not distinguish between bcc and primary cubic (pc). Roe et al. (24) carried out SAXS experiments on SB and SBS block copolymers and tentatively concluded that the morphology of their samples had either a face-centered cubic (fcc) or bcc arrangement of spherical domains. Finally, Richards and Thomason (25) proposed that an fcc arrangement of spheres exists in their set of

SI, SIS and perdeuterated SI block copolymers as determined by electron microscopy, SAXS and small angle neutron scattering (SANS). Clearly, the liquid crystalline structure of spherical microdomains is the most difficult to characterize and this topic will be further addressed in Chapter 5.

Microdomains of phase separated block copolymers generally exhibit a high degree of uniformity in domain dimensions, attributable to the monodisperse nature of these anionically synthesized polymers (Chapters 2,3). The governing parameter which determines domain size is the molecular weight of the block in the included phase. Under the criterion of constant density within a phase, phase dimensions could hypothetically range from that obtained for a single collapsed block to that corresponding to an assembly of fully extended blocks. The actual chain conformation and associated domain size is uniquely determined by minimizing the overall free energy of the system. Various authors have addressed this issue (8,9,26) with Helfand and Wasserman (9) recently presenting a comprehensive computer program for calculating domain type and size in diblock and triblock copolymers of styrene and isoprene or butadiene. Calculated dimensions for lamellar and cylindrical morphologies are in excellent agreement with values (27,28) reported in the literature. Predicted radii for microspheres of polystyrene in polydiene are also consistent with experimental findings (20). Surprisingly, theoretical values for radii of polyisoprene spheres included in a polystyrene matrix are consistently twice that observed experimentally (20). The analogous case of polybutadiene has not been examined.

4.1.3 Block Copolymer Interfaces: Recent refinements in both the

theoretical and experimental methods of polymer blend analysis have brought about an increased interest in understanding polymer-polymer interfacial behavior. Such behavior becomes particularly significant in microphase separated block copolymers since the surface-to-volume ratio, which scales inversely with characteristic domain dimension, becomes extremely large. For example, a typical microphase domain having a 10 nm radius has 10^3 times the interfacial surface area as the homopolymer analog with a characteristic phase dimension of 10 μm. Furthermore, placement of block pair junctions at phase boundaries might be expected to enhance interfacial mixing, thereby increasing the interfacial volume fraction.

The necessity of including a finite interfacial thickness in determining the lowest free energy state of a phase separated block copolymer system has been demonstrated by various authors (9,26,29). Helfand and Wasserman (9,20,27,28) in particular have published extensively on this topic. Using a mean field theory they have derived the following analytical expression for relating the concentration of polymer species B, ρ_B, to a given position r from the center of the interface,

$$\rho_B(r) = 1/2[1-\tanh(2r/a_I)] \qquad 4\text{-}2$$

$$a_I = 2b/(6\chi)^{1/2} \qquad 4\text{-}3$$

where b is the length of a single segment (Kuhn statistical length), χ is the segment-segment interaction parameter and $\rho_B(r)$ ranges from 0 to 1. In deriving this expression, the density and Kuhn statistical

length in each phase were assumed to be identical. a_I is defined as the interfacial thickness. Equation 4-3 is illustrated in Figure 4-4.

The existence of diffuse phase boundaries has been experimentally verified in the past few years, primarily by the use of small angle scattering (SAS) techniques. In a series of publications Hashimoto et al. (23,30-32) have investigated the domain boundary structure of block copolymer films of styrene and isoprene having spherical and lamellar microstructures using SAXS. Their results indicate that for the system studied, the interfacial thickness averages 1.8 nm relatively independent of domain type and size. Richards and Thomason (25) have also recently measured the interfacial thickness in a styrene-isoprene block copolymer system by means of SANS and report a value of 2.9 nm. This finding is considerably larger than that quoted by Hashimoto, although the SANS measurements were made on material containing predominately cis 1,4 polyisoprene while the SAXS study involved a vinyl 1,2-3,4 polyisoprene. Nevertheless, such a variation between these materials would not be expected. To date, no interfacial measurements by small angle scattering involving block copolymers of styrene and butadiene have been reported.

4.1.4 Blends of Block Copolymers and Homopolymers: Blending of block copolymers with their corresponding homopolymers is an obvious extension of the studies on the parent pure components. Since block copolymers are significantly more costly and difficult to obtain than their homopolymer counterparts, the economic incentives for such research are high.

Numerous investigators have found that most block copolymers will

emulsify otherwise macroscopically phase separated blends of homopolymers (33-35) and this behavior has been interpreted in terms of the concept of a polymeric oil in oil emulsion (36). Such behavior has been found to be limited to blends which contain homopolymer of molecular weight equal to or less than that of the respective blocks in the copolymer (35). Homopolymer of higher molecular weight tends to form separate macroscopic phases, while solubilized homopolymer modifies the size, type and long range ordering of microdomains (32). A recently reported study on blends of styrene and isoprene diblock copolymers and homopolymers concluded that the interfacial thickness as measured by SAXS is independent of homopolymer content (32).

As previously stated (Section 4.1.1), several polymeric systems exhibit heterogeneous homopolymer blends and homogeneous block copolymer behavior (1,7,11). Under these circumstances, addition of block copolymer has been found to have a compatabilizing influence on the homopolymers (Appendix D). These characteristics should also be strongly molecular weight dependent, although this awaits experimental verification.

The quantitative theoretical treatment of blends of block copolymers and homopolymers has lagged behind the extensive developments with pure components. Meier (37) has extended his earlier work on block copolymers in developing a theory concerning the solubilization of homopolymer by block copolymers. Unfortunately, his results are in poor agreement with all experiment findings (32-36). Many unanswered questions remain concerning the phase characteristics of block copolymer-homopolymer blends.

4.1.5 Processing: The preceding discussion concerning the phase behavior of multicomponent polymeric systems has been based upon the assumption of phase equilibrium. In practice, polymer blends are rarely at equilibrium due to severe diffusional restrictions on recovery from the processing state. This becomes particularly apparent in glassy materials such as polystyrene at room temperature, which for all practical purposed never achieves an equilibrium state (38). Therefore, the manner in which a multicomponent polymer blend is processed can have a lasting influence on the structural characteristics of the product.

Polymer blends are generally processed in bulk form at elevated temperatures in order to obtain a suitable blend viscosity. Under such conditions, homopolymer phase dimensions can be modified by the input of mechanical energy. Although microphase domains of block copolymers are stable under such processing, long range domain ordering may be dramatically affected. Pedemonte et al. (39) have shown that extruded plugs of Kraton 101 (SBS; Shell Chemical Co.) yield highly oriented cylinders of polystyrene in a polybutadiene matrix. Skoulios et al. (40) have extended this concept by applying a steady oscillatory shear field to sheets of SIS and SI block copolymers, thereby orienting cylindrical and lamellar microdomains.

A second method of sample preparation is to directly cast a film from a polymer-solvent solution. This technique has limited applicability to homopolymer blends since the components will generally completely phase separate into individual layers. Solvent casting of block copolymer films does not suffer from this drawback and its use

has been widely reported in the literature (1,17,23). Cast films must be carefully checked for residual solvent which can be removed by vacuum drying at an appropriate temperature.

The range of nonequilibrium states attainable with block copolymers can be greatly extended by the use of solvent casting. Unlike bulk processing, solvent cast films reflect morphologies generated in a highly solvated state. As with pure block copolymer, block copolymer-solvent behavior is dictated by the minimization of system free energy. Analagous to the case of solvent and homopolymers (2), the critical concentration at which phase separation occurs is determined by the molecular weight, χ_{12}, χ_{13} and χ_{23} (solvent-segment, solvent-segment and segment-segment interaction parameters). Due to restraining block-block covalent bonds, phase dimensions are restricted to a microregime. Upon removal of solvent by evaporation, shrinking domains become increasingly unable to reorganize due to severe diffusional restrictions, and the bulk morphology generally reflects the geometry which was established in solution. Judicious adjustment of χ_{12} and χ_{13} through choice of solvent provides great flexibility in specifying microdomain type. These interaction parameters can also be continually varied during the course of solvent casting by the use of a mixed solvent, e.g. different solubility parameters and vapor pressures. The theoretical treatment of block copolymer domain formation during solvent casting has been presented by Meier (29) and Inoue et al. (17) and numerous experimental examples have been documented (17,41). Inoue et al. (35) have also extended their work to include solvent casting of block copolymer-homopolymer

blends.

The influence of solvent on intradomain structure has only recently received attention. SAXS measurements on an SI diblock copolymer film containing polyisoprene spheres indicates domain size and interfacial thickness are independent of casting solvent (32). Diamant et al. (42) have claimed that the interfacial composition of an SBS triblock copolymer is strongly solvent dependant. Their method of analysis involves modeling the viscoelastic behavior of the material and will be discussed in Chapter 7.

4.2 EXPERIMENTAL METHODS OF STRUCTURAL ANALYSIS

4.2.1 Electron Microscopy: The most widely used method of composite material microstructure visualization is electron microscopy. After interacting with a sample object, electrons, emitted from an illuminating source ($\sim 10^5$kV), carry information in the amplitude and phase of their wave. Generally, the squared amplitude of the wave function can be utilized to produce amplitude contrast which is related to mass thickness contrast or diffraction contrast. A detailed treatment of the principles of electron microscopy can be found in Ref. (43).

Diffraction contrast in polymeric samples is dependent on crystalline structure. Since block copolymers and homopolymers of the type being discussed exhibit no crystallinity, attention will be focused on mass thickness contrast. Most hydrocarbon polymers have nearly the same atomic composition and density so that microstructural features cannot be distinguished in the electron microscope. This

difficulty can be overcome by preferentially enhancing the mass thickness of one component. Smith and Andries (44) developed an ebonite method, useful when working with several unsaturated (olefinic) polymers (1), while Kato (45) introduced a technique known as osmium staining for the case when only one phase contains olefinic unsaturation. Since osmium tetraoxide will react with the unsaturated sites in polydienes but not with polystyrene, the mass thickness contrast can be greatly increased by heavy-metal deposition in the polydiene phase. Use of this technique has been widely reported in the literature (27, 35) with respect to block copolymer microphase analysis.

Caution must be exercised when interpreting electron micrographs since the images obtained are two-dimensional projections of three-dimensional objects (46). In particular, inference of spherical microdomain packing order can be especially misleading (21). Determination of microdomain size is well suited to this method, particularly for spherical domains which can only project a single image. Nevertheless, staining and beam damage can lead to alteration of domain dimensions. Interfacial thickness is virtually impossible to resolve by amplitude contrast electron microscopy although Christner and Thomas (47) have proposed the studying of polymer interfaces via the phase part of the electron wave function (defocus electron microscopy).

An electron microscope specimen must transmit a reasonable fraction of the incident electron beam. In practice this requires extremely thin sections (300-2000Å) conveniently obtained on an ultramicrotome using glass or diamond knives (43).

4.2.2 Small Angle Scattering (SAS): The amplitude of radiation

diffracted by matter A, is related to that of the incident beam A_o, as follows (48) (Fig. 4-3),

$$A = A_o \sum_i p_i \exp[i(Q \cdot r_i)] \qquad 4\text{-}4$$

where p_i is the fraction of radiation scattered by the i-th scattering element and r_i is a vector from an arbitrary origin to the element. Q is proportional to the difference between unit vectors along incident rays and those scattered at an angle of 2θ having a magnitude,

$$Q = 4\pi \sin\theta/\lambda \qquad 4\text{-}5$$

where λ is the radiation wavelength.

The differences between small angle x-ray (SAXS), neutron (SANS) and light (SALS) scattering techniques lie primarily in p_i and λ. For SAXS, p_i is associated with the scattering electron densities, in SANS the nature of the scattering nuclei and in SALS the refractive indices. The long wavelength of light ($4 \cdot 10^3$Å for HeNe) prohibits application of SALS from the study of bulk block copolymers since the characteristic dimensions being examined ($d=2\pi/Q$) are of the order $10\text{-}10^3$Å. A commonly used x-ray wavelength is 1.54Å; larger wavelengths are significantly absorbed by matter. Thermal neutrons used in SANS instruments range in wavelength from 1 to 18Å, the longer variety being produced with the aid of a cold source (49). This range of wavelengths extends the lower limits of Q experimentally attainable by small angle scattering.

The nature of p_i is a particularly attractive aspect of SANS

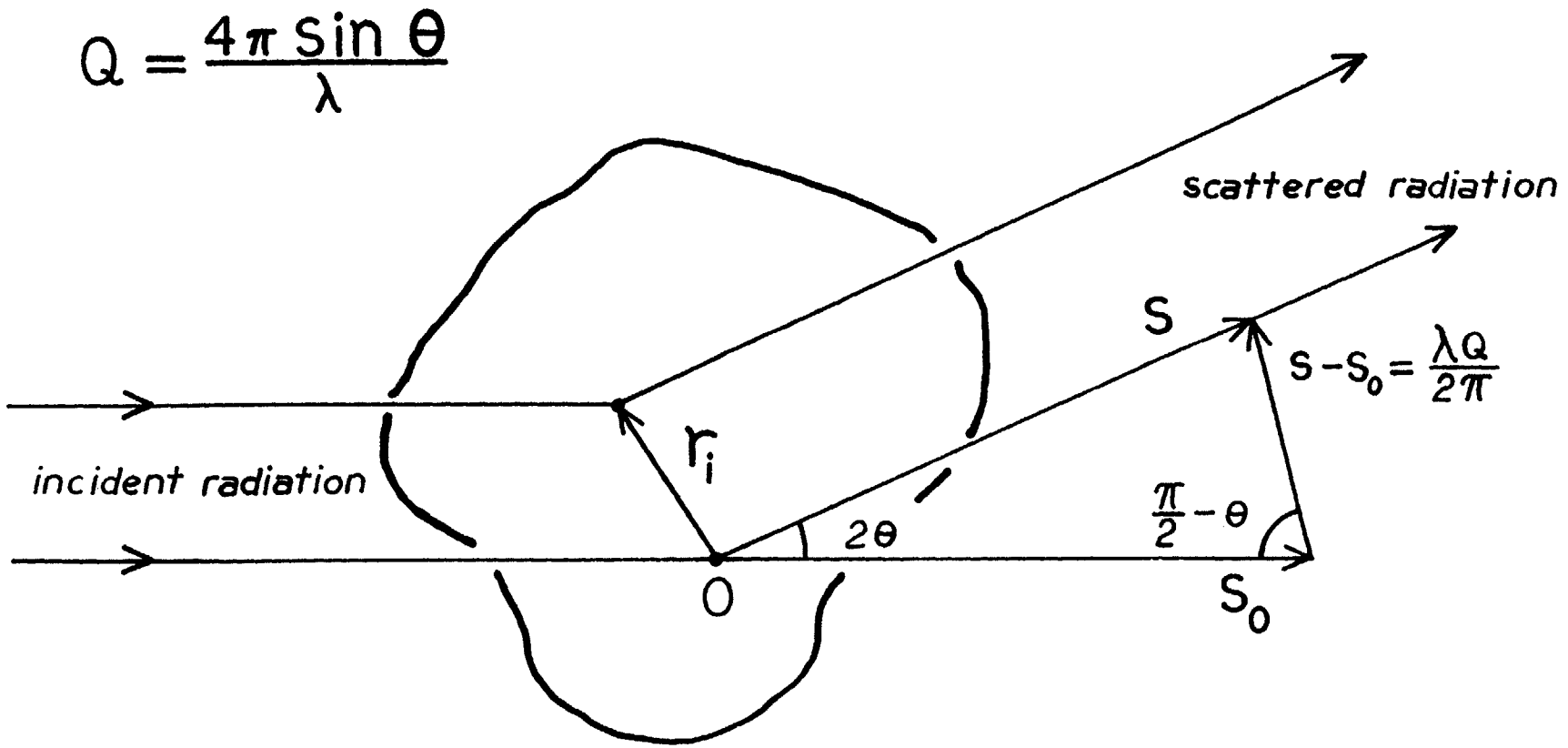

Figure 4-3 Scattering of radiation by matter

relative to the study of polymers. σ, the total scattering cross section of a nucleus, is composed of two terms (50),

$$\sigma = \sigma_{coh} + \sigma_{incoh} \qquad 4\text{-}6$$

where σ_{coh} is the cross section for coherent scattering and σ_{incoh} for incoherent scattering. It is only σ_{coh} which contributes to interference effects. For an assembly of nuclei the coherent cross section is given by the square of the mean scattering length b, averaged over the array:

$$\sigma_{coh} = 4\pi\langle b\rangle^2 \qquad 4\text{-}7$$

The incoherent cross section is proportional to the mean square of the deviation from the average over the array:

$$\sigma_{incoh} = 4\pi(\langle b^2\rangle - \langle b\rangle^2) \qquad 4\text{-}8$$

Incoherent scattering results from the interaction of neutrons with nuclei having non-zero spin states. It is isotropic and forms a flat background intensity, independent of Q (50).

b is the term equivilant to f_x, the atomic scattering factor for X rays and denoted p_i in equation 4-4. Table 4-1 lists the scattering length, total and coherent scattering cross sections, and nuclear spin for the atomic species which comprise the polymers associated with the present work. Immediately apparent are the large variations in b and σ between atomic hydrogen and deuterium. This fact was recognized several years ago and led to the selective deuterium substitution in

TABLE 4-1

Neutron Scattering Data for Elements and Isotopes [a]

Element	Specific Nucleus	Nuclear Spin	$10^{12} \cdot b$ (cm)	σ_{coh} [b] (barns)	σ [c] (barns)
H	H^1	1/2	-.376	1.79	81.5
	H^2	1	.654	5.40	7.6
C	C^{12}	0	.660	5.50	5.51
	C^{13}	1/2	.356	4.50	5.50

[a] From Ref. (50) [b] Coherent scattering cross section [c] Total scattering cross section

TABLE 4-2

Monomer Scattering Length and Scattering Length Density

Monomer	$10^{12} \cdot b$ (cm)	$10^{10} \cdot \rho_b$ ($cm \cdot cm^{-3}$)
styrene	2.328	1.416
butadiene	0.416	0.415
butadiene-d6	6.66	6.65

in polymer chains and subsequent SANS examination of the hydrogenated polymers in a deuterated matrix of the same polymer (or vice versa) (51-53). Such experiments are completely analagous to dilute solution SALS measurements. Isotope exchange contrast enhancement can also be effective in bulk multiphase polymeric systems although extraction of single chain scattering functions must take phase structure into account (54). This topic is further addressed in Appendix C. Values of b and $\rho_b = b/v_{ap}$ for the monomers employed in this study are presented in Table 4-2 where ρ_b is the scattering length density of a monomer unit of molecular volume v_{ap}.

Nearly all reported studies concerning the SAS analysis of bulk block copolymers have made use of SAXS. The same information is accessible by SANS with an increased range of Q and an ability to deuterium label individual molecules. Such investigations have only recently been reported (25). The major drawbacks to SANS are limited beam time, availability of materials (Chapter 2) and high incoherent scattering levels in hydrogenous polymers.

4.2.3 Structural Determination by SANS: The theory of SAS, primarily developed for X rays, can be easily adapted to unpolarized neutrons. The expressions utilized in the present work will be drawn from that field. Derivations of the fundamental equations involving SAXS can be found in Ref. (48,55,56) and a more recent treatise on neutron scattering including SANS has been presented by Kostorz (57).

Upon replacing p_i by a locally averaged scattering length density, $\rho_b(r)$, in equation 4-4, we can write the coherent scattering intensity per atom over N nuclei as,

$$I(Q) = \frac{1}{N}\left|\int_V \rho_b(r)\exp(iQ\cdot r)d^3r\right|^2 \qquad 4\text{-}9$$

where r is a continuously variable position vector and the integration extends over sample volume V. For a two-phase system of identical particles in which ρ_{bp} and ρ_{bm} are the particle and matrix scattering length densities, I(Q) can be shown to equal (57):

$$I(Q) = \kappa(\rho_{bp}-\rho_{bm})^2[<f_p^2(Q)>-<f_p(Q)>^2+<f_p(Q)>^2W(Q)] \qquad 4\text{-}10$$

The single particle form factor $f_p(Q)$ is given by,

$$f_p(Q) = \frac{1}{V_p}\int_V \exp(iQ\cdot r)d^3r \qquad 4\text{-}11$$

where V_p is the particle volume. κ in equation 4-10 is a constant which includes factors such as particle concentration, beam intensity, sample thickness and detector efficiency (25), and W(Q) is an interparticle interference function. 4-10 is a general equation for the scattering of randomly oriented identical particles.

Based on a regularity in shape and size, block copolymer microdomains readily lend themselves to either SAXS or SANS analysis. Cylindrical and lamellar microdomains must be highly oriented with the major axis parallel to the incident beam in order to obtain tractable scattering profiles, as demonstrated by Hashimoto et al. (31,58). Spherical microdomains may be directly investigated.

For spherical particles, $<f_p^2(Q)> = <f_p(Q)>^2$ and equation 4-10 reduces to:

$$I(Q) = \kappa(\rho_{bp}-\rho_{bm})^2 \langle f_p(Q)\rangle^2 W(Q) \qquad 4\text{-}12$$

For a sphere of radius R, $f_p(Q)$ is given by Rayleigh (59) as,

$$f_p(Q) = f_s(QR) = (9\pi/2)^{1/2} J_{3/2}(QR) \Big/ (QR)^{3/2} \qquad 4\text{-}13$$

where $J_{3/2}(QR)$ is a Bessel function of order 3/2. Various functional forms of W(Q) can be found in the literature. Fournet (60) derived the following expression for an ensemble of spherical particles,

$$W(Q) = \left\{1 + \frac{8v_o}{v_1} f_s(2QR)\right\}^{-1} \qquad 4\text{-}14$$

where v_o/v_1 is the volume fraction of spheres ($v_o/v_1 \leq .74$). Hosemann and Bagchi (56) have expressed W(Q) as the convolution product (*) of a paracrystalline lattice factor Z(Q), and shape amplitude S(Q):

$$W(Q) = Z(Q) * |S(Q)|^2 \qquad 4\text{-}15$$

In all derivations W(Q) reduces to 1 at large values of Q.

Applying equation 4-10 to SAS curves provides information concerning domain size and shape through $f_p(Q)$ and spacial distribution through W(Q). Investigation of domain boundary structure is accomplished in the Porod region of the curve and this topic has recently been reviewed by Koberstein et al. (61). Porod (62) has shown that SAXS from ideal two-phase systems with sharp boundaries in the limit of large Q gives:

$$\lim_{Q \to \infty} I_p(Q) = K_p/Q^4 \qquad 4\text{-}16$$

Equation 4-16 is known as Porod's law where K_p is Porod's constant,

$$K_p = 2\pi A_i(\rho_{bp}-\rho_{bm})^2 \qquad 4\text{-}17$$

and A_i is the total interfacial area of the system.

In practice, multiphase polymers exhibit systematic deviations from equation 4-16 which in SANS can be attributed to incoherent scattering and diffuse phase boundaries. The first of these can be subtracted by conventional methods (61) leaving the second which contributes to negative deviations from Porod's law.

The observed negative deviation from Porod's law can be accounted for by modeling the phase boundary with a scattering length density gradient. Following Ruland (63), this may be accomplished by convoluting the sharp scattering length density profile, $\Delta\rho(r)$, as found in Porod's law with a smoothing function h(r),

$$\Delta\rho(r)_{obs} = \Delta\rho(r)*h(r) \qquad 4\text{-}18$$

where r is the distance along an arbitrary vector within the scattering volume. Application of equation 4-18 is illustrated in Figure 4-4 using a smoothing function presented by Ruland (64). The resulting scattering length density profile corresponds to that derived by Helfand (9) as given by equation 4-2.

The scattered intensity is the Fourier transform of the square of

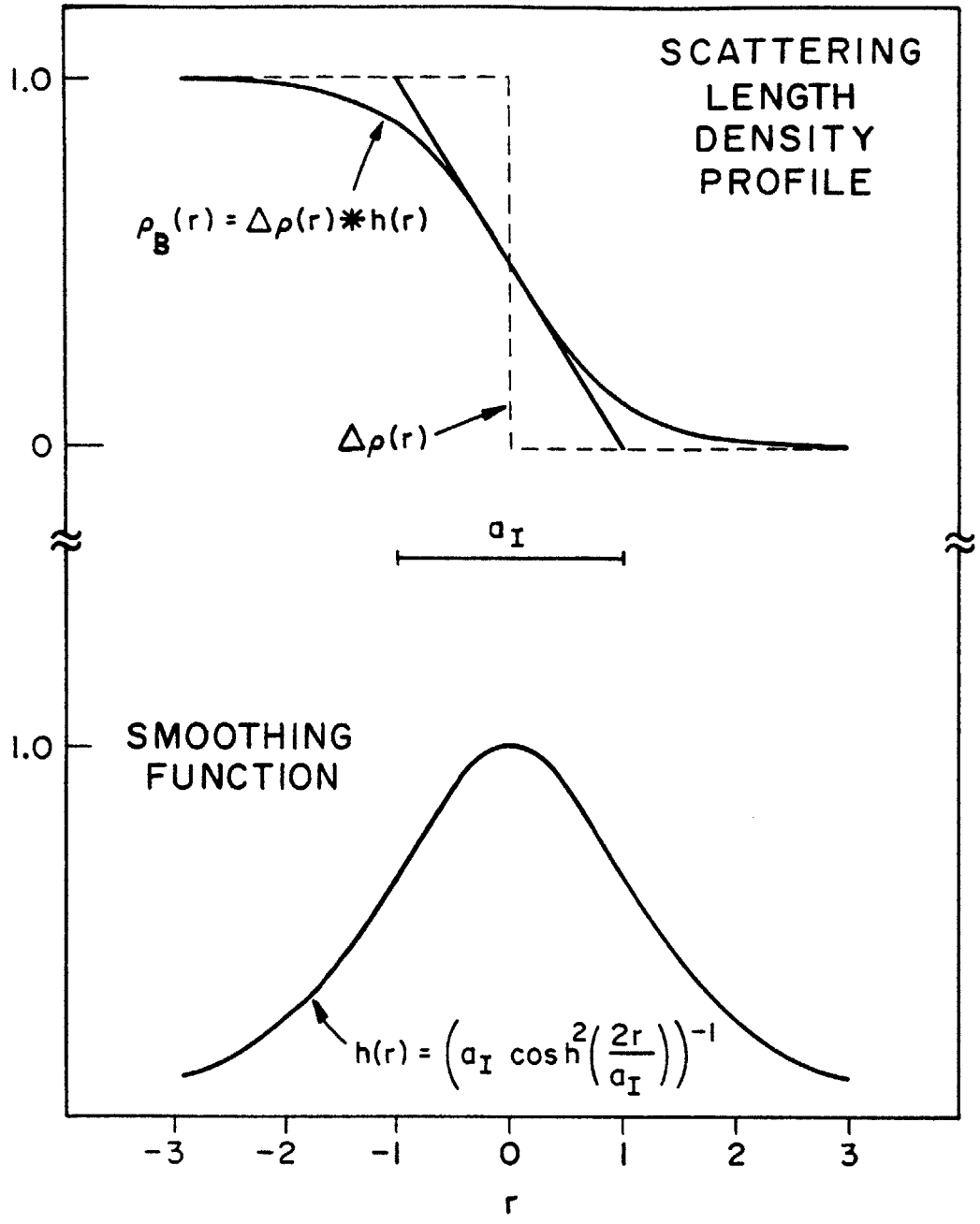

Figure 4-4 The interfacial composition profile is modeled by convoluting a sharp interface with a smoothing function. In this case ρ_B is given by equation 4-2.

the observed scattering length density profile, which in reciprocal space equals the product:

$$I_{obs}(Q) = I_p(Q)H^2(Q) \qquad 4\text{-}19$$

$I_{p'}(Q)$ is the Porod intensity given by equation 4-16 and H(Q) is the Fourier transform of h(r).

Several forms of H(Q), derived for different models of interfacial composition, are listed in Table 4-3 along with the associated working Porod expression. The Helfand and linear Porod equations have been obtained from a series expansion of $I_{obs}(Q)$ in which higher order terms in Q have been truncated. For the linear and Helfand gradient models, a plot of Q^2I versus Q^{-2} permits determination of E (the width of the box-shaped linear smoothing function) and a_I from the slope and intercept. σ, of the sigmoidal gradient model, is obtained from the slope of a plot of $\ln(Q^4I)$ versus Q^2.

Finally, the minimum value of Q which may be used in a Porod plot of a material with a spherical morphology is (61),

$$Q_{min} = (\pi/2R^2)^{1/2}\left[\{1+[8/(1+\Omega^2)](R/\sigma)^2\}^{1/2}-1\right]^{1/2} \qquad 4\text{-}20$$

where R is the sphere radius and Ω is the fractional deviation of the calculated standard deviation of the Gaussion smoothing function σ, from the true value (usually less than 0.05).

TABLE 4-3

Modified Porod Equations

Scattering length density profile	H(Q)	$I_{obs}(Q)$
linear [a]	$\frac{\sin(EQ/2)}{EQ/2}$	$\frac{K_p}{Q^4}\left[1 - \frac{(EQ/2)^2}{3}\right]$
sigmoidal [b]	$\exp(-\sigma^2Q^2/2)$	$\frac{K_p}{Q^4}\exp(-\sigma^2Q^2)$
Helfand [c]	$\frac{\pi a_I Q/4}{\sinh(\pi a_I Q/4)}$	$\frac{K_p}{Q^4}\left[1 - \frac{(\pi a_I Q/4)^2}{3}\right]$

[a] E equals the box smoothing function width (69) [b] σ equals the standard deviation of the Gaussian smoothing function (63) [c] a_I is given by equation 4-3 and H(Q) was obtained from Ref. (64)

4.3 EXPERIMENTAL EQUIPMENT

4.3.1 Electron Microscopy: A Phillips 200 electron microscope operated at 60 and 80 kV was utilized for determining microdomain type and size in block copolymers and blends. Samples were contrast enhanced by immersion for several days in a 1% aqueous solution of osmium tetroxide and microtomed on an LKB ultramicrotome fitted with either a diamond knife (Dupont) or a freshly prepared glass knife. Thin sections (30-100 nm) were collected on uncoated 200 mesh copper grids (Ted Pella, Inc.) and measurements were calibrated against a diffraction grating carbon replica (21,600 lines per cm).

4.3.2 Small Angle Neutron Scattering: SANS patterns were obtained at the National Center for Small Angle Scattering Research (NCSASR) located at Oak Ridge National Laboratories (ORNL). A schematic of the 30 meter SANS facility is shown in Figure 4-5. The neutron beam extracted from the High Flux Isotope Reactor (HFIR) is monochromated by Bragg reflection from two sets of pyrolytic graphite crystals and is subsequently filtered with a cooled block of polycrystalline beryllium. The emerging beam has a wavelength of 4.75 Å with a resolution of $\Delta\lambda/\lambda \simeq 0.06$. A pair of apertures, one at the exit of the monochromator and the second directly in front of the sample (separated by a 10 m evacuated flight path), define the beam incident on the sample. Scattered neutrons are intercepted by a 64-by-64 cm position sensitive area detector of the Barkowski-Kopp design (65). The detector is mounted on a motorized dolly and can be positioned anywhere from 1.8 to 19 m from the specimen in an evacuated flight chamber.

The resolution of the SANS instrument can be determined according

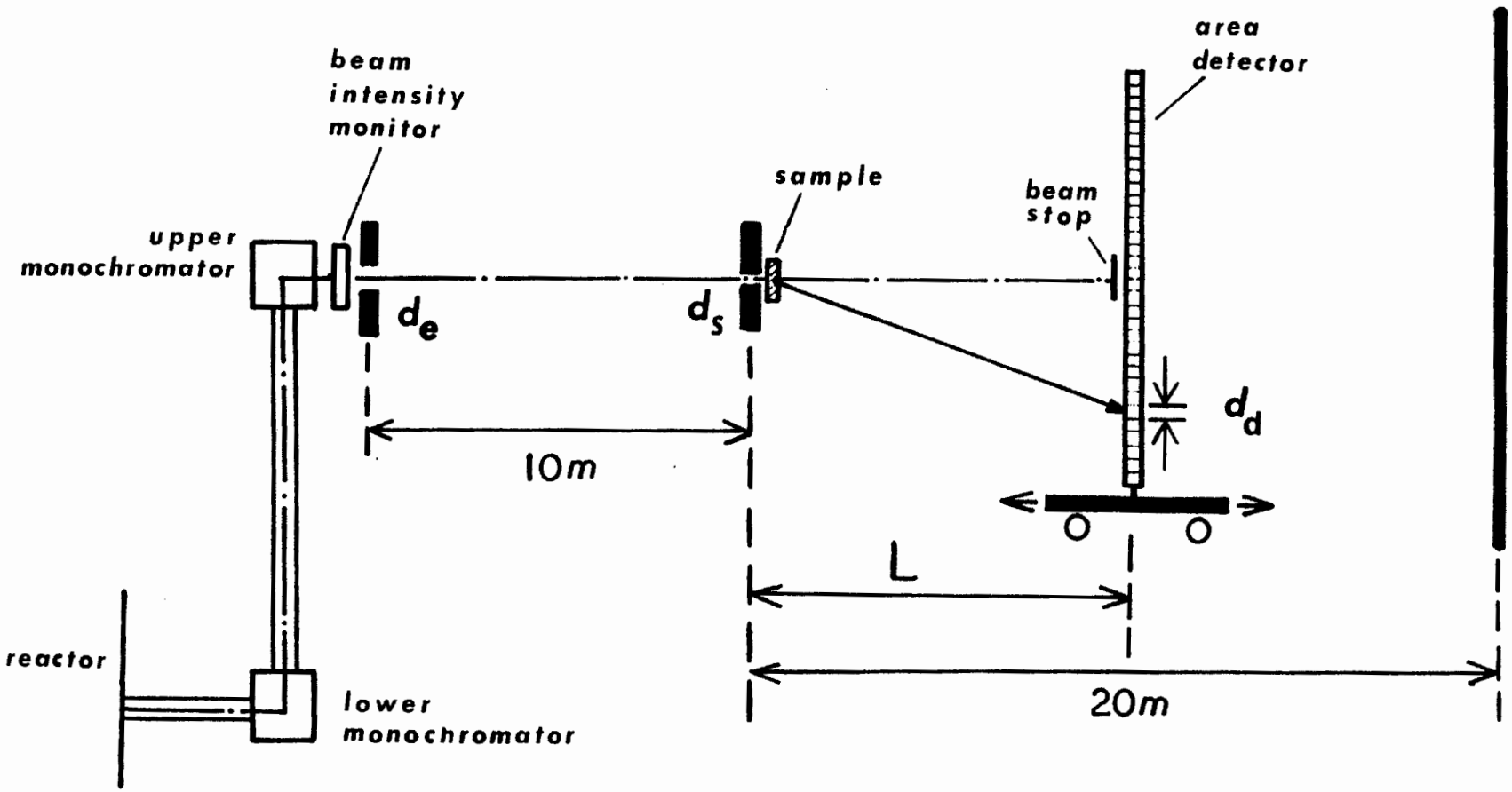

Figure 4-5 Schematic of the 30 meters SANS instrument at NCSASR, ORNL

to King (66),

$$\left(\frac{\Delta Q}{Q}\right)_{FWHM} = \left(\frac{2\cdot 1n2}{3}\right)^{1/2}\left\{\left(\frac{2\pi}{\lambda Q}\right)^2\left[\frac{d_e}{1^2} + \frac{d_d}{L^2} + d_s{}^2\left(\frac{1}{1} + \frac{1}{L}\right)^2\right] + 2\left(\frac{\Delta\lambda}{\lambda}\right)^2\right\}^{1/2} \qquad 4\text{-}21$$

where 1 equals 10 m and d_d equals 0.5 cm. Sample to detector distance L and aperture diameters d_e and d_s are specified by the user (see Figure 4-5).

4.4 SAMPLE PREPARATION

4.4.1 Why Spheres? From both a mechanical and structural viewpoint a composite made up of spherical particles readily lends itself to analysis. Packing anisotropy, unavoidable when processing block copolymers with lamellar and cylindrical morphologies (see Sec. 4.1.5), is not evident in films having a spherical microstructure. This eliminates the ambiguities in the viscoelastic characterization of the former which may arise from poorly defined coupling mechanisms (Chapters 6,7). Also, the SAS analysis of domain boundary structure requires no orientation when dealing with spherical domains while lamellar and cylindrical morphologies must be highly ordered.

For the above reasons the present study of the structural and viscoelastic behavior of block copolymers and block copolymer-homopolymer blends has focused on a spherical morphology. This permits both aspects of the investigation to be addressed in an optimal fashion on a material having a common processing history.

Disadvantages of the spherical morphology arise mainly from the fact that a non-equilibrium sphere size is generally obtained in

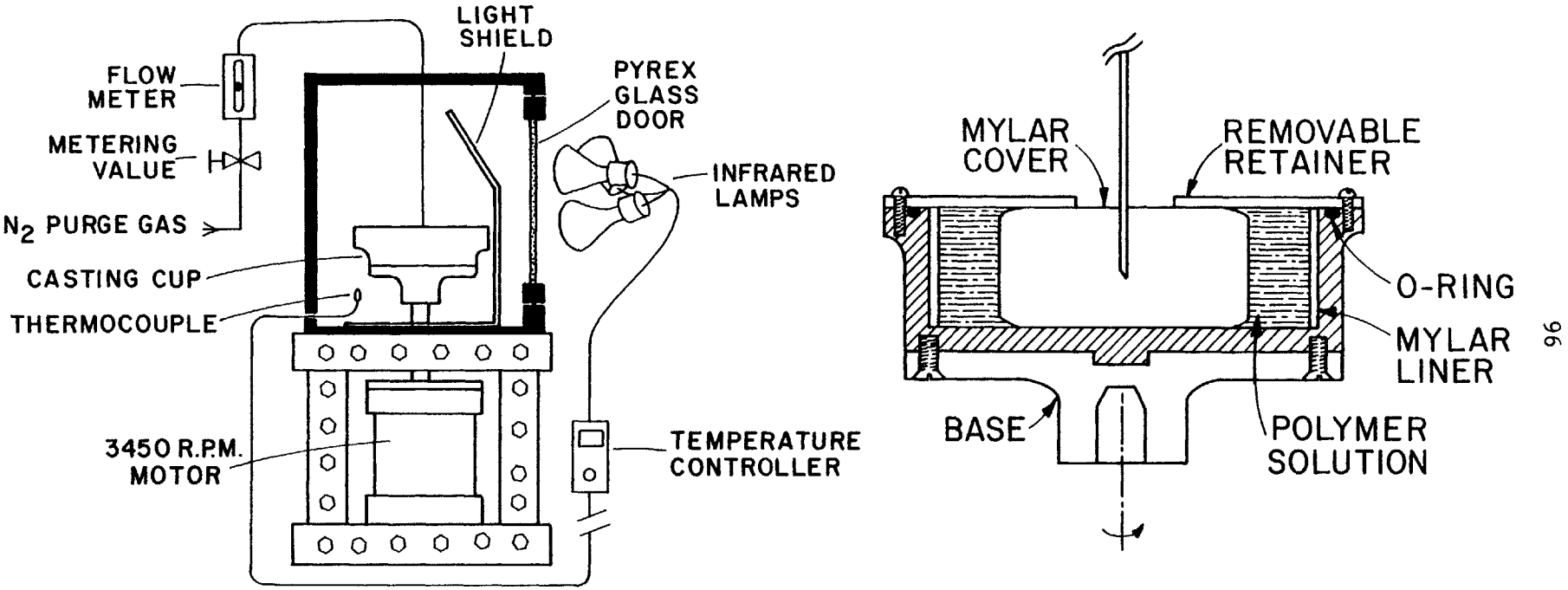

Figure 4-6 Solvent spin casting apparatus

polystyrene-polydiene systems containing a polystyrene matrix (23). This is not deemed to be a problem in the present study, in which domain dimensions are experimentally determined, since relative sphere size is of primary concern. Furthermore, this non-equilibrium behavior can be examined concurrently with the other aspects of this work.

4.4.2 Film Casting: Films for structural and mechanical analysis were prepared by a solvent spin casting technique (67). Polymer samples were dissolved in an organic solvent at a concentration of 2-5 weight percent, depending on molecular weight, and injected into the spinning caster. The injection is accomplished with a Millipore filtration unit (Millipore Corp.) containing a 10 μm filter and fitted with a 12 inch, 15 ga stainless steel needle.

The spin casting unit is illustrated in Figure 4-6. The aluminum casting cup has a 10.2 cm diameter, 3.2 cm wall height and a 1/8 inch groove fitted with a no. 243 neoprene O-ring. A mylar liner (10 mil) is placed along the caster wall and a mylar cover is secured against the O-ring with an aluminum retainer and six screws. The assembled caster is rotated at 3450 r.p.m. producing a centrifugal force of 730 G at the liner. Polymer solution is injected through a small hole (1/8 inch) in the mylar cover followed by the insertion of a nitrogen gas line. Passing nitrogen through the caster removes solvent and subsequently deposits a polymer film on the mylar liner. The solvent removal rate can be controlled by the gas flow rate. A temperature chamber, fitted with a pyrex glass door, encloses the spin caster which is heated by radiation from three 250 W infrared lamps. The unit can be temperature controlled between room temperature and 150°C. A

TABLE 4-4

Solvent Casting Parameters

Solvent(s)	$\delta(cal/cm^3)^{1/2}$ [a]	b.p. °C	Casting Temperature °C [b]
methylcyclohexane (30%) [c]	7.8	101	60→80
benzene (70%)	9.2	80	
toluene	8.9	110	80
benzene	9.2	80	60→80
tetrahydrofuran (70%)	9.1	67	50→80
methyl ethyl ketone (30%) [d]	9.3	80	
polystyrene	9.1	-	-
polybutadiene	8.5	-	-

[a]Obtained from Ref. (68) neglecting hydrogen bonding effects. [b]60→80 indicates temperature was increased from 60 to 80°C during casting. [c]Poor solvent for polystyrene. [d]Poor solvent for polybutadiene.

shield protects the casting cup from direct infrared radiation.

It was found that optimal film quality (smooth surface and uniform thickness) could be achieved at elevated casting temperatures over a period of 2 to 4 days. Table 4-4 lists the solvents utilized in preparing samples along with casting temperatures, set below the boiling point of the solvent. Film thickness, determined by the quantity of polymer (2-5 grams) charged to the caster, ranged from .2-.5 mm.

At the completion of solvent removal, polymer films were further dried and annealled at 120°C in a vacuum oven for 24 hours, cooled (20°C per hour) and stored under vacuum in the absence of light.

4.4.3 Blends: Figure 4-1 illustrates the expected equilibrium morphologies for the diblock copolymers listed in Table 3-2. Those falling in the lamellar and cylindrical category have been modified by the addition of homopolystyrene as indicated in Table 4-5. Based upon composition, all blended samples would then be expected to exhibit a spherical morphology (35). In practice, this was not found to be the case, as demonstrated in Figure 4-7. Sample SB6/S2, cast from toluene, consists of cylinders of polybutadiene while sample SB4, also cast from toluene, contains polybutadiene spheres. Since toluene is essentially a non-preferential solvent (see Figures 4-1 and 4-2), these are assumed to be equilibrium domain types. Using the technique outlined in Sec. 4.1.5, sample SB6/S2 has been cast into a spherical morphology (Fig. 4-7) from a mixed solvent of 70% THF and 30% MEK. Since the vapor pressure of THF exceeds that of MEK, the solubility parameter of the solution becomes continually poorer with

TABLE 4-5

Blends

	weight fraction			
Sample [a]	SB	S	B	polybutadiene (total)
SB2/S2	.523	.477	-	.113
SB3/S1	.363	.637	-	.115
SB3/S2	.363	.637	-	.115
SB5/S2	.523	.477	-	.127
SB6/S2	.363	.637	-	.119
SB8/S3	.523	.477	-	.112
SB9/S2	.363	.637	-	.119
SB9/S3	.363	.637	-	.119
SB_d2/S1	.392	.608	-	.142
SB4/S2/B1	.500	.441	.059	.118
SB_d3/S2/B1	.500	.445	.055	.108

[a] Sample specification is given in Table 3-2

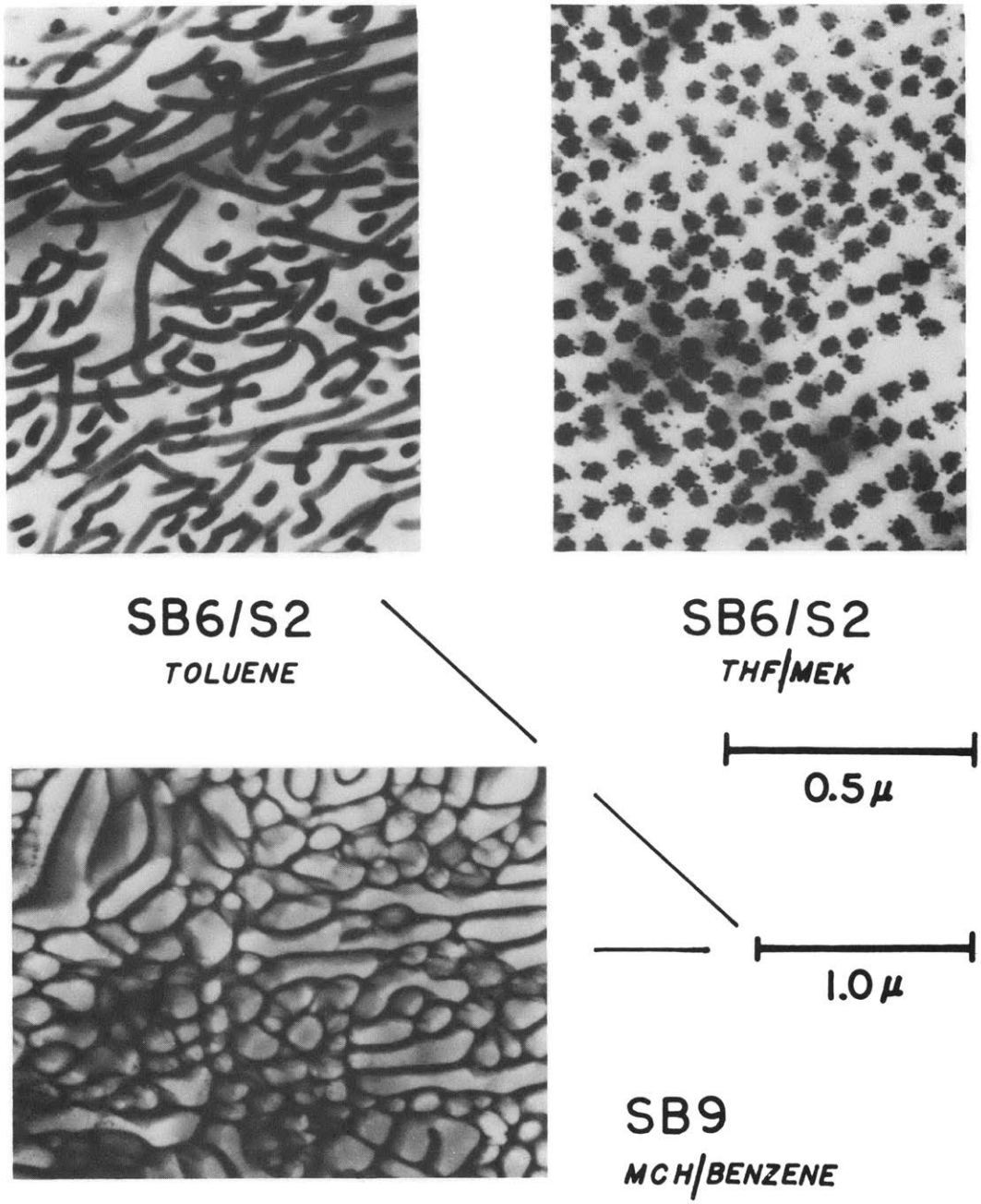

Figure 4-7 Effect of casting solvent on microphase morphology. Darkened regions are osmium stained polybutadiene.

respect to polybutadiene (Table 4-4) during the course of solvent removal. This leads to an increase in the volume fraction of the polystyrene-solvent phase and subsequently a spherical morphology. All blends listed in Table 4-5 were cast in this fashion (except SB4/S2/B1) and contained a microspherical morphology. In contrast, sample SB9, cast from a solution of methylcyclohexane/benzene, is phase inverted (Fig. 4-7) so that polybutadiene has become the continuous phase. This sample will be further discussed in Chapters 6 and 7.

Two of the blends listed in Table 4-5 contained macroscopically phase separated homopolymer. The film of sample SB9/S3 was only semi-transparent and under electron microscopic examination revealed large regions of homopolystyrene. Sample SB4/S2/B1 (cast from toluene) contained a separate layer of homopolybutadiene across the film. These problems were overcome by lowering the homopolymer molecular weight (SB9/S2) or increasing the block molecular weight (SB_d3/S2/B1). The significance of these findings will be further discussed in Chapter 7.

Electron micrographs of six representative samples are presented in Fig. 4-8, selected in order to illustrate the range of domain sizes which have been constructed from the diblock copolymers and blends of Tables 3-2 and 4-5. All samples prepared from pure diblock copolymer or blends with homopolystyrene exhibit a very narrow sphere size distribution, while sample SB_d3/S2/B1, which contains homopolybutadiene, contains a broad distribution (Fig. 4-8). Based on this inability to control structure in blends containing homopolybutadiene, this study has focused on materials containing homopolymer free rubber phases.

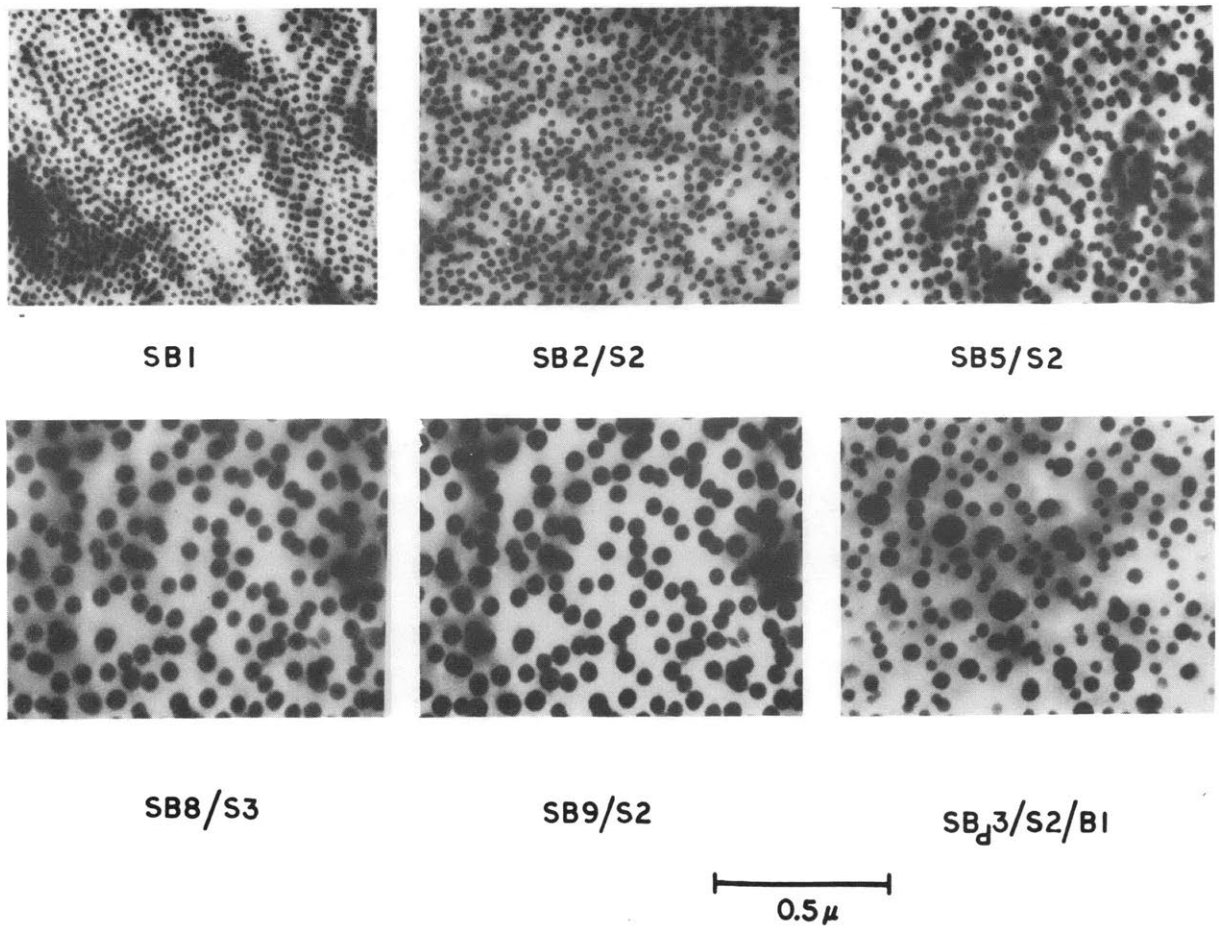

Figure 4-8 Electron micrographs representative of the samples discussed in this work. Dark spherical domains are osmium stained polybutadiene.

References

1 A. Ramos, Sc.D. thesis, Massachusetts Institute of Technology (1977).

2 P.J. Flory, Principles of Polymer Chemistry, Cornell University Press (1953).

3 L.P. McMaster, Macromolecules, 6, 760 (1973).

4 L.C. Sanchez and R.H. Lacombe, J. Phys. Chem., 80, 2352 (1976).

5 Ibid., p. 2568.

6 R.J. Roe and W.C. Zin, Macromolecules, 13, 1221 (1980).

7 R.E. Cohen and D.E. Wilfong, to appear in Macromolecules (1982)

8 D.J. Meier, J. Polymer Sci., C, 26, 81 (1969).

9 E. Helfand and Z.R. Wasserman, to appear in Developments in Block Copolymers, ed. I. Goodman, Applied Sciences Publishers Ltd.

10 L. Leibler, Macromolecules, 13, 1602 (1980).

11 S. Krause, D.J. Dunn, A.S. Mozzaffari and A.M. Biswas, Macromolecules, 10, 4, 786 (1977).

12 E.V. Gouinlock and R.S. Porter, Polym. Eng. Sci., 17, 573 (1977).

13 C.I. Chung, H.L. Griesbach and L. Young, J. Polym. Sci., Polymer Phys. Ed., 18, 1237 (1980).

14 A. Skoulios, G. Finaz and J. Parrod, Compt. Rend., 251, 739 (1960).

15 R.J. Ceresa, ed., Block and Graft Copolymers, J. Wiley, London (1973).

16 S.L. Aggarwal, ed., Block Copolymers, Plenum Press, N.Y. (1970).

17 T. Inoue, T. Soon, T. Hashimoto, and H. Kawai, J. Polym. Sci., A-2, 7, 1283 (1969).

18 B. Gallot, Liquid Crystalline Order in Polymers, ed. A. Blumstein, p. 191, Acad. Press, N.Y. (1978).

19 A. Skoulios, Advances in Liquid Crystals, ed. G.H. Brown, p. 169, Academic Press, N.Y. (1975).

20 E. Helfand and Z.R. Wasserman, Macromolecules, 11, 960 (1978).

21 E. Pedemonte, A. Turturro, V. Bianchi and P. Devetta, Polymer, 14, 145 (1973).

22 A. Douy and B. Gallot, Makromol. Chem., 182, 265 (1981).

23 T. Hashimoto, M. Fujimura and H. Kawai, Macromolecules, 13, 1660 (1980).

24 R.J. Roe, M. Fishkis and J.C. Chang, Macromolecules, in press.

25 R.W. Richards and J.L. Thomason, Polymer, 22, 581 (1981).

26 D.F. Leary and M.C. Williams, Polymer Letters, 8, 335 (1970).

27 E. Helfand and Z.R. Wasserman, Macromolecules, 9, 6, 879 (1976).

28 E. Helfand and Z.R. Wasserman, Macromolecules, 13, 4, 994 (1980).

29 D.J. Meier, Block and Graft Copolymers, eds., J. Burke and V. Weiss, Syracuse Univ. Press (1973).

30 A. Todo, M. Kiuno, K. Miyoshi, T. Hashimoto and H. Kawai, Polymer Eng. and Sci., 17, 8, 587 (1977).

31 T. Hashimoto, M. Shibayama and H. Kawai, Macromolecules, 13, 1237 (1980).

32 H. Hashimoto, M. Fujimura, T. Hashimoto and H. Kawai, Macromolecules, 14, 844 (1981).

33 J. Kohler, G. Riess and A. Banderet, Eur. Polym. J., 4, 173 (1968).

34 G.E. Molau and W.M. Wittkrodt, Macromolecules, 1, 260 (1968).

35 T. Inoue, T. Soon, T. Hashimoto, H. Kawai, Macromolecules, 3, 87 (1970).

36 E.J. Clayfield and E.C. Lumb, Colloid Interface Sci., 22, 269 (1966).

37 D.J. Meier, Polymer Preprints, 18, 340 (1977).

38 C.C. Wu, Sc.D. thesis, Massachusetts Institute of Technology, (1981).

39 Dlugosy, A. Keller and E. Pedemonte, Kolloid Z.Z. Polym., 242, 1125 (1970).

40 G. Hadziioannou, A. Mathis and A. Skoulios, Colloid and Polymer Sci., 257, 136 (1979).

41 M.B. Beuer and M. Shen, Materials Sci. and Eng., 15, 145 (1974).

42 J. Diamant, D.S. Soong and M.C. Williams, to appear in Contemporary Topics in Polymer Sci., vol 4, ed. W.J. Bailey, Plenum Press, N.Y. (1981).

43 F.A. Lenz, Electron Microscopy in Material Science, ed. V. Valdre, Academic Press, N.Y. (1971).

44 R.W. Smith and J.C. Andries, Rubber Chem. Tech., 47, 64 (1974).

45 K. Kato, Polym. Eng. and Sci., 7, 38 (1967).

46 E.J. Roche and E.L. Thomas, Polymer, 22, 333 (1981).

47 G.L. Christner and E.L. Thomas, J. Appl. Phys., 48, 10, 4063 (1977).

48 J.S. Higgins and R.S. Stein, J. Appl. Cryst., 11, 346 (1978).

49 K. Ibel, J. Appl. Cryst., 9, 296 (1976).

50 G.E. Bacon, Neutron Diffraction, Oxford (1962).

51 H. Benoit, D. Decker, J.S. Higgins, C. Picot, J.P. Cotton, B. Farnoux, G. Jannink and R. Ober, Nature, 245, 13 (1973).

52 R.G. Kriste, W.A. Kurse and K. Ibel, Polymer, 16, 120 (1975).

53 G. Lieser, E.W. Fischer and K. Ibel, J. Polym. Sci. Polym. Letters, 13, 39 (1975).

54 S.N. Jahshan and G.C. Summerfield, J. Polym Sci., Phys. Ed., 18, 8, 1859 (1980).

55 A. Guinier and D.C. Dexter, X ray Studies of Materials, J. Wiley and Sons (1963).

56 R. Hosemann and S.N. Bagchi, Direct Analysis of Diffraction by Matter, North Holland Publishing Co. (1962).

57 G. Kostorz, Treatise on Materials Science and Technology, vol. 15, ed. G. Kostorz, Academic Press (1979).

58 T. Hashimoto, K. Nagatoshi, A. Todo, H. Hasegawa and H. Kawai, Macromolecules, 7, 3, 364 (1974).

59 Lord Rayleigh, Proc. Royal Soc., London, Ser, A90, 219 (1914).

60 A. Guinier and G. Fournet, Small Angle Scattering of X rays, J. Wiley and Sons, N.Y. (1955).

61 J.T. Koberstein, B. Morra and R.S. Stein, J. Appl. Cryst., 13, 34 (1980).

62 G. Porod, Kolloid-Z., 125, 1, 51 (1952); ibid. 125, 2, 108 (1952).

63 W. Ruland, J. Appl. Cryst., 4, 70 (1971).

64 W. Ruland, "Colloquium Franca-American Sur La Diffusion Des Rayon-X et Des Neutrons Aux Petits Angles Par Les Polymeres," D26, 78, 16-18 Sept. 1980, Strasbourg, France.

65 C.J. Barkowski and M.K. Kopp, IEEE Trans. Nucl. Sci., 19, 161 (1972).

66 J.S. King, Methods of Experimental Physics: Polymers, vol. 16, ed. R.A. Fava, Academic Press (1980).

67 D.H. Kaelble, J. Appl. Polym. Sci., 9, 1209 (1965).

68 J. Brandrup and E.H. Immergut, eds., Polymer Handbook, second edition, (1975).

69 C.G. Vonk, J. Appl. Cryst., 6, 81 (1973).

CHAPTER 5: SMALL ANGLE NEUTRON SCATTERING

SANS data were obtained at the National Center for Small Angle Scattering Research (NCSASR) over a period of one year with the assistance of Dr. G.D. Wignall of NCSASR. Dr. C.V. Berney, of the Nuclear Engineering Department at M.I.T., has collaborated in collecting the data discussed in this chapter. SANS results presented in graphical form in the main text are tabulated in Appendix E with cross reference to NCSASR files.

The following presentation and analysis of SANS data have been organized according to the three structural regimes identified in Chapter 4: interfacial thickness, domain size and interdomain structure. This classification must be loosely applied since analysis of the scattering intensity in any limited regime of momentum transfer, Q, requires information obtained over a much broader range of Q. Discussion of the data as categorized begins at the highest values of Q and proceeds to the lowest. All samples examined are discussed concurrently in each regime.

SANS results presented in this chapter are discussed in Chapter 7.

5.1 EXPERIMENTAL PARAMETERS

5.1.1 Sample Preparation: Polymer films, prepared as discussed in Section 4.4, were cut into 1.5 cm square pieces and stacked together to obtain a desired thickness. This assembly was then annealled at 120°C under an applied force of approximately 8×10^3 Pa. The resulting

samples were one piece, clear, polymer blocks of uniform thickness. All samples, with one exception, were annealled at 120°C (see Chapter 4) prior to SANS examination in order to eliminate variations in aging time. One sample was aged six months following SANS analysis and then re-examined to determine the effects of aging on these measurements.

Sample thickness was chosen so as to optimize on scattering efficiency which reaches a maximum at a transmission of 0.37% (1). Transmission measurements were performed on the SANS instrument in the following manner. A strongly scattering glassy carbon specimen was placed over the sample aperture (Figure 4.5) and the total intensity on the detector was measured over several minutes. The polymer specimen was then mounted in front of the monochromator aperture and the measurement repeated. Both measurements were corrected for background intensity (see Sec. 5.1.2) and the transmission determined from the ratio between the corrected counts. Using Beer's law (2), we can calculate the reciprocal attenuation coefficient μ, which applies to all types of scattering and adsorption, from,

$$\log(1/T) = \mu t \qquad 5\text{-}1$$

where T is the transmission of a sample of thickness t. μ was found to be approximately 2.1 cm^{-1} for all samples so that a thickness of 0.2 cm provides for nearly optimal scattering efficiency.

Samples were prepared with thicknesses ranging from 0.17 to 0.25 cm and the transmission of each sample was measured prior to analysis. A 0.043 cm thick sample was also included in order to

TABLE 5-1

SANS Samples

Sample [a]	Preparation [b]
SB_d1-T	Toluene
SB_d1-B	Benzene
SB_d1-M	THF/MEK
SB_d1-TA	Toluene - aged 6 months
SB_d1-MT	THF/MEK - thin specimen (1/4 the thickness of SB_d1-M)
SB_d3-T	Toluene
SB_d3-B	Benzene
SB_d3-M	THF/MEK
$SB_d2/S1$-M [c]	THF/MEK
SB1-T	Toluene
SB7-T	Toluene
S3-T	Toluene

[a] Sample designation prior to hyphen is the same as in Table 3-2
[b] Casting conditions are listed in Table 4-4 [c] Sample $SB_d2/S1$ is listed in Table 4-5

ascertain how sample thickness influences the SANS results. Sample thickness and transmittance values are included in Appendix E.

A listing of the samples investigated by SANS is given in Table 5-1 and three representative electron micrographs of perdeuterated specimens are presented in Figure 5-1. The two hydrogenated samples listed in Table 5-1 were included for comparison with the perdeuterated analogs where applicable.

5.1.2 Instrument Parameters: Utilization of a two-dimensional area detector greatly increases the efficiency of counting scattered neutrons making feasible the use of a pinhole sample aperture. This eliminates the difficulties encountered in employing slit collimation, e.g. the necessity of desmearing scattering data (3,4). Therefore, all SANS spectra were obtained using a pinhole sample aperture. The size of both the sample and monochromator apertures varied depending upon the sample-to-detector distance which ranged from 1.8 to 15.3 m. Table 5-2 lists the sample-to-detector distance, aperture setting and associated resolution (eq. 21) at detector mid-range, for the various geometries utilized in SANS data acquisition.

Various corrections must be applied to data obtained directly from the SANS instrument. Background radiation is accounted for by taking a scattering pattern with a cadmium plate placed over the sample aperture. Since cadmium is a strong neutron absorber, the measured intensity can be attributed to gamma and cosmic rays along with stray neutrons (outside the primary beam) impinging on the detector. A second spectrum taken with an empty sample aperture corrects for primary beam contributions to the background intensity

TABLE 5-2

SANS Instrument Settings

Sample-to-detector distance (m)	Monochromator aperture (cm)	Sample aperture diameter (cm)	Resolution [b] $(\Delta Q/Q)_{FWHM}$
1.8	3.2 X 3.6	1.3	0.089
4.2	2.5 X 2.5	1.0	0.099
7.0	1.0 [a]	0.6	0.075
15.3	1.0 [a]	0.6	0.093

[a] Diameter of pinhole [b] Calculated at detector mid-range using equation 4-21

level. Both of these corrections were obtained at each sample to detector distance. A spectrum was also obtained from a 0.081 cm thick specimen of polyethylene having a transmission of 0.56%. This material scatters isotropically and with an intensity nearly independent of Q. Therefore, the intensity actually registered as a function of Q can be used to correct for channel-to-channel detector sensitivity fluctuations. One such spectrum was taken during each session of data collection (a period of 3-5 days). All uncorrected scattering data were corrected channel by channel at NCSASR using these three correction spectra, and subsequently divided by sample transmission, thickness and normalized to 1000 monitor counts. Three scattering patterns, representing each of the three perdeuterated materials, are presented in Figure 5-2 in the form of contour plots, with contour lines designating relative intensity. Lack of intensity at the center of these plots is due to beam blockage by a cadmium beam stop.

The radial symmetry exhibited at all intensity levels in the three profiles given in Figure 5-2 can be attributed to isotropic scattering, characteristic of unoriented two-phase materials. All samples were determined to be structurally isotropic by this method and the scattering profiles were subsequently reduced to two-dimensional form by radially averaging the corrected scattering data from the center of the scattering pattern. In this manner, use of structurally isotropic samples greatly increases the counting efficiency, thereby lowering the collection time required to obtain specific counting statistics. The differential radial spacing used in radial averaging corresponded to the spatial resolution of the detector

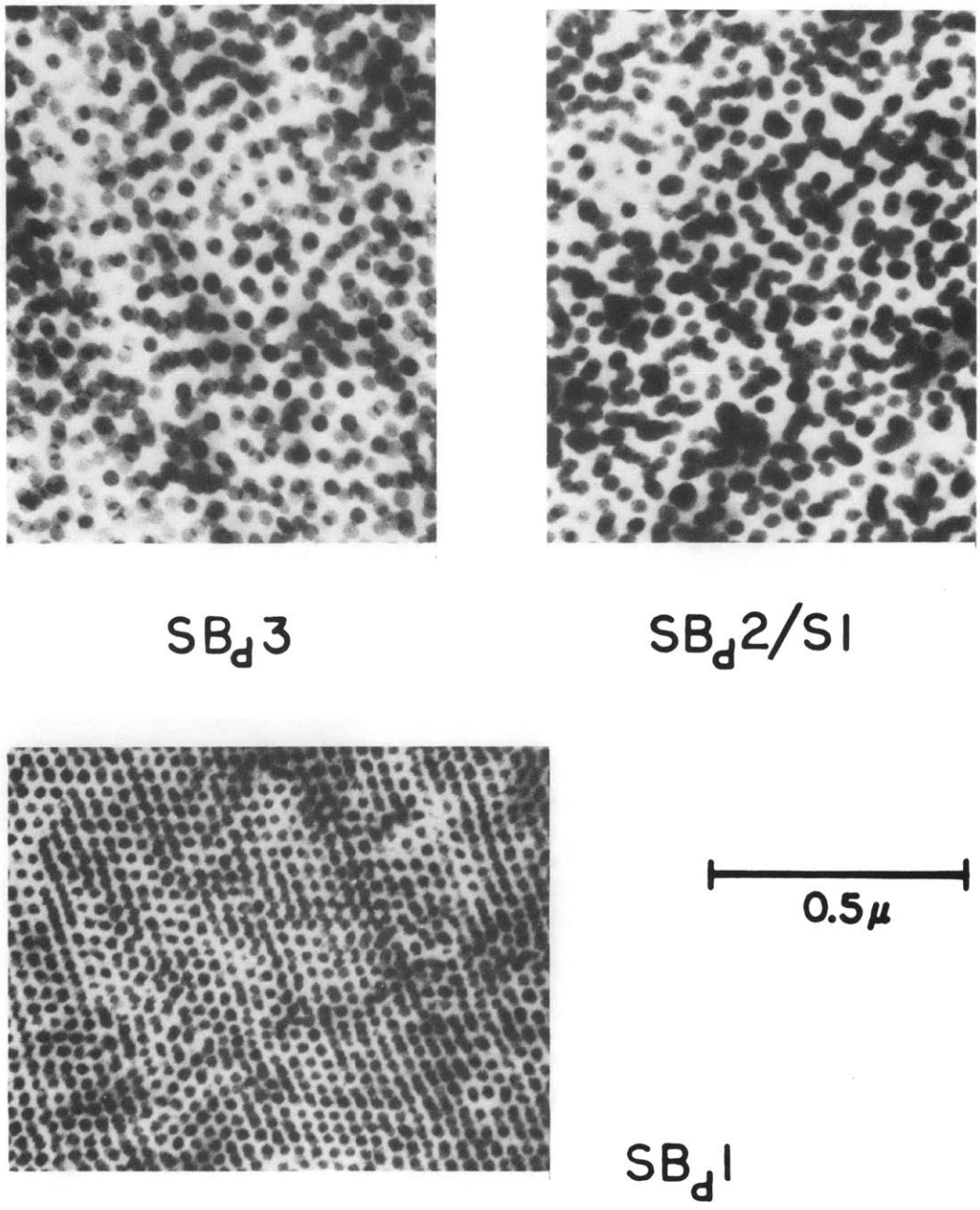

Figure 5-1 Typical electron micrographs taken from the samples examined by SANS.

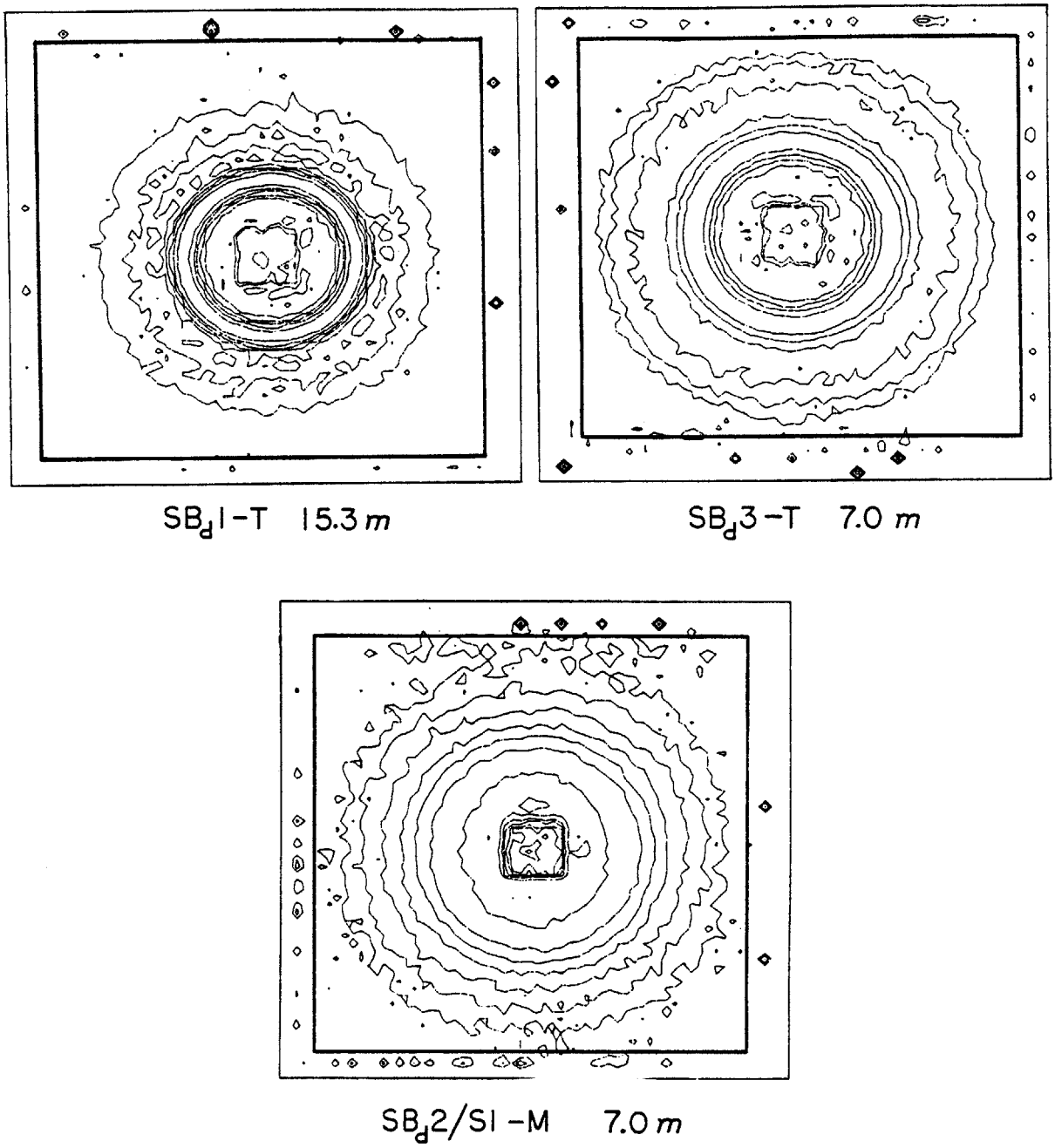

Figure 5-2 Typical SANS intensity contour plots. Radial averaging was performed over area delineated by inner box.

(0.5 cm).

Radially averaged data can be converted to an absolute differential scattering cross section per unit solid angle $\frac{d\Sigma}{d\Omega}(Q)$ cm^{-1} by the following formula,

$$\frac{d\Sigma}{d\Omega}(Q) = I_R \cdot \frac{L^2}{K_N A} \qquad 5\text{-}2$$

where I_R is the radially averaged result, L is the sample-to-detector distance in meters, A is the area of the sample aperture (cm^2) and K_N is a neutron calibration constant determined for each monochromator aperture setting. Values for K_N have been determined by the staff at NCSASR and are listed in Appendix E. Since none of the analysis performed in the text requires absolute calibration (although this is required in Appendix C), results will be reported in terms of relative intensity. Nevertheless, data collected on a given sample at different values of L, K_N or A were correlated using equation 5-2.

5.2 INTERFACIAL THICKNESS

The characteristics of the domain boundary in a two-phase material can be investigated using the Porod region of a small angle scattering curve as discussed in Chapter 4. 1.8 meters SANS data, obtained from the samples listed in Table 5-1, have been subjected to such an analysis and are presented in this section.

5.2.1 Corrections: Three sets of SANS data are plotted for large values of Q in Figure 5-3. As seen in this illustration, the scattering intensity from sample S3-T is nearly independent of Q. This result is

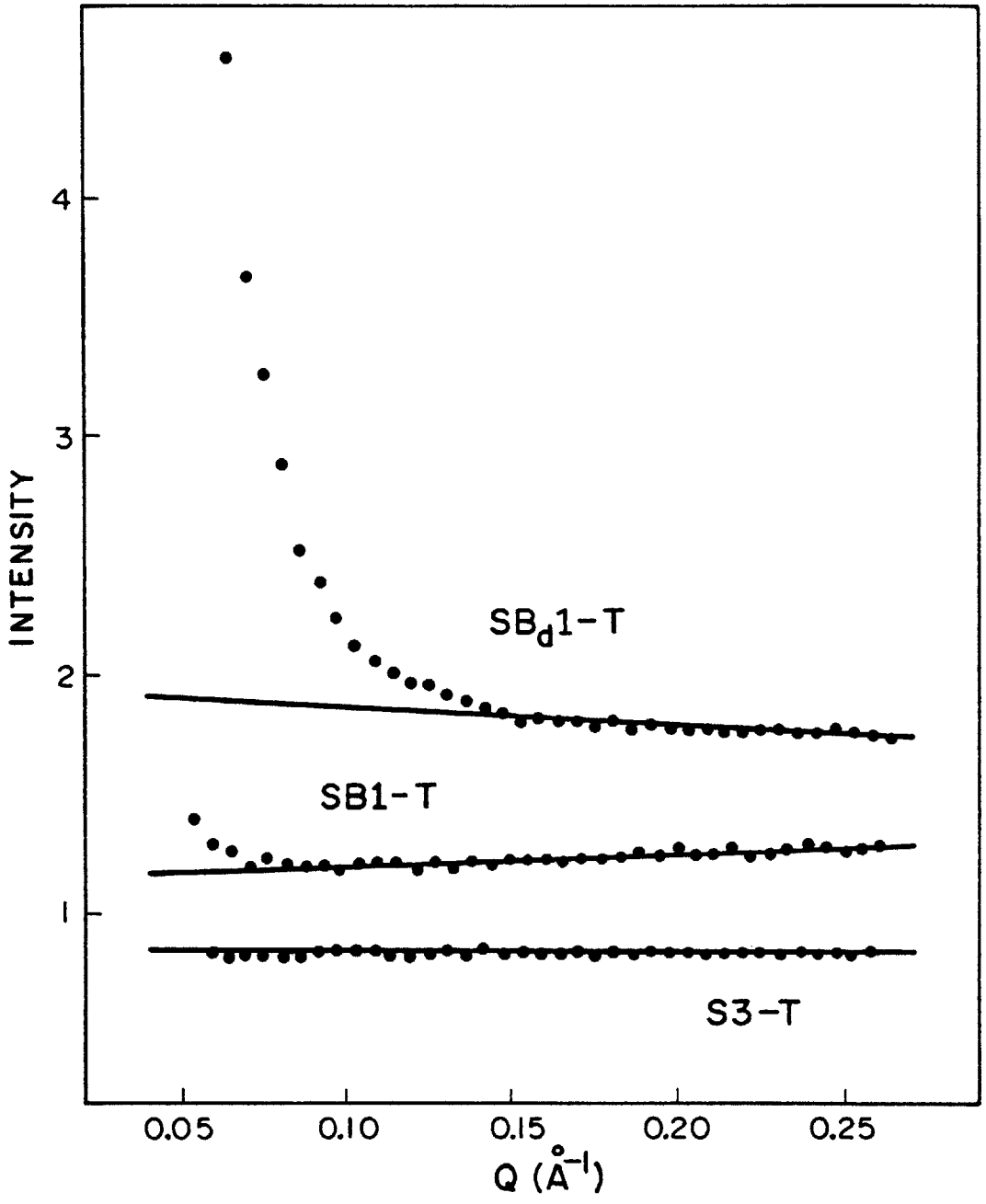

Figure 5-3 Porod scattering. Solid lines are best fits to the linear data and are used to correct for incoherent scattering. Curves SB_d1-T and SB1-T have been shifted 0.5 and 1.0 intensity units respectively.

expected, since sample S3-T consists of pure polystyrene containing no observable heterogeneities; therefore, the intensity can be attributed to incoherently scattered neutrons (Section 4.2.2). Data from sample SB1-T exhibits similar behavior for values of Q greater than 0.09 $Å^{-1}$. The observed increase in intensity for Q less than 0.09 $Å^{-1}$ results from inter- and intra-particle interference effects, e.g. arising from the spherical microdomains, as discussed in Chapter 4. These effects become much more significant in sample SB_d1-T, extending to a value of Q equal to 0.15 $Å^{-1}$. For values of Q greater than 0.15 $Å^{-1}$ the intensity as a function of Q is nearly constant, resembling samples S3-T and SB1-T. The dramatic difference in the coherent scattering intensity between samples SB1-T and SB_d1-T, which have nearly identical molecular (see Table 3-2) and structural (see Figures 4-8 and 5-1) characteristics, is brought about by a twenty-seven fold increase in the contrast factor $(\rho_B-\rho_S)^2$ (see Table 4-2) of SB_d1-T relative to SB1-T. This fact has been exploited in obtaining SANS data in the Porod region.

Figure 5-3 serves to illustrate the method in which incoherent scattering has been accounted for in all samples. To an excellent approximation, data occuring beyond the region of Q in which coherent scattering is evident, can be fit with a straight line. Straight line fits appearing in Figure 5-3 have been obtained using a least square linear regression with a statistical weighting of the points (5). In regions of Q where coherent scattering is present, the incoherent intensity level can be determined by extrapolation of this regressed line. Samples S3-T and SB1-T provide evidence supporting the assumption

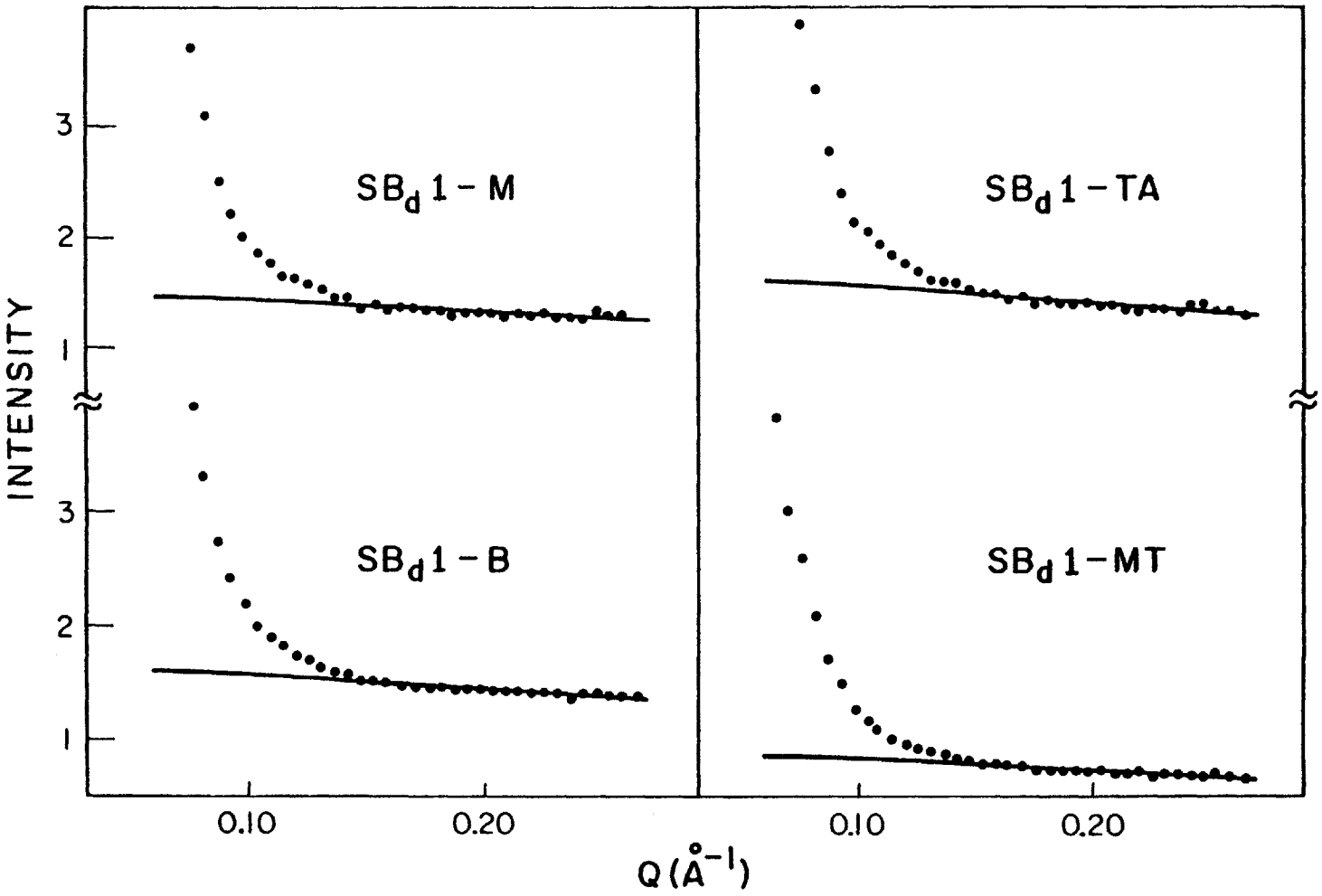

Figure 5-4 (first of two pages) Porod scattering and incoherent scattering corrections (solid lines)

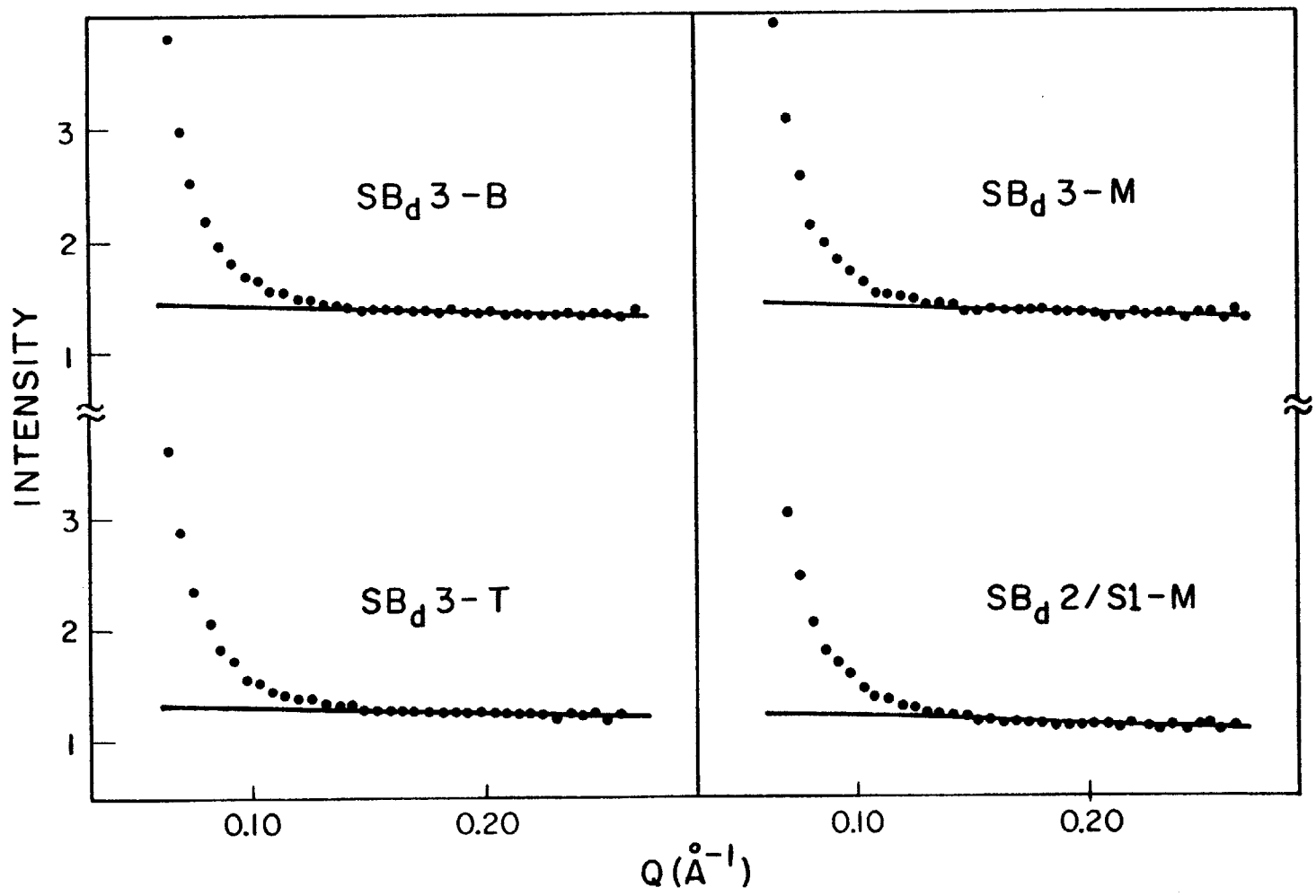

Figure 5-4 (second of two pages)

that the incoherent scattering intensity remains linear in Q for values lower than can be experimentally determined in sample SB_d1-T.

SANS data and linear incoherent scattering corrections for the remaining samples given in Table 5-1 (except SB7-T) are shown in Figure 5-4 (2 pages) along with straight line best fits through points in Q greater than 0.15 $Å^{-1}$. The slight slope associated with the incoherent intensity levels shown in Figures 5-3 and 5-4 can be attributed to minor inaccuracies in the background and detector sensitivity corrections (6). Both the sign and magnitude of this slope were found to change between visits to NCSASR (see Fig. 5-3), although the corrections always remained linear. Also, Porod's law calculations (Table 4-3) on a given sample gave consistent results in each case.

Schelten and Schmatz (7) have recently addressed the issue of correcting small angle scattering data for multiple scattering, specifically examining the case of randomly distributed homogeneous spheres. The necessity for such a correction in Porod law calculations depends upon the total scattering probability given by,

$$\frac{s(0)}{k_o^2} = \frac{Dp6\pi^2R}{k_o^2}(\rho_B-\rho_S)^2 \qquad 5\text{-}3$$

where p is the volume fraction of spheres of radius R, k_o is the wavenumber and D is the sample thickness. For values of $s(0)/k_o^2$ less than one, the measured versus true Porod constant varies by only several percent. Using parameters representative of samples having the highest total scattering probability (D=.2 cm, p=.13 and R=220 Å, see Sec. 5.3) $s(0)/K_o^2$ equals 0.54. Therefore, none of the Porod data

should require a multiple scattering correction. In order to experimentally verify this conclusion, SB_d1-MT was included in the set of samples examined. As seen in Figure 5-4, the incoherent scattering intensity of SB_d1-MT is half that of SB_d1-M. This difference is due to multiple incoherent scattering and is accounted for in the incoherent scattering correction.

5.2.2 Porod Analysis: The domain boundary thickness was determined for each of the samples listed in Table 5-1 containing perdeuterated polybutadiene. The three modified versions of Porod's law, given in Table 4-3, were used to obtain an interfacial thickness based upon a Helfand (8), linear, and sigmoidal interfacial composition profile.

Plots of Q^2I versus Q^{-2} are presented in Figure 5-5 (3 pages). Minimum values of Q for data appearing in Figure 5-5 are in each case greater than that calculated by equation 4-20. The standard deviation of each point, as indicated by an error bar, was calculated from the uncertainty in estimating the incoherent background intensity and the statistical uncertainty associated with the coherent scattering intensity. Each set of data in Figure 5-5 has been fit with a straight line using a least square linear regression in which each point was weighted with its associated variance (5). Values of the interfacial thickness, as defined by Helfand, a_I (8), and Vonk, E (9), can be determined from the slope and intercept of these straight lines (see Table 4-3). The results are presented in Table 5-3.

The date shown in Figure 5-5 are replotted as $\ln(Q^4I)$ versus Q^2 in Figure 5-6. Straight line best fits to the points have been determined

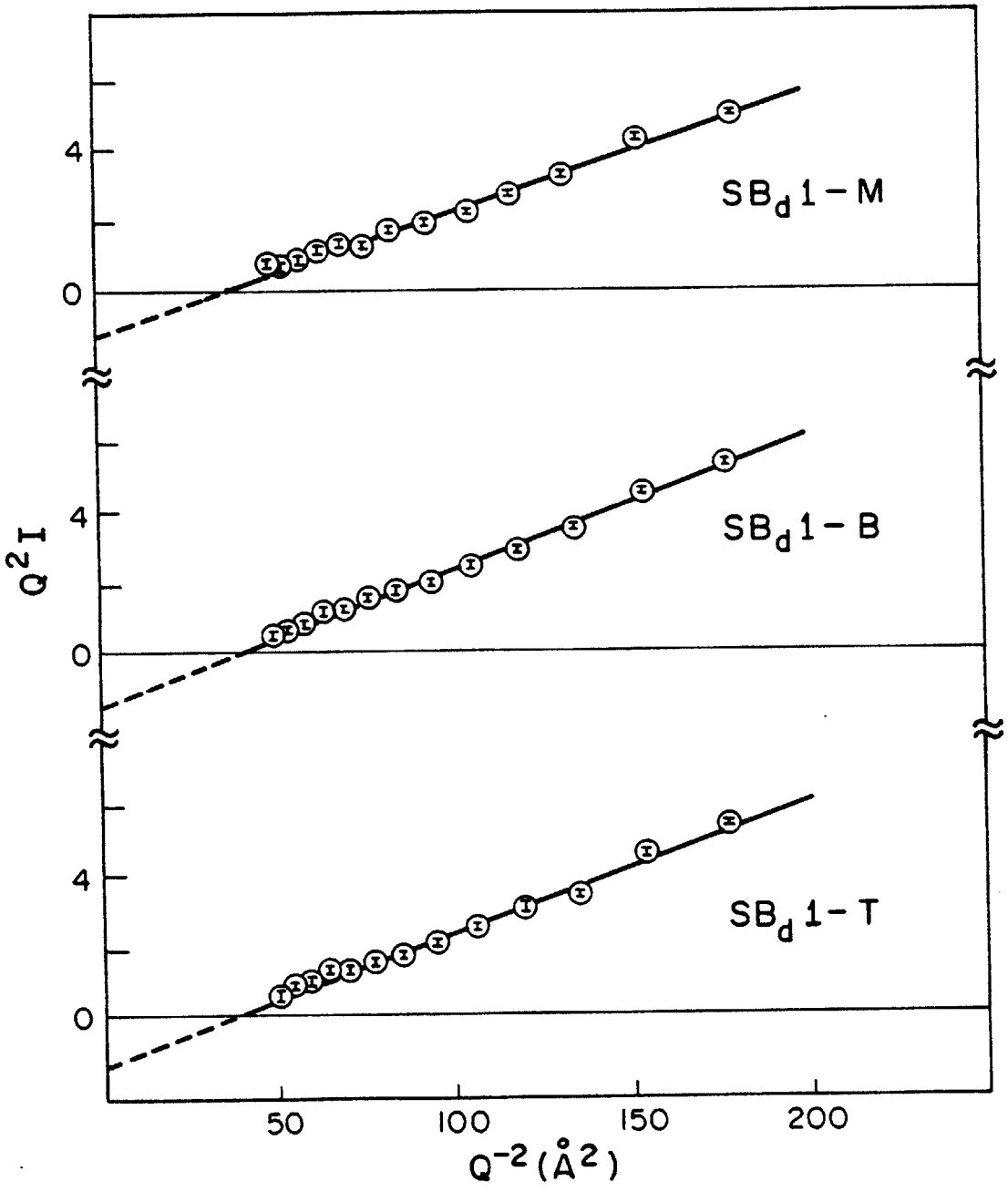

Figure 5-5 (first of three pages) Porod plots for the linear and Helfand interfacial composition profile models

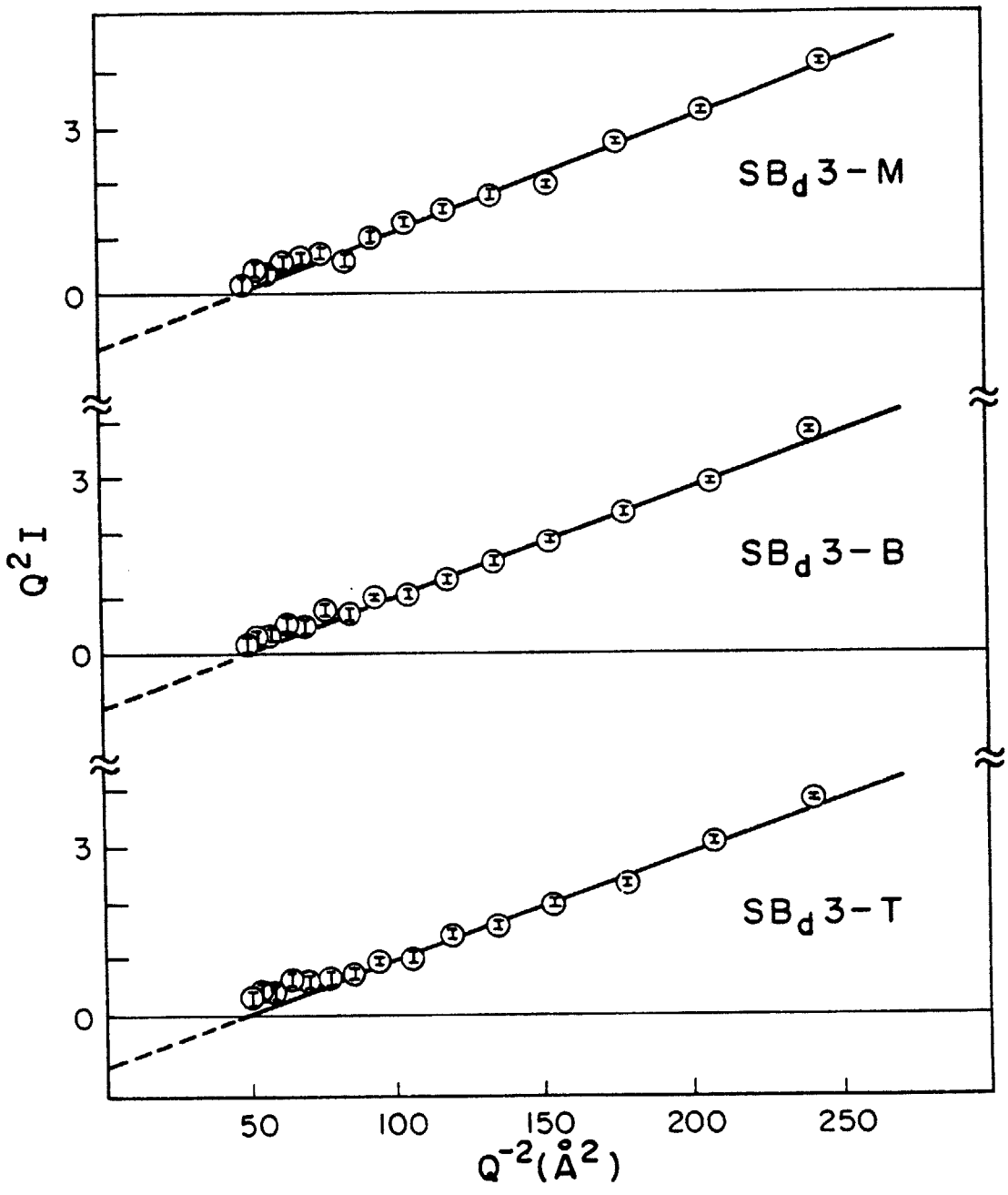

Figure 5-5 (second of three pages)

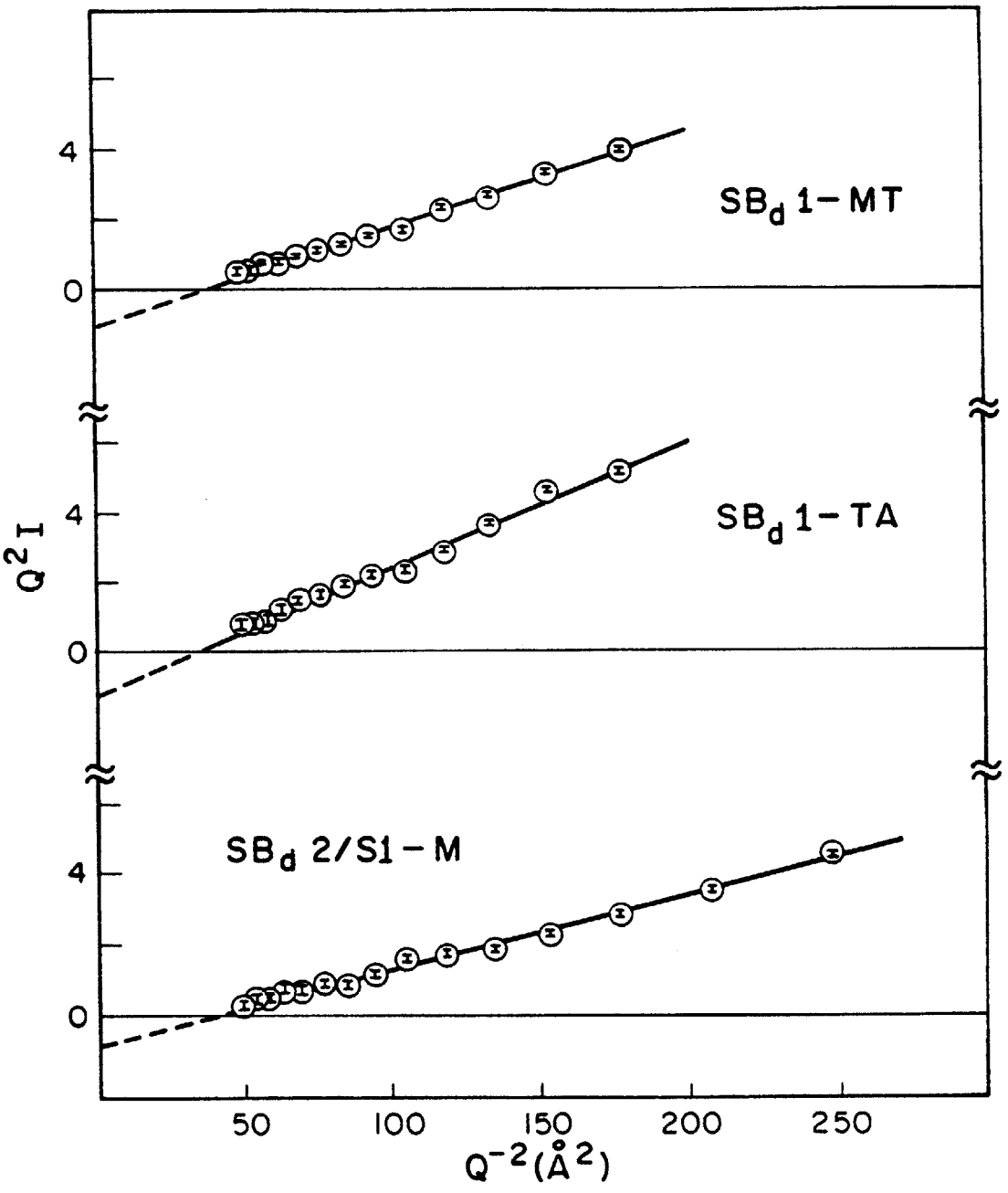

Figure 5-5 (third of three pages)

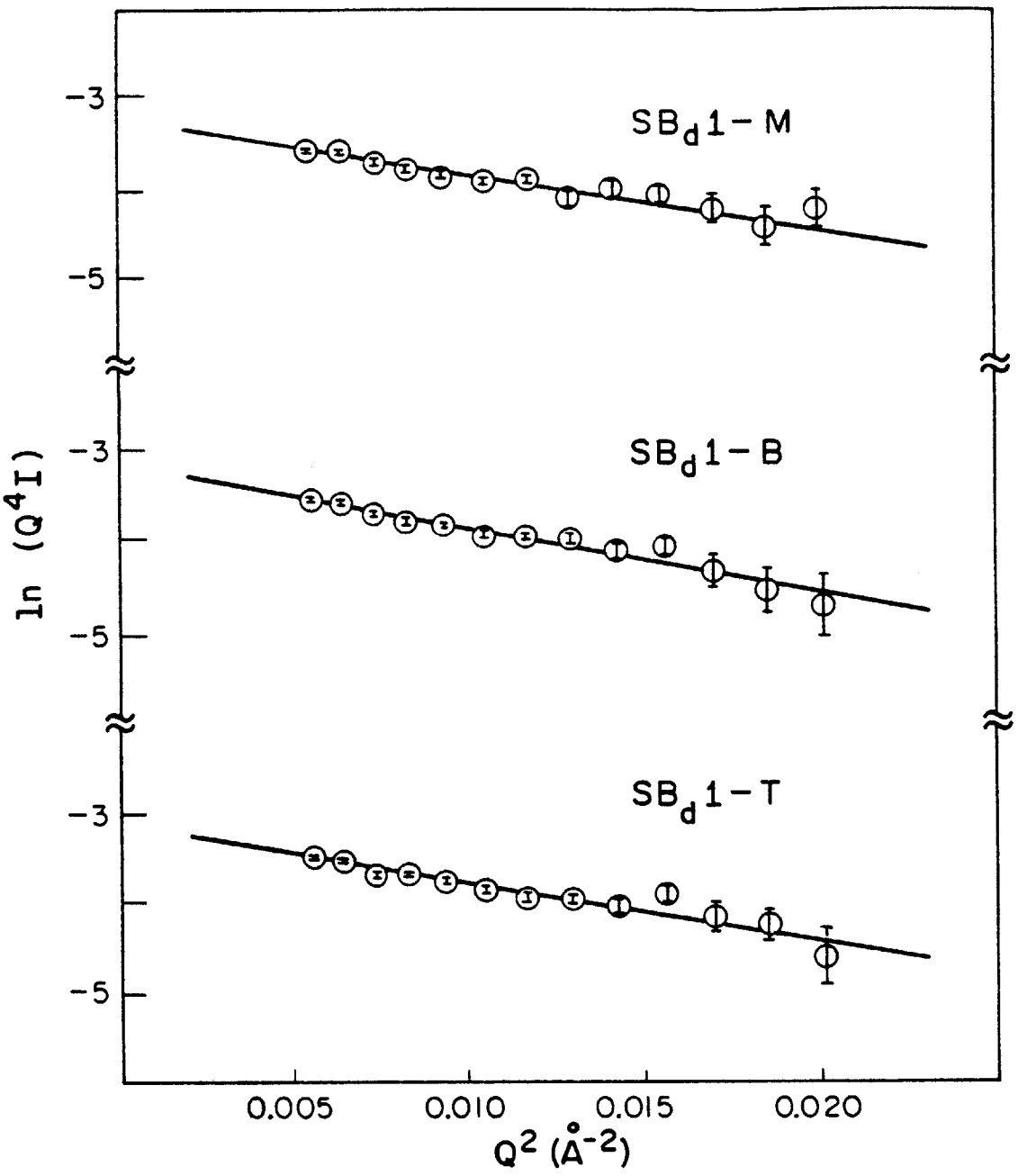

Figure 5-6 (first of three pages) Porod plots for sigmoidal interfacial composition profile model

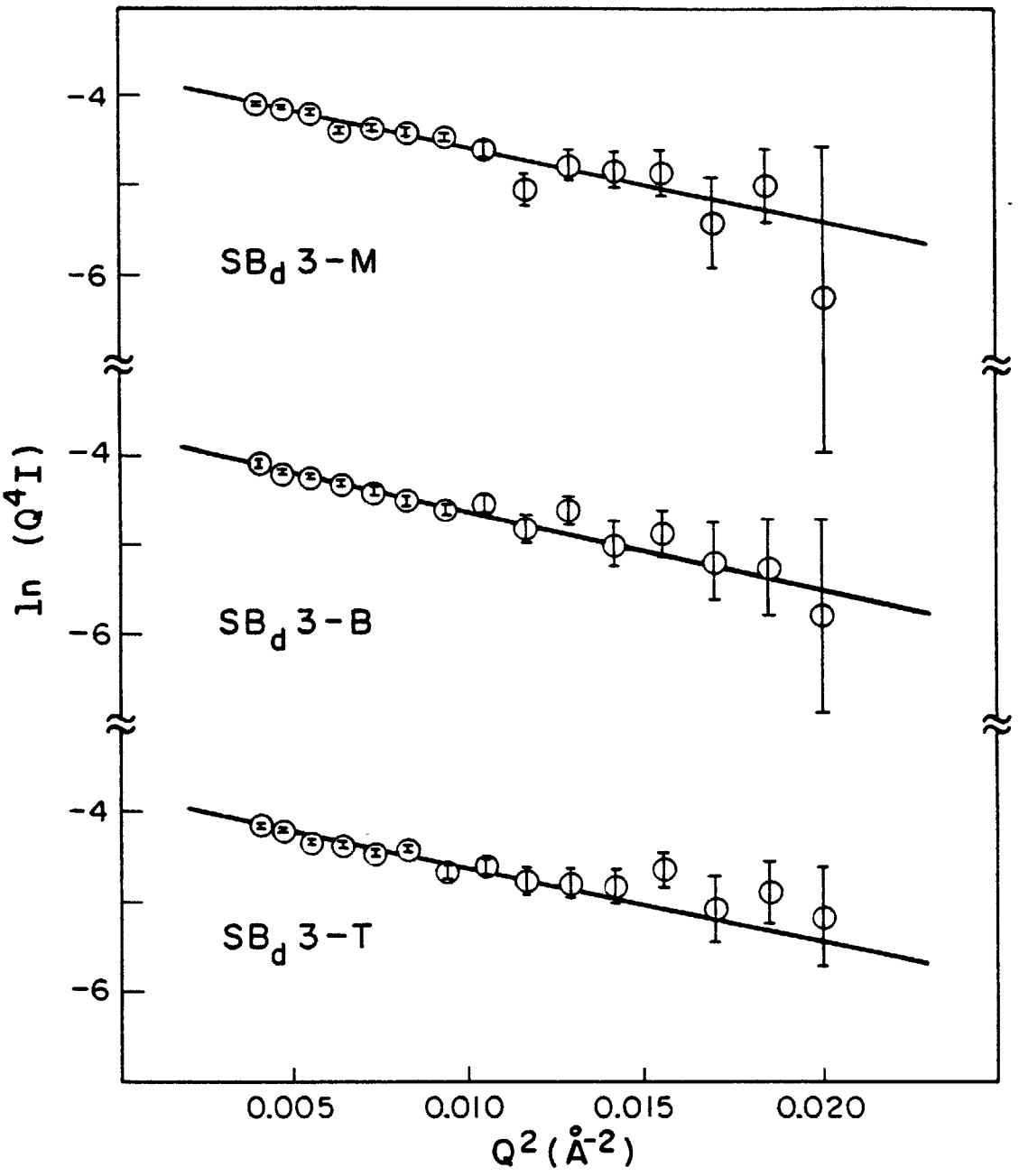

Figure 5-6 (second of three pages)

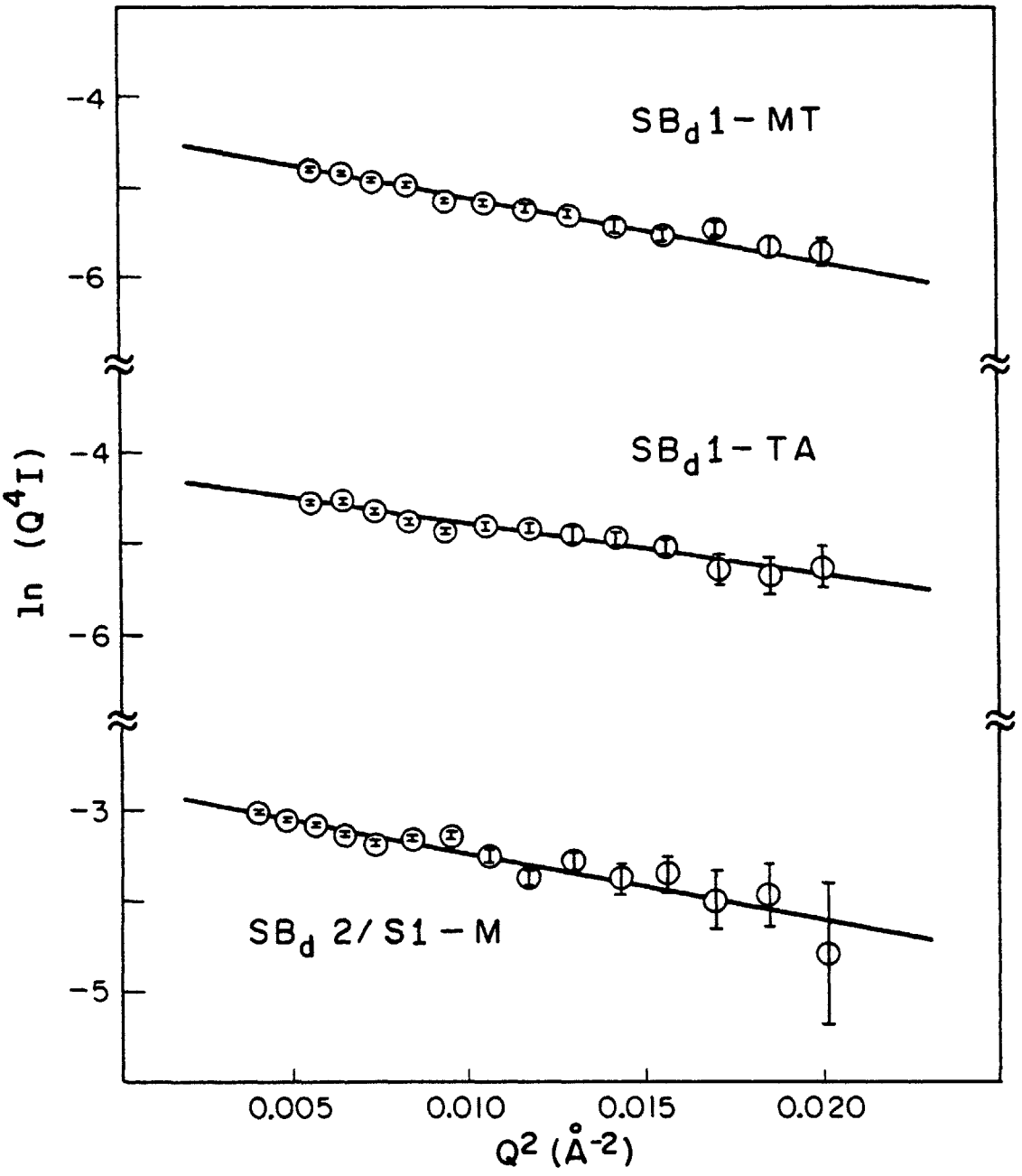

Figure 5-6 (third of three pages)

TABLE 5-3

Domain Boundary Dimensions

Sample [a]	Linear model E(±2 Å)	Helfand model a_I(±2 Å)	Sigmoidal model ΔR(±2 Å)
SB_d1-T	22	14	20
SB_d1-B	22	14	21
SB_d1-M	22	14	20
SB_d1-TA	21	13	19
SB_d1-MT	22	14	21
SB_d3-T	24	15	23
SB_d3-B	25	16	23
SB_d3-M	25	16	23
SB_d2-B-M	24	15	22

[a] Samples are referenced in Table 5-1

in the same manner as in the previous case. Values for the standard deviation σ, of the Gaussion smoothing function used in deriving the sigmoidal interfacial concentration profile can be obtained from the slopes of these lines (see Table 4-3). The results of this analysis are also given in Table 5-3, where the interfacial thickness has been defined as (10):

$$\Delta R = (2\pi)^{1/2} \sigma \qquad 5\text{-}4$$

Comparison of the interfacial thickness calculated for samples SB_d1-M and SB_d1-MT confirms that there is no detectable multiple scattering contribution in the measurement of the thicker sample.

Figure 5-7 illustrates the three scattering length density profiles determined for average values of E, a_I and ΔR given in Table 5-3.

5.3 DOMAIN DIMENSIONS

Information pertaining to the size of the spherical domains, seen in Figure 5-1, can be obtained from single particle scattering described in Chapter 4. SANS data collected at 1.8, 4.2, 7 and 15.3 meters have been utilized for this purpose and are described in this section.

5.3.1 Scattering Model: Scattering from a uniform set of spheres can be described by the spherical form factor, $f_s^2(QR)$, given by equation 4-13. This function is periodic, producing local maxima at QR = 5.765, 9.10, 12.33, etc. Hence, identification of maxima (or shoulders) in a SANS profile permits estimation of the sphere radius. In order to more accurately describe the features observed in the SANS data, $f_s(QR)$ was modified so as to account for a dispersity in sphere size and a

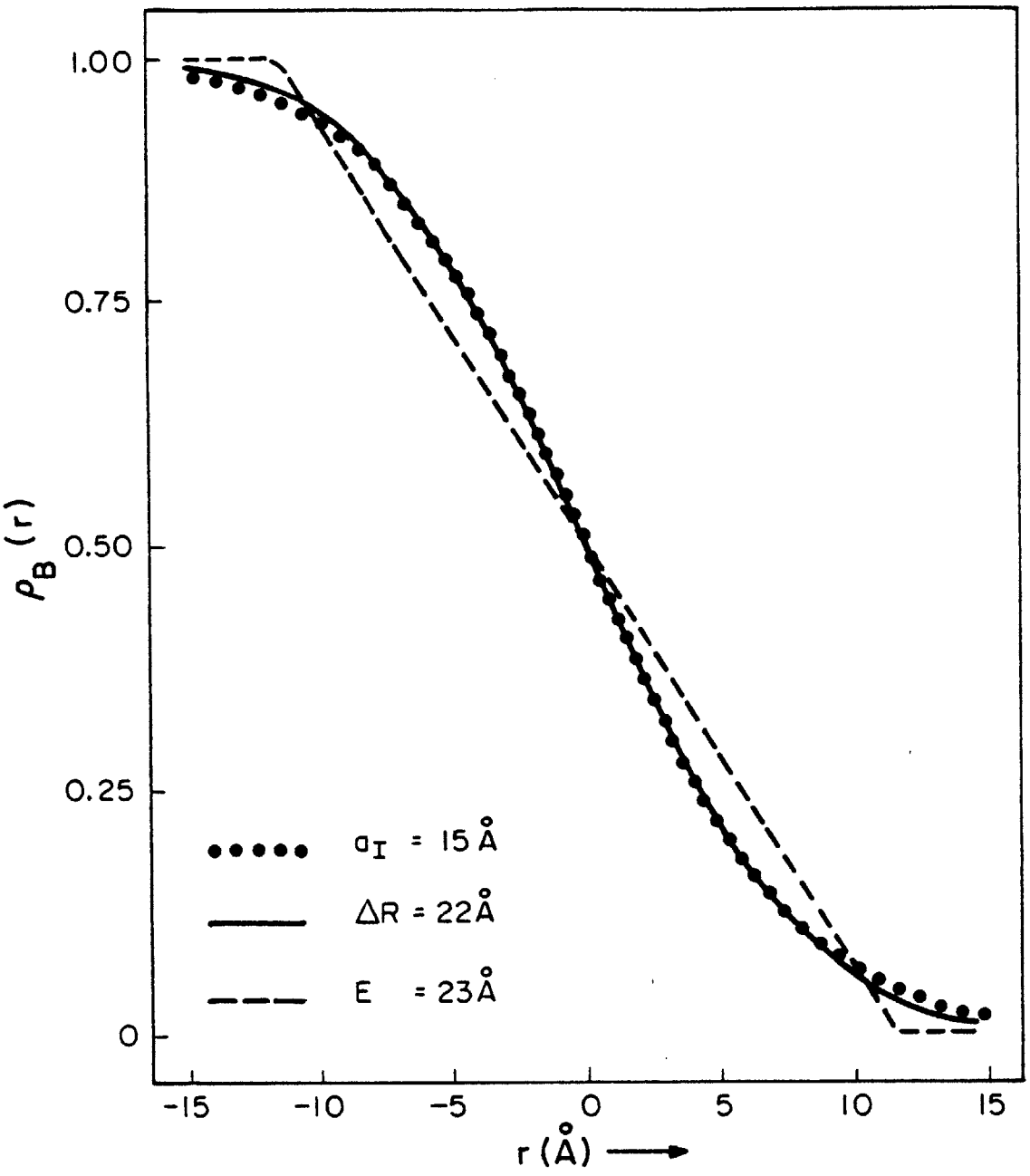

Figure 5-7 Scattering length density profiles obtained from average SANS results listed in Table 5-3

diffuse domain boundary. The latter was modeled using the previously discussed sigmoidal scattering length density profile (Sec. 4.2) (10),

$$f(QR) = (4\pi R^3/3) f_s(QR) \exp(-\sigma^2 Q^2/2) \qquad 5\text{-}5$$

where σ is obtained from the Porod region of the scattering curve (Table 5-3 and equation 5-4).

The distribution in sphere sizes has been assumed to follow the Gaussion function P(R):

$$P(R) = (\text{const}) \exp[-(R-\bar{R})^2/2\sigma_R^2] \qquad 5\text{-}6$$

Incorporating equations 5-5 and 5-6 into equation 4-12 yields:

$$I_{obs}(Q) = \kappa(\rho_B-\rho_S)^2 \left[\int_0^\infty P(R) f^2(Q;R) dR \Big/ \int_0^\infty P(R) dR \right] W(Q) \qquad 5\text{-}7$$

5.3.2 Modeling Results: Composite scattering profiles have been modeled with equation 5-7, which was numerically evaluated using a Gauss-Jacobi quadrature method (11). The incoherent scattering intensity level and domain boundary smoothing parameter σ were experimentally determined at high values of Q (Sec. 5.2) while the interparticle interference function W(Q), was assumed to be unity for the region of Q presently being discussed. Although κ can theoretically be calculated, SANS data must then be scaled to absolute intensity units for comparison. Since the features being modeled are not affected by the absolute intensity scaling constant, κ was selected so as to match the relative level of intensity exhibited by the data.

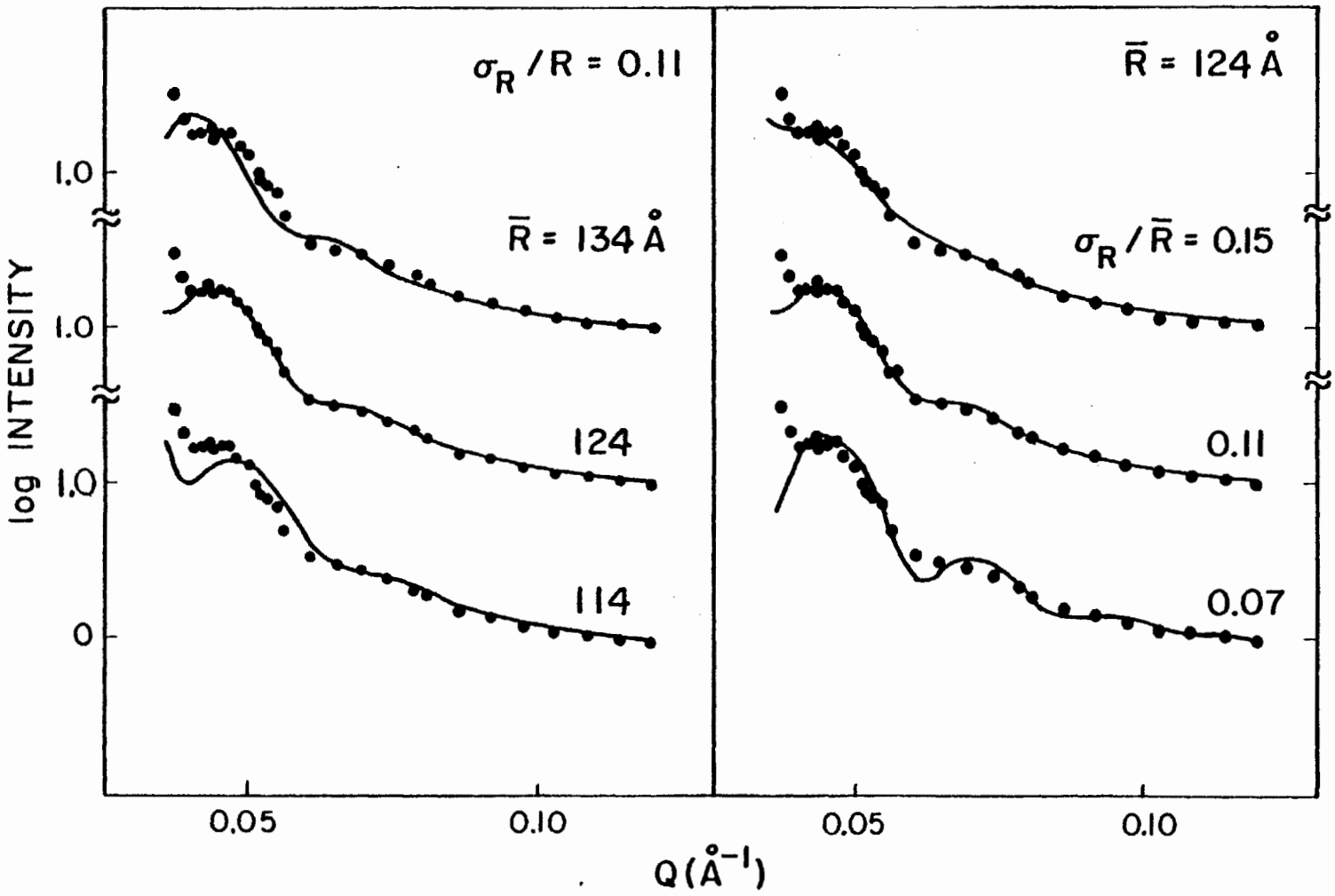

Figure 5-8 Sensitivity of scattering model (equation 5-7) to variations in the fitting parameters. SANS data correspond to sample SB_d1-T.

Figure 5-8 illustrates the sensitivity of equation 5-7 to variations in $\bar{R}$ and σ_R. Changes in mean sphere radius produce a shift in the Q location of the periodic peaks generated by the Bessel function (equation 4-13) with little effect on their shape. Varying the sphere size standard deviation modifies the resolution of this periodic function but has no influence on the Q location of the maxima. In this manner both parameters can be fit independently. SANS results can only be represented within a narrow range of parameter values, e.g. $\bar{R}$ = 124±2 Å and $\sigma_R/\bar{R}$ = 0.11±0.01 for sample SB_d1-T as shown in Figure 5-8.

The effects of perdeuteration on the observed intraparticle scattering intensity are clearly demonstrated in Figure 5-9. Although samples SB7-T and SB_d2/S1-M contain polybutadiene spheres of equal size (Table 5-4), $(\rho_B-\rho_S)^2$ is twenty-seven times greater in the latter.

SANS results from all samples examined for intraparticle scattering have been modeled using equation 5-7, and best fit results are presented in Figures 5-9 to 5-11. In each case, the calculated curve adequately predicts the behavior of the experimental points for QR>5. $\bar{R}$ and σ_R have been determined from these fitted curves and are listed in Table 5-4.

The lack of agreement between the simulated curves and experimental points for values of QR<5 is due to interparticle interference effects, neglected (W(Q) = 1) in the simulations presented in Figures 5-9 to 5-11. This mode of scattering is addressed in the following section.

As with the Porod region of the scattering curve, multiple

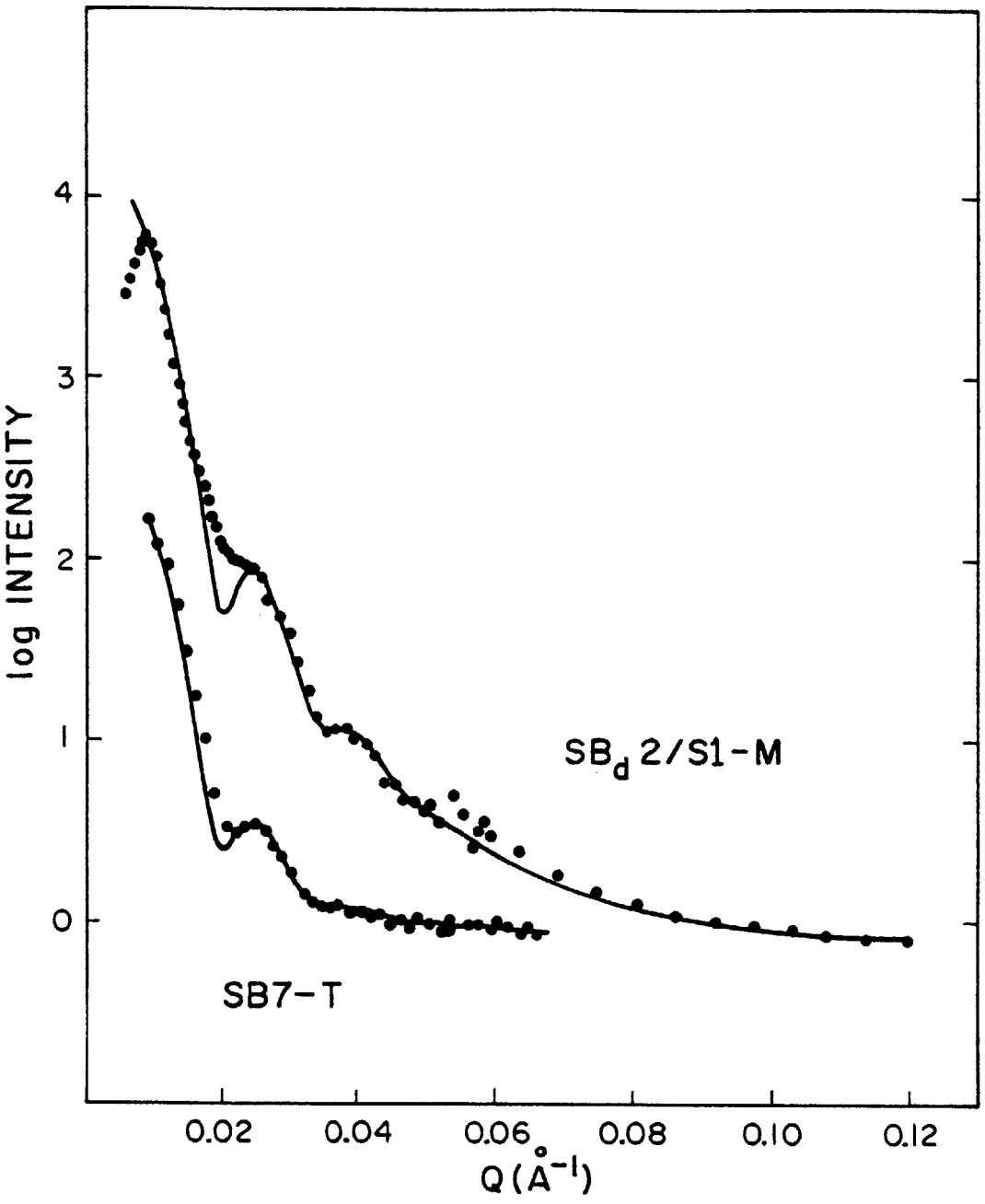

Figure 5-9 Single particle scattering from hydrogeneous (SB7-T) and perdeuterated (SB$_d$2/S1-M) spheres of polybutadiene. Solid curves are best fits of equation 5-7 to the data.

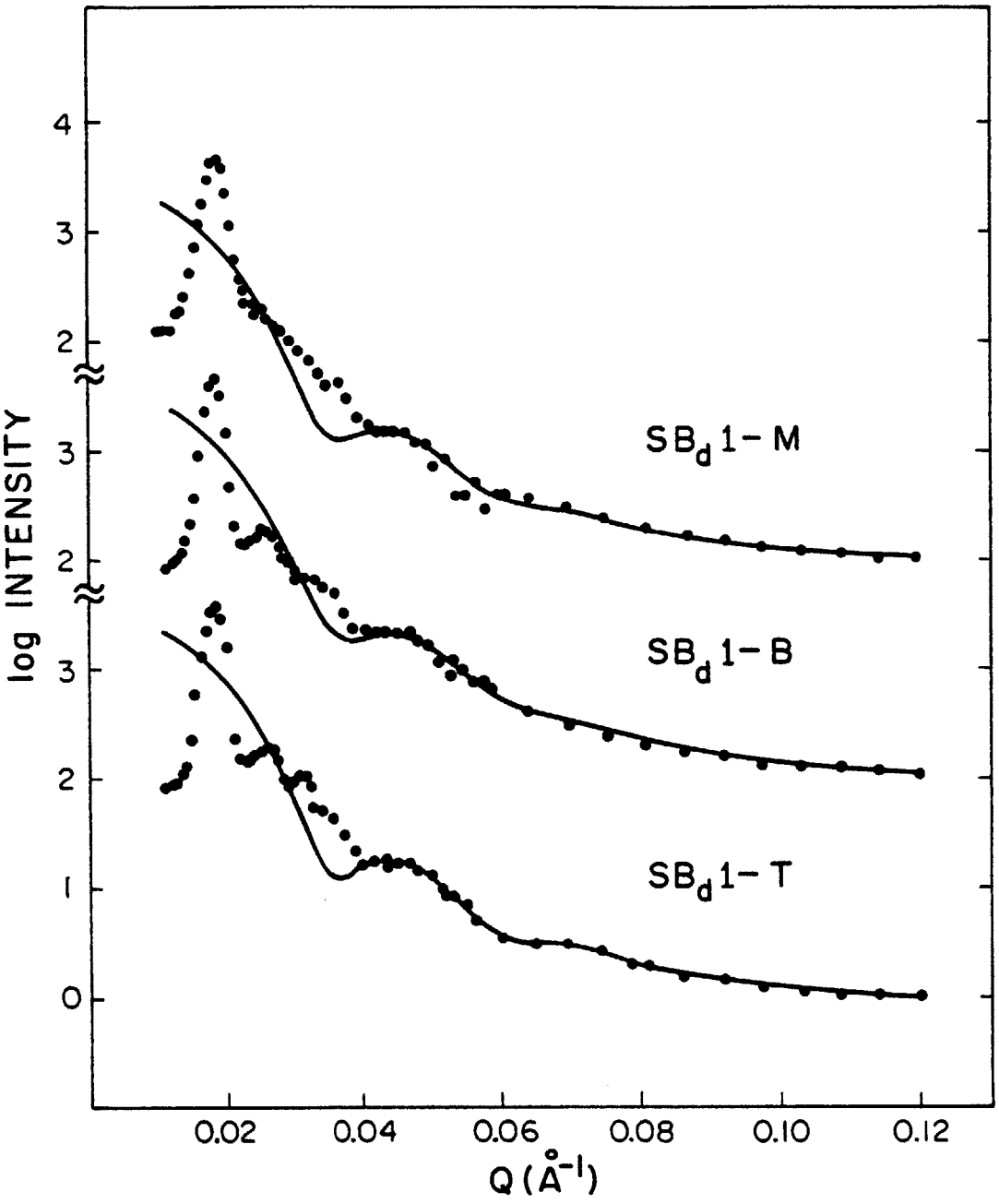

Figure 5-10 SANS results from sample SB_d1 for three casting solvents. Solid curves are best fits of equation 5-7 to the data.

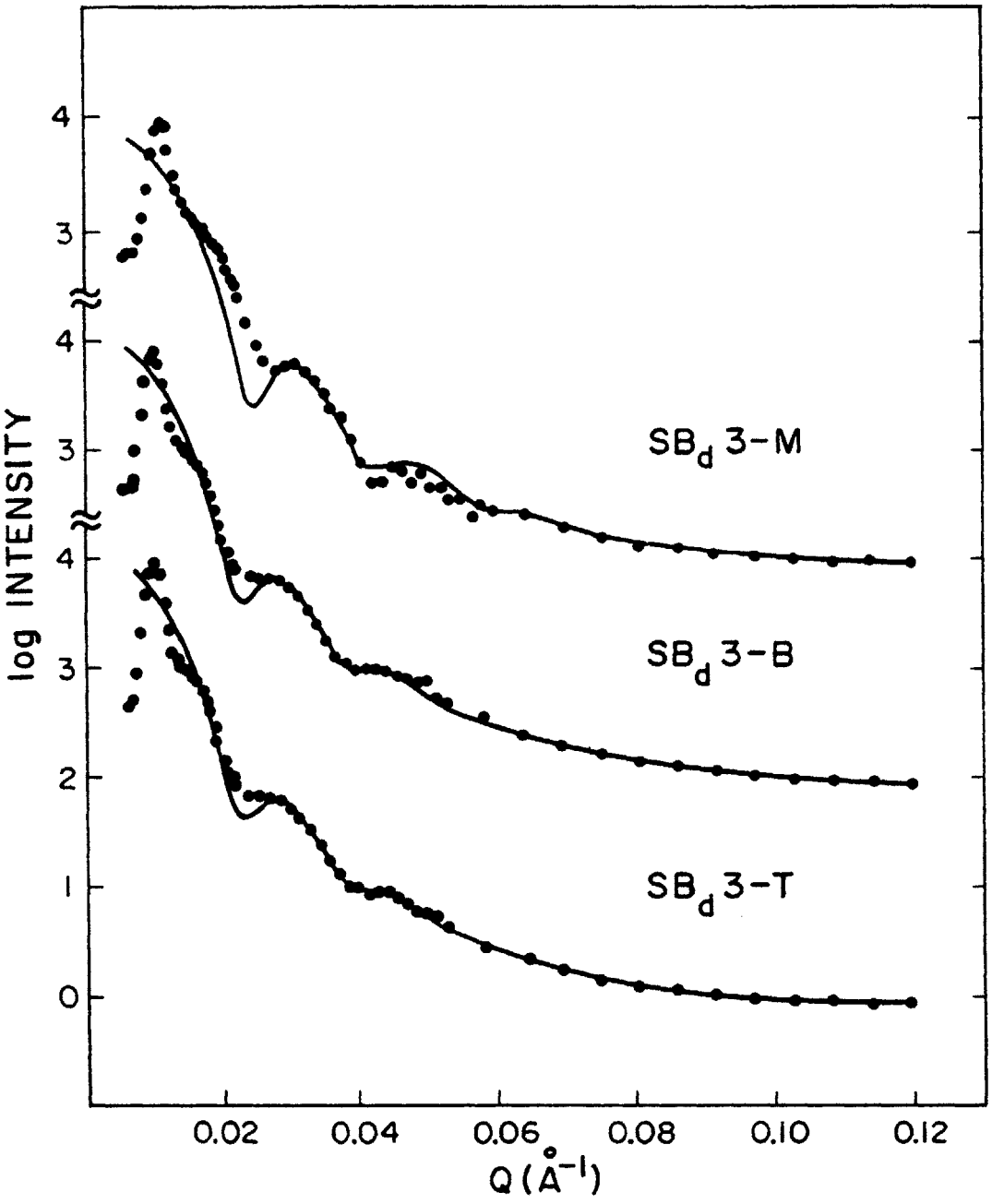

Figure 5-11 SANS results from sample SB_d3 for three casting solvents. Solid curves are best fits of equation 5-7 to the data

scattering contributions to the observed intraparticle scattering can be evaluated in terms of equation 5-3. Calculated values for the total scattering probability of the samples listed in Table 5-1 indicate a maximum possible error of 2% on the evaluated sphere radius (7). The influence of multiple scattering on the calculated values of σ_R can be determined by comparing the results from sample SB7-T with all the perdeuterated samples. As indicated by equation 5-3 the total scattering probability is directly dependent on the contrast factor. Therefore, if multiple scattering were significant, there would be a noticeable difference in $\sigma_R/\bar{R}$ between the hydrogenated and perdeuterated samples. This is not the case as shown in Table 5-4.

5.4 DOMAIN PACKING

The SANS facility at NCSASR is particularly useful for investigating the domain packing structure in the samples being discussed. A combination of longer wavelength and larger sample-to-detector distance permits the collection of scattering data at low Q with much greater resolution than is attainable with available SAXS instruments. Such results obtained at 15.3 m are presented in this section.

5.4.1 Interparticle Interference: Deviation of the intraparticle scattering model from the experimental data at low values of Q, as seen in Figures 5-9 to 5-11, is the result of excluding interparticle interference effects, e.g. setting W(Q) = 1. Therefore, the model (eq. 5-7) has been modified in each case by including the Fournet approximation (eq. 4-14) (3) for W(Q), without changing the other parameters.

TABLE 5-4

Intra- and Inter-Domain Dimensions

Sample	$\bar{R}$ (Å)	$\sigma_R/\bar{R}$	$\bar{D}$ (Å) [a]		
SB_d1-T	124±2	0.11±.01	347±2	246±3	203±3
SB_d1-B	121±2	0.13±.01	345±2	246±3	(196)
SB_d1-M	124±3	0.12±.02	340±3	(250)	
SB_d3-T	197±3	0.11±.01	635±4		
SB_d3-B	196±3	0.10±.01	638±4		
SB_d3-M	181±3	0.09±.02	579±4		
SB_d2-B-M	221±3	0.10±.01	690±5		
SB1-T	[117] [b]	----	325±2	230±4	
SB7-T	222±3	0.11±.01	---		

[a] Dimensions not clearly resolved are given in parenthesis [b] Calculated from $\bar{D}$ and V_B^{UV} (Table 5-6) assuming a bcc packing mode

These results are shown in Figures 5-12 and 5-13 (dashed lines) along with the 15.3 m data for each sample. With the possible exception of sample $SB_d2/S1-M$, this modification fails to explain the scattering behavior of these samples over the range of Q shown. Therefore, a paracrystalline structure of the type described by Hosemann and Bagchi (eq. 4-15) (12) is indicated. Such a structure is also indicated by Figure 5-1 for sample SB_d1-T, although the quantitative determination of packing order is impossible using this electron micrograph (two-dimensional projection).

The local maxima in intensity apparent in Figure 5-12 (and to a lesser extent in Fig. 5-13) can be interpreted in terms of Bragg scattering from a mosaic of paracrystals, e.g. a Debye-Scherrer powder pattern is observed (13). Each peak is associated with reflections from a specific crystallographic plane having a spacing $\bar{D}$, as described by Bragg's law:

$$2\bar{D} \cdot \sin\Theta = \lambda \qquad 5\text{-}8$$

Such planar spacings have been identified by fitting the resolvable peaks in Figures 5-12 and 5-13 with Gaussion functions,

$$I_{Bragg}(Q) = \sum c_i \exp\left[-\frac{1}{2}\left(\frac{Q-q_i}{\sigma_i}\right)^2\right] \qquad 5\text{-}9$$

added to an arbitrary background. The lattice spacings $\bar{D}$, associated with each q_i are given in Table 5-4.

5.4.2 Packing Order: Table 5-5 lists the lattice spacings associated with the allowed Bragg reflections predicted for a powder pattern

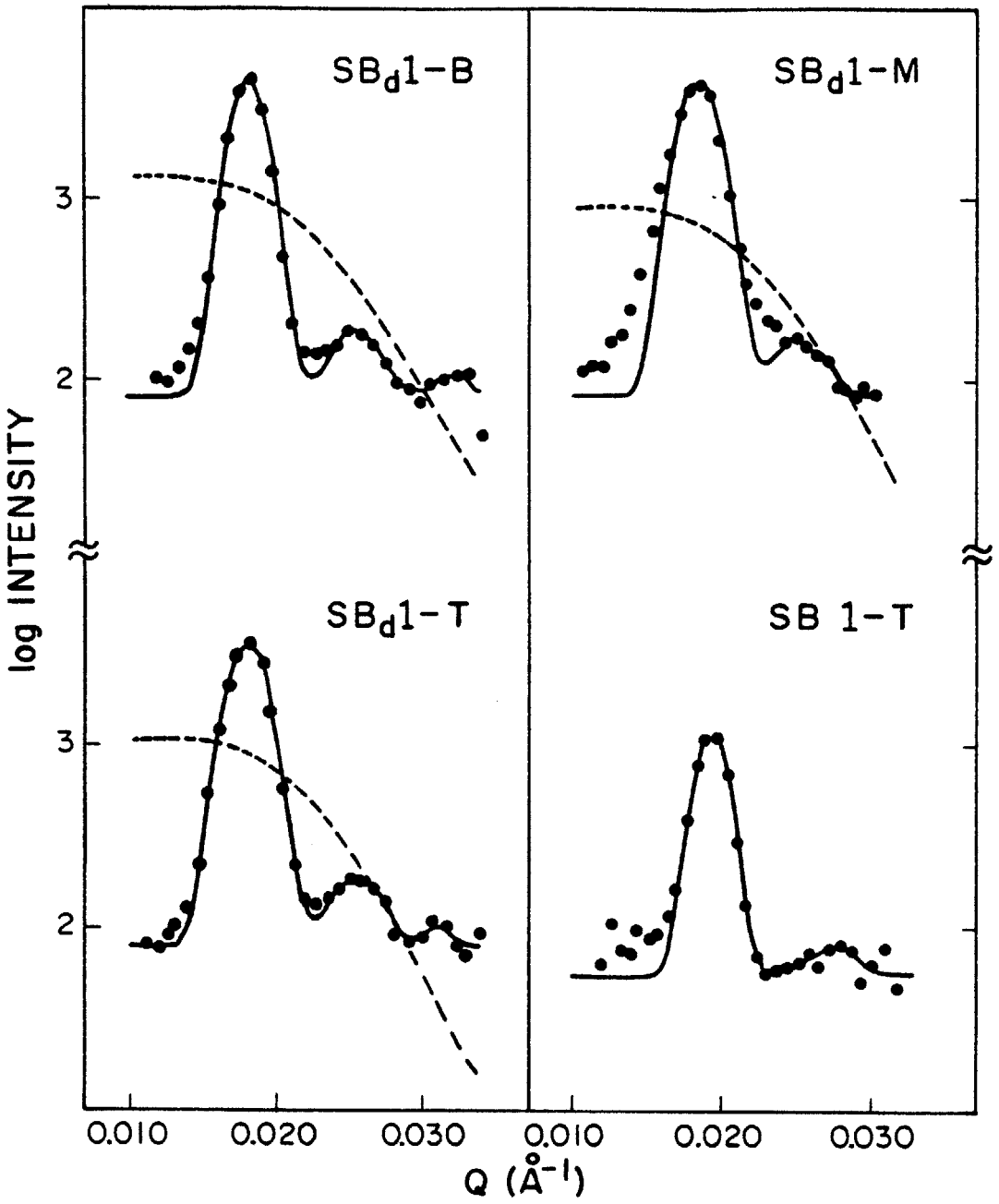

Figure 5-12 Solid curves represent best fits of equation 5-9 to the resolvable peaks. Dashed curves were determined from equation 5-7 using a Fournet interparticle interference approximation (eq. 4-14). The SB1-T results have been shifted up one decade.

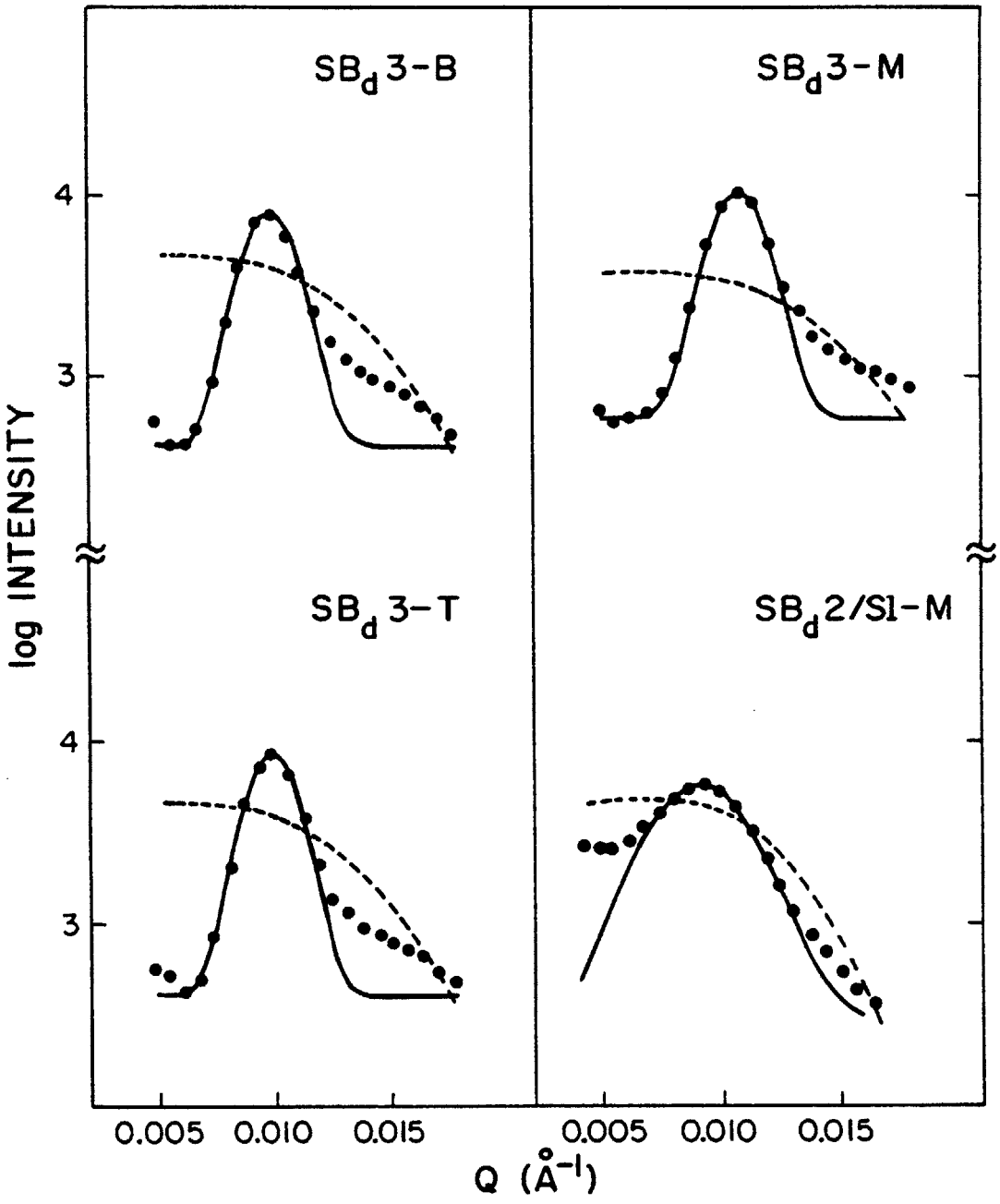

Figure 5-13 Solid curves represent best fits of equation 5-9 to the resolvable peaks. Dashed curves were determined from equation 5-7 using a Fournet interparticle interference approximation (eq. 4-14).

TABLE 5-5

Predicted Bragg Peaks for Simple Packing Arrangements

	Allowed Peaks (h,k,l)	Relative $\bar{D}$	Predicted $\bar{D}$ (Å)
body centered cubic (bcc)	(110)	(1)	(345)
	(200)	0.707	244
	(211)	0.577	199
simple cubic (pc)	(100)	(1)	(345)
	(110)	0.707	244
	(111)	0.577	199
face centered cubic (fcc)	(111)	(1)	(345)
	(200)	0.866	299
	(220)	0.612	211
hexagonal close pack (hcp) (c/a = 1.633)	(001)	(1)	(345)
	(100)	0.530	183
	(002)	0.500	173

from four different simple domain packing arrangements (13). Comparison of the results in Table 5-4 with those in Table 5-5 clearly indicates that samples SB_d1-T,B,M and SB1-T are composed of either a body centered cubic (bcc) or simple cubic paracrystalline macrolattice. It is theoretically possible to distinguish between these two packing modes at higher Q since the (321) reflection in bcc materials gives rise to a peak at $\sqrt{7}$ times the Q of the main peak, while a simple cubic lattice exhibits no such reflection. However, this peak would occur in a region where intraparticle scattering (rather than Bragg scattering) is the dominent mechanism, making its resolution impossible. Nevertheless, the actual packing mode can be determined by utilizing the mean radii listed in Table 5-4. The volume fraction of polybutadiene V_B, can be calculated as follows,

$$V_B = n \cdot \frac{4}{3}\pi \bar{R}^3 / a^3 \qquad 5\text{-}10$$

where n = 1 sphere per unit cell and a = $2\pi/q(100)$ for simple cubic packing. For a body centered cubic arrangement, n = 2 and a = $\pi\sqrt{8}/q(110)$. Volume fractions determined in this manner are listed in Table 5-6. Weight fractions of polybutadiene obtained by UV absorption spectroscopy (Table 3-1), and converted to volume fractions using ρ_S = 1.05, ρ_{B_d} = 0.99 and ρ_B = 0.895 g/cm^3 (14) are also given in Table 5-6.

From these results it is apparent that samples SB_d1-T, B and M are constructed of an arrangement of body centered cubic paracrystals. No such conclusions can be drawn concerning the remaining samples. Although the results of V_B calculations show near agreement for a simple cubic arrangement in sample SB_d2/S1-M, a paracrystalline hypothesis for this

material is not warranted (see below).

A mean crystallite size can be determined for a given sample from the Bragg peaks in a powder pattern using a modified Scherrer formula. Assuming a spherical geometry, the crystallite radius is evaluated from (15),

$$\bar{R}_{CRYSTAL} = \frac{0.277\lambda}{B\cos\Theta} \qquad 5\text{-}11$$

where B is the full width at half maximum intensity (in radians) of the Bragg peak observed at a mean scattering angle of 2Θ. The standard deviation of the Gaussian functions fit to the main Bragg peaks seen in Figures 5-12 and 5-13 are listed in reduced form in Table 5-6. These values have been used to calculate $B(2.354\sigma)$. Combining equation 5-11 with the previously calculated values of $\bar{R}$ (Table 5-4) and V_B (Table 5-6) provides for the determination of the number of spherical domains per paracrystal. These results are tabulated in Table 5-6.

The contrast between SANS data and predicted interparticle interference found in Figure 5-12 can be explained by the results given in Table 5-6. In samples where a high degree of order exists (more than 100 domains per paracrystal) several Bragg peaks are discernable and the packing order can be clearly established (bcc). Less domain ordering (about 40 domains per paracrystal) results in the resolution of only a single interference maximum with no specific packing mode indicated. Sample SB_d2/S1-M exhibits essentially no order (5 domains per paracrystal), and correspondingly is nearly predicted by the Fournet amorphous spheres approximation (eq. 4-14).

TABLE 5-6

Domain Packing

Sample	UV [a]	bcc	Simple Cubic	$10 \cdot \sigma/q$ [b]	Domains/paracrystal [c]
SB_d1-T	0.143	0.135±.007	0.191±.010	0.72±.03	110
SB_d1-B	0.143	0.128±.007	0.181±.010	0.63±.03	172
SB_d1-M	0.143	0.144±.012	0.204±.017	0.68±.05	124
SB_d3-T	0.112	0.089±.005	0.125±.007	1.06±.05	40
SB_d3-B	0.112	0.086±.005	0.121±.006	1.12±.05	36
SB_d3-M	0.112	0.091±.006	0.128±.010	1.04±.05	42
SB_d2-B-M	0.149	0.097±.005	0.138±.007	2.20±.10	5
SB1-T	0.138	---	---	0.54±.03	241

[a] Using UV data from Table 3-1 with $\rho_{B_d} = 0.99$, $\rho_B = 0.895$ and $\rho_S = 1.05$ (g/cm^3)

[b] q and σ are obtained from the Gaussian function fit to the first Bragg peak

[c] Obtained using σ/q, V_B^{UV} and $\bar{R}$ (Table 5-4)

Finally, all SANS patterns of samples SB_d1 and SB_d3 exhibit shoulders at twice the principle Bragg peaks (Figs. 5-10,11), which can be attributed to multiple Bragg scattering. This point is confirmed by the lack of such a shoulder in samples SB_d2/S1-M and SB7-T (Fig. 5-9). There is no paracrystalline structure in the former (e.g. no Bragg scattering) while in the latter, a reduction in contrast factor precludes such an effect (see eq. 5-3).

References

1 G.E. Bacon, Neutron Diffraction, Oxford (1962).

2 D.G. Peters, J.M. Hayes and G.M. Hieftje, Chemical Separations and Measurements, W.B. Saunders Co. (1974).

3 A. Guinier and G. Fournet, Small Angle Scattering of X rays, J. Wiley and Sons, N.Y. (1955).

4 J.T. Koberstein, B. Morra and R.S. Stein, J. Appl. Cryst., 13, 34 (1980).

5 P.R. Bevington, Data Reduction and Error Analysis for the Physical Sciences, McGraw Hill Book Co. (1969).

6 G.D. Wignall, personal communication.

7 J. Schelten and W. Schmatz, J. Appl. Cryst., 13, 385 (1980).

8 E. Helfand and Z.R. Wasserman, Macromolecules, 11, 960 (1978).

9 C.G. Vonk, J. Appl. Cryst., 6, 81 (1973).

10 T. Hashimoto, M. Fujimura and H. Kawai, Macromolecules, 13, 1660 (1980).

11 J. Villadsen and M.L. Michelsen, Solution of Differential Equation Models by Polynomial Approximation, Prentice-Hall, Inc., N.J. (1978).

12 R. Hosemann and S.N. Bagchi, Direct Analysis of Diffraction by Matter, North Holland Publishing Co. (1962).

13 J.B. Cohen, Diffraction Methods in Material Science, Macmillan, New York (1966).

14 J. Brandrup and E.H. Immergut, eds., Polymer Handbook, second edition (1975).

15 B.E. Warren, J. Appl. Cryst., 11, 695 (1978).

CHAPTER 6: Mechanical Properties

Diblock copolymers and blends reported in Tables 3-2 and 4-5 were mechanically tested in a linear viscoelastic regime and the results are presented in the following chapter. The mechanical properties exhibited by these materials will be discussed in conjunction with their structural features in Chapter 7.

6.1 MECHANICAL BEHAVIOR OF BLOCK COPOLYMERS AND BLENDS

6.1.1 Large Deformation Properties: Exploitation of the structural features present in block copolymers on a commercial scale originated when Shell Chemical Company introduced a new class of polymers known as thermoplastic elastomers in 1965. Previous work by Millkovich and coworkers (1) led to the understanding that, upon phase separation, glassy polystyrene microdomains effectively crosslink center block elastomers in triblock copolymers (SBS or SIS). Furthermore, raising the temperature above the glass transition point of polystyrene permits easy processing, hence the name thermoplastic.

These elastomers, marketed under the tradename KRATON, have been investigated in great detail with regards to their large deformation properties (2-11). Their elastic behavior can be adequately described by conventional rubber elasticity theory, providing the reinforcing contribution of the domains is taken into account (9). Ultimate properties are characterized by extension ratios at break as high as 15 (4). These materials along with SOLPRENE, a similar product marketed by Phillips Petroleum Co., have had a significant impact on the

elastomers industry.

Glassy continuous block copolymers and blends have received an increasing amount of industrial and academic interest in the past several years. While conventional high impact polystyrene (HIPS) exhibits considerable toughness, it is on opaque material due to the size of the rubber inclusions (1-10 microns). Polystyrene, rubber modified with block copolymers, is highly transparent since the wavelength of visible light is considerably longer than the microdomain inclusions. Phillips Petroleum Co. capitalized on this fact and in 1972 began producing a new series of rubber-modified polystyrene under the tradename K-Resins (12,13). This product, consisting of a polystyrene-polybutadiene block copolymer (unspecified block geometry) combines toughness with excellent transparency.

Incorporation of rubber particles in polystyrene, as found in HIPS, leads to increased craze initiation upon deformation. Since the formation of craze matter absorbs energy, an increase in the amount of craze formation enhances the material toughness. The phenomena of crazing has been extensively studied for bulk materials such as polystyrene and polymethylmethacrylate and rubber-modified plastics such as HIPS and ABS. A review of the subject can be found in References (14-16).

Only recently has attention turned to investigating the large deformation behavior of glassy continuous block copolymers and blends. Kawai et al. (17) have examined a set of di- and triblock copolymers of polydienes and polystyrene along with blends of the corresponding homopolymers. These authors have recognized the importance of crazing in the macroscopic deformation process and conclude that crazing in

block copolymers and blends proceeds via the same mechanism as in HIPS. In a more quantitative study of crazing in block copolymers (K-Resins), Argon et al. (18) have shown that, in fact, craze propagation rates depend strongly on molecular structure and/or structural morphology. Craze propagation in KRO-1 resins (polybutadiene cylindrical morphology) was adequately described by the Taylor meniscus instability model (19) while for KRO-3 (lamellar morphology) an Anderson-Bergkvist model (20) was necessary. In both cases, craze velocity as a function of stress was significantly different than for polystyrene.

Through accumulated industrial experience it has been established that many factors are important in assuring adequate toughness in heterogeneous polymer among which the size, shape, volume fraction and internal constitution of rubbery particles together with the characteristics of their interfaces (e.g. thickness) play important roles (16,18,21). A fundamental investigation into the mechanisms of crazing in block copolymer systems requires an ability to control phase morphology and molecular architecture. This cannot be accomplished with industrially available materials. Therefore, the block copolymers and homopolymers reported in Table 3-2 have been designed so as to fulfill the requirements for such a study. As seen in Figures 4-1 and 4-2, the diblock copolymers span a wide range of molecular weights and cover the three basic equilibrium morphologies found in polystyrene continuous regime. Morphology can be further manipulated by blending (diblocks and homopolymers) and selective solvent casting.

The large deformation analysis of these materials is being conducted in this laboratory by Chris Schwier in an attempt to better understand

the underlying mechanisms of craze initiation and propagation in block copolymers and blends. Crazing is not discussed in the present work which focuses on the dynamic mechanical behavior of the same materials.

6.1.2 Small Deformation Properties: The small deformation (particularly dynamic mechanical) analysis of block copolymers and blends has proven to be an extremely valuable method of determining the structure-property relationships in these composite materials. Major phase transitions are the most obvious features observed in a dynamic mechanical test, e.g. scanning temperature at a constant frequency. Phase separated block copolymers such as KRATON and K-Resins exhibit multiple loss tangent ($\tan\delta$) peaks which correspond to the glass transition temperatures (T_g) of each component. A random copolymer having an equivalent monomer composition displays only one $\tan\delta$ peak (22). This aspect has been successfully exploited by Cohen and Ramos (23) in identifying the state of phase separation in polybutadiene, polyisoprene diblock copolymer-homopolymer blends.

Dynamic mechanic properties are also strongly dependent on composition and processing. Mechanical processing can affect properties by influencing microphase orientation. Kraus et al. (24) investigated a set of styrene-butadiene linear and star-shaped block copolymers (75% wt. polystyrene) and found significant variations in the dynamic mechanical properties as a function of lamellar and cylindrical domain orientation in extruded and molded films. Samples having a spherical morphology were mechanically isotropic.

As previously discussed (Sec. 4.1.5), solvent casting has a well

documented effect on the structural characteristics of block copolymers and blends. Nevertheless, the resulting dynamic mechanical behavior of these materials has never been fully resolved. Miyomoto et al. (25) conducted one of the earliest investigations into the influence of casting solvent on the dynamic mechanical properties of block copolymers. Their work on SBS (30%wt. polystyrene) demonstrated that the storage modulus, E', was significantly dependent on casting solvent. Also, a third loss tangent peak was observed in samples cast from methethylketone (MEK) and ethylacetate (EA). The authors suggested that this intermediate peak was due to a mixed interfacial material. Electron micrographs confirmed major structural differences between samples cast from different solvents. A similar but more extensive study was later conducted by Beamish et al. (26) on two SBS triblock copolymers. Their results were in good agreement with the previous study. E' and E'' (loss modulus) varied dramatically with casting solvent along with the microstructure. One difference was that the intermediate $\tan\delta$ peak found in the first study was only apparent as a small shoulder appearing at 60°C. The authors suggested that this shoulder might reflect a β-transition previously observed in atactic polystyrene. Two recent investigations have further examined the effects of solvent and structure on the dynamic viscoelasticity of SBS polymers (7,27). In neither case was an intermediate $\tan\delta$ peak observed, although both studies found large variations in dynamic properties as a function of casting solvent. Kotaka et al. (7) clearly demonstrated the accompanying structural changes.

Over the past decade, considerable effort has been directed at

examining how a mixed interlayer region influences the dynamic mechanical properties of block copolymers and blends. Numerous authors have attributed intermediate peaks and shoulders in modulus and tanδ to relaxations due to an interphase (10,25,26). In most cases, these conclusions are clouded by morphological variations arising from casting solvent effects (25,26). Wilkes et al. (28) recognized this point but nevertheless suggested that casting solvents influence interfacial mixing and the resulting dynamic mechanical properties. Diamant et al. (29) have recently extended this idea in modeling the viscoelastic behavior of SBS block copolymers. Details concerning the interfacial composition are inferred from parameters used in fitting a modified two-phase Nielson model (30) to torsion pendulum data. In this manner variations in viscoelastic behavior, resulting from different casting solvents, were ascribed to changes in interfacial composition. Unfortunately, the structural state of their samples were not clearly identified.

In this author's opinion, Kraus and Rollmann (31) have conducted the only systematic investigation into the nature of the dynamic viscoelastic behavior of block copolymer domain boundaries. Triblock copolymers (SBS, SIS, BSB) covering a wide range of molecular weights at constant composition (50%wt. polystyrene) were analyzed at 35 Hz using a Rheovibron. Casting solvent (toluene) and morphology (lamellar) were kept constant over all samples. Although no secondary loss maximum was found between the two domain glass transitions, increasing the interfacial volume fraction did lead to major changes in the material properties. Kraus and Rollmann also concluded that the mixed interlayer is

asymmetric, rich in polystyrene.

The following conclusions can immediately be drawn from the above discussion. A mixed domain boundary does in fact influence the dynamic mechanical properties of block copolymers although the phenomenon is not entirely understood and, most significantly, all these investigations have been performed on triblock copolymers containing a minimum of 50% rubber. The latter point is rather surprising since the characteristics of the glassy-rubbery interface purportedly affect crazing (16,18,21) in rubber-modified thermoplastics.

The present study has attempted to eliminate those structural features which might obscure identification of viscoelastic behavior attributable to a mixed interphase. Choice of a spherical morphology avoids the possibility of mechanical anisotropy while maintaining the ability to film cast diblock copolymers containing 13% by volume polybutadiene from a variety of solvents. Furthermore, this morphology is well-suited for structural analysis (Chapters 4 and 5) and complements the large deformation study being conducted in this laboratory. For these reasons, the present investigation focuses almost exclusively on a morphology of polybutadiene microspheres dispersed in a polystyrene matrix.

6.2 EXPERIMENTAL METHODS

6.2.1 Sample Preparation: Polymer films were solvent cast using the previously described spin casting technique (Sec.4.4.2). All blends appearing in Table 4-5 (except SB4/S2/B1) were cast from a solvent mixture of tetrahydrofuran and methylethylketone (THF/MEK) (Table 4-4).

Diblock copolymers containing approximately 12 wt% polybutadiene (Table 3-1) and sample S3 were cast from toluene and, in addition, films of SB_d1 and SB4 were prepared from THF/MEK. As previously mentioned blended samples SB9/S3 and SB4/S2/B1 contained phase-separated homopolymer and therefore were not mechanically tested. In each case film thicknesses ranged from 0.22 to 0.30 mm.

Films prepared from SB3/S1 were found to be extremely brittle, due to the low molecular weight of S1, making dynamic mechanical testing nearly impossible. Blending SB3 with S2 resulted in a transparent film, containing no discernible heterogeneities, which was suitably tough for mechanical analysis. Likewise, sample SB2 was blended with S2 in order to increase toughness. In both cases the microstructure remained unaffected.

Films prepared from SB_d1, SB1 and SB2/S2 were also found to be quite brittle, which consistently led to specimen fracture between 30° and 70°C during dynamic mechanical testing. These materials could be considerably toughened by lightly crosslinking the polybutadiene phase. Such specimens were obtained by irradiating cast films with a 3 MeV electron beam to a total dose of 10 Mrads.

Sample SB9 was cast into a 0.6 mm film from a solution of methylcyclohexane/benzene (Table 4-4). The resulting morphology was rubber continuous (phase inverted) as illustrated in Figure 4-7.

All films were annealled as previously specified (Sec. 4.4) and cut into 1 mm (±.05) wide sections. Test specimens ranged in length from 5.5 to 6.5 cm.

6.2.2 Dynamic Mechanical Testing: Dynamic mechanical properties of the various samples were determined using a direct reading dynamic viscoelastometer, Rheovibron Model DDV-II-C (Toyo Baldwin Company, Ltd., Tokyo, Japan). This instrument was fitted with a low temperature chamber (IMASS, Inc., Accord, Mass.) thereby extending the range of operation down to -150°C. During operation, this chamber is kept under nitrogen in order to avoid moisture condensation.

Takayanagi (32) has detailed the principles of operation of this instrument which can be operated in tension, shear, flexure and compression. All the measurements to be discussed were obtained in the tensile mode. Briefly, a sample is subjected to a sinusoidal displacement on one end, and the resulting force generated measured at the other end. Under steady-state conditions it is found that the strain lags the stress by an angle δ and the Rheovibron displays this phase angle as $\tan\alpha$.

Massa (33) has provided a complete analysis of the Rheovibron, including corrections for various instrument and sample-induced errors. In tensile geometry the complex modulus is defined as,

$$|E^*| = \left[\frac{F}{X}\right]\left[\frac{L}{S}\right] \qquad 6\text{-}1$$

where
F = force (N)
X = displacement (m)
L = sample length (m)
S = sample cross sectional area (m^2)

Equation 6-1 has been modified as follows (33),

$$|E^*| = \frac{(C/A - M\omega^2 D_{oc})}{\left\{D[1+(D_{oc}/D)^2 - 2(D_{oc}/D)\cos\alpha]^{1/2} - D_{ov}\right\}} \left[\frac{L}{S}\right] \qquad 6\text{-}2$$

where
- M = sample mass (Kg)
- C = constant = 2 MN/m
- ω = frequency (Hz)
- α = phase angle (from instrument)
- D = dynamic force (from instrument)
- A = preset amplification factor
- D_{oc} = instrument compliance correction
- D_{ov} = grip correction

Several correction terms appear in equation 6-2. D_{oc} is a result of the finite stiffness of the instrument and can be determined by replacing the sample with a short metal strip. The resulting dynamic force reading equals the correction, and was found to be $D_{oc} = 24/A$, which is consistent with a previous study (34) conducted on this instrument. $M\omega^2 D_{oc}$ represents an inertial correction term which for low frequencies and small masses can be neglected.

D_{ov} is a grip correction which depends upon sample characteristics and operating frequency and can be eliminated by employing an end-butting technique introduced by Voet and Morawski (35). This method involves epoxying both ends of a tensile sample to small aluminum plates which are in turn held in the sample grips. Ramos (34) found this method particularly useful in studying elastomers. Unfortunately, the small sample cross-sectional areas necessitated by working with glassy polymers, along with increased applied forces, prohibits the use of end-butting in the present case.

In order to eliminate grip slippage, all specimens were epoxied (Epoxi-Patch, Dexter Corp.) to the broad side of a 0.5 mm thick

aluminum tab, insuring that the polymer film was entirely potted in epoxy. The assembly was then annealled at 120°C for 24 hours to fully cure the epoxy and raise its glass transition temperature above that of polystyrene. Subsequent mechanical testing was generally conducted within two weeks. This end-tabbing technique necessitated determination of D_{ov}, which was accomplished by measuring D at various sample lengths. A plot of D vs. L yielded a straight line for which the zero length intercept equals $D_{ov}+D_{oc}$. Based on structural similarities, a single specimen geometry sufficed for all Rheovibron measurements. Therefore, only one grip correction was necessary throughout the study which was determined to be $D_{ov} = 15$.

Corrected equations for the storage modulus E', loss modulus E'' and $\tan\delta$ are given by (33),

$$|E'| = \frac{|E^*|\,(1-D_{oc}/D\cos\alpha)}{[1+(D_{oc}/D)^2-2(D_{oc}/D)\cos\alpha]^{1/2}}\,(\cos\alpha) \qquad 6\text{-}3$$

$$|E''| = \frac{|E^*|}{[1+(D_{oc}/D)^2-2(D_{oc}/D)\cos\alpha]^{1/2}}\,(\sin\alpha) \qquad 6\text{-}4$$

$$\tan\delta = E''/E' = (1-D_{oc}/D\cos\alpha)^{-1}\tan\alpha \qquad 6\text{-}5$$

Although Massa (33) dismissed the necessity of correcting $\tan\delta$ with equation 6-5, Ramos et al. (36) clearly demonstrated its importance and therefore, all $\tan\delta$ data have been corrected in this manner. Wedgewood and Seferis (37) have recently published an extensive updated

analysis of the Rheovibron with emphasis placed on identifying sources of measurement error. Since the present study focuses on determining the differences between samples, and all samples have very similar geometry and composition, such errors have been essentially eliminated.

Rheovibron measurements were conducted between -135°C and 110°C. The instrument was cooled to -150°C and subsequently slowly heated at a rate of less than 1°C per minute. Sample temperature was monitored by means of a copper-constantan thermocouple placed in close proximity to the sample and connected to a Hewlett Packard digital multimeter through a cold junction. All data were acquired at an operating frequency of 3.5 Hz.

6.3 DYNAMIC MECHANICAL PROPERTIES

6.3.1 Block Copolymers and Blends: Dynamic mechanical data collected on all samples (except SB_d3/S2/B1) were found to be well correlated with polybutadiene molecular weight. This result was expected based upon the structural similarities of these samples which will be discussed in detail in Chapter 7. Therefore, in order to facilitate property analysis, Rheovibron data have been reduced into the following four categories (see Tables 3-2 and 4-5):

Category	Samples
SB-A	SB1, SB_d1
SB-B	SB2/S2, SB4
SB-C	SB3/B2, SB5/S2 SB_d3, SB6/S2, (SB7)
SB-D	SB8/S3, SB9/S2

Determination of the influence on dynamic mechanical properties of casting solvent, perdeuteration and crosslinking of the polybutadiene phase was accomplished using category SB-A. None of these variables had any significant influence on the SB-A samples. This point is illustrated in Figure 6-1 in which E' and E'' are plotted for each of the three variables. The solid curves in Figure 6-1 were obtained from the interpolation of data from three separate Rheovibron spectra, e.g. SB_d1 and SB1 cast from toluene and SB_d1 cast from THF/MEK, each lightly crosslinked. Although the individual data points are not specified (for clarity), they are all well represented by the "hybrid" curves, particularly in the case of E' and for temperatures less than -50°C and greater than 20°C in E''. Data from the uncrosslinked sample (SB_d1 cast from THF/MEK), shifted vertically for the purpose of identification, also exhibits no noticeable variations from the hybrid curves.

Hybrid curves for SB-B, SB-C and SB-D have been obtained in the same manner as SB-A and are shown in Figures 6-2, 6-3 and 6-4. In all but one case (SB7) the data are well represented by the composite curves, particularly in the polybutadiene and polystyrene phase transition regions. Since no trends in individual data were apparent within hybrid plots, individual sample specification has been deleted to avoid confusion. For no apparent reason, the mechanical spectra of sample SB7 deviates considerably from the others in Figure 6-3 in the region of the polybutadiene phase transition. This is believed to be an artifact of the experiment and so these data were not included in determining the SB-C hybrid data set.

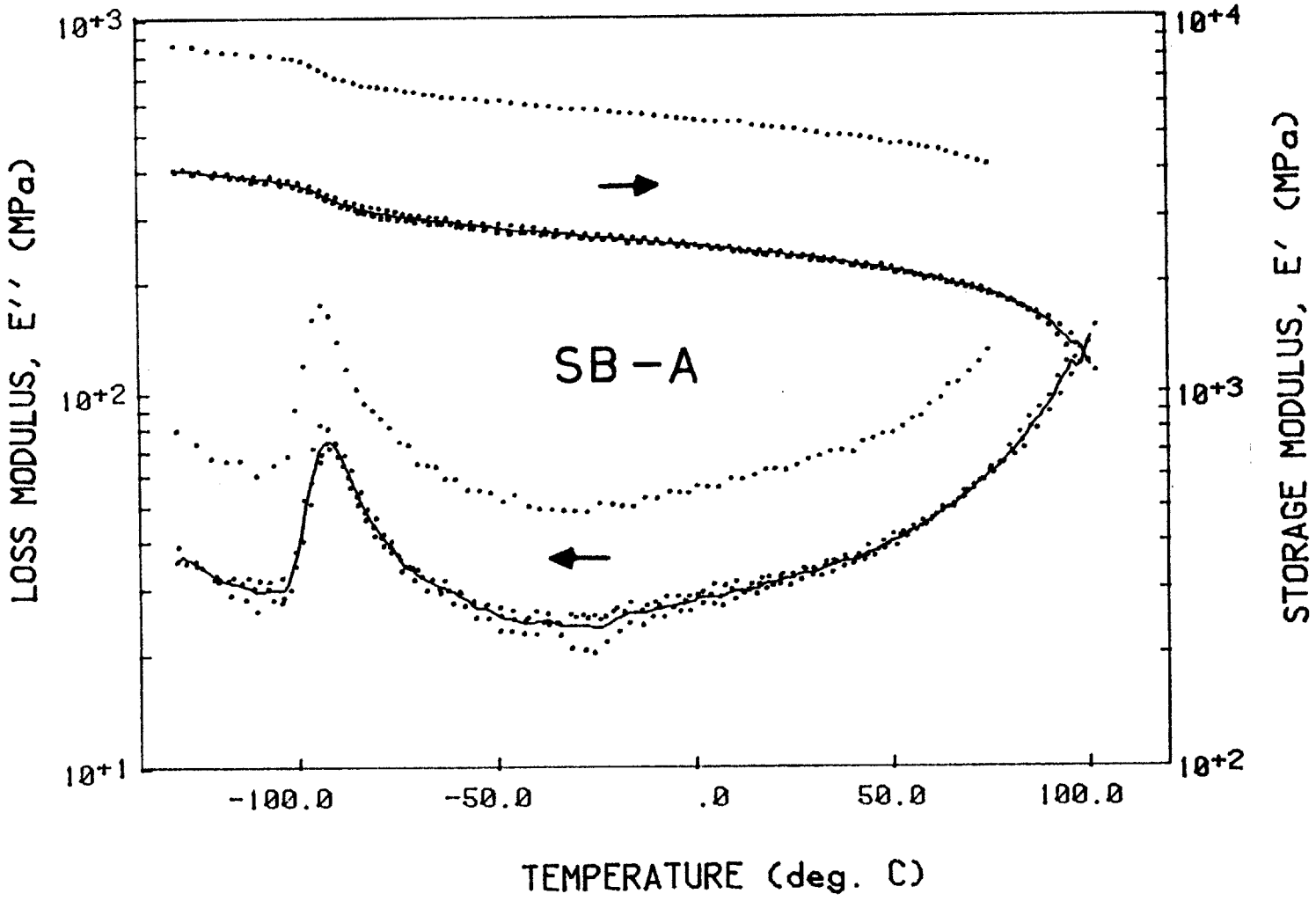

Figure 6-1 Category SB-A hybrid curves obtained from lightly crosslinked specimen of samples SB_d1 and SB1. Vertically shifted data are from an uncrosslinked SB_d1 sample.

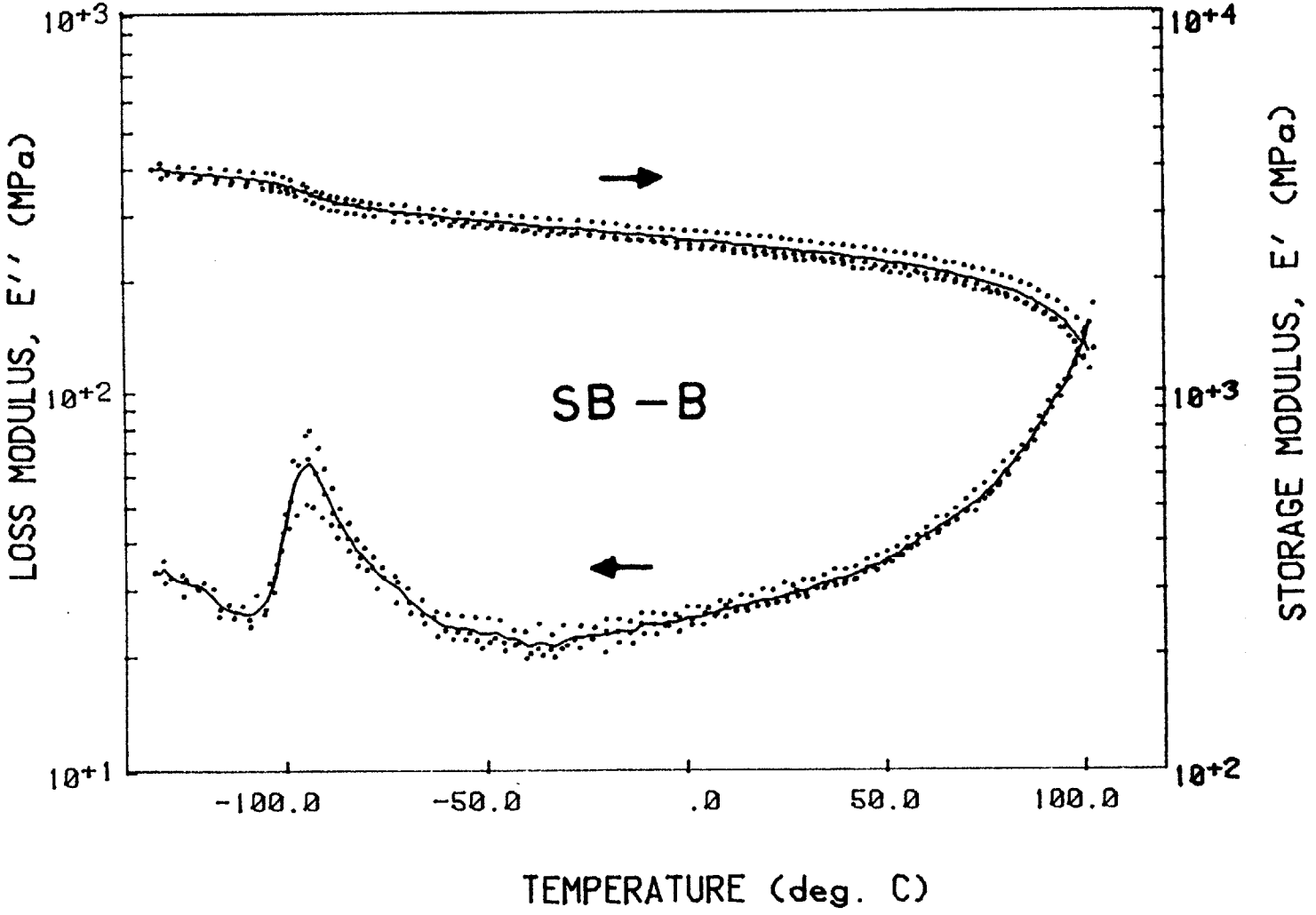

Figure 6-2 Category SB-B hybrid curves obtained from samples SB4 and lightly crosslinked SB2/S2

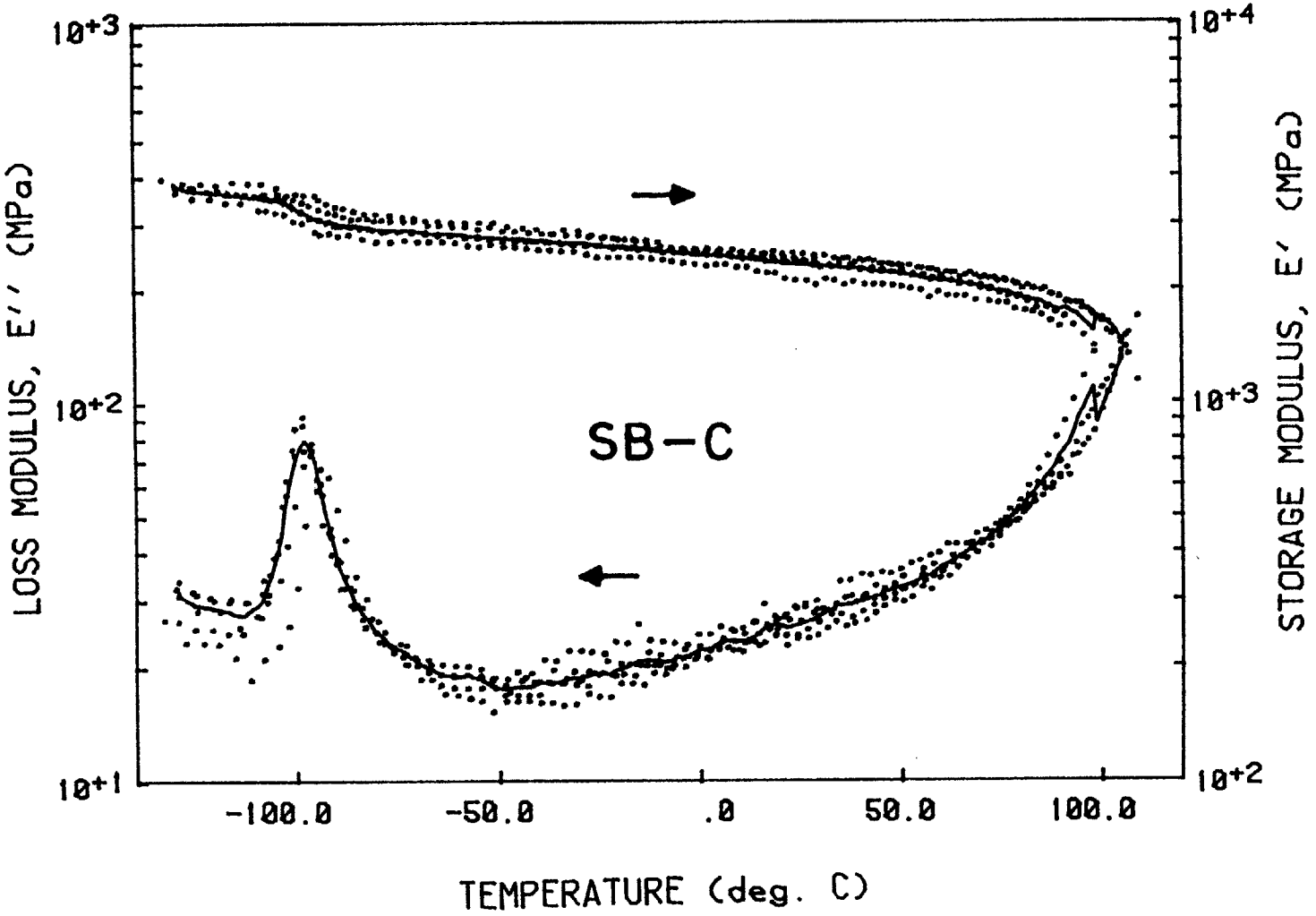

Figure 6-3 Category SB-C hybrid curves obtained from samples SB_d3, SB3/S2, SB5/S2 and SB6/S2. SB7 data are also included in this graph.

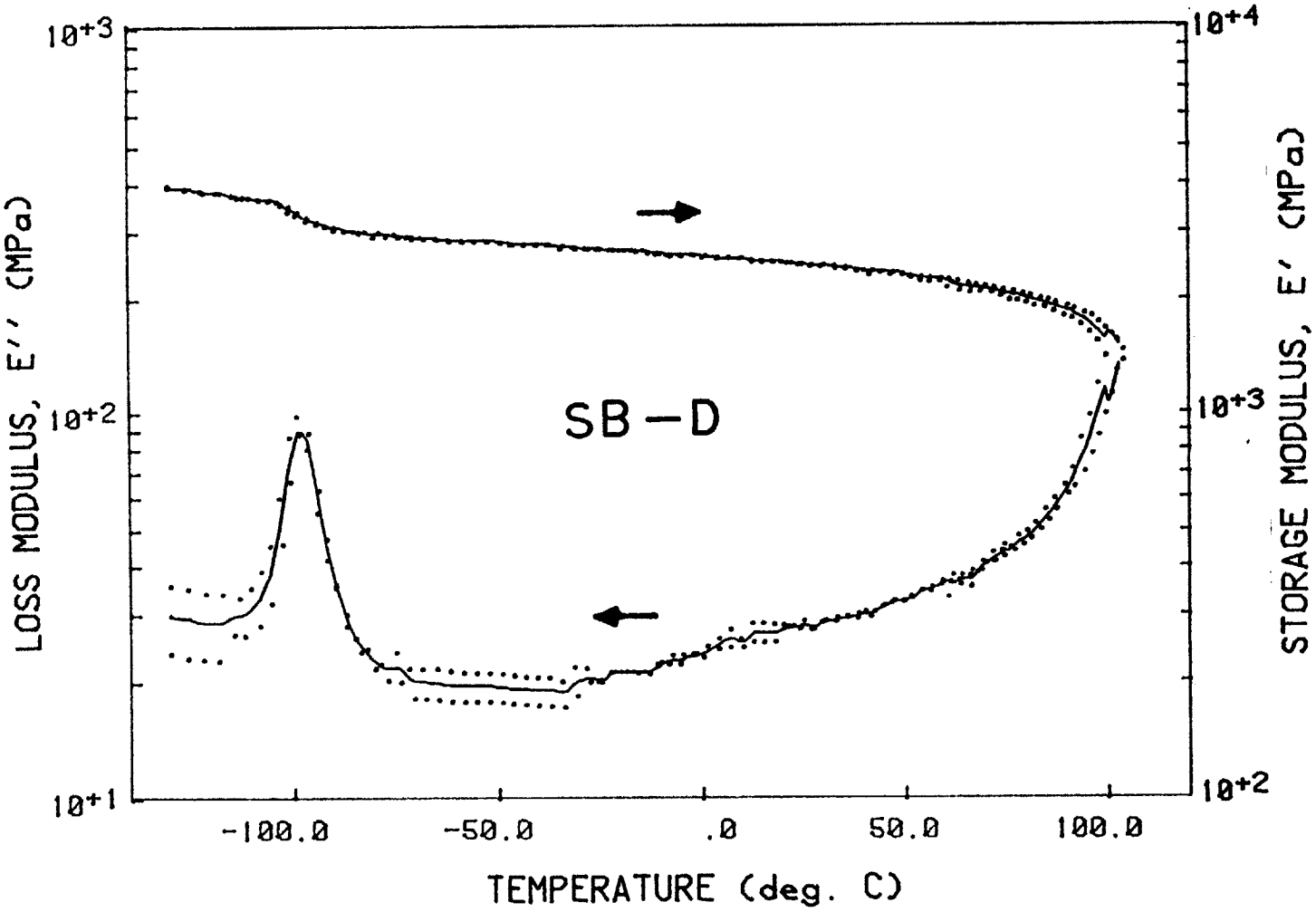

Figure 6-4 Category SB-D hybrid curves obtained from samples SB8/S3 and SB9/S2

6.3.2 Composite Properties: Dynamic mechanical spectra were also obtained from polybutadiene (sample B2) and polystyrene (sample S3) for comparison with the hybrid curves reported in the previous section. The Rheovibron data for the polybutadiene specimen were taken by José Torradas of this laboratory on a lightly crosslinked (10 Mrad) toluene cast specimen.

A plot of storage modulus versus temperature for samples B1, S2, SB_d3/S2/B1 and the four hybrid data sets are given in Figure 6-5 with the corresponding plot for the loss modulus appearing in Figure 6-6. As expected, the composite materials exhibit a storage modulus intermediate to that of the corresponding homopolymers. A combination of low rubber content (~13% volume) and near complete parallel coupling (16) leads to the observed high levels of E'. Most significant is the similarity exhibited between each hybrid curve and SB_dB/S2/B1 in Figure 6-5. In contrast, noticeable differences are apparent between these curves in the loss modulus plot (Figure 6-6). Discussion of the detailed behavior of E' and E'' in these materials will be taken up in Chapter 7 and therefore, no attempt has been made to identify individual hybrid curves in Figures 6-5 and 6-6.

Comparison of the composite curves in Figures 6-5 and 6-6 with that of polybutadiene, in its glass transition region, is complicated by the three decade change in E' and E'' in the latter. Instead, tanδ has been plotted versus temperature in Figure 6-7 for comparitive purposes. Composite tanδ curves very closely resemble those obtained for E'', a result of the near constant character of E'. Immediately obvious is the large difference in the polybutadiene glass transition

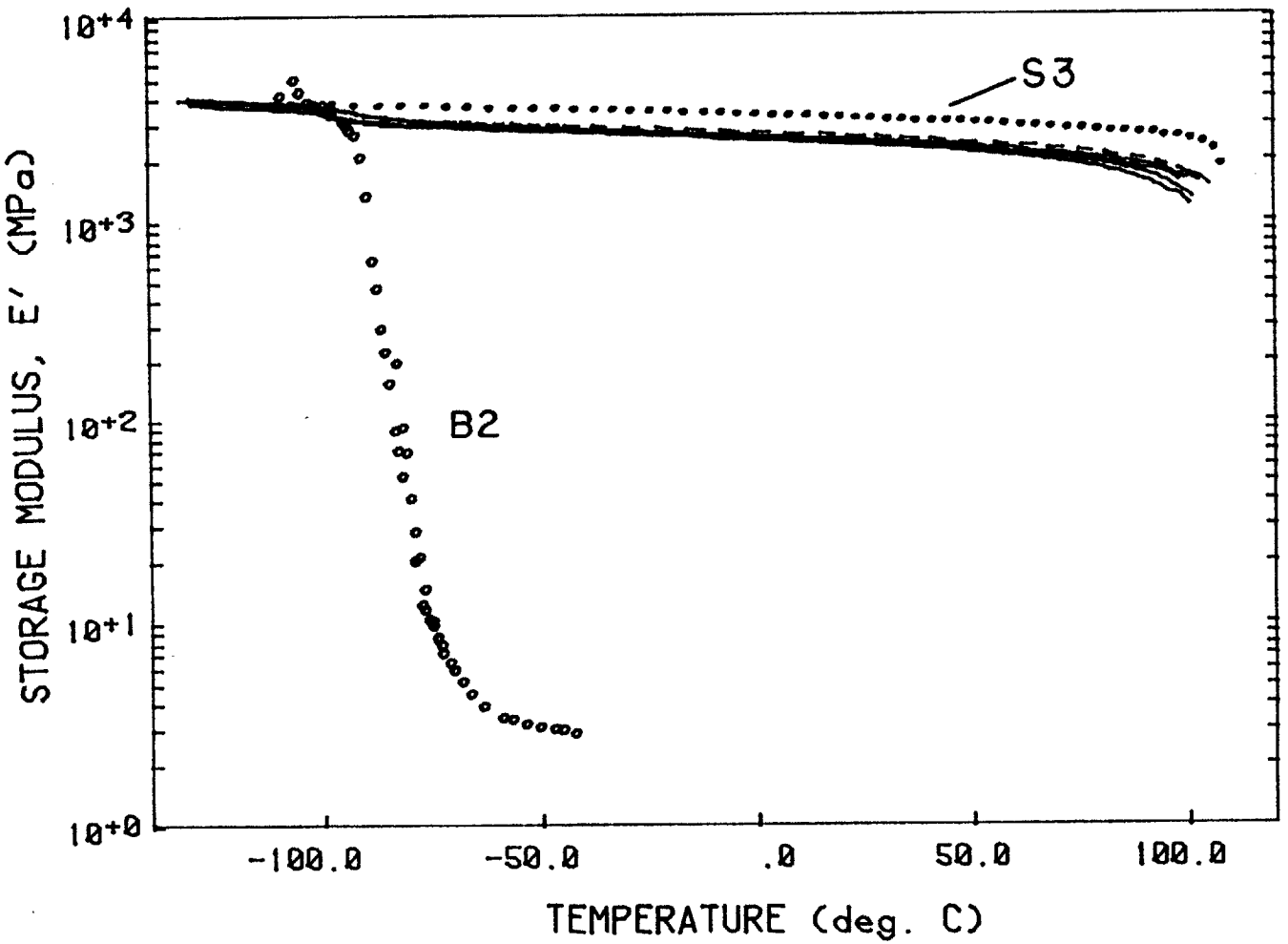

Figure 6-5 Solid curves are hybrid composite materials and dashed curve is sample $SB_d3/S2/B1$.

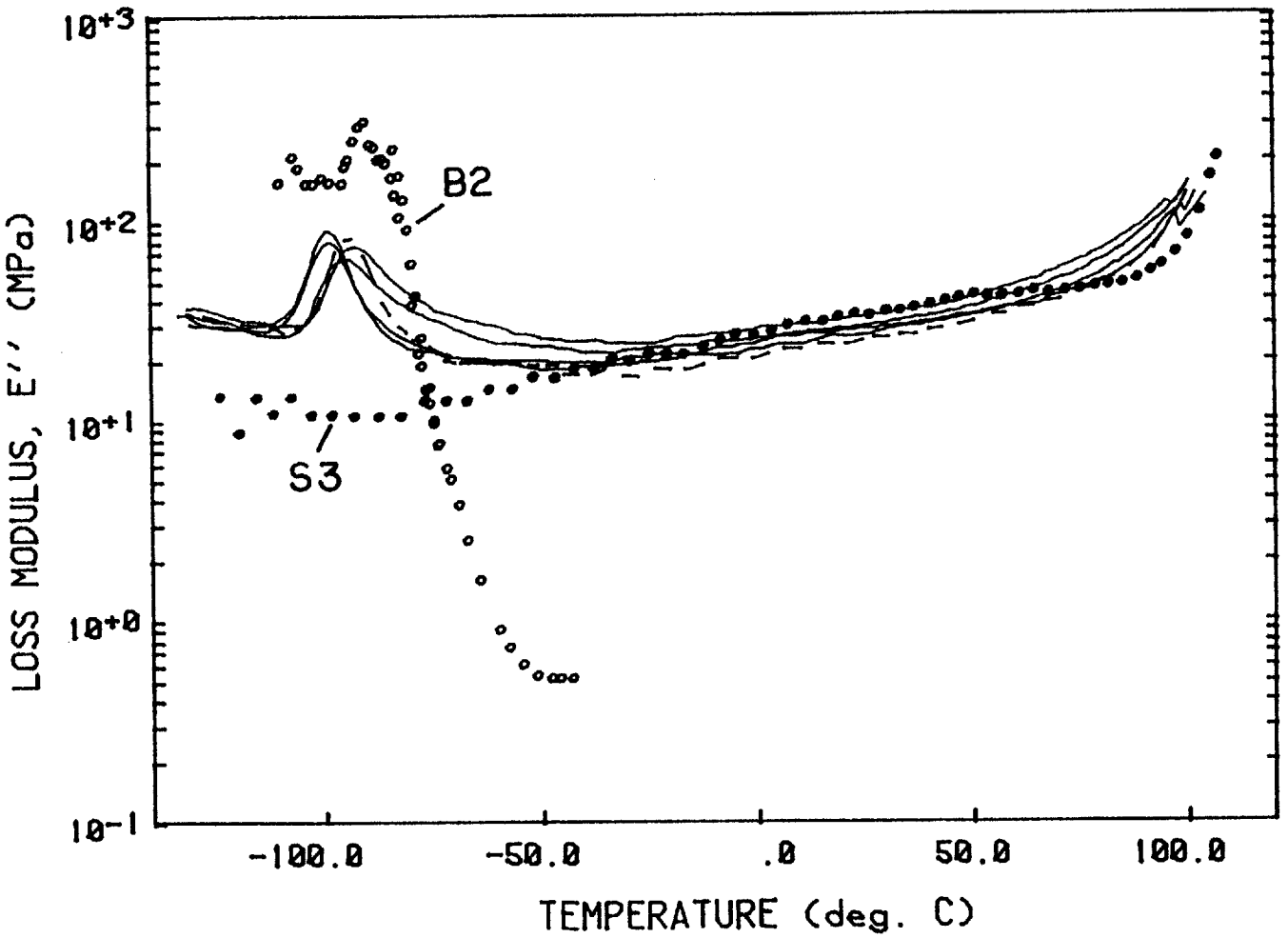

Figure 6-6 Solid curves are hybrid composite materials and dashed curve is sample $SB_d3/S2/B1$.

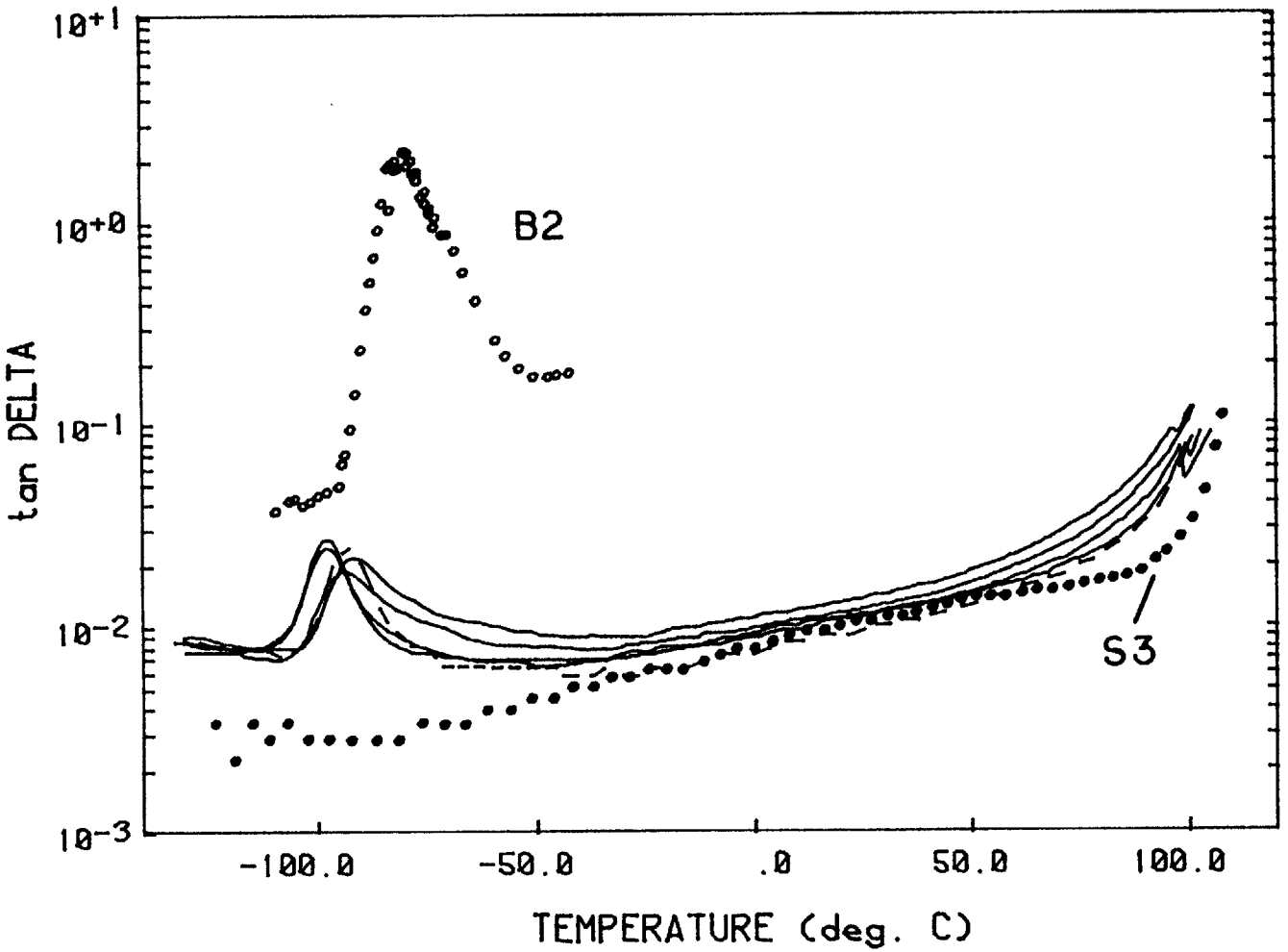

Figure 6-7 Solid curves are hybrid composite materials and dashed curve is sample $SB_d3/S2/B1$.

temperature T_g^B, determined by tanδ peak location, for the composite materials relative to that of homopolybutadiene. As discussed in Chapter 7, this temperature shift can be attributed to a rubbery dispersed, glassy continuous morphology.

In order to test this hypothesis and preclude the possibility that a microstructural variation between sample B2 and the composite samples is responsible for the T_g^B shift, sample SB9, cast from methylcyclohexane/benzene (see Fig. 4-7), was examined. These results, together with those for samples B2 and SB9/S2 are presented in Figure 6-8. The increased size of the SB9 tanδ peak relative to that of SB9/S2 is the combined result of a higher rubber content and a different morphology; this is analogous to the B2 peak being larger than that for SB9. Therefore, since SB9 exhibits the same T_g^B as B2 and SB9/S2 contains the same polybutadiene molecules as SB9, the T_g^B shift observed in the composite samples, as represented by SB9/S2, must be morphology related.

Both the large T_g^B shift exhibited by all composite samples and the smaller variation in T_g^B between individual hybrid curves as seen in Figure 6-7 will be discussed in Chapter 7.

6.3.3 Aging effects: While the present study does not focus on the phenomenon of aging, any investigation involving glassy polymers must take its effects into account. This subject has been reviewed in the literature (38) and a related topic (glass transition phenomena) has recently been investigated by a member of this research group (39). To date almost all work has dealt with single phase systems.

Potential property differences arising from aging amongst samples was minimized by annealling and cooling all specimens under the same

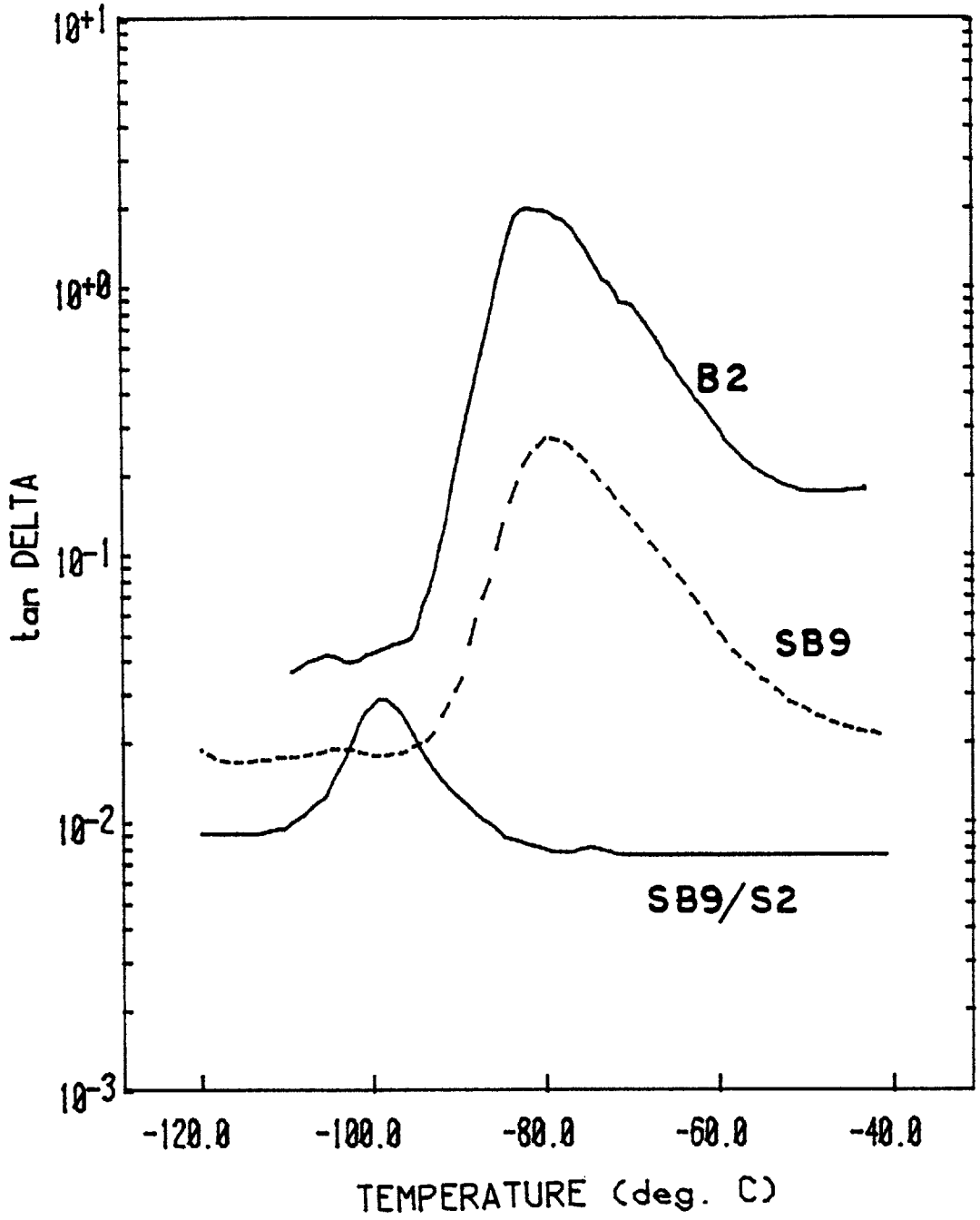

Figure 6-8 Identification of T_g^B in polybutadiene homopolymer (-80°C) rubber continuous diblock copolymer (Fig. 4-7) (-80°C) and polybutadiene microspheres (Fig. 4-8) (-99°C).

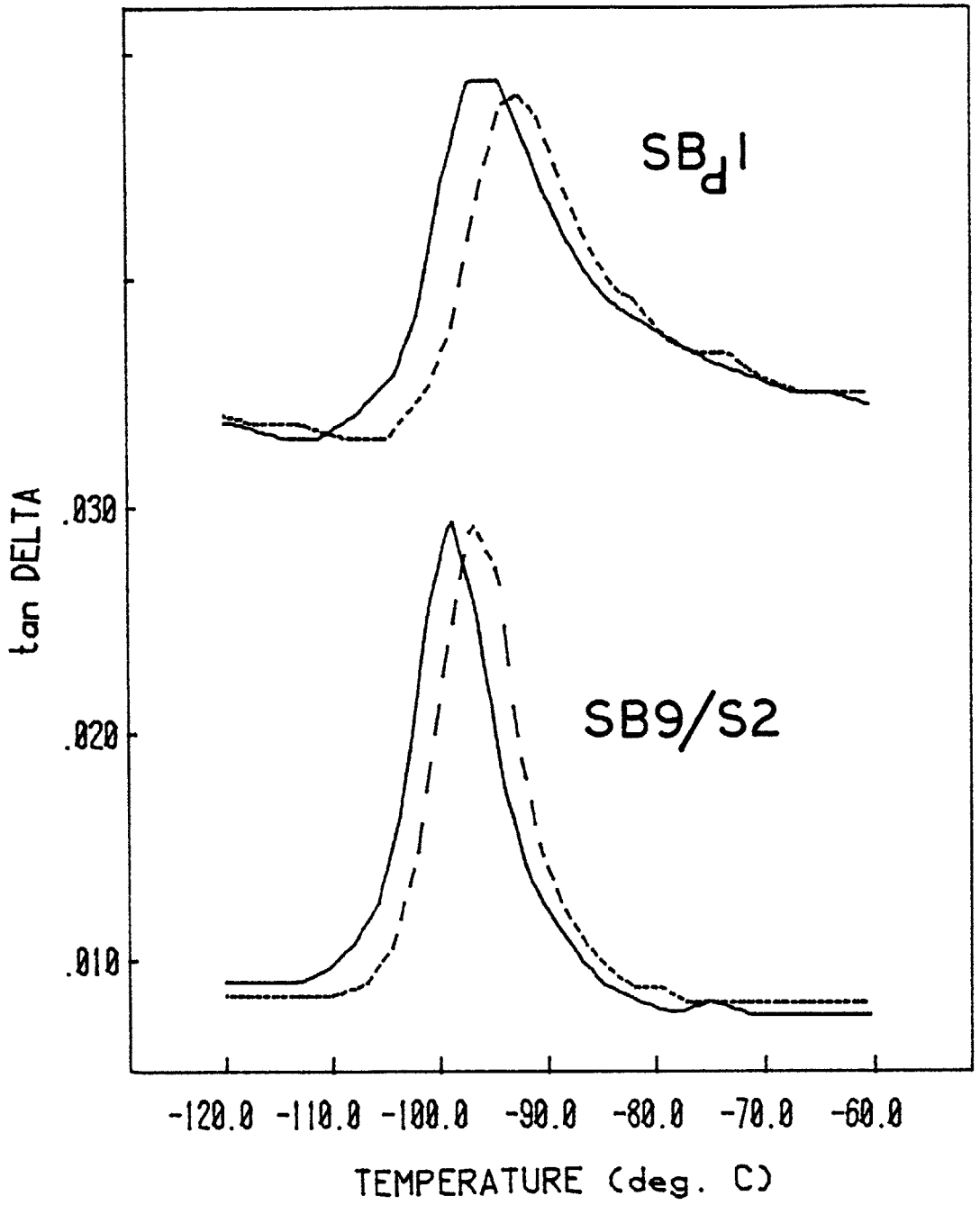

Figure 6-9 Effects of aging on the polybutadiene glass transition spectra. Solid curves are from freshly annealled specimens and dashed curves are from the same specimens after aging 100 days at room temperature. SB_dl curves have been shifted vertically 0.025 units in tan δ.

conditions (Sec. 4.4.2) and examining them within two weeks. In order to assess the magnitude and possible domain-size dependence of aging on their dynamic mechanical properties, specimens of SB_d1 and SB9/S2, each cast from THF/MEK, were examined within 24 hours of annealling and subsequently after 100 days at room temperature. A noticeable variation in tan δ was found in both samples below -80°C after 100 days of aging. As seen in Figure 6-9, each curve has shifted 2°C higher in temperature while essentially maintaining the same shape. These results, representing the limits in polybutadiene molecular weight (domain dimensions), will be discussed in conjunction with the other dynamic mechanical properties in Chapter 7.

References

1 (a) R. Milkovich, S. African Pat. Application 642,271 (1964), Brit. Pat. 1,000,090 (1965) (b) R. Milkovich, G. Holden, E.T. Bishop and W.R. Hendricks, Brit. Pat. 1,035,873 (1966).

2 G. Holden, E.T. Bishop and N.R. Legge, J. Polymer Sci., C, 26, 37 (1969).

3 E.T. Bishop and S. Davison, ibid., p. 59.

4 M. Morton, J.E. McGrath and P.C. Juliano, ibid., p. 99.

5 T.L. Smith and R.A. Dickie, ibid., p. 163.

6 R.F. Fedors, ibid., p. 189.

7 T. Kotaka, T. Miki and K. Arai, J. Makromol. Sci.-Phys., B17(2), 303 (1980).

8 R.E. Cohen and N.W. Tschoegl, Intern. J. Polymeric Mater., 2, 49 (1972).

9 Y.-D.M. Chen and R.E. Cohen, J. Appl. Polymer Sci., 21, 629 (1977).

10 R.E. Cohen and N.W. Tschoegl, Trans. Soc. Rheology, 20, 1, 153 (1976).

11 G. Kraus, J. Appl. Polymer Sci., 7, 861 (1963).

12 L.M. Fodor, A.G. Kitchen and C.C. Biard, A.C.S. Plast. Chem. Org. Casting Preprints, 34 (1), 130 (1974).

13 A.G. Kitchen and F.J. Szalla (Phillips Petroleum Co.), U.S. Pat. 3,639,517 (1972).

14 R.P. Kambour, J. Polymer Sci.: Macromolecular Reviews, vol. 7, 1-154 (1973).

15 S. Rabinowitz and P. Beardmore, CRC Crit. Revs. Macromol. Sci., 1, 1 (1972).

16 C.B. Bucknall, Toughened Plastics, Applied Sci. Publishers, London (1977).

17 H. Kawai, T. Hashimoto, K. Miyoshi, H. Uno and M. Fujimura, J. Macromol. Sci. Phys., B17 (3), 427 (1980).

18 A.S. Argon, R.E. Cohen, B.Z. Jang and J.B. VanderSande, J. Polymer Sci., Phys. Ed., 19, 2, 253 (1981).

19 A.S. Argon and M.M. Salama, Phil. Mag., 36, 1217 (1977).

20 H. Andersson and H. Bergkvist, J. Mech. Phys. Solids, 18, 1, (1970).

21 A.S. Argon, Pure Appl. Chem., 43, 247 (1975).

22 C.W. Childers and G. Kraus, Rubber Chem. Tech., 40, 1183 (1967).

23 R.E. Cohen and A.R. Ramos, Macromolecules, 12, 131 (1979).

24 G. Kraus, L.M. Fodor and K.W.Rollmann, Adv. Chem. Series, no. 176, 277 (1979).

25 T. Miyomoto, K. Kodama and K. Shibayama, J. Polymer Sci., A-2, 8, 2095 (1970).

26 A. Beamish, R.A. Goldberg and D.J. Hourston, Polymer, 18, 49 (1977).

27 N.K. Kalfoglou, J. Appl. Polymer Sci., 23, 2385 (179).

28 G.L. Wilkes, S. Bagrodia, Z. Ophir and J. Emerson, J. Appl. Phys., 49, 10, 5061 (1978).

29 J. Diamant, D.S. Soong and M.C. Williams, to appear in Contemporary Topics in Polymer Sci., vol 4, ed. W.J. Bailey, Plenum Press, N.Y. (1981).

30 L.E. Nielson, Rheol. Acta., 13, 86 (1974).

31 G. Kraus and K.W. Rollmann, J. Polymer Sci. Phys. Ed., 14, 1133 (1976).

32 M. Takayanagi, Mem. Fac. Eng. Kyushu Univ., 23, 1 (1963).

33 D.J. Massa, J. Appl. Phys., 44, 2595 (1973).

34 A. Ramos, Sc.D. thesis, Massachusetts Institute of Technology (1977).

35 A. Voet and J.C. Morawski, Rubber Chem. Tech., 47, 758 (1974).

36 A.R. Ramos, F.S. Bates and R.E. Cohen, J. Polymer Sci. Phys. Ed., 16, 753 (1978).

37 A.R. Wedgewood and J.E. Seferis, Polymer, 22, 966 (1981).

38 L.C.E. Struik, Physical Aging in Amorphous Polymers and Other Materials, Elsevier Scientific Publishing Company, Amsterdam (1978).

39 C.C. Wu, Sc.D. thesis, Massachusetts Institute of Technology, (1981).

CHAPTER 7: Structure-Property Analysis

The dynamic mechanical properties of the block copolymers and blends discussed in Chapter 6 can be related to their structural characteristics which were identified in Chapter 5. Findings concerning both the structural and mechanical properties of these materials touch on several current issues in polymer science. These points are developed in the following chapter.

7.1 STRUCTURAL ANALYSIS

7.1.1 Interface: As demonstrated in Figure 5-7, SANS data analysis, using each of the three modified Porod expressions, led to consistent domain boundary profiles. In particular, the Helfand and sigmoidal models led to nearly identical interfacial profiles. A more careful examination of Table 5-3 reveals several important additional facts. The measured values of interfacial thickness are essentially the same for each of the three samples studied. From this one can infer that neither molecular weight nor homopolystyrene content influences this parameter. Furthermore, the measured interfacial thicknesses of both a low molecular weight (SB_d1) and high molecular weight (SB_d3) diblock copolymer were found to be independent of casting solvent. Finally, aging sample SB_d1-T for 6 months at room temperature had no effect on the domain boundary.

Several authors have predicted the existence and dimensions of a diffuse domain boundary in phase separated block copolymers (1-5). All

these theories are based upon an interaction parameter χ (or Λ), defined in terms of a particular model of the mixing free energy. In order to critically compare theoretical predictions of the interfacial thickness with experimental results, we must first determine this parameter.

Fortunately, the interaction parameter for polystyrene and 1,4 polybutadiene has been reported in the literature. Several recent publications (4,6) have made use of an expression determined by Rounds (7) for predicting the interaction parameter for the polystyrene-polybutadiene (polyisoprene) pair. Examination of the original study reveals that based upon 95% confidence limits, χ can only be estimated within $\pm$72% at 25°C. Roe and Zin (8) have recently presented new results concerning the determination of the interaction parameter for the polystyrene-polybutadiene pair. They found Λ to be weakly dependent on temperature and composition ϕ,

$$\Lambda = \lambda_0+\lambda_1\phi_1+\lambda_T T \ (\text{cal/cm}^3) \qquad 7\text{-}1$$

where T is given in degrees Centigrade; ϕ for the present case will be taken to be 0.5. The constants appearing in equation 7-1 have been averaged over all the reported values and with 95% confidence limits are given by: $\lambda_0 = 0.996\pm.174$, $\lambda_1 = 0.040\pm.243$ and $\lambda_T = -0.00200\pm.00116$. This corresponds to a 22% confidence limit in Λ (and subsequently $\chi = \Lambda V_r/RT$) at 25°C. Using an average segment volume of $V_r = 75$ cm^3/mol (5), χ is determined from equation 7-1 to equal 0.123, which is nearly identical to that predicted by Rounds ($\chi = 0.125$). Nevertheless, the significant improvement in accuracy provided by Roe and Zin is an

important contribution.

Two popular theories concerning the interface in phase separated block copolymers have been examined in relation to the experimental findings of this work. Since the glass transition temperature of interfacial material should be intermediate to that of polystyrene and polybutadiene, the interfacial thickness is not expected to be "frozen" at the glass transition temperature of polystyrene. Therefore, a temperature of 25°C will be used in theoretical calculations.

Meier (1) has modeled the interface with the following sigmoidal profile,

$$\rho_B(r) = \sin^2\left(\frac{\pi r}{2\lambda}\right) \qquad 7\text{-}2$$

where $\rho_B(0) = 0$, $\rho_B(\lambda) = 1$ and λ represents the interfacial thickness. In order to compare the SANS results with this theory, λ must be proportioned to one of the previously defined interfacial thicknesses. To a good approximation this may be accomplished by matching the slope of the sigmoidal gradient model,

$$\rho_B(r) = 1/2[1-\mathrm{erf}(r/\sigma)] \qquad 7\text{-}3$$

with that of equation 7-2 at the inflection point. The proportionality constant so determined, $\lambda = 1.1\Delta R$ ($=1.8\ a_I$), results in a good correlation between profiles generated by equations 7-2, 7-3 and 4-2.

Meiers' (1) theory predicts that λ is a single valued function of the product of molecular weight and interaction parameter, ΛM. Although this theory was derived for a lamellar morphology, the author claims it

can be applied to other domain types as well. Based upon this assumption, the interfacial thickness for sample SB_d1 was determined to be λ = 35 Å in contrast to that obtained experimentally, λ_{exp} = 22 Å; for sample SB_d3, λ = 24 Å while λ_{exp} = 25 Å. Clearly the experimental results do not support the molecular weight dependence of λ predicted by this theory.

Direct comparison can be made between the value of a_I experimentally obtained and that predicted by Helfand and Wasserman (4,5) using equation 4-3:

$$a_I = 2b/(6\chi)^{1/2} \qquad 4\text{-}3$$

Here a_I is independent of molecular weight, consistent with the experimental findings. Using a Kuhn statistical length averaged over polystyrene and polybutadiene, b = 6.5 Å (5), and χ = 0.123±.027, the interfacial thickness is determined to be a_I = 15±2 Å. This value equals the average of the interfacial thicknesses reported in Table 5-3.

In a series of publications, Hashimoto et al. (6,9,10) have conducted a similar analysis of microdomain boundaries by SAXS in a set of diblock copolymers and blends consisting of polystyrene and vinyl (1,2-,3,4) polyisoprene. Consistent with this study, they found that the interfacial thickness is essentially independent of molecular weight, domain type and homopolymer content (up to 60% weight). In a limited study they also found no dependence of this parameter on casting solvent. As indicated above and demonstrated by Figure 5-7, the definition of "interfacial thickness" is model dependent and not a unique parameter. This point was overlooked by Hashimoto et al. in

comparing their results, ΔR = 18 Å, with Helfand's theory (4,5). Based upon an average segment volume of V_r = 84 cm^3/mol (5) and b = 6.5 Å, a polyisoprene-polystyrene interface is predicted to be $a_I = 14 \pm 2$ Å thick. The interfacial thickness determined by Hashimoto et al., when proportioned for comparison (4) is $a_I = .64\Delta R$ = 12 Å. This slightly lower than predicted value is not surprising since χ for polystyrene-vinyl polyisoprene is expected to be larger than that for polystyrene-1,4 polybutadiene (11) which was used in the calculation.

Richards and Thomason (12) have also recently measured the interfacial thickness of a polystyrene-polyisoprene diblock copolymer by SANS, although in this case the rubber consisted of a high cis 1,4 microstructure. Using a linear gradient model, they obtained an interfacial thickness of E = 29 Å, which upon conversion yields $a_I = 0.64E$ = 19 Å. Since only one sample was examined it is not possible to assess the significance of the difference between this result and that found in the present work and predicted by Helfand.

The findings of this study concerning the domain boundary in block copolymers, in conjunction with the improved estimate of Λ provided by Roe and Zin (8), clearly demonstrate the capabilities of equation 4-3 in predicting a_I.

7.1.2 Domain Dimensions: Sphere radii have been determined for all samples by electron microscopy (EM) and for five of these by SANS (Table 5-4). A comparison of these two techniques reveals an unexpected inconsistency as illustrated in Figure 7-1; $\bar{R}_{EM} \simeq 0.77 \bar{R}_{SANS}$, independent of

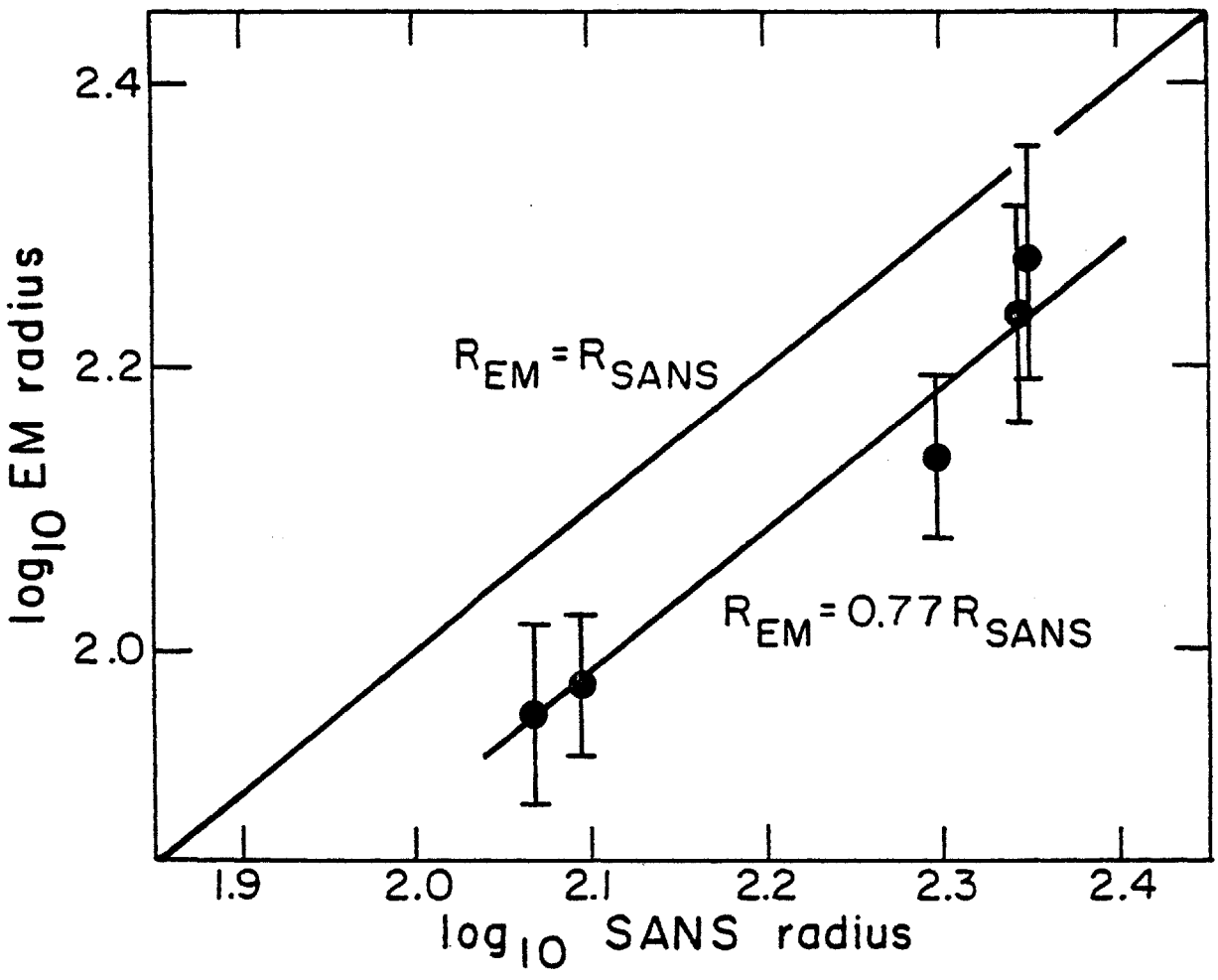

Figure 7-1 Comparison of sphere radii as measured by SANS and electron microscopy. Error bars indicate the standard deviation in the measurement of a representative population of ~100 spheres.

sphere size. Recently, Stribeck[1] (13) observed a similar phenomenon while examining crystalline polypropylene by SAXS and EM; samples subjected to EM analysis were contrast enhanced with chlorosulfonic acid. The results of Stribeck, $\bar{L}_{EM} \simeq 0.71\bar{L}_{SAXS}$ where L was the measured long period, are very similar to the findings of this work.

The mean radius measured from the projection of a set of uniform spheres is related to the section thickness and sphere radius as follows,

$$R_{meas} = R\left[\frac{1+ \frac{\pi R}{2t}}{1+ 2\frac{R}{t}}\right] \qquad 7\text{-}4$$

where R is the true radius and t is the sample thickness. For a specimen of thickness t = R, $R_{meas} = 0.86R$ while for conditions relevant to sample SB_d1, $t \geq 4R$, $R_{meas} \geq 0.93R$. Also, measured sphere size distributions were narrow ($\sigma_R/R \leq 0.13$) which would be inconsistent with that predicted for a thin film. Therefore, microtoming effects cannot account for the observed discrepancy.

Sample preparation for EM involves osmium staining followed by thin sectioning with subsequent bombardment by high energy electrons, known to cause damage in polymers, and the effects of these processes on apparent image size have not been thoroughly studied. The instrument was calibrated each time it was used, thereby excluding the possibility of magnification errors. Since the SANS experiments were

[1]Professor E.L. Thomas, University of Massachusetts, brought this reference to the author's attention.

TABLE 7-1

Domain Dimensions (Å)

Sample	[a] $\bar{R}$	[b] $\sigma_R/\bar{R}$	[c] $\bar{R}_{theoretical}$
[d] SB1	117	.07	129
SB2/S2	159	.08	199
SB3/S2	231	.13	333
SB4	152	.09	193
SB5/S2	200	.07	340
SB6/S2	243	.07	430
[d] SB7	243	.09	394
SB8/S3	298	.12	647
SB9/S2	355	.07	1032
[d] SB_d1	122	.06	137
[d] SB_d2/S1	224	.08	357
[d] SB_d3	177	.07	309
SB_d3/S2/B1	267	.42	-

[a] 1.30 times electron microscope value (see Fig. 7-1) [b] Based on a representative population of ~100 spheres in EM micrograph [c] Helfand and Wasserman (5), assuming blends are pure diblock copolymers
[d] Also determined by SANS, see Table 5-4 and Figure 7-1

carried out on unperturbed samples of macroscopic dimensions and since sphere size determination from the neutron scattering curves is relatively direct and unambiguous, the $\bar{R}_{SANS}$ values will be accepted as correct and the low EM values regarded as an artifact. It should also be noted that the mean standard deviation in sphere radii obtained by SANS, $\langle\sigma_R/\bar{R}\rangle_{SANS} = 0.11$ (Table 5-4), is slightly higher than that determined by EM, $\langle\sigma_R/\bar{R}\rangle_{EM} = 0.08$ (Table 7-1). This results from neglecting instrument resolution effects (Table 5-2) in equation 5-7; this has no bearing on the outcome of the present work which only requires knowledge of $\bar{R}$.

Domain dimensions not determined by SANS have been measured by EM and corrected using the proportionality constant cited above and are listed in Table 7-1. These sphere radii are also plotted against polybutadiene molecular weight in Figure 7-2. Based on the theory of Helfand and Wasserman (5), sphere radii have been calculated for each sample at a temperature of 90°C and are listed in Table 7-1 and plotted in Figure 7-2. In calculating predictions for blends, the polystyrene block molecular weight was adjusted in order to agree with the polybutadiene molecular weight and volume fraction; this was necessary because the theory does not account for homopolymer. Also included in Figure 7-2 are the SAXS results of Hashimoto et al. (6) obtained from a set of SI diblock copolymers.

The results shown in Figure 7-2 illustrate several interesting points. Sphere size is apparently dictated by polybutadiene molecular weight, independent of homopolystyrene content and casting solvent (see Table 5-4). Most striking is the discrepancy between the experimental

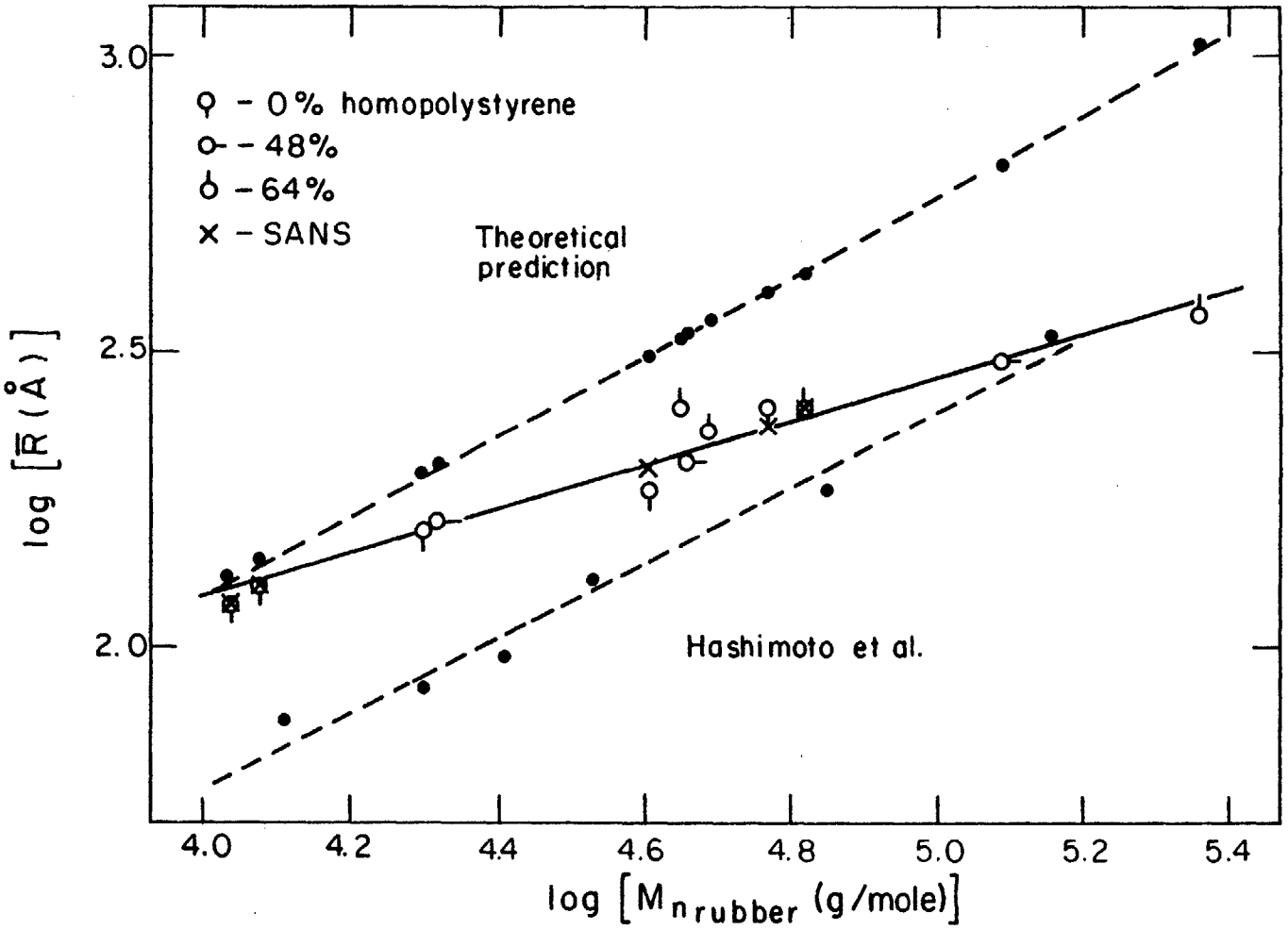

Figure 7-2 Open circles are 1.30 times the radius measured by electron microscopy (see Fig. 7-1). SANS points correspond to the open circle data of equal polybutadiene molecular weight.

and predicted results, each of which can be modeled by equation 7-5,

$$R = \kappa M^{\beta} \qquad 7\text{-}5$$

where $\beta_B = 0.37$, $\beta_I = 0.63$ (Hashimoto's results) and $\beta_{theory} = 0.68$. The power low dependence of $\beta_B = 0.37$ found in the present study is very surprising, particularly in light of the fact that in bulk polymers the radius of gyration increases with the square root of the degree of polymerization. Imposing the restrictions associated with a microphase should increase β to 0.68.

Solvent cast block copolymers reflect a morphology established in a solvated state (Sec. 4.1.5) and, as pointed out by Hashimoto et al. (6), in the case of spherical domains the bulk domain size is fixed by the number of chains per sphere, N, equilibrated with solvent at the point of phase separation. Subsequent adjustment of N requires the transport of SB chains through an S(B)-solvent matrix, an energy barrier which increases as solvent is removed. The magnitude of this energy barrier is illustrated by the fact that at constant polybutadiene molecular weight, (~50 kg/mol) a four-fold decrease in diblock molecular weight (i.e. a large decrease in viscosity) attained by blending homopolystyrene results in little or no effect on domain size. Therefore, the large variation in β between theory and experiment cannot be attributed to a decrease in diblock diffusivity with increasing molecular weight. Instead the explanation must lie with the state of the solvated polybutadiene domains.

The importance of micelle formation during block copolymer solvent casting was originally recognized by Inoui et al. (14), further

developed by Meier (15) and with one exception (16) little else has ensued. Pico and Williams (16) have presented an extension of the Leary and Williams theory (2,3), applicable to solvated ABA triblock copolymers and valid at the low solvent end of the composition scale. Unfortunately, computation of the criteria for micelle formation requires a cumbersome numerical scheme. Nevertheless, the concepts developed by Pico and Williams permit formulation of a qualitative model which can adequately explain the discrepancy between the results presented in Figure 7-2.

For a fixed composition, the temperature at which a block copolymer phase separates is proportional to its molecular weight and interaction parameter, $T_s \sim M\chi$. This product was estimated for a composition of 12% by weight polybutadiene at 90°C using the theory of Helfand and Wasserman (4). According to Leibler (17), for a given composition, $M\chi$ at the spinoidal point is a constant. Therefore, the value calculated at 90°C, $M\chi$ = 3.6 kg/mol, will be assumed to hold for all molecular weights and temperatures. Equation 7-1 provides the required temperature dependent relationship for $\chi(\Lambda)$.

Addition of a diluent to a block copolymer decreases T_s, hence it is possible to observe microphase homogenization at room temperature in the presence of a solvent (18). The results of Pico and Williams (16) indicate that, for a given composition and microstructure, T_s is linearly dependent on ϕ_s, the volume fraction of solvent at phase separation (homogenization). Lacking sufficient information for a complete analysis, the solvent dependent behavior of T_s has been modeled by simply modifying the bulk equilibrium relationship, determined by the

constant $M\chi$,

$$T_s = \left[\frac{16.4M}{1+.021M}\right](1-\phi_s) \qquad 7\text{-}6$$

where T_s is given in degrees Kelvin. Equation 7-6 applies to block copolymers containing 12% by weight polybutadiene which, in the limit of $\phi_s = 0$, reduces to the Helfand prediction. Using equation 7-6, T_s has been plotted versus M for several values of ϕ_s in Figure 7-3 (solid curves). These results are in qualitative agreement with the results presented by Pico and Williams (16), although these authors have neglected the temperature dependence of χ; this results in linear ϕ_s curves.

Figure 7-3 reveals the source of the discrepancy in β. At low molecular weight (SB1, SB_d1) the solvent content at phase separation is calculated to be only 30%, and correspondingly the bulk domains exhibit near equilibrium size. On the other hand, increasing molecular weight steadily increases the solvent content at phase separation; ϕ_s = 40% in SB4 and ϕ_s = 50% in SB7. This results in a deviation from bulk equilibrium structure since the bulk domain size is controlled by that which is established in solution. Pico and Williams have also predicted that T_s (and ϕ_s) is relatively insensitive to solvent type, provided the solubility parameter of the solvent is close to the range of parameters of the two blocks, consistent with the presently reported SANS results (Table 5-4).

Differences between the present data and that of Hashimoto et al. (6) can be explained in the same manner. The latter study was conducted

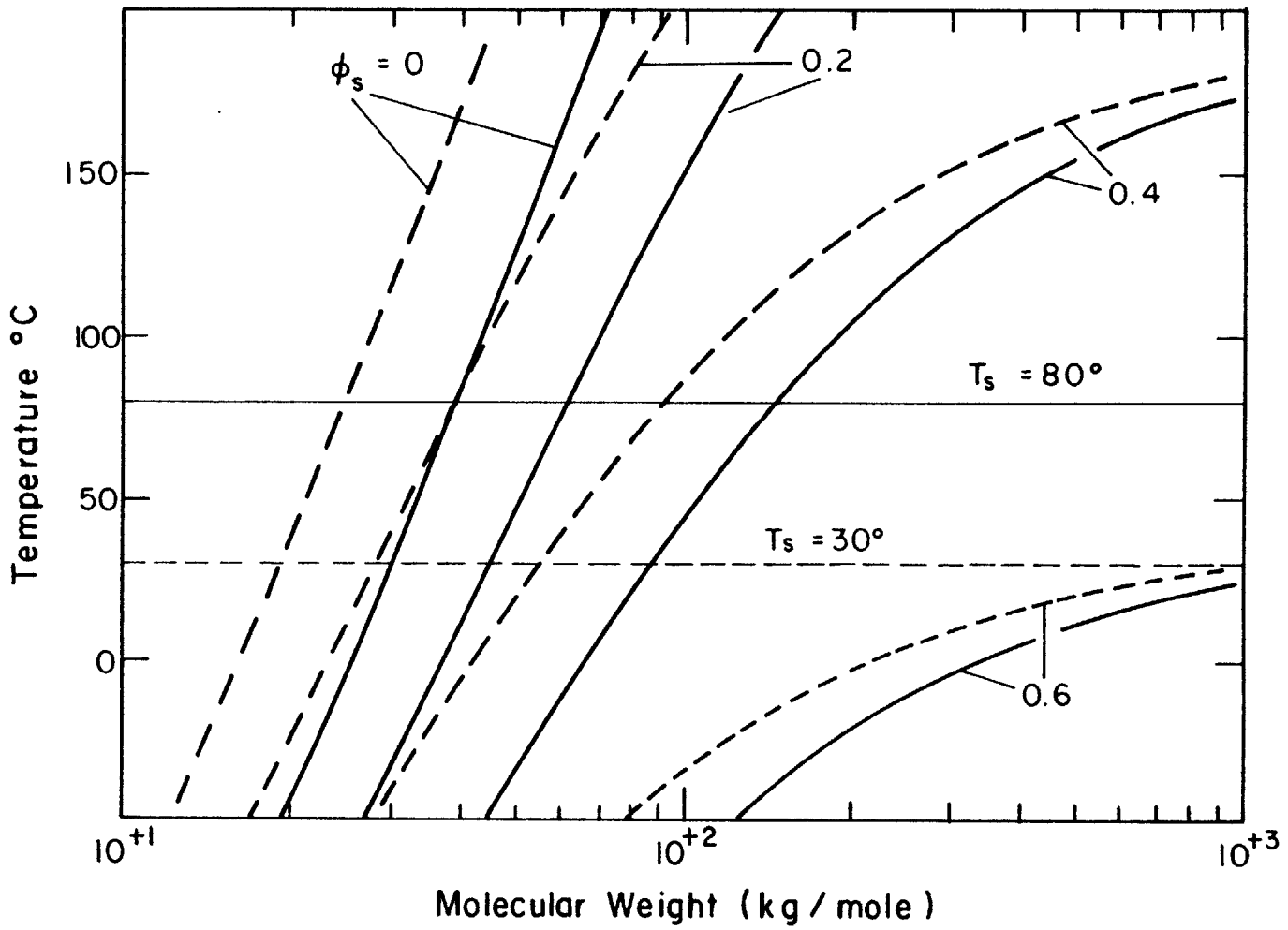

Figure 7-3 Solvent content, ϕ_s, at phase separation in solutions of diblock copolymer. Solid curves correspond to 12% and dashed curves 17% by weight polybutadiene.

under conditions which varied in three ways. First, χ in their system is different than in the present system although this difference is expected to be small, a point substantiated in Sec. 7.1.1. Second, SI samples were cast at 30°C whereas SB samples have been cast at or close to 80°C. Third, the average sample composition in Hashimoto's study was 17% by weight polyisoprene while this study has dealt with an average composition of 12% polybutadiene. The second and third points can be accounted for in equation 7-6 by re-evaluating the constant $M\chi$. As illustrated in Figure 7-3, this substantially shifts the bulk equilibrium and ϕ_s curves (dashed lines). Together with the lower casting temperature, this results in a higher solvent content at phase separation for a given molecular weight than is obtained for the SB samples. For example, SI (67-13) which has a rubber molecular weight equivilant to SB_d1 and SB1 ($\phi_s \simeq 0.3$) is calculated to phase separate at $\phi_s = 0.46$. Not surprisingly, the resulting bulk sphere radius is considerably further from equilibrium than in the SB case (Fig. 7-2). At higher molecular weight this difference is reduced, ϕ_s(SB6/S2) = 0.5 and ϕ_s(SI(251-71)) = 0.58, and accordingly the resulting bulk domain dimensions become comparable. These observations are consistent with the notion that decreasing ϕ_s brings the bulk radius closer to equilibrium, hence the variation in β between the two experimental sets of data.

It is important to note that the calculations using equation 7-6 are for comparative purposes only and should not be considered as quantitative. Nevertheless, they do provide a qualitative explanation as to the source of the discrepancies found in Figure 7-2; Figure 7-3

clearly indicates these are related to the solvent content at phase separation.

Why then does the phase separation of a diblock copolymer in solution result in the establishment of fewer chains per domain than would be present in the bulk equilibrium state? Although developed specifically for the case of block copolymers in the bulk state, the thermodynamic principles employed by Helfand and Wasserman (4,5) in defining system free energy are relevant to the present discussion. The free energy expression can be divided into three components: joint placement, chain configuration and interfacial free energy. The last of these can be minimized by reducing the surface to volume ratio of the system; in the case of spheres this corresponds to increasing the radius. This term is directly related to the interfacial tension which is expressed as,

$$\gamma = (\chi/6)^{1/2}\rho bkT \qquad 7\text{-}7$$

for a symmetrical interface of uniform density ρ, where b is the Kuhn statistical length and k is Boltzmann's constant. This tendency to increase domain size is opposed by the other two terms. Since placement of the block joint is restricted to the interface, an increase in interfacial area increases the degrees of freedom of joint placement. Under the criterion of uniform density across the domain, a balance must be struck between domain size and optimal chain configuration. The effects of solvent addition can now be examined with respect to these three free energy terms.

Addition of solvent would not be expected to reverse the tendency of the joint placement term to minimize domain size.

The chain expansion coefficient of a polymer in concentrated solution can be estimated from (19),

$$\alpha^5-\alpha^3 = \frac{K}{v_s}\,[1/2 - \chi(1-\phi)](1-\phi) \qquad 7\text{-}8$$

where v_s is the molar volume of solvent, ϕ is the volume fraction of polymer and K is a concentration independent parameter for a given polymer system; K can be determined from intrinsic viscosity measurements. $\alpha^3 = [\eta]/[\eta]_\Theta$ where $[\eta]_\Theta$ refers to the intrinsic viscosity at theta conditions (20). For a polybutadiene molecular weight of 50 kg/mol the solvent fraction at phase separation is estimated to be $\phi_s = 0.50$ (equation 7-6, 80°C). A polybutadiene spherical domain, swollen with 50% solvent from the bulk equilibrium state, will have undergone a radial expansion of 1.26. Using literature data (21) the chain expansion coefficient for the same polybutadiene chain in toluene was determined to be $\alpha = 1.36$. Therefore, the relative influence of solvent addition on the chain configurational free energy should be small.

In contrast, addition of solvent will have a pronounced effect on the interfacial free energy term. Diluting each phase with a common solvent will rapidly reduce χ thereby lowering γ (equation 7-7) which in turn leads to an increase in interfacial area and the associated decrease in sphere size, e.g. the number of chains per domain decreases. Here then lies the fundamental reason for the apparent discrepancy between theory ($\beta = 0.68$) and experiment ($\beta = 0.37$).

In order to qualitatively test this conclusion, the theoretical

sphere size calculations (Table 7-1) were repeated with reduced values of χ, keeping the other parameters constant. In no way can this be construed as a quantitative calculation . Still, if the above arguments are correct, then reducing χ should reduce sphere radius, and this in fact occurs; for $\chi_s = 0.5\chi$, $R_s = 0.89R$, nearly independent of molecular weight. Quantitatively predicting the equilibrium behavior of block copolymers in solution awaits future theoretical developments.

7.1.3 Domain Packing: Leibler (17) has predicted a body centered cubic (bcc) packing order in the spherical microstructure of diblock copolymers, which is supported by the SANS findings on sample SB_d1. Yet sample SB_d3 exhibits a lower degree of order with no identifiable packing regime. This loss of packing order may be attributed to a higher solvent content at microphase separation as discussed above. It is interesting to note that the calculated polyisoprene volume fractions, determined from the main Bragg peaks in the SI samples of Hashimoto et al. (6), using either a bcc or simple cubic paracrystal are higher than those obtained from their reported molecular weights. This would be expected since it has already been shown that ϕ_s in these samples is considerably larger than in the SB samples of this work.

Complete loss of order is displayed by sample $SB_d2/S1$ and in this case solvent content cannot be responsible based upon the arguments given in Sec. 7.1.2, e.g. sphere radius in the bulk state reflects solvent content at phase separation and $SB_d2/S1$ and SB_d3 exhibit very similar domain dimensions (Table 5-4). Instead, it appears

as though decreasing the fraction of matrix polystyrene covalently bound to the domains has increased the packing freedom of the system. While these observations are interesting, they have no direct bearing on the other structural aspects or mechanical properties of these materials and so will not be dealt with further.

7.1.4 Blending: The accepted "rule of thumb" states that if the molecular weight of a homopolymer is equal to or less than that of the analogous block of a diblock copolymer, the former will be incorporated by the latter into the microphase separated state (22). Meier (23) challenges this claim on the basis that the homogenization of homopolymer is actually determined at the point of phase separation in solution, comparable to the situation previously discussed (Sec. 7.1.2). As the solvent content at phase separation is decreased, the molecular weight and/or volume fraction of homopolymer must also be decreased if it is to remain homogenized.

This point became important in the present work. Sample SB4/S2/B1 did not incorporate homopolybutadiene (B1) into the domains of SB4, even though the polybutadiene molecules are equal in molecular weight. By doubling the diblock molecular weight complete homogenization of homopolybutadiene was accomplished (sample SB_d3/S2/B1); this also resulted in a dramatic increase in sphere size distribution (see Fig. 4-8). This deviation from the "rule of thumb" can be easily understood in light of the developments of Sec. 7.1.2, that is, the solvent content at phase separation is lower than has commonly been encountered in the literature. Only one such difficulty arose with respect to the polystyrene blends (sample SB9/S3) and this was easily rectified by

lowering the homopolymer molecular weight (SB9/S2); apparently the effect is more dramatic within the included phase. Because of the difficulties in controlling sphere size, distribution and rubber content when adding homopolymer, the present work focused primarily on samples in which polybutadiene was present in block form, with very satisfying results. In one situation examination of a sample containing blended homopolybutadiene was critical and $SB_d3/S2/B1$ proved invaluable, as discussed in the following section.

Finally, in light of the popularity of preparing blends of block copolymers and homopolymers from solution, it is very surprising to note that the work of Meier (23) is little recognized and has not been further developed. Any blend (rubbery or glassy) cast from solution will rarely be in a true state of phase equilibrium, a point overlooked by many authors.

7.2 PROPERTY ANALYSIS

7.2.1 Glass Transition Temperature Shift: As shown in Figure 6-7 the polybutadiene glass transition temperature, T_g^B, in all the composite samples is markedly shifted down in temperature relative to homopolybutadiene. This variation arises from a mismatch between the thermal expansion coefficients of polystyrene ($\alpha_S = 2.0 \cdot 10^{-4} K^{-1}$) and polybutadiene ($\alpha_B = 7.5 \cdot 10^{-4} K^{-1}$) (21) which places the included rubber particles in a state of triaxial tension upon cooling from the liquid state (~90°C), assuming the interfacial adhesion is sufficiently good. It is well knwon that dilation of a polymer sample lowers the glass transition temperature (24). This phenomenon has also been noted by

several authors investigating ABS and HIPS (25,26) although the magnitude was not as great as is presently reported.

The thermal stresses developed within a spherical rubber particle can be readily determined (27),

$$\sigma_B = \sigma_{rr} = \frac{2(\alpha_B-\alpha_M)E_B E_M \Delta T}{6(1-2\mu_B)E_M+3E_B(1-\mu_M)} \qquad 7\text{-}9$$

where μ is Poisson's ratio, E the tensile modulus and the subscripts M and B refer to the matrix and polybutadiene respectively. Here, the matrix is defined as the composite material external to a spherical rubber particle. In the glass the stresses are given by,

$$\sigma_{rr} = \left(\frac{r}{R}\right)^3 \sigma_B \qquad 7\text{-}10$$

$$\sigma_{\psi\psi} = \sigma_{\theta\theta} = -1/2\ \sigma_{rr} \qquad 7\text{-}11$$

in which r is the radius of the inclusion and R is the radial distance from its center. Pure component tensile properties were taken from the experimental data (Fig. 6-5) at -50°C; this is above the glass transition range of polybutadiene but sufficiently low in temperature to represent the properties near T_g^B. Poisson's ratio for polystyrene was taken from the Polymer Handbook (21) and for polybutadiene it was calculated using the experimental tensile modulus and a literature value (21) for the bulk modulus ($2.3 \cdot 10^3$ MPa, based upon polyisoprene and corrected for temperature and pressure). In order to accurately estimate the necessary matrix parameters in equation 7-9, the effects of

the filler (domains) on the polystyrene must be accounted for. Chow (28,29) has derived the general equations for calculating the composite modulus and thermal expansion coefficient from pure component properties for a system composed of elliptical filler particles. It is inappropriate to reproduce these cumbersome sets of equations and therefore only the calculated results will be given.

	E(MPa)	μ	$\alpha(K^{-1})$
B	3.0	0.49978	$7.5 \cdot 10^{-4}$
S	$3.6 \cdot 10^{3}$	0.33	$2.0 \cdot 10^{-4}$
M (calculated)	$3.0 \cdot 10^{3}$	0.35	$2.5 \cdot 10^{-4}$
M (experimental)	$2.8 \cdot 10^{3}$	-	-

The predicted drop in tensile modulus falls reasonable close to that determined experimentally, the latter being the one used in stress calculations. Also, the presence of the polybutadiene filler has a small effect on μ_M and a modest influence over α_M.

Assuming equation 7-9 is valid between 90°C and -90°C the level of stress within a domain is calculated to be σ_B = -78 MPa. Since the temperature-pressure shift factor for polybutadiene was not found, the reported value for polyisoprene has been substituted, $dT_g/dP = 0.24°C \cdot MPa^{-1}$ (30) leading to $\Delta T_g^B = 18.7°C$. This value falls at the upper limit of the values exhibited by the data ($19 \geq \Delta T_g^B \geq 12$ °C) which quantitatively explains the phenomena. Since the level of stress induced by thermal contraction is independent of sphere radius the variation in ΔT_g^B between data sets must derive from a separate mechanism. This will be discussed in the following section.

In light of the above discussion, the effects of aging, as

evidenced by Figure 6-9, can be explained. Aging corresponds to the densification, or loss of free volume, in a glass. To some extent this mitigates the hydrostatic tension imposed on the polybutadiene following annealling, which translates into an increase in T_g^B. It is important to note that the effects on samples SB_d1 and SB9 are nearly identical, ~2°C shift in each transition peak, even though they represent the upper and lower limits in sphere radii (Table 7-1). Based on equation 7-9, this would be expected. It has also been demonstrated by SANS analysis that aging does not affect the interfacial thickness (Table 5-3) so that the observed variations in T_g^B must derive from a different mechanism (see below).

7.2.2 Structure versus Property: The structural characteristics of the four hybrid data sets discussed in Chapter 6, along with sample SB_d3/S2/B1, are presented in Table 7-2. Hybrid sample results were obtained by averaging over all the constituent samples.

The fact that all composite storage modulus curves are nearly identical (Fig. 6-5) is the result of almost complete parallel coupling between the phases. As was shown in the previous section the polybutadiene spheres modify the polystyrene modulus by only 22%, pure parallel coupling would result in a 13% reduction in E'. In this situation, inclusion of a small fraction of interfacial material (Table 7-2) has a negligible influence on the storage modulus and therefore this parameter will not be further considered.

Loss modulus curves, shown in Figure 6-6, do exhibit significant differences amongst composite samples which become more apparent in Figure 7-4. For the moment this discussion will be limited to the

TABLE 7-2

[a] Structural Characterization of Composite Materials

	[b] $\bar{M}_n^B$	$\bar{R}$ (Å)	[c] v_S	[c] v_B	[d] $v_{\Delta R}$
SB-A	12	120	.820	.102	.078
SB-B	20	155	.838	.106	.056
SB-C	50	223	.851	.111	.038
SB-D	177	326	.853	.120	.027
$SB_d3/S2/B1$	16 [e](27)	267	.865	.105	.030

[a] Taking $\rho_B = 0.895$, $\rho_{Bd} = 0.99$, $\rho_S = 1.05$ g/cm^3 (21) [b] Polybutadiene molecular weight (kg/mol) per free chain end [c] Volume fraction of pure component [d] Interfacial volume fraction based on $\Delta R = 22$ Å [e] Molecular weight per chain

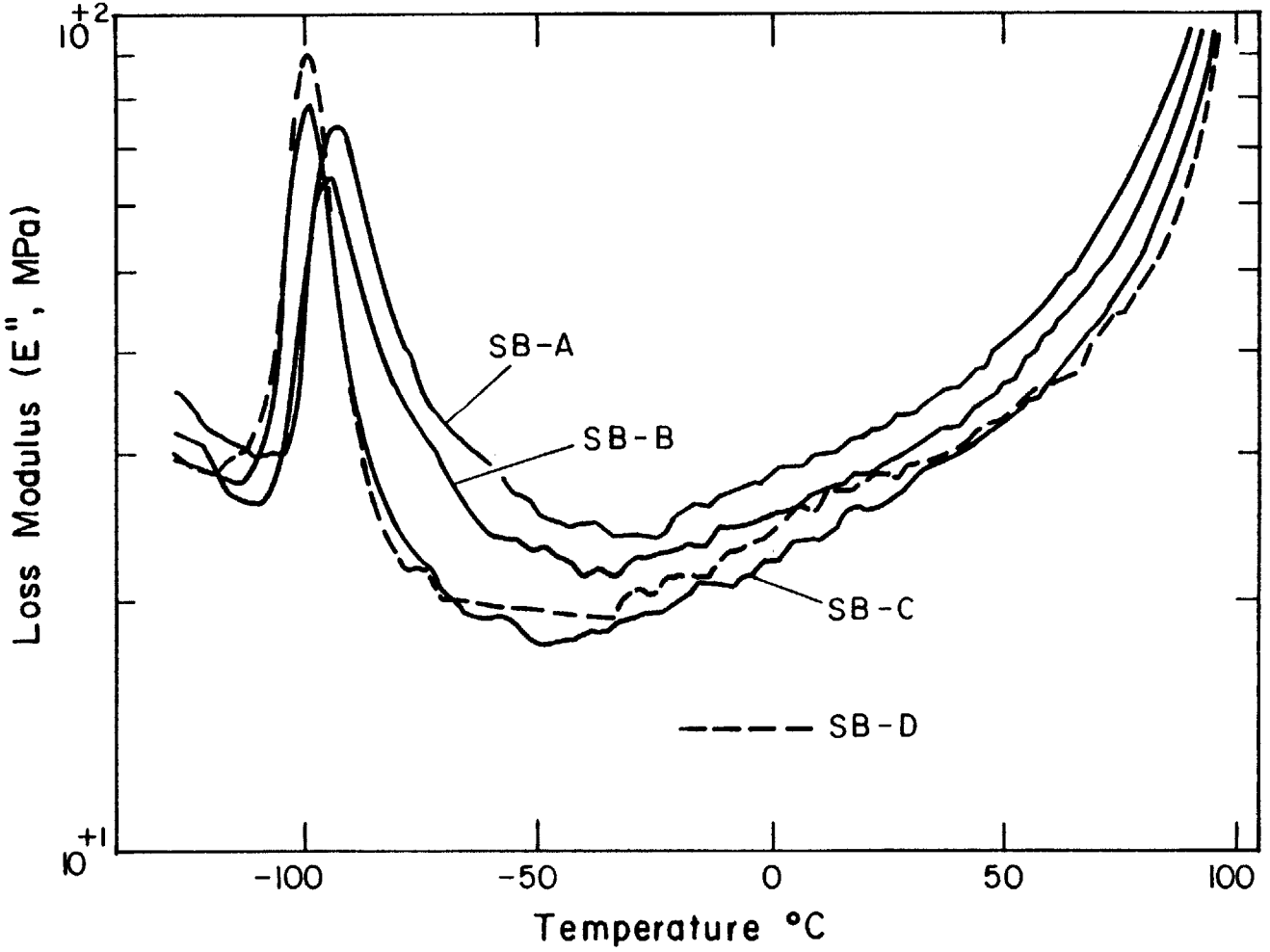

Figure 7-4 Hybrid composite materials. Structural characteristics are given in Table 7-2.

four hybrid curves, sample $SB_d3/S2/B1$ will be considered later. Two distinct property variations in E'' can be identified. First, the level of viscoelastic loss increases over the entire temperature range as the domain radius decreases, which also corresponds to a decrease in polybutadiene molecular weight. Second, T_g^B increases as domain radius (molecular weight) decreases. This second point will be considered first.

The observed increase in T_g^B with decreasing molecular weight is rather surprising. There are only two parameters which change in these samples, sphere radius (structural) and molecular weight (molecular). It is well known that the glass transition temperature is related to free volume and can be represented by,

$$T_g = T_{g,\infty} - K/M_n \qquad 7\text{-}12$$

where $T_{g,\infty}$ corresponds to a liquid with an infinite molecular weight and K is a constant. Regardless of the magnitude, equation 7-12 predicts that decreasing M_n will lower T_g, which in practice is a proven fact (31).

Therefore, attention turns to the structural differences in these samples. Couchman and Karasz (32) have discussed the domain size dependence of the glass transition temperature and conclude "unequivocally" that T_g increases as particle size decreases, as a result of interfacial tension. Interfacial tension can be directly calculated using equation 7-7 which for the present case gives $\gamma = 3.0$ dynes/cm. The corresponding domain pressure, $P = 2\gamma/r$, is inversely related to the sphere radius, r. For the set of materials listed in Table 7-2, the highest pressure will

be generated in SB-A, P = 0.5 MPa, which corresponds to a 0.1°C temperature shift. Clearly this is not the source of the deviation.

The possibility exists that the bulk modulus of the interfacial material, $K_{\Delta R}$, is lower than that for polybutadiene, so that an increase in interfacial volume fraction, $v_{\Delta R}$, results in a greater compliance of the domain as a whole, with an accompanying increase in T_g^B. Assuming that the interfacial region and polybutadiene couple in series, it can be easily shown that the differential pressure associated with ΔT_g^B would then be related to the interfacial bulk modulus as follows,

$$K_{\Delta R} = K_B \times \frac{\alpha_{\Delta R}}{\alpha_B}\left[\frac{P_2\phi_2^{\Delta R} - P_1\phi_1^{\Delta R}}{P_1\phi_1^B - P_2\phi_2^B}\right] \qquad 7\text{-}13$$

where

$$\phi_i^{\Delta R} + \phi_i^B = 1$$

P_i, ϕ_i^j and α_i represent the pressure, volume fraction and thermal expansion coefficient associated with phase j $\{\Delta R, B\}$ in material i $\{1,2\}$. Assuming $\alpha_{\Delta R} = \alpha_B$ and calculating pressures as $P = \Delta T_g^B/0.24$ (MPa), equation 7-13 predicts $K_{\Delta R} = 0.07\ K_B$ based on the structural data associated with samples SB-A and SB-C. Such a large difference in bulk modulus is essentially impossible, which eleminates the above argument.

Although the stress developed within a domain is independent of radius, stress distribution in the matrix is strongly dependant on the radius of the inclusion (equations 7-10,11). The possibility exists that the glass surrounding the smaller domains has yielded, thereby

reducing the internal stress and raising T_g^B. A recent publication by Earmme et al. (33) treats this problem in detail.

Sample $SB_d3/S2/B1$ was prepared specifically to resolve the question at hand; that is, are these variations in ΔT_g^B molecular or structural in nature? These two parameters cannot be separated within the set of composite materials thus far discussed, e.g. increasing polybutadiene molecular weight also increases sphere radius. But, by blending with homopolybutadiene this can be accomplished. As documented in Table 7-2, blending SB_d3 with B1 has increased domain size while decreasing the number average molecular weight. This results in an interfacial volume fraction which is close to that in SB-D, but a molecular weight which is slightly lower than that in SB-B. For the purposes of the present discussion it is more appropriate to treat molecular weight with respect to free chain ends (24) and therefore, M_n for B1 has been corrected in order to account for two free chain ends per molecule as opposed to one in block polybutadiene.

The loss modulus curve for sample $SB_d3/S2/B1$ is plotted together with that for SB-B in Figure 7-5 and here the influence of structure and polybutadiene molecular weight on E'' becomes apparent. As clearly shown in Figure 7-6, the shift in T_g^B is directly correlated with $\bar{M}_n^B$ and not domain size. The variation in interfacial volume fraction does produce a significant change in the entire level of viscoelastic loss, a point which will be considered following discussion of the glass transition temperature shift. Most fascinating is the fact that in the present system, decreasing molecular weight increases T_g^B!

This apparent paradox must be examined with respect to the thermal

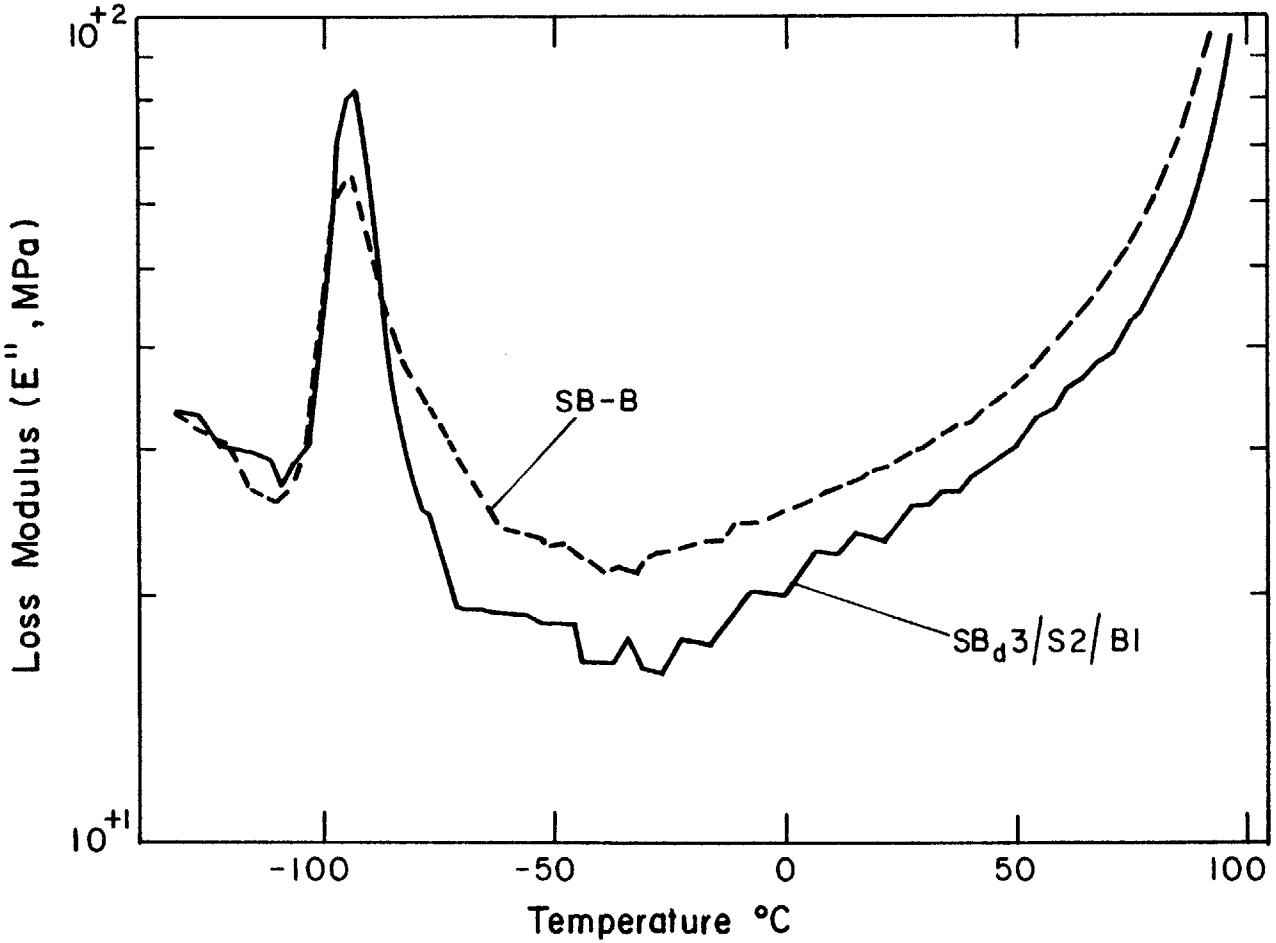

Figure 7-5 Effect of varying the interfacial volume fraction on the loss modulus where $v_{\Delta R}$ = 0.055 in sample SB-B and $v_{\Delta R}$ = 0.029 in sample $SB_d3/S2/B1$.

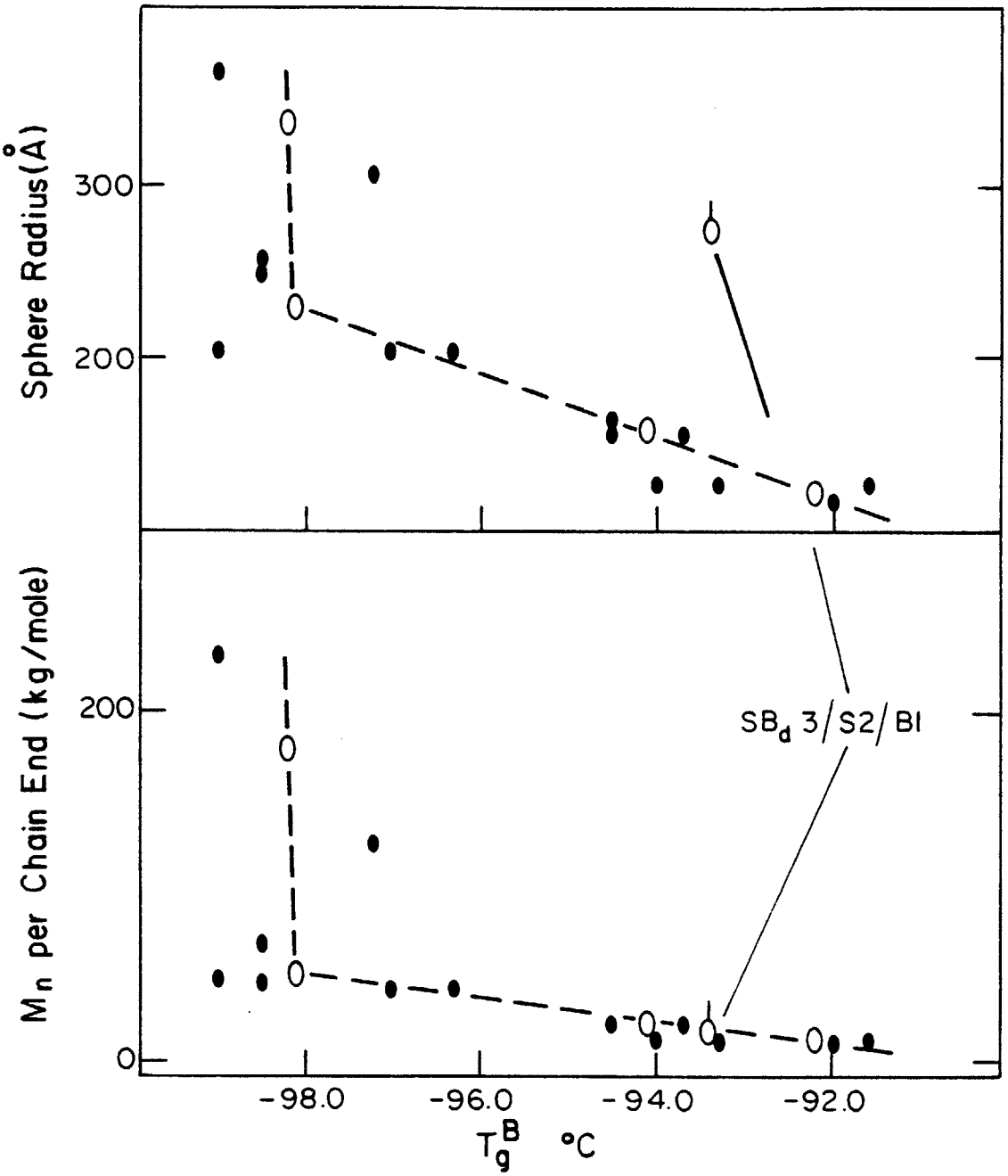

Figure 7-6 Polybutadiene glass transition temperature as a function of domain size and rubber molecular weight. Solid points correspond to individual data and open circles were taken from hybrid curves.

stress equation. In practice, samples measured in the Rheovibron are loaded and cooled over a relatively short, but consistent (~5°C/min) period of time. Under these conditions equation 7-9 is more properly represented, after rearrangement, by,

$$\sigma_B(t) = \int_{-\infty}^{t} \frac{K_B(t-t')}{\xi K_B(t-t')+1} \dot{\gamma}_v(t')dt' \qquad 7\text{-}14$$

where ξ contains only matrix terms, assumed to be constant, and $\dot{\gamma}_v$ is the time dependent rate of volumetric stain, determined by the sample cooling rate and thermal expansion coefficient difference. $K_B(t)$ is the time dependent bulk relaxation modulus for polybutadiene. Equation 7-14 assumes that the polybutadiene is behaving as a linear viscolastic material. Under this assumption the observed shift in T_g^B must derive from a molecular weight dependence of α_B, dT_g^B/dP or K_B, or any combination of these.

Since α is known to be inversely proportional to molecular weight (24) (i.e. directly proportional to free volume), it seems unlikely that this would be the source of the dilemma. It is difficult to predict how molecular weight would affect dT_g^B/dP, although since this parameter is also related to free volume (24), one would expect it to be smoothly dependent on M_n (as are α and T_g), particularly for the polymerization indices under consideration (>200). Examination of Figure 7-6 reveals that there is a marked difference between the T_g^B behavior of high ($\geq$41 kg/mol) and low ($\leq$21 kg/mol) molecular weight polybutadiene, the former being essentially independent, while the latter directly dependent, on molecular weight. This leaves as suspect the bulk modulus

term.

Neither the time dependent relaxation modulus nor forcing function of equation 7-14 are known, so that this constitutive equation cannot be solved. Nevertheless, it is probably safe to assume that for the cooling rate applied, the polybutadiene bulk properties are essentially at equilibrium for $T>T_g^B+20°C$ (24) which represents 90% of ΔT (i.e. σ_B). Under this assumption the bulk modulus of the polybutadiene in sample SB-A would have to be, $K_B = 1 \cdot 10^3$ MPa in order to satisfy the equilibrium version of equation 7-14 for the observed $\Delta T_g^B = 12°C$. A literature value of $K_B = 2.3 \cdot 10^3$ MPa has previously been shown to almost exactly predict the shift exhibited by the higher molecular weight polybutadiene, $\Delta T_g^B = 18°C$. Bulk viscoelastic behavior depends on very local motions of polymer molecules so that molecular weight should have virtually no effect on the bulk modulus of a rubber. Therefore, these calculations strongly suggest that equation 7-14 does not actually represent the state of deformation in the lower molecular weight polybutadiene.

Perhaps the most relavant observation concerning this phenomenon is the fact that the polybutadiene is under a tremendous state of strain. Based upon equation 7-14 at equilibrium, the volumetric strain in samples SB-C and SB-D is calculated to be $\Delta V/V = 0.034$. It is likely that this extensive dilation leads to a non-linear behavior of the low molecular weight polybutadiene which results in the observed shift in the glass transition temperature.

Unfortunately, the topic of dilation and cavitation in rubbery materials has received very little attention, mainly due to obvious

experimental impediments. Gent (34,35) has provided a theoretical expression for calculating the triaxial tension required to inflate a pre-existing hole in an elastic solid. This expression contains a surface energy and an elastic deformation term which for small holes results in a maximum pressure at a given level of dilation. For example, according to this theory, a 10 Å radius cavity in a rubber will expand indefinitely under a 100 MPa triaxial tensile load. Although this theory looks attractive, it is inappropriate to apply a continuum analysis to the present problem which deals with polymers at a molecular level, e.g. single chain dimensions are on the order of domain dimensions (see Appendix C).

Nevertheless, based on the above discussion concerning T_g^B, it must be concluded that the low molecular weight polybutadiene within the microdomains is actually failing, either by cavitation or yielding (rupture). The (brittle) strength of various polymers, including polystyrene, polyethylene and butyl rubber has been shown (36) to conform to an equation originally proposed by Flory (37):

$$\text{(Brittle) strength} = A - B/M_n \qquad 7\text{-}15$$

Lacking any evidence to the contrary, it must be assumed that equation 7-15 also applies in triaxial tension which would be consistent with the present experimental findings. Samples SB-C and SB-D exhibit equivalent values of T_g^B because the level of stress did not reach the {brittle, yield} point of the higher molecular weight polybutadiene, hence the consistency with the calculated stress. Furthermore, Argon et al. (38) have shown that in the case of intergranular cavitation in

metals, maximum stress is obtained at the point of nucleation, after which additional strain results in a significant drop in stress; this might account for the magnitude of the differences in T_g^B. At this point it becomes impossible, without further experimentation, to prove whether the true mechanism governing this phenomenon has been identified. The required experiments will be discussed in Chapter 8 and a discussion of what has been deduced thus far taken up in the following section.

The second variation between samples observed in Figure 7-4 is an increase in loss level and assymetry in the polybutadiene transition peak with decreasing sphere radius and rubber molecular weight. In this case Figure 7-5 clearly demonstrates that this effect is due to a structural change; the interfacial volume fraction of SB-B is twice that of $SB_d3/S2/B1$. Therefore, the influence of the domain boundary on these diblock copolymer-homopolymer blends has been unequivocally identified, independent of all molecular and structural effects. A discussion of these results will be presented in the following section.

7.3 DISCUSSION

Several important features concerning the structural characteristics of block copolymers and blends have been identified in this work. The characterization of these materials has been divided into three separate categories, interfacial, domain and interdomain dimensions. Structural analysis revealed that regardless of the molecular composition or processing history of the composite the interfacial

thickness remains unaffected. Specifically, diblock copolymer molecular weight, homopolystyrene content, casting solvent and aging had little or no influence over this parameter. Helfand and Sapse (39) have shown that non-local interactions need only be considered when $\chi \gtrsim 3$, hence equation 4-3 includes only local interaction contributions. The excellent agreement obtained between equation 4-3 and the SANS results validates this approach. Therefore, since local interactions completely dictate the interfacial composition, it is not surprising that this structural feature is insensitive to the perturbations mentioned above; the interface was always found to be at or near equilibrium.

On the other hand, domain and inter-domain structure were dependent on one or more of the above variables. The predicted equilibrium behavior was only approached in diblock copolymers containing no homopolymer and a low solvent content at phase separation. Increased solvent content at phase separation results in fewer chains per domain (e.g. smaller spheres in the bulk state) and degeneration of the equilibrium body centered cubic paracrystalline macrolattice. Addition of homopolystyrene leads to a loss of paracrystallinity, although this parameter has no apparent effect on the subsequent dynamic mechanical properties. Therefore, it appears as though only those structural features which involve long range interactions are affected by molecular composition and processing variations.

Two important property characteristics of the composites investigated in this study have been examined in detail, the dynamic mechanic behavior of the domain boundary and the bulk properties of the glass entrapped rubber. The latter of these will be considered first.

Since all structural changes have been accounted for, the most plausible explanation for the variations in T_g^B illustrated in Figure 7-6 is that a decrease in polybutadiene molecular weight is accompanied by a decrease in triaxial stress at rubber failure. It seems likely that this behavior is associated with the fractional free volume of the rubber, f_B. This is consistent with the fact that sample $SB_d3/S2/B1$ is better correlated with hybrid samples SB-A and SB-B based upon the number average molecular weight per free chain end (Fig. 7-6) rather than M_n. Also, lightly crosslinking samples SB1, SB_d1 and SB2/S2, which leaves f_B essentially unaffected, produced no variation in T_g^B .

In general, regardless of the mechanism, these characteristics can be expected to have a profound influence on the large deformation behavior of rubber modified glasses. Indeed, investigators are beginning to recognize the importance of rubber failure in determining the ultimate properties of materials such as ABS and HIPS (39-43). Manson and Hertzberg (39) and Durst et al. (40) have documented the importance of rubber-matrix adhesion in obtaining fracture resistant rubber modified polystyrene, e.g. the rubber particle must be capable of supporting large hydrostatic stresses. Donald and Kramer (43) have recently shown that internal voiding and cavitation in both solid and occluded large (>1 μm) rubber particles in ABS are of prime importance to craze initiation. Cavitation in small particles (<1 μm) promotes shear deformation, another toughening mechanism. It is impossible to deduce the contributing role of f_B in rubber failure from the studies cited above. Instead, it is more likely that an investigation involving

block copolymers, which readily lend themselves to both molecular and structural control, will provide the answer.

The original motivation for conducting a combined structure and property analysis of the reported materials was to better understand the mechanical behavior of the interface. In the present work the interfacial properties have been separated from both molecular and other structural variables, and these results will be discussed in conjunction with previously reported findings as briefly outlined in Section 6.1.2.

Figures 7-4 and 7-5 demonstrate that the development of a mixed domain boundary does not lead to the generation of an intermediate loss peak as has been speculated by various investigators (44-46). Instead, this work confirms the findings of Kraus and Rollmann (47) conducted on a set of triblock copolymers containing a lamellar microstructure. With the exception of SB-D, the entire loss level between T_g^B and T_g^S of the samples listed in Table 7-2 increases proportionately with interfacial volume fraction. A re-examination of Figures 6-6 and 6-7 provides a convincing explanation as to why sample SB-D appears to deviate from this behavior. SB-D contains the lowest fraction of interfacial material (Table 7-2) so that the broad intermediate shoulder in E'' found in pure polystyrene begins to become apparent. As $v_{\Delta R}$ increases this feature becomes masked, particularly since the greater fraction of the interfacial relaxation spectra occurs at temperatures near each component's T_g (see below and Figure 6-7). This might resolve a question which has circulated for more than a decade. Miyomoto et al. (44), Beamish et al. (45), Cohen and Tschoegl

(46) and Kalfoglou (48) have each observed a similar phenomenon and interpreted it in a different fashion. As demonstrated by Cohen and Tschoegl (46) this response shifts to higher temperatures with increasing frequency, which is why most studies (110 Hz) have found this shoulder to be closer to T_g^S than in the present work (3.5 Hz). All these findings are consistent with the β transition mechanism in atactic polystyrene, long ago established by Illers (49,50).

The viscoelastic behavior shown in Figures 7-4 and 7-5 can be described by treating the material as a three-phase composite. Since the interfacial "phase" has a gradient composition, its loss modulus at any given temperature and frequency is actually determined by a series of composite loss moduli, or more precisely,

$$E''_{\Delta R}(T,t) = \frac{\int_{-\Delta R/2}^{\Delta R/2} E''(T,t,\rho_B)\rho_B(r)dr}{\int_{-\Delta R/2}^{\Delta R/2} \rho_B(r)dr} \qquad 7\text{-}16$$

where $\rho_B(r)$ represents a given interfacial composition profile. The overall material behavior is determined by the coupling mechanism between the three phases, the limiting cases being,

$$E''(T,t) = \left[\frac{v_S}{E''_S(T,t)} + \frac{v_B}{E''_B(T,t)} + \frac{v_{\Delta R}}{E''_{\Delta R}(T,t)}\right]^{-1} \qquad 7\text{-}17$$

for series coupling and,

$$E''(T,t) = v_S E''_S(T,t) + v_B E''_B(T,t) + v_{\Delta R} E''_{\Delta R}(T,t) \qquad 7\text{-}18$$

for parallel coupling. In practice, a composite material will exhibit elements of both coupling modes, the actual combination being strongly dependent on sample structure. A variety of mechanical models have been developed to account for this behavior, most notably those by Takayanagi (51) and Nielsen (52). Using a similar set of equations, Kraus and Rollmann (47) have demonstrated that a weighted combination of equations 7-17 and 7-18 predicts the experimental trends obtained upon increasing $v_{\Delta R}$, which is an overall increase in the E'' plateau level. Regardless of the coupling mechanism, this can be easily understood based solely upon equations 7-16 to 7-18. The composition profile determines how the interfacial loss spectrum will be distributed as a function of temperature. If $\rho_B(r)$ were described by the linear gradient profile (Fig. 5-7) there would be an even distribution of interfacial loss between T_g^B and T_g^S. Development of a sigmoidal profile of the type shown in Figure 5-7 displaces a greater volume fraction of interfacial material towards each pure component, e.g. a higher composition gradient exists at the center of the interface. If the interfacial profile were asymmetric, this displacement would occur preferentially towards a given pure component. Although a symmetric interphase has only been assumed in the present work for convenience, the results given in Figures 7-4 and 7-5 do not contradict this premise. Finally, based upon either 7-17 or 7-18, increasing $v_{\Delta R}$ will increase the overall level of loss, provided $E''_{\Delta R} > (E''_S + E''_B)/2$. This would be

expected since at any given temperature in the plateau region of the E'' curve a fraction of the interfacial material will be in its transition state and correspondingly at a high loss level.

Detailed application of the two-phase mechanical models to the present three-phase situation is not simple, and in most cases, such as with the Takayanagi model (51), the introduction of additional adjustable parameters is required. In the present case, there are few incentives to conduct such an exercise; the properties have been clearly associated with a proven structure and the variations between samples are rather small. Diamant et al. (53) have taken the opposite approach. They modified the two-phase Nielsen model (52) into a multiphase model in which the domain boundary of a set of SBS triblock copolymers were treated as seventy discreet phases. All coupling constants were statistically averaged to a single fitting parameter Φ_{max} and a polystyrene continuous matrix was assumed. The authors contend that $v_{\Delta R}$ and $\rho_B(r)$ can be determined by fitting $G''(T)$ torsion pendulum data with the model. Φ_{max} is independently fit to G' data which they claim is insensitive to $\rho_B(r)$ and $v_{\Delta R}$. The latter point is consistent with the findings of this study. While the loss modulus trends predicted by their model are in agreement with this work, Diamant arrives at several conclusions, based on fitting data, which conflict with the present findings. First, they find that varying casting solvent brings about as much as a four-fold variation in $v_{\Delta R}$. Second, they report that $v_{\Delta R} = 0.04$ for SBS (7-36-6 kg/mol) and $v_{\Delta R} = 0.10$ for SBS (16-78-16), both cast from the same solvent! The first point conflicts with the concept that local interactions dictate interfacial composition, which

the present work has substantiated. The second is directly opposed to the results given in Table 7-2. Unfortunately, the authors included neither EM nor small angle scattering structural data. Kotaka et al. (54) have established a strong correlation between solvent induced structure and dynamic mechanical properties in similar SBS triblock copolymers.

It is difficult to anticipate how variations in the interfacial volume fraction would affect the large deformation behavior of rubber modified glasses. As illustrated in Figures 7-4,5 and 6-5, this parameter only exerts a modest influence over the dynamic loss modulus and virtually none over the storage modulus. In materials such as HIPS and ABS in which the rubber content is low (5-15%), and phase dimensions significantly larger than in block copolymers, these effects would be immeasurable. In this case, a mixed domain boundary is probably most influential in maintaining good adhesion between matrix and particle under an applied stress. On the other hand, a high loss domain boundary may enhance the impact resistance of block copolymers such as K-Resins where the interfacial volume fractions are comparable to that of SB-A.

References

1 D.J. Meier, Polymer Preprints, 15, 171 (1974).

2 D.F. Leary and M.C. Williams, J. Polymer Sci. Phys. Ed., 11, 345 (1973).

3 D.F. Leary and M.C. Williams, J. Polymer Sci. Phys. Ed., 12, 265 (1974).

4 E. Helfand and Z.R. Wasserman, to appear in Developments in Block Copolymers, ed. I. Goodman, Applied Sciences Publishers Ltd.

5 E. Helfand and Z.R. Wasserman, Macromolecules, 11, 960 (1978).

6 T. Hashimoto, M. Fujimura and H. Kawai, Macromolecules, 13, 1660 (1980).

7 N.A. Rounds, Doctoral dissertation, University of Akron (1971).

8 R.J. Roe and W.C. Zin, Macromolecules, 13, 1221 (1980).

9 T. Hashimoto, M. Shibayama and H. Kawai, Macromolecules, 13, 1237 (1980).

10 H. Hashimoto, M. Fujimura, T. Hashimoto and H. Kawai, Macromolecules, 15, 844 (1981).

11 R.E. Cohen and D.E. Wilfong, to appear in Macromolecules (1982).

12 R.W. Richards and J.L. Thomason, Polymer, 22, 581 (1981).

13 N. Stribeck, Ph.D. dissertation, Philipps-Universität, Marburg/ Lahn (1980).

14 T. Inoue, T. Soon, T. Hashimoto and H. Kawai, J. Polym. Sci., A-2, 7, 1283 (1969).

15 D.J. Meier, Block and Graft Copolymers, ed. J. Burke and V. Weiss, Syracuse Univ. Press (1973).

16 E.R. Pico and M.C. Williams, J. Polymer Sci. Phys. Ed., 15, 1585 (1977).

17 L. Leibler, Macromolecules, 13, 1602 (1980).

18 E.R. Pico and M.C. Williams, J. Appl. Polym. Sci., 22, 445 (1978).

19 W.W. Graessley, Adv. Polym. Sci., 16, 1 (1974).

20 P.J. Fory, Principles of Polymer Chemistry, Cornell University Press (1953).

21 J. Brandrup and E.H. Immergut, eds., Polymer Handbook, second edition (1975).

22 G. Riess and Y. Jolivet, Adv. in Chem. Series, 142, 243 (1975).

23 D.J. Meier, Polymer Preprints, 18, 340 (1977).

24 J.D. Ferry, Viscoelastic Properties of Polymers, second edition, John Wiley and Sons (1970).

25 L. Bohn, Angew, Makromol. Chem., 20, 129 (1971).

26 L. Marbitzer, K.H. Ott, M. Schuster and D. Kranz, Angew Makromol. Chem., 7, 57 (1972).

27 R.H. Beck, S. Gratch, S. Newman and K.C. Rusch, Polymer Letters, 707 (1968).

28 T.S. Chow, J. Polymer Sci. Phys. Ed., 16, 959 (1978).

29 T.S. Chow, J. Polymer Sci. Phys. Ed., 16, 967 (1978).

30 J.M. O'Reilly, J. Polym. Sci., 57, 429 (1962).

31 R.F. Fedors, Polymer, 20, 518 (1979).

32 P.R. Couchman and R.E. Karasz, J. Polym. Sci. Phys. Ed., 15, 1037 (1977).

33 Y.Y. Earmme, W.C. Johnson and J.K. Lee, Metallurgical Trans., A, 12A, 1521 (1981).

34 A.N. Gent, Science and Technology of Rubber, ed. F.R. Eirich, p. 419, Academic Press, N.Y. (1978).

35 A.N. Gent and D.A. Tompkins, J. Polym. Sci., A-2, 7, 1483 (1969).

36 R.G.C. Arridge, Mechanics of Polymers, Oxford University Press (1975).

37 P.J. Flory, J. Am. Chem. Soc., 67, 2048 (1945).

38 A.S. Argon, I.W. Chen and C.W. Lau, conference proceedings TMS-AIME, Milwaukee, Wisconsin, Sept. 18-19, 1979.

39 J.A. Manson and R.W. Hertzberg, J. Polym. Sci. Phys. Ed., 11, 2483 (1973).

40 R.R. Durst, R.M. Griffith, H.J. Urbanic and W.J. von Essen, ACS Div. Org. Coat. Plast. Prepr., 34(2), 320 (1974).

41 H. Breuer, F. Haaf and J. Stahenow, J. Macromol. Sci. Phys., B14(3), 387 (1977).

42 F. Ramsteiner, Polymer, 20, 839 (1979).

43 A.M. Donald and E.J. Kramer, submitted to J. Mat. Sci. (1981).

44 T. Miyomoto, K. Kodama and K. Shibayama, J. Polymer Sci., A-2, 8, 2095 (1970).

45 A. Beamish, R.A. Goldberg and D.J. Harriston, Polymer, 18, 49 (1977).

46 R.E. Cohen and N.W. Tschoegl, Trans. Soc. Rheology, 20, 1, 153 (1976).

47 G. Kraus and K.W. Rollmann, J. Polymer Sci. Phys. Ed., 14, 1133 (1976).

48 N.K. Kalfoglou, J. Appl. Polymer Sci., 23, 2385 (1979).

49 K.M. Illers and E. Jenchel, J. Polym. Sci., 41, 528 (1959).

50 K.M. Illers, Electrochem., 65, 679 (1961).

51 M. Takayanagi, Mem. Fac. Eng. Kyushu Univ., 23, 1 (1963).

52 L.E. Nielson, Rheol. Acta., 13, 86 (1974).

53 J. Diamant, D.S. Soong and M.C. Williams, to appear in Contemporary Topics in Polymer Sci., vol. 4, ed. W.J. Bailey, Plenum Press, N.Y. (1981).

54 T. Kotaka, T. Miki and K. Arai, J. Makromol. Sci.-Phys., B17(2) 303 (1980).

CHAPTER 8: Summary

8.1 CONCLUSIONS

This study has evolved along three distinct lines: molecular engineering via anionic polymerization, microstructural analysis via SANS and EM, and finally property characterization by means of dynamic mechanical testing. Motivation to develop the first originally grew out of a desire to investigate the third. Understanding the third required inclusion of the second, which in turn necessitated a re-examination of the first. All three aspects of this work have been important in arriving at the following conclusions.

While not directly related to the main body of this thesis, development of the "living" polyvinyl gels (Appendix A) was crucial in establishing the means of producing the desired materials. Using the methods detailed in Chapter 2 and Appendix A, large quantities of block copolymer, of predetermined composition and molecular weight, can be prepared in a straight-forward and reproducible manner. Such control of molecular architecture has proven to be invaluable in pursuing the stated objectives.

Structural features in these materials can be divided into two categories, those governed by local interactions, such as microdomain boundary thickness, and those which are strongly influenced by long range interactions, such as domain type, size and ordering. Structural features of the first type are insensitive to processing, and in the case of interfacial thickness can be accurately predicted by the

equilibrium theory of Helfand and Wasserman (1). Those of the second type are greatly affected by processing conditions which can lead to non-equilibrium structures. Spherical domain size and order in solvent cast films are dictated by the solvent content at microphase separation, ϕ_s. At low values of ϕ_s, the predicted equilibrium domain size (2) is approached and a body centered cubic paracrystalline macrolattice is established, in accordance with the equilibrium prediction of Leibler (3). Increasing ϕ_s results in a decrease in the bulk size of the domains (fewer chains per domain) and a degeneration of paracrystalline order. Understanding these processes provides an added dimension of control over the structural features attainable with block copolymers.

Investigation of the dynamic mechanical behavior of these materials has led to several notable conclusions. Probably the most significant of these was to demonstrate the importance of establishing the molecular and structural groundwork before attempting to analyze a given mechanical behavior. In this manner a variety of plausible hypotheses were eliminated when trying to explain an unexpected increase in the polybutadiene glass transition temperature. It seems likely that this behavior is brought about by a dependence of rubber failure in triaxial extension on the polybutadiene fractional free volume. This may have a significant influence on the large deformation characteristics of rubber modified glasses in general. Incorporation of a diffuse domain boundary leads to a predictable increase in the loss modulus of these materials, the distribution in temperature and/or time being determined by the interfacial composition profile and the magnitude by the interfacial volume fraction.

8.2 RECOMMENDATIONS FOR FUTURE WORK

Several interesting questions have been raised in the course of this study which in the author's opinion warrant further investigation.

The polyvinyl gels, reported in Appendix A, offer a versatile substrate for a variety of purposes. Application to solvent purification has been convincingly demonstrated. Further development will require a more quantitative understanding of the reaction parameters pertaining to gel synthesis. Development of the rate expressions governing monomer conversion and gelation as a function of anion concentration, solvent content and type will be necessary in order to control residual vinyl content and network structure. Further application might include gel utilization as a catalyst substrate, since the pendant vinyl groups represent an attractive site for immobilizing various organic and organometallic moieties.

An obvious extension of the findings of this work concerning the importance of solvent content at microphase separation in block copolymer solutions would be a combined theoretical and experimental investigation of this phenomenon. The concepts developed by Helfand and Wasserman (1) could be readily extended to include the effects of solvent. A variety of techniques could be employed in order to ascertain the point of phase separation in such solutions as a function of solvent content and temperature, the most powerful being small angle scattering.

A surprising finding of the structural analysis in this study was the significant discrepancy identified between the measurement of sphere radii by EM and SANS. There is no apparent explanation for this result although the error almost certainly lies with the EM values. Here lies

an interesting and important topic for further research.

Finally, several unanswered questions remain concerning the polybutadiene glass transition temperature shifts which have been reported. The existence of a voiding mechanism in the low molecular weight polybutadiene could be easily established by examining the samples both at room temperature and in a cryogenic cell using either a SAXS or SANS instrument. Similarly, use of the deformation device, presently in operation on the 10 m SAXS instrument at NCSASR, would provide a clear cut means of determining whether cavitation occurs in rubbery microdomains prior to macroscopic sample failure.

A simple method also exists for testing the rubber fractional free volume concept which has been advanced. With a trivial extension of the synthetic techniques presented in Chapter 2, SBS triblock copolymers having the same compositions and overall molecular weights as hybrid samples SB-A through SB-D could be prepared. If the fractional free volume concept is correct, they would all exhibit the same rubber glass transition temperature since none of the samples contain free polybutadiene chain ends. As an incentive, it might be noted that K-Resins, developed by Phillips Petroleum Co as tough, impact resistant thermoplastics, consist of styrene-butadiene star-block and linear multiblock blends which in all probability contain few if any free polybutadiene chain ends (4).

References

1 E. Helfand and Z.R. Wasserman, to appear in Developments in Block Copolymers, ed. I. Goodman, Applied Sciences Publishers Ltd.

2 E. Helfand and Z.R. Wasserman, Macromolecules, 11, 960 (1978).

3 L. Leibler, Macromolecules, 13, 1602 (1980).

4 A.G. Kitchen and F.J. Szalla (Phillips Petroleum Co.), U.S. Pat. 3,639,517 (1972).

APPENDIX A: Preparation of Homogeneous "Living" Polyvinyl Gels for Application to Solvent Purification

INTRODUCTION

In this appendix the polymerization of divinylbenzene (DVB) into homogeneous gels containing a significant concentration of residual vinyl groups is reported. Methods are described whereby microsyneresis (1), commonly observed in the polymerization of DVB, is eliminated. These methods of synthesis, therefore, place no restrictions on overall sample size and yield materials of substantial mechanical strength. The utility of these novel homogeneous polyvinyl macrogels is demonstrated in solvent purification.

EXPERIMENTAL SECTION

Materials: Divinylbenzene (Matheson Coleman and Bell, practical grade) was washed with 10% NaOH and with distilled water and was stored over molecular sieves at 0°C. Proton NMR analysis confirmed a monomer composition of 60% DVB and 40% ethylstyrene (ES). The [m-DVB]/[p-DVB] was reported as 3:1 by the manufacturer. Reagent grade benzene, tetrahydrofuran (THF), 1,4-dioxane, and toluene were dried over molecular sieves. n- and sec-butyllithiums were diluted in hexane or used as received from Aldrich; concentrations were verified by titration, using the method of Eppley and Dixon (2).

Gel Synthesis: Reactions were performed at room temperature in sealed, flamed and argon-flushed Pyrex test tubes. Solvents and monomer were each introduced to the vessel by syringe and mixed. Addition

of initiator was followed by a color change from colorless to burgundy brown and subsequent gelation. The reacting solution/gel was left for 24 hours and recovered in benzene. During storage in benzene, slow reaction with oxygen terminated the living gels, as indicated by loss of color.

Gelation reactions were conducted in solution over a range of monomer concentrations from 2 to 40% (v/v) and at an initiator concentration of 0.016 M. Varying the [THF]/[I] molar ratio between 0 and 4 in benzene has a dramatic effect on the product obtained. Initiation in the absence of THF leads to slow development of color with subsequent polymerization and gelation dominated by extensive microsyneresis; the opaque gel so produced has little mechanical strength and crumbles upon handling. Addition of initiator to a solution with [THF]/[I] = 4 instantaneously produces a burgundy color followed by rapid homogeneous gelation. The product is a clear uniform gel of superior strength. Varying [THF]/[I] between 0 and 4 results in large changes in reaction time and product characteristics. A value of [THF]/[I] = 4 provides adequate time for mixing prior to gelation and yields a product suitable for application to solvent purification (see below). This gel can be readily cut into serviceable pieces as recovered in the swollen state while also containing a significant concentration of accessible vinyl groups. The conditions for the synthesis of this gel are summarized in Table A-1. As described in the Discussion, homogeneous gels were also obtained from reactions carried out in a mixed solvent composed of 75% dioxane and 25% toluene (v/v).

TABLE A-1

Experimental Conditions for the Synthesis of Gels Used in Solvent Purification

reagent	conc., M
DVB (75% meta, 25% para)	0.83
ethylstyrene (mixed isomers)	0.55
benzene	9.01
n-BuLi	0.016
THF	0.064

TABLE A-2

Variations Observed in Gelation Reactions and Products [a]

solvent	benzene	benzene/THF (0.994/0.006)	dioxane/toluene (0.750/0.250)
time to full color, s	>120	instantaneous	instantaneous
time to gel,[b] s	~1200	~20	~160
expected overall rate constant[c] L mol^{-1} s^{-1}	0.01	25.3[d]	0.9
clarity of gel	opaque	clear	clear
structural characteristics of gel	inhomogeneous (powder)	homogeneous (swollen rubber)	homogeneous (swollen rubber)

[a]Experimental conditions are as in Table A-1 keeping the relative volume of solvent constant
[b]Subject to small deviations due to an inability to accurately control reaction temperature
[c]Based on values for lithium polystyryl (Ref. 4) [d]Assuming propagation is via monoetherate of lithium polystyryl (Ref. 4)

Characterization: The gel of Table A-1 was analyzed for accessible vinyl content in the following manner. 1.5 g (dry weight) of 0.5 cm^3-size swollen particles was suspended in toluene, charged with excess n-BuLi, and allowed to react under purified argon for 1 week. The presence of available vinyl groups in the gels was evidenced by the appearance of a deep reddish brown color. The solution was then drained and a 250-mL aliquot of a standardized solution of toluene and benzoic acid was added. The activated gel particles turned colorless. Aliquots (50 mL each) of the remaining solution were titrated for benzoic acid content with a standardized solution of methanol and sodium methoxide. Phenophthalein was added as an end point indicator. The titration technique was verified independently on a known solution of benzoic acid in toluene. This method yielded a value of 1.4×10^{-3} mol of available vinyl groups per gram of dry gel.

The method of characterization was chosen in order to duplicate conditions employed during solvent purification, as discussed in the following section. Presumably the true vinyl content is considerably higher since this chemical reaction is expected to be diffusion limited and because reaction of more than one vinyl group per initiator molecule is possible.

Application: The polyvinyl gel was used for solvent purification in all the anionic polymerizations reported in Chapter 2. Approximately 2.0 g (dry weight) of gel was suspended over 2000 mL of distilled solvent under argon. Since the polymerizations were later initiated with n-butyllithium, a suitable amount of anisole was added to the solvent to provide for a high rate of initiation (3).

Sufficient n-BuLi (1.6 M) was added to the impure solvent and the solution was stirred for several days. Sequential lowering of clear gel particles into this solvent provided fresh vinyl material for excess initiator removal as evidenced by the appearance of a reddish brown color in the gel. When the newly added gel particles remained colorless, the purification of the solvent was assumed to be complete. Gas chromatographic analysis was used to confirm the purity of the gel-treated solvent; the absence of DVB at a sensitivity of 1 ppm was verified. The purity of the solvent was also verified through its use in anionic polymerizations as discussed in the text (Chapter 2).

A polymerization under similar conditions to those described in Chapter 2, with solvent prepared in an identical fashion except for the gel purification, resulted in complete deactivation of the calculated quantity of initiator and no polymerization. This clearly illustrates the capabilities of the polyvinyl gel material in this solvent purification application.

It should also be noted that the counterion utilized in solvent purification can be matched with that used during polymer synthesis, thereby eliminating difficulties which might arise due to counterion exchange. Another potential complication of this method of solvent purification is the presence of products of the reaction between initiator and impurities in the solvents. Under many conditions (diene polymerization being one possible exception) such byproducts have no detrimental influence on the polymerization. Furthermore, sufficient gel activation should provide an adequate number of "living" sites to

bind these complexing compounds, which otherwise would be destined to remain in solution. However, to test the possible influence of these byproducts, NMR analysis of polybutadiene sample B2 was carried out. This experiment identified a microstructure composed of 87% 1,4 (cis and trans) and 13% 1,2 addition (see Fig. 3-1). This is consistent with previously documented values for lithium-catalyzed anionic polybutadiene prepared in nonpolar solvents, using conventional methods of solvent purification (4).

DISCUSSION

The unfavorable structural characteristics of DVB gels prepared by anionic polymerizations in benzene can be attributed to microsyneresis. An analogous situation develops when DVB is emulsion polymerized, although the product is recovered as a microgel (5). Chemical and physical applications of such materials are limited to a "microregime", e.g., as multifunctional initiators for star polymers (6-8) in paint formulations (5) or as column packing for gel permeation chromatography. Addition of THF to benzene at a molar concentration four times that of initiator suppresses microsyneresis, permitting the synthesis of macroscopically homogeneous gels. The following discussion addresses the underlying chemical mechanism by which microsyneresis is believed to be avoided.

Substitution of sec-butyllithium for n-butyllithium in the absence of THF decreases the time to gelation but does not, by itself, suppress the undesirable microsyneresis. Addition of THF also increases the rate of initiation and thus also decreases gelation times. However,

in view of the results obtained with sec- and n-butyllithiums in the absence of THF, the major contribution of THF in suppressing syneresis in the gelation reactions must be attributed to something other than rapid initiation.

It can be assumed that the mechanisms of vinyl addition to lithium polystyryl and lithium poly(divinylbenzyl) are identical, based on the reported similarity between the reaction kinetics of each in benzene and in benzene/THF (9,10). It is well established that lithium polystyryl exists primarily in the dimeric form in benzene, although vinyl addition proceeds predominantly via dissociated contact ion pairs (4). The presence of THF has two significant effects on lithium polystyryl in benzene. First, it eliminates ion pair associations; unassociated lithium polystyryl etherates are the predominant living species in solution. Second, the mechanism of propagation in the presence of THF is dramatically changed so that vinyl addition occurs via a coordinated vinyl-etherate complex (4). This author believes that it is the first of these two effects which leads to the suppression of microsyneresis in the gelation reactions.

In order to test this hypothesis, a series of gelation reactions in a mixed solvent composed of 75% dioxane and 25% toluene (v/v) were performed. It has been shown that lithium polystyryl in dioxane exists as and propagates via unassociated contact ion pairs (4). Therefore by carrying out a gelation in this solvent, the same addition mechanism as for the case of reaction in pure benzene solvent has been maintained while essentially eliminating living-end association. The 25% toluene was added to the dioxane in order to obtain a solubility parameter

comparable to that of benzene while having the dielectric characteristics of the solvent mixture for the most part unchanged from that of pure dioxane. The results of these experiments appear in Table A-2 along with analogous information from the previous two solvent systems. The clarity and structural characteristics of the dioxane/toluene and benzene/THF gels were indistinguishable. The gelation times for the three cases are consistent with the reported values for the rates of polymerization of styrene in the respective solvents (Table A-2). This supports the earlier assumption regarding the similarity in reaction mechanism between styrene and divinylbenzene in each system.

In the case of dimeric lithium poly(divinylbenzyl), as found in benzene without THF, the proximity of the terminal pendent vinyl group of one living chain to the active end of its associated counterpart greatly enhances the probability of interchain reaction. Such reaction essentially doubles the molecular weight and the "living" functionality of the resulting species as illustrated in Figure A-1. Successive dimerization and cross-linking of separate species quickly increases the molecular weight, cross-link density and "living" functionality of the growing polymer, which all lead to microsyneresis. Adding THF to benzene or using dioxane-toluene eliminates lithium poly(divinylbenzyl) dimerization. In the absence of such association early stage polymerization is expected to be predominantly linear chain growth due to the high concentration of monomer units relative to polymer repeat units. Linear polymerization is also enhanced by a factor of 2 for the vinyl content of DVB monomer compared to polymer repeat unit and by the inability of ethylstyrene to contribute to cross-linking. Prior to

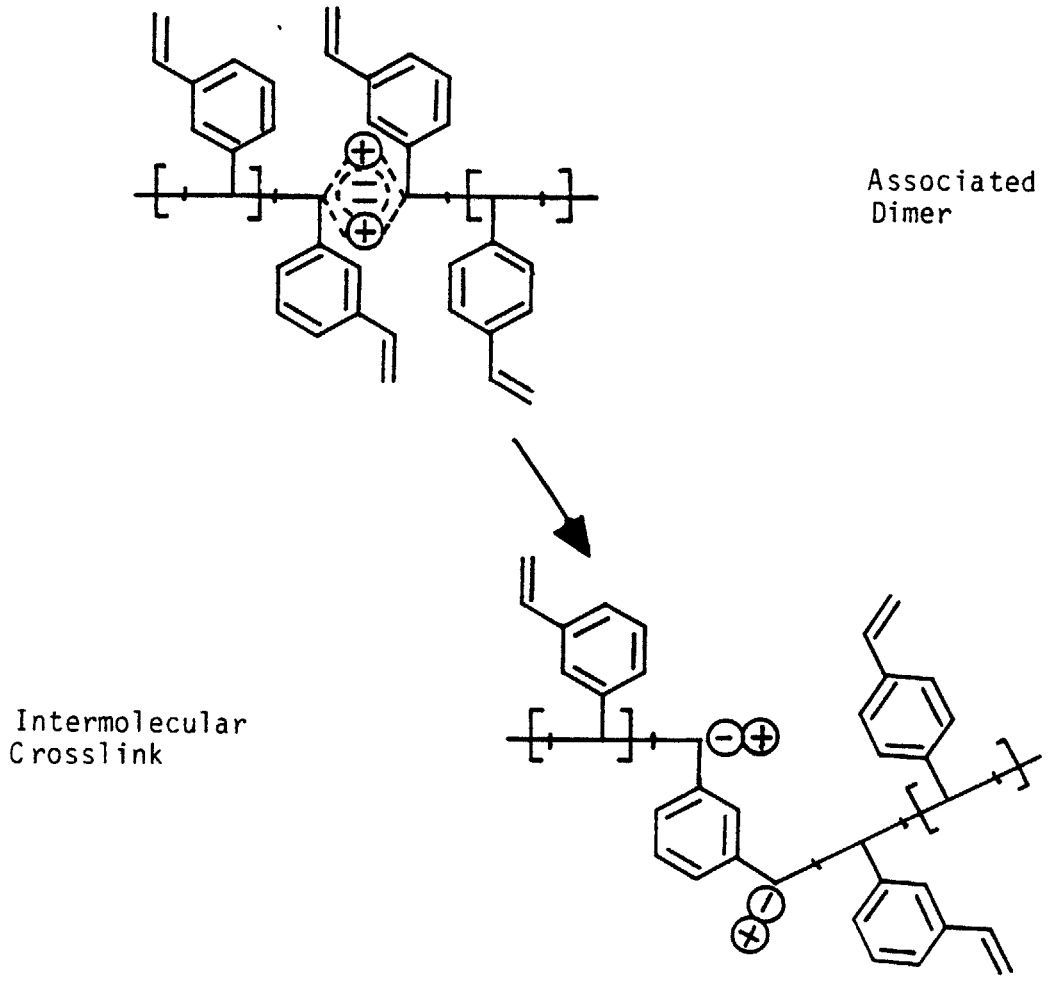

Figure A-1 Proposed mechanism leading to microsyneresis in the polymerization of DVB in non-polar solvents in the absence of a polar modifier such as THF.

gelation, the reaction medium is composed of soluble living polymer which then forms a macroscopic homogeneous network.

The termination-free nature of this polymerization and high ceiling temperature ensure virtually complete incorporation of monomer into the gel. Also observed was the fact that the gelation reaction stops at the point of swelling equilibrium; i.e., the "living" gel does not undergo macrosyneresis (1) nor does the recovered product swell further in excess solvent. Future work should be aimed at clarifying this phenomenon, the kinetics of the homogeneous gelation reactions, and the detailed structural features of the products.

References

1 K. Dusek, Polymer Networks--Structure and Mechanical Properties, eds., A.J. Chompff and S. Newman, p. 245, Plenum Press, N.Y. (1971).

2 R.L. Eppley and J.A. Dixon, J. Organomet. Chem., 8, 176 (1967).

3 R.J. Ceresa, ed., Block and Graft Copolymerization, vol. 1, J. Wiley and Sons, N.Y. (1973).

4 M. Szwarc, Carbanions, Living Polymers and Electron Transfer Processes, Interscience, N.Y. (1968).

5 W.J. Funke, Oil Colour Chem. Assoc., 60, 483 (1977).

6 H. Eschwey, M. Hallensleben and W. Burchard, Makromol. Chem., 173 235 (1973).

7 M. Eschwey and W. Burchard, Polymer, 16, 180 (1975).

8 M. Eschwey and W.J. Burchard, J. Polym. Sci., Polym. Symp., no. 53 (1975).

9 D.J. Worsfold, Macromolecules, 3, 514 (1970).

10 D.J. Worsfold, J.G. Zilliox and P. Rempp, Can. J. Chem., 47, 3379 (1969).

APPENDIX B: HPSEC Chromatographs

The high pressure size exclusion chromatographs used to obtain the characterization results given in Table 3-2 are presented in this appendix. Diblock copolymer chromatographs have been paired with those obtained from the corresponding polystyrene (S) blocks (see Chapter 2). Retention volumes in milliliters are indicated by numbered markers. All the S-block chromatographs shown in Figure B-1 (5pages) exhibit a secondary peak at a retention volume corresponding to twice the molecular weight determined from the primary peak. This is particularly apparent in samples SB_d1, SB5, SB6, SB7 and SB9. In the case of diblock copolymers containing a low weight fraction of polybutadiene, the peak position is shifted only slightly lower in retention volume than for the precursor S-block. Therefore, if the secondary peak displayed by the former were representative of the polystyrene in the reactor, it would be clearly identifiable in the diblock chromatograph. Samples SB_d1 and SB7 clearly demonstrate that this is not the case. Instead, this secondary peak is actually an artifact of the sampling procedure (see Chapter 2). For this reason, these peaks have been represented by a dashed curve.

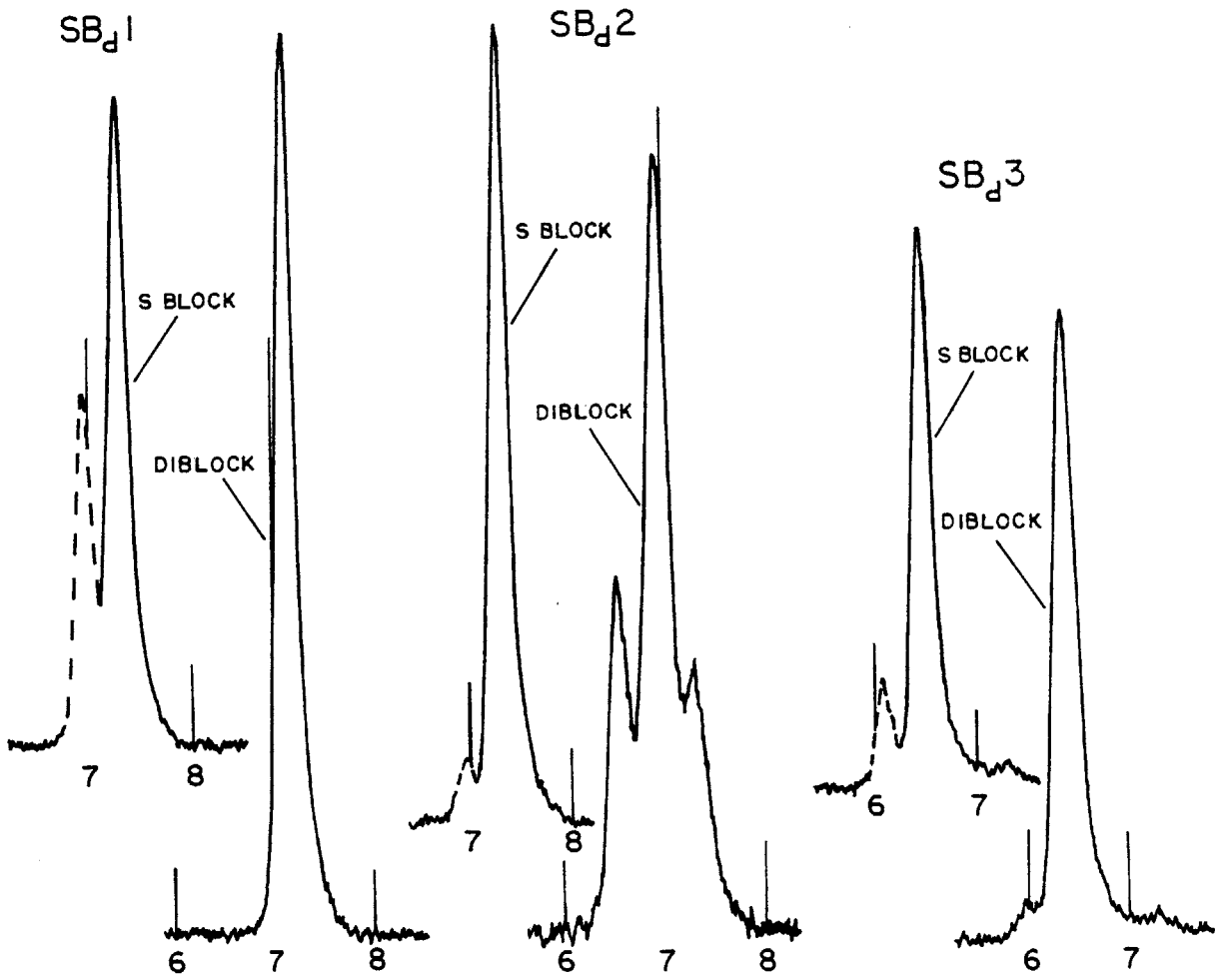

Figure B-1 (page one of five) HPSEC chromatographs. Numbered markers indicate retention volume in milliliters.

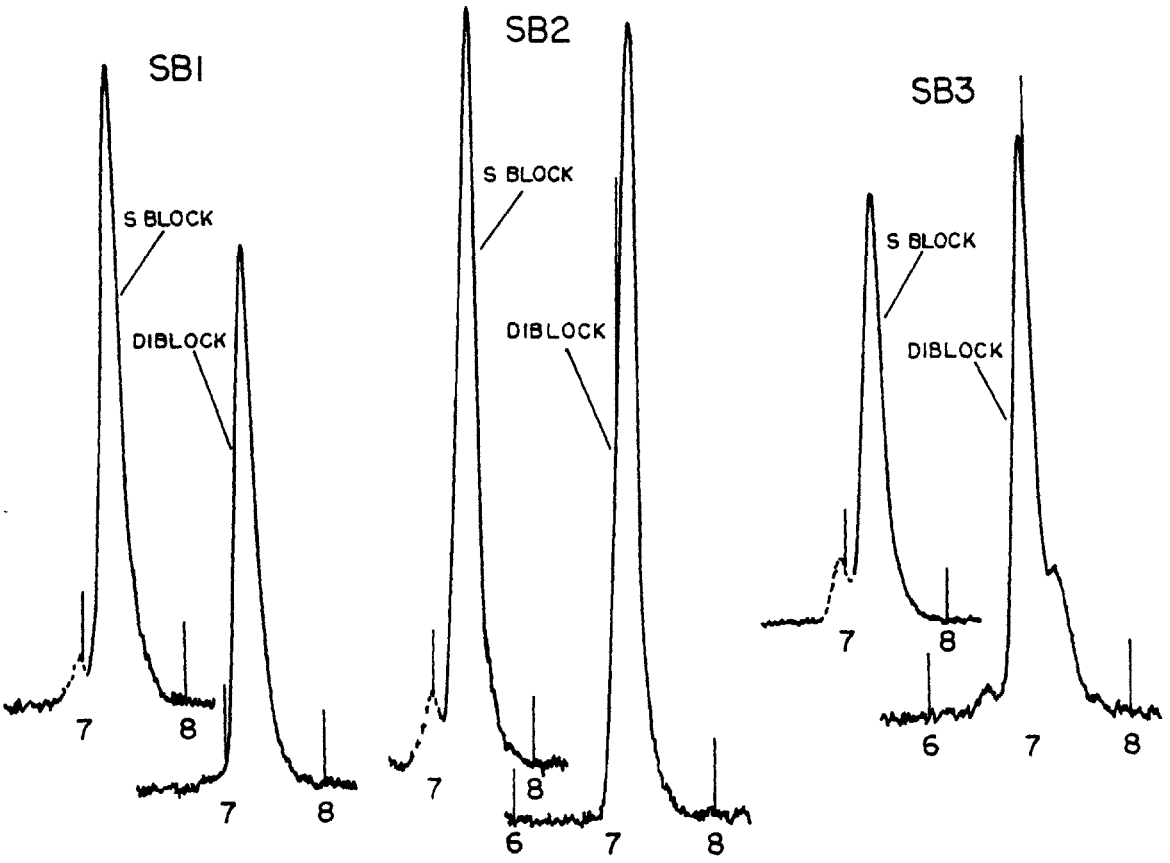

Figure B-1 (page two of five)

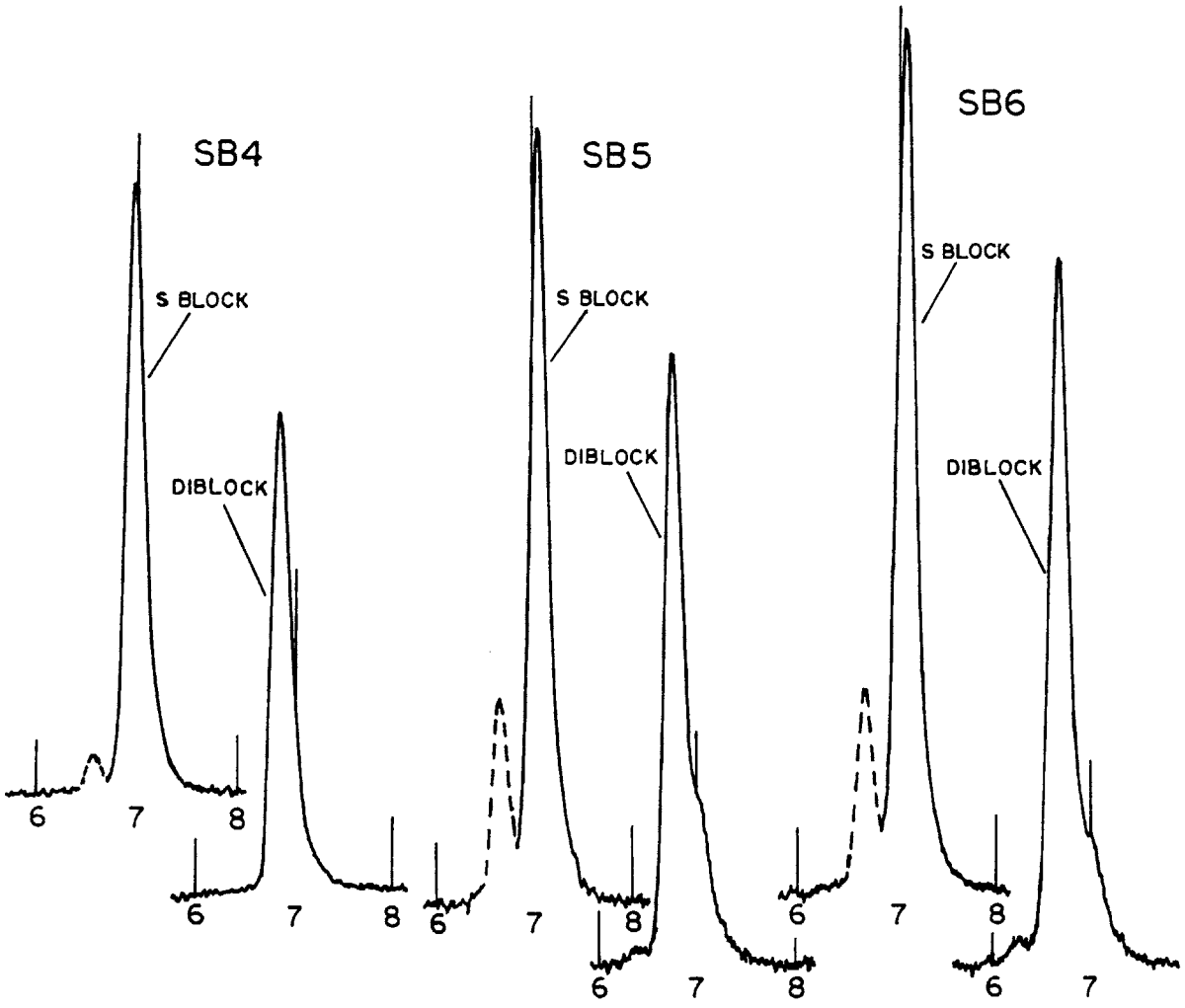

Figure B-1 (page three of five)

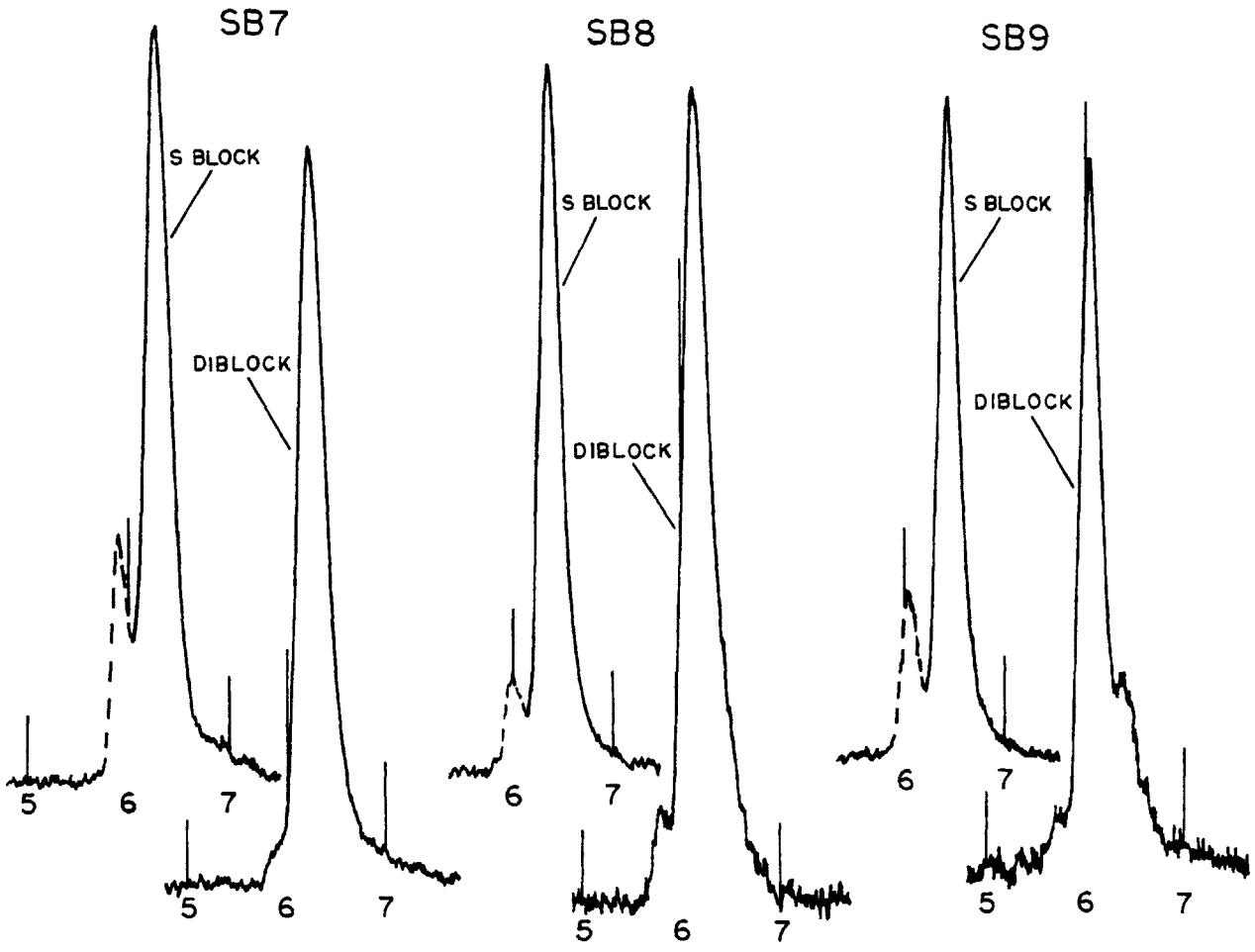

Figure B-1 (page four of five)

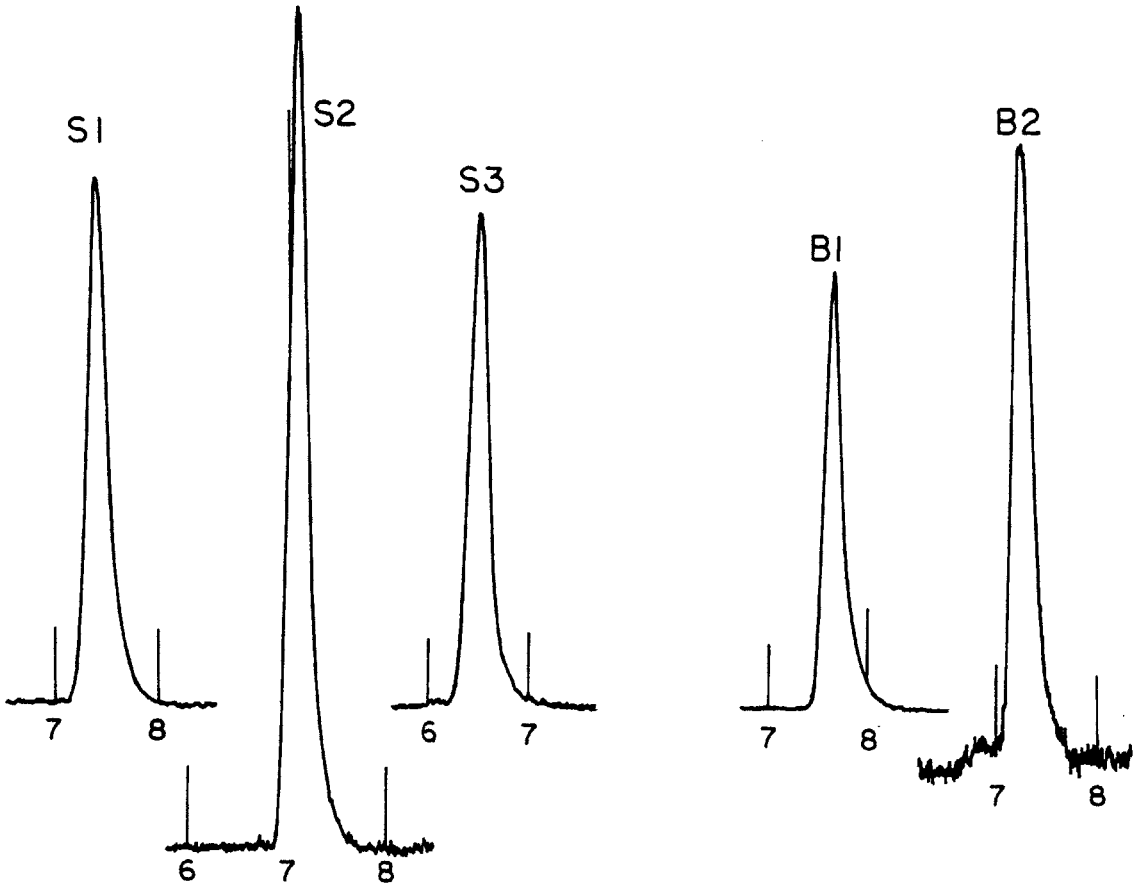

Figure B-1 (page five of five)

APPENDIX C: Single Chain Scattering

The data discussed in this appendix have been collected and analyzed in collaboration with Dr. G.D. Wignall of NCSASR, ORNL. Details concerning the methods of data collection and correction may be found in Chapter 5.

INTRODUCTION

Small angle neutron scattering has recently gained wide popularity in the area of polymer physics, primarily due to the powerful deuterium substitution staining technique discussed in the main text. The data presented in Chapter 5 utilized this contrast enhancement in order to improve the signal-to-noise ratio obtained from the two-phase scattering, which included Bragg, single sphere and Porod scattering. A SAXS instrument could also have been used to obtain the Porod and single sphere measurements. Although theoretically feasible, it would have been impossible to obtain the high resolution (15.3 m) Bragg data with available SAXS equipment. The real advantage to using SANS lies in the ability to extract single chain scattering functions from bulk materials. Four of the diblock copolymers reported in the text were designed to permit investigation of the single chain scattering behavior of these two-phase materials.

Measurement of polymer single chain dimensions by SANS originated less than a decade ago (1) and remains in a state of infancy. Brief reviews of the topic are included in References (2,3). Scattering from

any isotropic substance in the limit of low Q has been shown by Guinier and Fournet (4) to be exponential in the radius of gyration, R_g:

$$I(Q) = I(0)\exp(-R_g^2Q^2/3) \qquad 1$$

This can be illustrated on a molecular level for polymer chain coils which obey Gaussian statistics. The scattering from a Gaussian coil is characterized by the Debye function (5),

$$I(Q) = I(0°)(2/v^2)[v-1+\exp(-v)] \qquad 2$$

$$v = Q^2R_g^2 \qquad 3$$

$$Q = 4\pi\sin\theta/\lambda \qquad 4$$

where R_g is the coil mean square radius of gyration. For $v<1$ equation 2 can be expanded to give,

$$I(Q) = I(0°)\left(1-\frac{R_g^2Q^2}{3} + O(Q^4)\ldots\right) \qquad 5$$

where, to the approximation of the first two terms, equation 5 is identical with the expansion of equation 1. Equation 5 predicts that a plot of $I(Q)^{-1}$ versus Q^2 will directly yield R_g^2 through the slope and intercept for values of $R_gQ < 1$, independent of the concentration of labelled chains. Recently, Wignall et al. (6) have verified this latter point, reporting a constant measured value of R_g for various concentrations up to 50 mole % perdeuterated polystyrene in hydrogenous polystyrene.

Forward scattering at zero angle in a system composed of isotropically distributed molecules is related to the weight-average molecular weight as given by (7,8),

$$M_w = \frac{1}{cK_N}\left(\frac{d\Sigma}{d\Omega}\right)_{Q=0} \qquad 6$$

$$\text{where} \qquad K_N = \bar{v}^2(\rho_p-\rho_m)^2/N_A$$

$\frac{d\Sigma}{d\Omega}(Q)$ must be specified in units of absolute intensity (cm^{-1}), $\bar{v}$ is the polymer specific volume (cm/g), and c is the concentration of labelled chains (g/cm^3). $(\rho_p-\rho_m)(cm\cdot cm^{-3})$ represents the contrast factor and N_A is Avogadros number. Wignall et al. (6) have recently shown that for blends of equal molecular weight polystyrenes, the forward scattering is actually related to the mole-fraction of labelled polymer, x:

$$\frac{I(0°)}{x(1-x)} = \text{constant} \qquad 7$$

Therefore, c in equation 6 must be proportioned accordingly.

SINGLE CHAIN SCATTERING IN BLOCK COPOLYMERS

The preceding discussion has been developed under the assumption that single chain scattering derives from a single phase material, e.g. I(Q) can be represented by a single chain correlation function. Obviously, phase separated block copolymers are not consistent with this premise. These materials exhibit strong interference effects,

attributable to both inter and intraparticle scattering, the intensity of which is directly related to the contrast factor. As was shown in Chapter 5, these effects remain significant in fully hydrogenated samples. Therefore, extraction of a single chain scattering function in these materials requires the subtraction of this structure scattering, or its elimination by appropriate deuterium labelling (see below).

Richards and Thomason (8) have determined the single chain dimensions of a perdeuterated polystyrene block contained in a diblock copolymer with cis 1,4 polyisoprene. In order to account for phase structure, these authors subtracted the scattered intensity obtained from an unlabelled sample from that taken on a labelled (4% w/w) specimen. The resulting molecular weight obtained from a Debye plot (eq. 5) was reportedly in excellent agreement with that determined by gel permeation chromatography. These authors neglected equation 7, although in this case it only represents a minor correction.

Recently, Jahshan and Summerfield (9) have shown that the scattering intensity obtained from a two-phase polymer system, in which one of the phases is composed of a mixture of labelled and unlabelled chains of equal dimensions, is given by:[1]

$$I_L(Q) - \frac{\left[\rho_S - \rho_{B_d} x - \rho_B(1-x)\right]^2}{(\rho_S - \rho_B)^2} I(Q) = \left[\bar{v}^2 (\rho_{B_d} - \rho_B)^2 / N_A\right] x(1-x) c_B M_w P_B(Q) \qquad 8$$

[1]Professor J.T. Koberstein also independently arrived at this result which he provided to this author prior to its appearing in the literature.

According to equation 8, in order to extract the single chain scattering function P_B, the scattered intensity from a labelled sample, I_L, must be corrected by subtracting a weighted fraction of the scattered intensity obtained from an unlabelled sample, I. Application of equation 8 requires that each sample contain an identical phase structure. x represents the fraction of B species which are labelled (B_d) and ρ_S,ρ_B, and ρ_{B_d} are the segment scattering length densities. Values of ρ for the present case can be found in Table 4-2 in Chapter 4.

EXPERIMENTAL

Examination of equation 8 reveals that determination of P_B can be greatly simplified by choosing x such that the term multiplying I(Q) becomes zero. For the polystyrene-polybutadiene system presently being considered, this corresponds to x = 0.16. Therefore, two specimens were film cast from toluene in which 16% of the polybutadiene was of the perdeuterated form and these two samples are designated as SB_d1/SB1 and SB_d3/SB7. As documented in Table 3-2 (Chapter 3), the molecular characteristics of these paired polymers are very similar, particularly in the case of SB1 and SB_d1. Sample preparation, data acquisition and corrections were carried out as reported in Chapters 4 and 5. SANS spectra were obtained for these samples at sample-to-detector distances of 2.74 (SB_d1/SB1) and 6 (SB_d3/SB7) meters and for sample S3-T at both detector settings. The resulting data files are listed in Appendix E.

While absolute intensity calibration is not required for determining R_g, it is necessary in order to calculate M_w using equation 6

or 8. Therefore, background and detector sensitivity corrected data were converted to an absolute differential scattering cross section per unit solid angle, in units of cm^{-1}, by means of equation 5-2 given in Chapter 5, where the neutron calibration constant K_N was determined by the staff at NCSASR (see Appendix E). The resulting scattering patterns are shown in Figures C-1 and C-2.

Comparison of the labelled results given in Figures C-1 and C-2 with those from the unlabelled samples found in Chapter 5 clearly demonstrate the validity of equation 8. The strong structure scattering apparent in Figures 5-9 to 5-11 has been entirely eliminated in the spectra obtained from the 16% labelled samples. Therefore, the observed coherent intensity can be attributed to single chain scattering.

Sample S3-T was also examined in order to calculate the incoherent background intensity which must be subtracted from the labelled spectra prior to analyzing the scattering pattern. Calculations of the normalized incoherent scattering cross section for the blended samples, averaged over all species (10), reveals that to within one-half of one percent, they can be represented by bulk polystyrene. Although polybutadiene contains a higher incoherent scattering cross section than does polystyrene, inclusion of 16% perdeuteropolybutadiene balances the overall polybutadiene incoherent cross section with that of polystyrene. Also, since the major component of these block copolymers is polystyrene, anomalies such as the slight slope observed in Figure C-1 for sample S3-T will be accounted for in labelled samples using this sample for incoherent background corrections. Linearly regressed fits

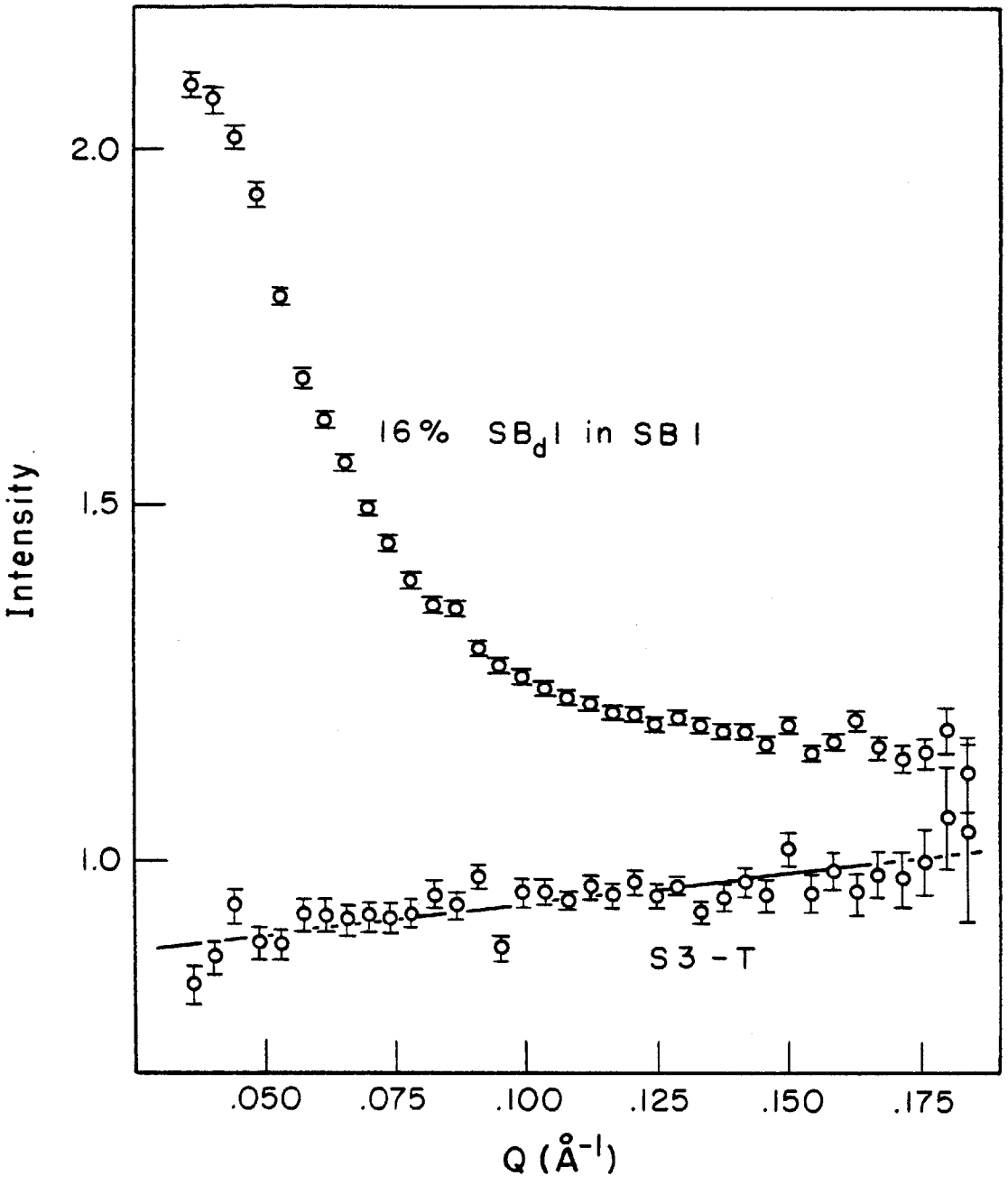

Figure C-1 SANS pattern for single chain scattering from block polybutadiene in SB_dl. Scattering pattern for SB_dl is given in Figure 5-10. The S3-T data were used to correct for incoherent scattering.

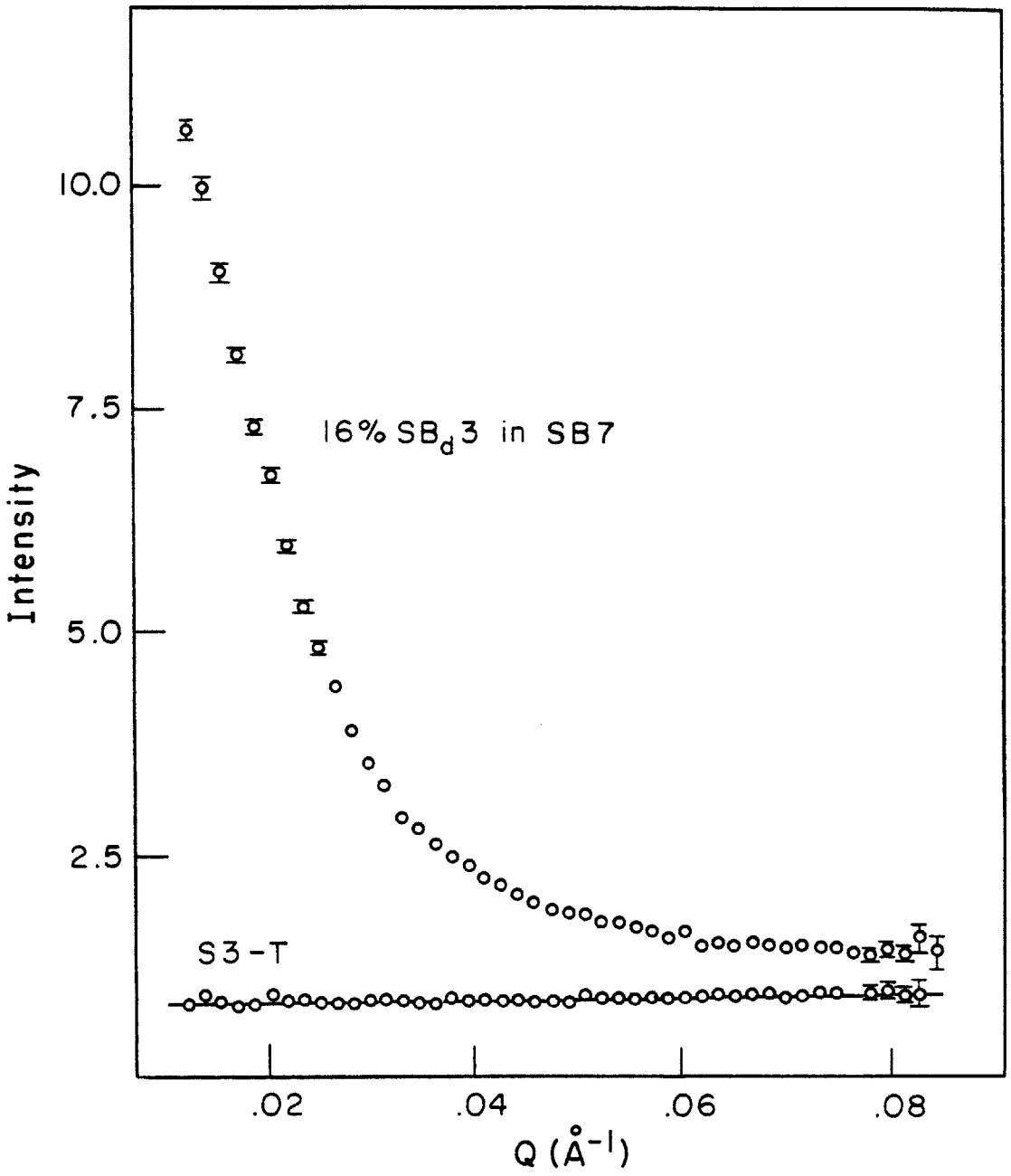

Figure C-2 SANS pattern for single chain scattering from block polybutadiene in SB_d3. Scattering patterns for SB_d3 and SB7 are given in Figures 5-9 and 5-11. The S3-T data were used to correct for incoherent scattering.

to the S3-T data have been used to obtain the incoherent scattering correction for the blended samples; these fits are also shown in Figures C-1 and C-2.

The data appearing in Figures C-1 and C-2 have been corrected for incoherent scattering and recast in the form of Debye plots (I^{-1} versus Q^2) which are presented in Figures C-3 and C-4. Straight line best fits to the low Q^2 linear data are also given in these plots. In the case of $SB_d1/SB1$ this corresponds to $Q^2 < 55 \cdot 10^{-4}$ and for $SB_d3/SB7$, $Q^2 < 4.1 \cdot 10^{-4}$. Based on equation 5 the radii of gyration of the polybutadiene in SB_d1 and SB_d3 have been determined and are given in Table C-1, each value subject to ~15% error. M_w has also been calculated by means of equation 6 with $\bar{v} = 1.12$ cm^3/g and c corrected according to equation 7, $c = (0.16)(1-0.16)c_B$ (g/cm^3) where the concentration of polybutadiene, c_B, has been determined from Table 3-1 (Chapter 3). In the present case, the contrast factor must be determined from the hydrogenated and deuterated polybutadiene scattering length densities (see equation 8), $(\rho_{B_d} - \rho_B)^2 = 3.89\ 10^{21} (cm \cdot cm^{-3})$. It should be noted that Richards and Thomason (8) have made an error in calculating their contrast factor. They took ρ_m to be the weighted sum of the unlabelled scattering length density from each phase rather than from hydrogenated polystyrene. Calculated weight average molecular weights are tabulated in Table C-1. These measurements are subject to ~15% error, primarily determined by the accuracy of the absolute intensity calibration constant. Also included in Table C-1 are the values of M_w for the perdeuterated polybutadiene as measured by HPSEC and UV absorption (Chapter 3).

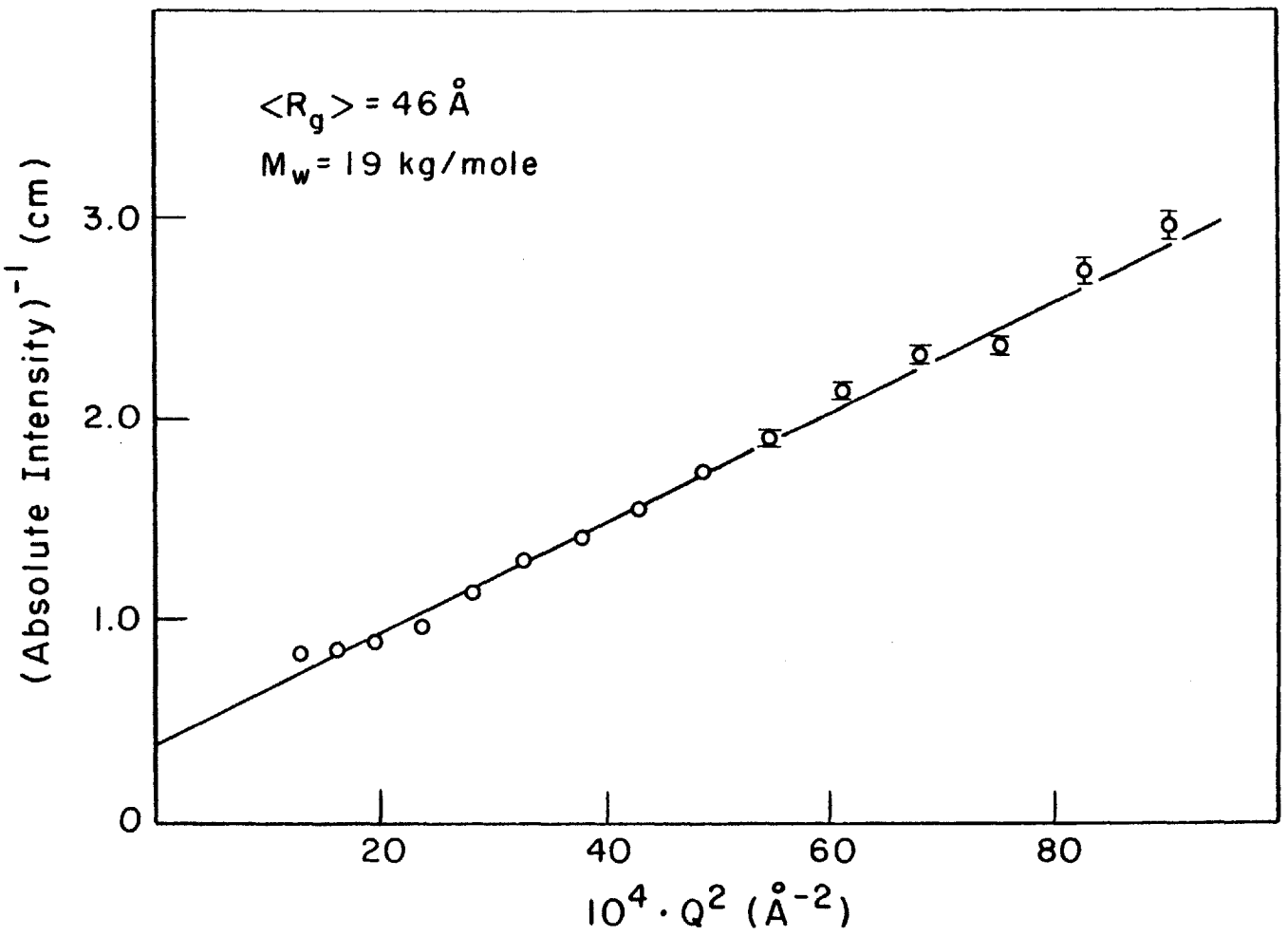

Figure C-3 Debye plot of the single chain scattering data obtained from sample SB_d1/SB1 (see Fig. 1).

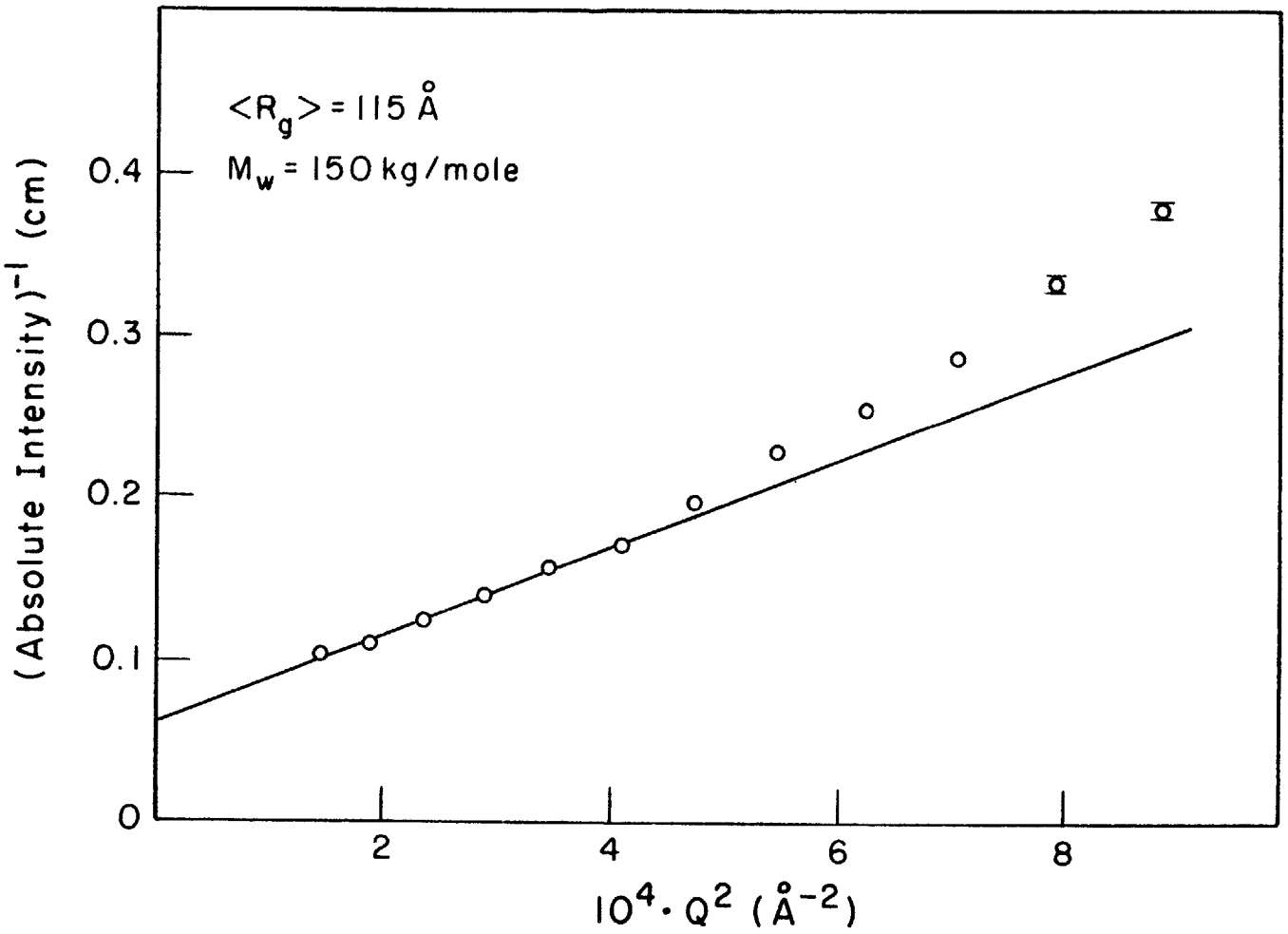

Figure C-4 Debye plot of the single chain scattering data obtained from sample $SB_d3/SB7$ (see Fig. 2).

TABLE C-1

Single Chain Scattering Results

Sample	$\bar{R}_{SPHERE}$ (Å)	R_g (Å)		M_w (kg/mol)	
		SANS	[b]predicted	SANS	molecular characterization
SB_d1/SB1	[a]119	46	44	19	[c]14
SB_d3/SB7	[a]224	115	84	150	[c]46
[d]DSI1	(130)	40	40	[e]36	[f]21

[a]Weighted average of SANS results from pure components (Chapter 5) [b]Based on homopolymer data [c]Determined by HPSEC and UV absorption (Chapter 3) [d]Results of Richards and Thomason (8) [e]The reported value, 26 kg/mol, was obtained using an incorrect contrast factor [f]Determined by GPC

DISCUSSION

Unperturbed polymer chain dimensions were long ago predicted to follow the simple expression (11), $R_g/M_w^{1/2} = (K/\Phi)^{1/3}$ where K/Φ is constant for a given polymer at a fixed temperature. SANS measurements on bulk polystyrene have verified this behavior (1) where $(K/\Phi)_S^{1/3} = 0.27\text{-}0.28(\text{Å } g^{-1/2}\text{mol}^{1/2})$. Therefore, in the case of polybutadiene this parameter can be estimated from intrinsic viscosity data obtained at theta conditions, $(K/\Phi)_B^{1/3} \simeq 0.37$ $(\text{Å } g^{-1/2}\text{mol}^{1/2})$ (12). Based on these constants the predicted values of R_g for the polymers presently being considered have been determined, and are listed in Table C-1. The results presented in Table C-1 have been contrasted with those obtained by Richards and Thomason (8) on block polystyrene.

Implicit in the calculation of M_w is the assumption that labelled polymer chains are randomly distributed within the sample. In practice it has been shown that this measurement is very sensitive to the degree of dispersion of single chains. Ballard et al. (7) demonstrated that in crystalline polyethylene M_w apparent directly correlates with the number of labelled chains contained within a "cluster." These authors have also shown that clustering has very little influence on the measured R_g; clustering of 600 chains only led to a 10% increase in measured R_g. Therefore, the R_g results will be considered independent of the calculated M_w.

The restrictions associated with interfacial block joint placement and domain boundary reflection violate the premise of equation 2, i.e. Gaussian chain statistics. Nevertheless, as indicated above, the

Guinier approximation (eq. 1) is valid regardless of particle form. As indicated in Table C-1, labelled block chains in samples SB_d1/SB1 and DSI1 assume conformations having radii of gyration equivalent to those of the corresponding homopolymers. However, labelled chains in sample SB_d3/SB7 exhibit a significantly larger radius of gyration than would a homopolymer counterpart.

It was demonstrated in Chapter 7 that samples SB_d1 and SB1 are essentially in a state of phase equilibrium, e.g. the spherical domain radii measured by SANS nearly equal those predicted by Helfand and Wasserman (13). It should be noted that reported polystyrene spherical domain dimensions are also consistently in agreement with equilibrium theory (13). In contrast, the domains found in samples SB_d3 and SB7 are markedly smaller than is predicted from theory (see Chapter 7). Using weighted pure component SANS values given in Chapter 5, the domain size in sample SB_d3/SB7 is estimated to be R = 224 Å, as opposed to 380 Å at equilibrium. This represents a five-fold decrease in sphere volume from equilibrium.

As discussed in Chapter 7, the development of smaller, non-equilibrium spheres in bulk is brought about by the establishment of fewer chains per domain at the point of phase separation in solution. This reduction in sphere size will increase the influence of the domain boundary and joint placement restrictions on polymer chain conformations. Indeed, the polybutadiene chains in sample SB_d3/SB7 show a significant increase in R_g over that predicted for an equivalent homopolymer. This explains the discrepancy between the results presented in Table C-1. In the case of equilibrium block domains, the chains

assume an unknown conformation, but one which has essentially the same radius of gyration as would be found in an equivalent homopolymer. A deviation from equilibrium, brought about by reducing the number of chains per domain, results in a significant perturbation in this chain conformation, as evidenced by a marked increase in R_g.

The above results are paralleled by the molecular weight behavior as measured by SANS. Since the block joints must reside along the domain surface, it would be unreasonable to assume that the chains were isotropically distributed within the domains. It is not surprising therefore that the measured M_w in sample $SB_d1/SB1$ is somewhat higher than was obtained by molecular characterization. Richards and Thomason (8) obtained a similar result. A dramatic increase in this discrepancy is found in sample $SB_d3/SB7$. Based on the above discussion this is not surprising since the restrictions placed on single chains within these domains have been increased. Yet it is impossible to establish the specific source of these M_w deviations. Clustering, as found in crystalline polyethylene (7) seems unlikely in the present situation. Instead, the statistical ordering of block joints on the domain surface may be the source of additional scattering which leads to a higher extrapolated zero angle intensity and the resulting increase in M_w.

CONCLUSIONS

This single chain scattering study has resulted in two significant findings. First, the theory of Jahshan and Summerfield (9) concerning the scattering from two-phase systems has been verified, so that

structural scattering can be eliminated by properly labelling a given phase. Second, at equilibrium, block copolymer chains exhibit radii of gyration equal to the corresponding homopolymers. Under non-equilibrium conditions, as frequently occurs in solvent cast polymer films, the chain dimensions may deviate from this behavior. In particular, reduction in spherical domain size from equilibrium results in an increase in the single chain radius of gyration.

References

1 H. Benoit, D. Decker, J.S. Higgins, C. Picot, J.P. Cotton, B. Farnaux, G. Jannink and R. Ober, Nature, 245, 13 (1973).

2 J.S. Higgins and R.S. Stein, J. Appl. Cryst., 11, 346 (1978).

3 J.S. King, Methods of Experimental Physics: Polymers, vol. 16, ed. R.A. Fava, Academic Press (1980).

4 A. Guinier and G. Fournet, Small Angle Scattering of X rays, J. Wiley and Sons, N.Y. (1955).

5 P. Debye and B. Bueche, J. Chem. Phys., 20, 1337 (1952).

6 G.D. Wignall, R.W. Hendriks, W.C. Koehler, J.S. Lin, M.P. Wai, E.L. Thomas and R.S. Stein, Polymer, 22, 886 (1981).

7 D.G.H. Ballard, A. Cunningham and J. Schelten, Polymer, 18, 259 (1977).

8 R.W. Richards and J.L. Thomason, Polymer, 22, 581 (1981).

9 S.N. Jahshan and G.C. Summerfield, J. Polym. Sci. Phys. Ed., 18, 1859 (1980).

10 G.E. Bacon, Neutron Diffraction, Oxford (1962).

11 P.J. Flory, Principles of Polymer Chemistry, Cornell University Press (1953).

12 J. Brandrup and E.H. Immergut, eds., Polymer Handbook, second edition (1975).

13 E. Helfand and Z.R. Wasserman, Macromolecules, 11, 960 (1978)

APPENDIX D: A Re-examination of the Phase Behavior in Polyisoprene-Polybutadiene Diblock Copolymer-Homopolymer Blends

INTRODUCTION

The past decade has seen considerable advances made in the theoretical treatment of polymer-polymer miscibility (1,2) particularly in the area of block copolymers (3,4), which have well outpaced experimental developments. In this regard, the experimental findings of Ramos and Cohen (5-7) have attracted this author's attention. This brief note demonstrates that the results reported by these authors, concerning the phase behavior of a set of block copolymer-homopolymer blends, can be readily explained in terms of current theories concerning polymer-polymer miscibility.

DISCUSSION

Ramos (8) examined the phase characteristics of a set of cis 1,4 polyisoprene-1,4 polybutadiene diblock copolymer-homopolymer blends. Table D-1,reproduced from Ref.(8), lists the molecular characteristics of the samples he examined. Dr. Paul Rempp, CNRS, Strasbourg, France, synthesized the diblock copolymers, the polyisoprene was obtained from Shell Nederland Chemie B.V. (Cariflex 309), and the polybutadiene was obtained from Phillips Petroleum Company (Solprene 233).

As documented in a series of publications, Ramos and Cohen (5-7) have demonstrated that the blends of these materials can exhibit either one-phase or two-phase behavior. The authors relied on the dynamic

[a]TABLE D-1

[b]Polymer	Mol% I	Wt% I	[c]Overall M_w	Repeat Units B/I
Diblock 2143	0.50	0.56	250000	1
Diblock 2144	0.34	0.39	264000	2
Diblock 2148	0.66	0.71	270000	0.5
Polyisoprene	1.00	1.00	133000	0
Polybutadiene	0	0	120000	∞

[a]Taken from Ref. (8) [b]Polyisoprene - 90% cis 1,4; polybutadiene - 45% cis and 45% trans 1,4, 10% vinyl [c]Diblocks via light scattering, homopolymers via intrinsic viscosity

mechanical spectrum of a sample in order to ascertain the state of phase separation. If two distinct peaks or shoulders could be identified in the glass transition region of the damping (tan δ) and storage modulus (E') spectra, the blend was assumed to be heterogeneous. Resolution of a single tan δ peak and shoulder-free glass transition in the E' spectrum indicated a homogenous mixture.

Using the above method the authors constructed three ternary phase diagrams composed of diblock copolymer, polyisoprene and polybutadiene; these are designated as COP 2143, COP 2144 and COP 2148 (see Table D-1). All three diblock copolymers were found to be homogeneous while the phase behavior in the blended regions of each ternary diagram varied. A schematic representation of these phase diagrams can be found in Ref. (7). These three sets of data need not be discussed individually as has been presented by the authors. As shown below all the data derive from a single phase diagram.

The data originally reported by Ramos (8) have been replotted as mole fraction isoprene n_I, versus mole fraction diblock copolymer n_{COP}, in Figure D-1. It should be noted that diblock copolymer 2148 does not lie at $n_{COP} = 1$. An analysis of the three block copolymer samples by HPSEC revealed that diblock copolymer 2148 contained ~15% by weight homopolybutadiene; Ramos was apparently unaware of this since light scattering was used in diblock copolymer characterization. A solid curve, symmetrical about $n_I = 0.5$, has been included in order to distinguish between regions of two-phase (open circles) and one phase (filled circles) behavior.

What is observed in Figure D-1 can now be interpreted in terms of

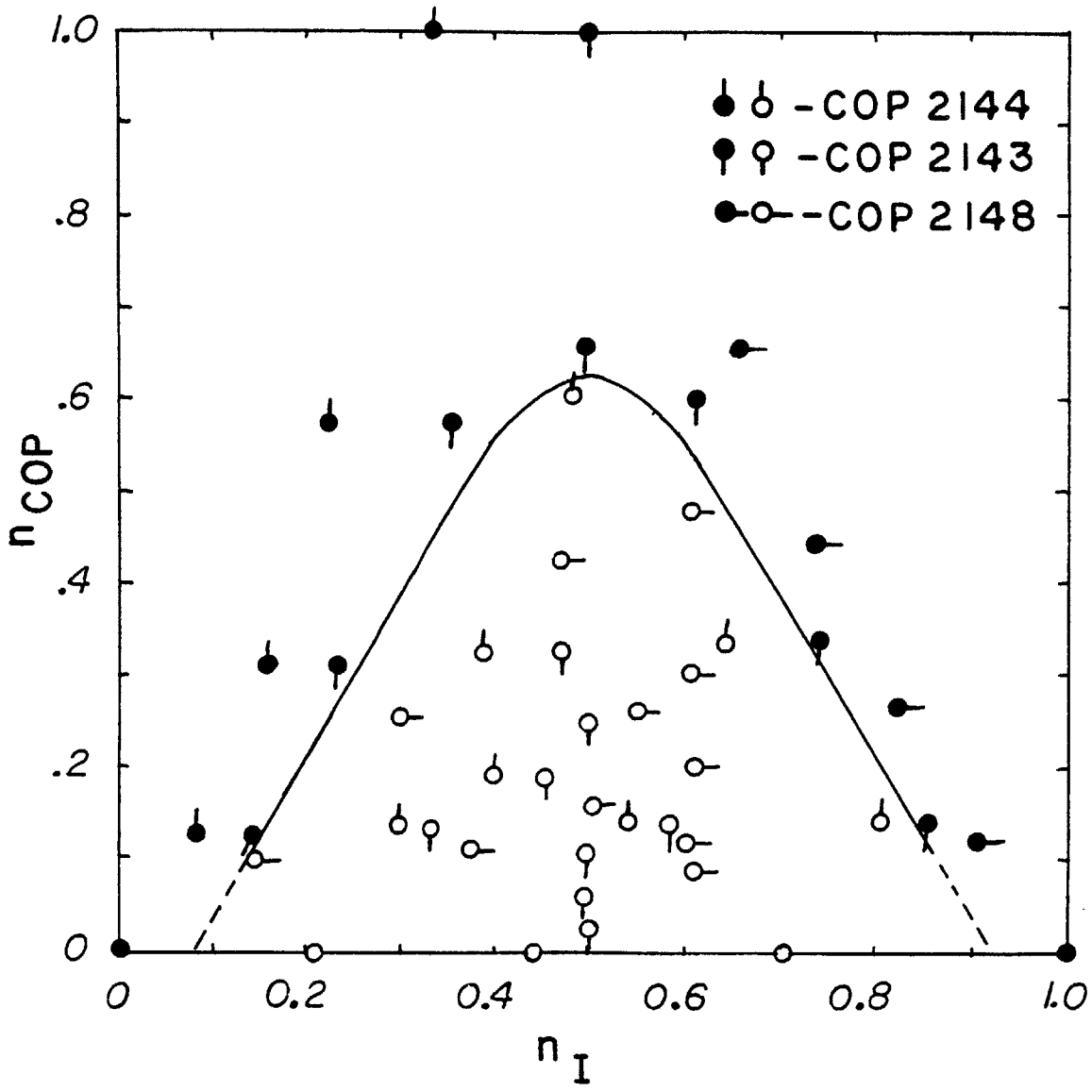

Figure D-1 Mole fraction polyisoprene, n_I, versus mole fraction diblock copolymer, n_{COP}. Filled circles indicate one phase and open circles two-phase behavior as taken from Ramos (8).

a three component phase diagram as illustrated in Figure D-2. The base plane of this three-dimensional plot is equivalent to the two-dimensional plot given in Figure D-1. The third vertical axis represents $N\chi$, the product of polymerization index N and interaction parameter χ.

In mixtures of two homopolymers the critical point of demixing is given by $(\chi N)_{crit} = 2$ (2,9) and the stability curve in the plane $n_{COP} = 0$ has been drawn accordingly. Leibler (3) has recently shown that a universal phase diagram can be used to represent the regions of stability in diblock copolymers where $(N\chi)_{crit} = 10.5$. The stability curve as predicted by Leibler is included in the plane $n_{COP} = 1$.

As indicated in Table D-1, to a good approximation, $(N\chi)_{COP} = 2(N\chi)_{HOP}$, where HOP signifies homopolymer. Therefore, all the data shown in Figure D-1 lie on a plane in composition space dictated by this relationship. Since χ is related to segment-segment interactions it may be assumed to be independent of chain geometry (homopolymer versus block polymer). Unfortunately, the absolute location of this plane cannot be established since χ is not known. Although in theory one could attempt to fit the extrapolated (dashed line) intercept of the stability curve, deduced from Figure D-1, to the homopolymer-homopolymer stability curve (2,9), the uncertainties involved mitigate the usefulness of such an approach. Nevertheless, this plane is constrained to a region defined by $(N\chi)_{n_{COP}=0} > 2$, $(N\chi)_{n_{COP}=1} < 10.5$ and $(N\chi)_{COP} = 2(N\chi)_{HOP}$. An example of a plane which falls within these limits is also shown in Figure D-2. Therefore, the data of Ramos as plotted in Figure D-1, merely represents a projection of a $(N\chi)_{COP} = 2(N\chi)_{HOP}$

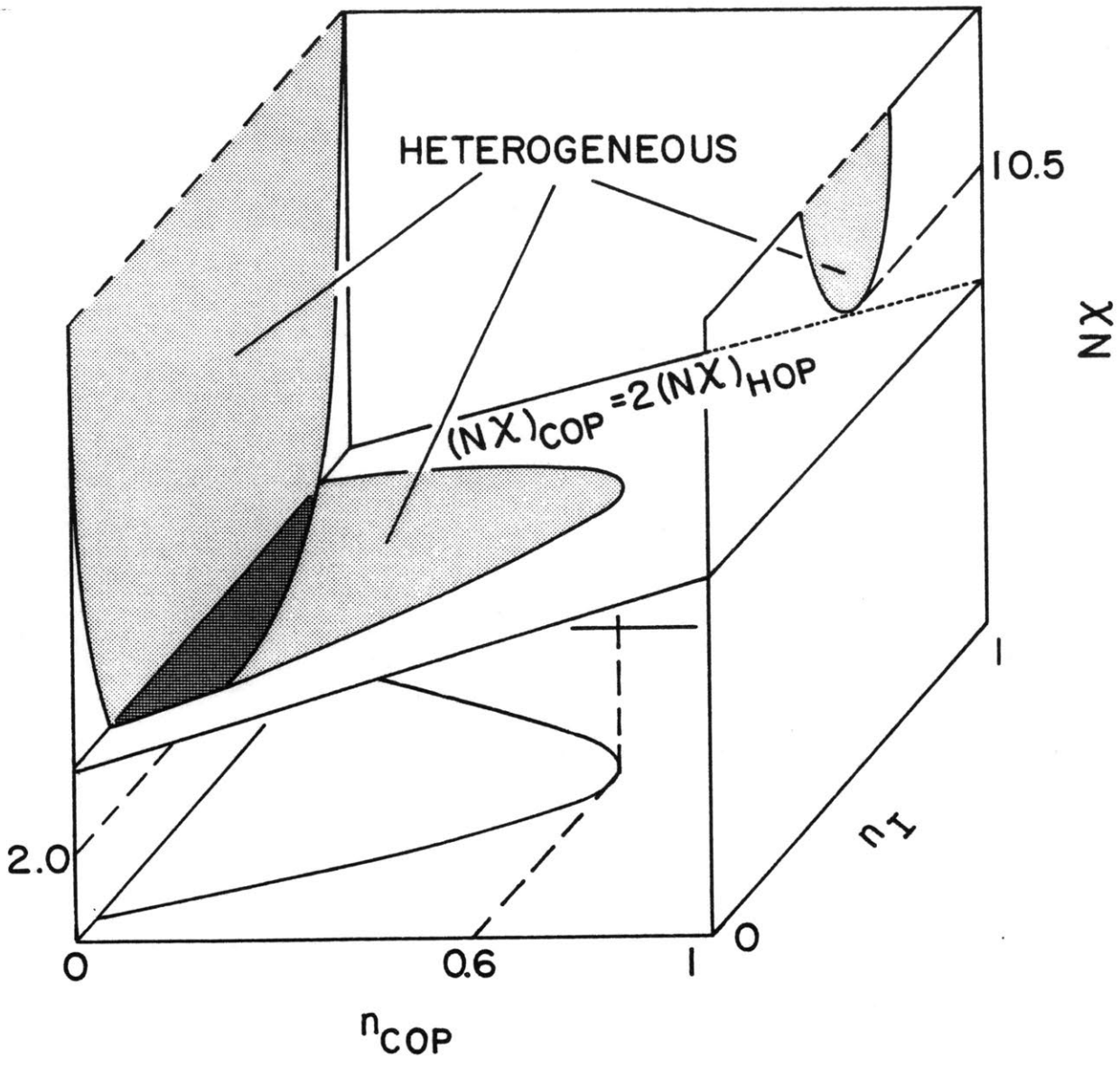

Figure D-2 Diblock copolymer-homopolymer-homopolymer phase diagram. Homopolymer ($n_{COP} = 0$) and diblock copolymer ($n_{COP} = 1$) stability curves are given by Flory (9) and Leibler (3) respectively. Data lie on $(N\chi)_{COP} = 2(N\chi)_{HOP}$ plane.

plane which has sliced through the three component stability dome.

CONCLUSION

The data of Ramos (8) are entirely consistent with current theories concerning phase separated diblock copolymers and homopolymers as demonstrated in Figure D-2. Further use of this information will require a knowledge of χ, which would enable specification of the data in composition space. Since the critical point for this operating plane has been established, $n_{COP} = 0.6$ (see Figures D-1 and D-2), the critical line could then also be inferred. Such information would be very useful in developing theoretical predictions concerning the miscibility of block copolymers and homopolymers in general.

References

1 L.P. McMaster, Macromolecules, 6, 5 (1973).

2 P.G. deGennes, Scaling Concepts in Polymer Physics, Cornell University Press, Ithaca, N.Y. (1979).

3 L. Leibler, Macromolecules, 13, 6 (1980).

4 E. Helfand and Z.R. Wasserman, to appear in Developments in Block Copolymers, ed. I. Goodman, Applied Sciences Publishers, Ltd.

5 A.R. Ramos and R.E. Cohen, Polymer Eng. Sci., 17, 639 (1977).

6 A.R. Ramos and R.E. Cohen, Adv. Chem. Series, 176, 237 (1979).

7 R.E. Cohen and A.R. Ramos, Macromolecules, 12, 131 (1979).

8 A.R. Ramos, Sc.D. thesis, Massachusetts Institute of Technology (1977).

9 P.J. Flory, Principles of Polymer Chemistry, Cornell University Press, Ithaca, N.Y. (1953).

APPENDIX E: SANS data

SANS data used to generate the results reported in Chapter 6 are compiled in this appendix. Also included are the single chain scattering data pertaining to the results of Appendix C. All files are listed by sample designation and cross referenced to ORNL file numbers. In each case the sample-to-detector distance, pinhole diameter and source aperture setting are given. The latter (source A) can be related to the neutron calibration constant K_N as determined by the staff at NCSASR. For $\lambda = 4.75$ the values for aperture settings presently reported are:

Source A	K_N
3.6 X 3.2 cm	1670 ± 200
2.5 X 2.5 cm	1170 ± 140
1.0 cm diameter (D)	177 ± 21

In all files the scattering intensity has been normalized by sample thickness (t) and transmission (T), each of which are given in the file heading.

Files falling under a four digit ORNL number have also been normalized to 1000 beam monitor counts, as indicated by, "scaled-YES." In these files the intensity may be converted to absolute units (cm^{-1}) by making direct use of the given K_N values and equation 5-2 (Chapter 5).

Files listed under three digit ORNL numbers are not beam monitor count normalized as indicated by, "scaled - NO." Comparison of three digit with four digit files requires scaling of the former with the

latter by means of the given beam counts. Also, three digit ORNL number data were taken using a different beam monitor than the four digit data and the monitor sensitivities were different. This becomes apparent when attempting to correlate three and four digit data as illustrated by files 1164 and 416 each obtained from sample SB_d1-T. Since the neutron flux from the reactor remained essentially constant, the sensitivity correction can be obtained by comparing the normalized beam counts of each. The newer monitor (1164) is calculated to be 78% as sensitive as the older one (416); this is in close agreement with what was reported by the staff at NCSASR. Therefore, when correlating data all three digit ORNL number files should be corrected accordingly since the reported K_N values correspond to the four digit files.

SAMPLE - SBd1-T ORNL # - 1164

SDD = 1.8m Pinhole Diam. = 1.3cm Source A.= 3.2x3.6 cm

t =.200cm T =.378 time = 3599sec beam cts- 7965 scaled -YES

	Q (A*-1)	INTENSITY	ERROR
1	.38100E-02	.99540E+02	.90860E+01
2	.85900E-02	.68680E+02	.47740E+01
3	.13820E-01	.88110E+02	.40300E+01
4	.19380E-01	.13320E+03	.41230E+01
5	.24970E-01	.34440E+03	.59760E+01
6	.30440E-01	.15120E+04	.11200E+02
7	.35840E-01	.14750E+05	.32620E+02
8	.41610E-01	.13690E+05	.27520E+02
9	.47590E-01	.10870E+05	.23370E+02
10	.53150E-01	.71660E+04	.18980E+02
11	.58420E-01	.41060E+04	.13390E+02
12	.63960E-01	.24550E+04	.98470E+01
13	.69640E-01	.18110E+04	.79120E+01
14	.75130E-01	.15450E+04	.74640E+01
15	.80530E-01	.12860E+04	.62860E+01
16	.86080E-01	.10420E+04	.55560E+01
17	.91610E-01	.94590E+03	.51140E+01
18	.97180E-01	.84220E+03	.46360E+01
19	.10270E+00	.76970E+03	.43980E+01
20	.10836E+00	.71820E+03	.39590E+01
21	.11400E+00	.68950E+03	.39580E+01
22	.11954E+00	.65870E+03	.36960E+01
23	.12507E+00	.65180E+03	.36540E+01
24	.13056E+00	.62070E+03	.34600E+01
25	.13618E+00	.60600E+03	.33060E+01
26	.14168E+00	.58650E+03	.32000E+01
27	.14736E+00	.57290E+03	.31970E+01
28	.15265E+00	.55680E+03	.30860E+01
29	.15822E+00	.56030E+03	.29470E+01
30	.16392E+00	.55540E+03	.28810E+01
31	.16946E+00	.55270E+03	.29140E+01
32	.17497E+00	.53900E+03	.27530E+01
33	.18058E+00	.54960E+03	.27680E+01
34	.18606E+00	.53190E+03	.27340E+01
35	.19169E+00	.53640E+03	.28310E+01
36	.19732E+00	.53160E+03	.29400E+01
37	.20294E+00	.52370E+03	.31780E+01
38	.20850E+00	.53270E+03	.36320E+01
39	.21388E+00	.52200E+03	.37680E+01
40	.21933E+00	.52310E+03	.40850E+01
41	.22483E+00	.52990E+03	.43250E+01
42	.23030E+00	.52340E+03	.47180E+01
43	.23575E+00	.51120E+03	.49940E+01
44	.24137E+00	.51240E+03	.53230E+01
45	.24707E+00	.52870E+03	.61750E+01
46	.25265E+00	.52020E+03	.69240E+01
47	.25834E+00	.51200E+03	.80830E+01
48	.26437E+00	.51130E+03	.97080E+01

SAMPLE - SBd1-T ORNL # - 413

SDD = 1.8m Pinhole Diam. = 1.0cm Source A.= 3.2x3.6 cm

t =.203cm T =.375 time = 900sec beam cts- 2500 scaled -NO

	Q (A*-1)	INTENSITY	ERROR
1	.36000E-02	.85290E+02	.10660E+02
2	.84900E-02	.98610E+02	.66190E+01
3	.13850E-01	.10210E+03	.52160E+01
4	.19660E-01	.99610E+02	.40730E+01
5	.25270E-01	.18060E+03	.51720E+01
6	.30970E-01	.61630E+03	.81060E+01
7	.36630E-01	.15500E+04	.12600E+02
8	.42010E-01	.18960E+04	.12770E+02
9	.47800E-01	.15640E+04	.10470E+02
10	.53520E-01	.10280E+04	.82740E+01
11	.59120E-01	.60310E+03	.59760E+01
12	.64660E-01	.40330E+03	.48340E+01
13	.70100E-01	.31490E+03	.39790E+01
14	.75950E-01	.27390E+03	.34590E+01
15	.81520E-01	.22600E+03	.32800E+01
16	.86990E-01	.19790E+03	.27850E+01
17	.92730E-01	.18320E+03	.26410E+01
18	.98340E-01	.17130E+03	.24840E+01
19	.10395E+00	.16010E+03	.23390E+01
20	.10957E+00	.14630E+03	.21810E+01
21	.11517E+00	.14260E+03	.20900E+01
22	.12081E+00	.14180E+03	.20380E+01
23	.12641E+00	.13870E+03	.19730E+01
24	.13202E+00	.13270E+03	.18900E+01
25	.13765E+00	.13350E+03	.18410E+01
26	.14334E+00	.13140E+03	.18010E+01
27	.14885E+00	.12620E+03	.17650E+01
28	.15439E+00	.13140E+03	.17300E+01
29	.16011E+00	.12820E+03	.16600E+01
30	.16573E+00	.12330E+03	.16420E+01
31	.17143E+00	.12710E+03	.15740E+01
32	.17708E+00	.12750E+03	.16290E+01
33	.18249E+00	.12790E+03	.16320E+01
34	.18806E+00	.13180E+03	.16760E+01
35	.19382E+00	.12870E+03	.17050E+01
36	.19937E+00	.12680E+03	.18570E+01
37	.20512E+00	.13020E+03	.20570E+01
38	.21074E+00	.12710E+03	.22320E+01
39	.21628E+00	.13090E+03	.24110E+01
40	.22186E+00	.12670E+03	.25480E+01
41	.22744E+00	.13250E+03	.28330E+01
42	.23305E+00	.13000E+03	.29430E+01
43	.23884E+00	.12960E+03	.33380E+01
44	.24432E+00	.14470E+03	.40090E+01
45	.24986E+00	.12680E+03	.42180E+01
46	.25532E+00	.12570E+03	.50760E+01
47	.26120E+00	.13500E+03	.63240E+01

SAMPLE - SB1-T ORNL # - 416

SDD = 1.8m Pinhole Diam. = 1.0cm Source A.= 3.2x3.6 cm

t =.173cm T =.458 time = 900sec beam cts- 2544 scaled -NO

	Q (A*-1)	INTENSITY	ERROR
1	.35900E-02	.26230E+02	.53540E+01
2	.85700E-02	.55370E+02	.44910E+01
3	.14120E-01	.26230E+02	.22830E+01
4	.19980E-01	.36480E+02	.22320E+01
5	.25730E-01	.44410E+02	.22600E+01
6	.31320E-01	.48180E+02	.20950E+01
7	.36840E-01	.84990E+02	.26730E+01
8	.42130E-01	.10650E+03	.27860E+01
9	.47610E-01	.11420E+03	.26330E+01
10	.53330E-01	.11510E+03	.24770E+01
11	.59140E-01	.10260E+03	.21850E+01
12	.64820E-01	.98270E+02	.21380E+01
13	.70320E-01	.90320E+02	.19300E+01
14	.75850E-01	.94310E+02	.19360E+01
15	.81350E-01	.91270E+02	.18080E+01
16	.87050E-01	.90140E+02	.17150E+01
17	.92820E-01	.89470E+02	.16480E+01
18	.98460E-01	.88120E+02	.16240E+01
19	.10406E+00	.92300E+02	.15980E+01
20	.10946E+00	.91600E+02	.16230E+01
21	.11508E+00	.91920E+02	.14780E+01
22	.12088E+00	.89190E+02	.14640E+01
23	.12657E+00	.92000E+02	.14320E+01
24	.13246E+00	.90090E+02	.13960E+01
25	.13833E+00	.92680E+02	.14450E+01
26	.14419E+00	.90660E+02	.13610E+01
27	.15034E+00	.92830E+02	.13400E+01
28	.15660E+00	.92990E+02	.13010E+01
29	.16290E+00	.94390E+02	.13060E+01
30	.16900E+00	.93000E+02	.12960E+01
31	.17510E+00	.94960E+02	.12730E+01
32	.18139E+00	.94870E+02	.12440E+01
33	.18775E+00	.94750E+02	.12250E+01
34	.19399E+00	.97690E+02	.12770E+01
35	.20048E+00	.95130E+02	.13110E+01
36	.20680E+00	.99940E+02	.14490E+01
37	.21327E+00	.96360E+02	.16030E+01
38	.21956E+00	.96790E+02	.17260E+01
39	.22586E+00	.10030E+03	.18810E+01
40	.23247E+00	.96100E+02	.19030E+01
41	.23904E+00	.97080E+02	.21480E+01
42	.24588E+00	.10060E+03	.21860E+01
43	.25306E+00	.10240E+03	.25290E+01
44	.25983E+00	.10050E+03	.29070E+01
45	.26592E+00	.97750E+02	.34450E+01
46	.27210E+00	.99860E+02	.36940E+01
47	.27850E+00	.10300E+03	.47440E+01

SAMPLE - SBd1-B ORNL # - 1163

SDD = 1.8m Pinhole Diam. = 1.3cm Source A.= 3.2x3.6 cm

t =.240cm T =.321 time = 3599sec beam cts- 7958 scaled -YES

	Q (A*-1)	INTENSITY	ERROR
1	.38100E-02	.95530E+02	.88320E+01
2	.85900E-02	.75450E+02	.49640E+01
3	.13820E-01	.92180E+02	.40900E+01
4	.19380E-01	.11610E+03	.38180E+01
5	.24970E-01	.16420E+03	.40940E+01
6	.30440E-01	.10900E+04	.94340E+01
7	.35840E-01	.10700E+05	.27560E+02
8	.41610E-01	.15430E+05	.28980E+02
9	.47590E-01	.10740E+05	.23050E+02
10	.53150E-01	.75150E+04	.19280E+02
11	.58420E-01	.41470E+04	.13350E+02
12	.63960E-01	.25330E+04	.99230E+01
13	.69640E-01	.19530E+04	.81520E+01
14	.75130E-01	.16050E+04	.75490E+01
15	.80530E-01	.13480E+04	.63850E+01
16	.86080E-01	.11160E+04	.57050E+01
17	.91610E-01	.98390E+03	.51750E+01
18	.97180E-01	.89800E+03	.47500E+01
19	.10270E+00	.82090E+03	.45070E+01
20	.10836E+00	.78130E+03	.40970E+01
21	.11400E+00	.74910E+03	.40930E+01
22	.11954E+00	.71260E+03	.38140E+01
23	.12507E+00	.69950E+03	.37550E+01
24	.13056E+00	.67000E+03	.35670E+01
25	.13618E+00	.65260E+03	.34030E+01
26	.14188E+00	.64020E+03	.33170E+01
27	.14736E+00	.62020E+03	.33000E+01
28	.15265E+00	.62070E+03	.32330E+01
29	.15822E+00	.61880E+03	.30730E+01
30	.16392E+00	.60100E+03	.29740E+01
31	.16945E+00	.60300E+03	.30200E+01
32	.17497E+00	.59080E+03	.28590E+01
33	.18058E+00	.59540E+03	.28580E+01
34	.18606E+00	.58890E+03	.28550E+01
35	.19169E+00	.59010E+03	.29460E+01
36	.19732E+00	.58990E+03	.30730E+01
37	.20294E+00	.58360E+03	.33290E+01
38	.20850E+00	.57520E+03	.37440E+01
39	.21388E+00	.58740E+03	.39650E+01
40	.21933E+00	.57700E+03	.42570E+01
41	.22483E+00	.57180E+03	.44570E+01
42	.23030E+00	.56920E+03	.48820E+01
43	.23575E+00	.55420E+03	.51590E+01
44	.24137E+00	.57190E+03	.55800E+01
45	.24707E+00	.56890E+03	.63550E+01
46	.25265E+00	.56230E+03	.71420E+01
47	.25834E+00	.56930E+03	.84570E+01
48	.26437E+00	.56790E+03	.10150E+02

SAMPLE - SBd1-M ORNL # - 1162

SDD = 1.8m Pinhole Diam. = 1.3cm Source A.= 3.2x3.6 cm

t =.200cm T =.388 time = 3599sec beam cts- 7969 scaled -YES

	Q (A*-1)	INTENSITY	ERROR
1	.93000E-03	.48590E+02	.88710E+01
2	.88100E-02	.51020E+02	.32140E+01
3	.15270E-01	.69280E+02	.35310E+01
4	.20010E-01	.77150E+02	.33700E+01
5	.24670E-01	.17420E+03	.41990E+01
6	.30740E-01	.11510E+04	.90040E+01
7	.36760E-01	.11630E+05	.28020E+02
8	.42060E-01	.12900E+05	.28900E+02
9	.46820E-01	.95910E+04	.23550E+02
10	.52420E-01	.67390E+04	.17180E+02
11	.58390E-01	.36430E+04	.12140E+02
12	.64210E-01	.23140E+04	.92290E+01
13	.69290E-01	.18160E+04	.86830E+01
14	.74530E-01	.14810E+04	.68590E+01
15	.80590E-01	.12350E+04	.58220E+01
16	.86650E-01	.10010E+04	.51990E+01
17	.91930E-01	.88790E+03	.52090E+01
18	.97050E-01	.80220E+03	.44710E+01
19	.10297E+00	.74100E+03	.40550E+01
20	.10880E+00	.70590E+03	.40130E+01
21	.11405E+00	.65570E+03	.39230E+01
22	.11913E+00	.64880E+03	.37180E+01
23	.12478E+00	.62640E+03	.34750E+01
24	.13067E+00	.60350E+03	.32420E+01
25	.13620E+00	.58540E+03	.34000E+01
26	.14135E+00	.58550E+03	.32100E+01
27	.14709E+00	.54760E+03	.29340E+01
28	.15303E+00	.55790E+03	.29060E+01
29	.15879E+00	.53510E+03	.28730E+01
30	.16395E+00	.54340E+03	.30280E+01
31	.16930E+00	.53760E+03	.27280E+01
32	.17513E+00	.53380E+03	.27070E+01
33	.18093E+00	.53600E+03	.26350E+01
34	.18619E+00	.51920E+03	.28030E+01
35	.19136E+00	.52800E+03	.28670E+01
36	.19705E+00	.52330E+03	.28140E+01
37	.20263E+00	.51950E+03	.31650E+01
38	.20816E+00	.51320E+03	.34460E+01
39	.21372E+00	.52110E+03	.36600E+01
40	.21948E+00	.51130E+03	.38120E+01
41	.22530E+00	.52080E+03	.42360E+01
42	.23081E+00	.51290E+03	.46150E+01
43	.23632E+00	.50530E+03	.49060E+01
44	.24191E+00	.49850E+03	.53700E+01
45	.24730E+00	.53360E+03	.64150E+01
46	.25236E+00	.51270E+03	.72040E+01
47	.25731E+00	.52500E+03	.84180E+01
48	.26401E+00	.50770E+03	.11050E+02

SAMPLE - SBd1-TA ORNL # - 1165

SDD = 1.8m Pinhole Diam. = 1.3cm Source A.= 3.2x3.6 cm

t =.202cm T =.369 time = 3599sec beam cts- 7964 scaled -YES

	Q (A*-1)	INTENSITY	ERROR
1	.18200E-02	.99370E+02	.12940E+02
2	.84300E-02	.85410E+02	.45330E+01
3	.14780E-01	.93980E+02	.39780E+01
4	.19940E-01	.12850E+03	.44350E+01
5	.24660E-01	.21320E+03	.48930E+01
6	.30330E-01	.13030E+04	.99890E+01
7	.36500E-01	.13790E+05	.29880E+02
8	.41920E-01	.14900E+05	.32340E+02
9	.46910E-01	.10240E+05	.23980E+02
10	.52560E-01	.69130E+04	.17740E+02
11	.58590E-01	.39640E+04	.12760E+02
12	.64110E-01	.23620E+04	.10100E+02
13	.69300E-01	.17700E+04	.81390E+01
14	.74900E-01	.15510E+04	.71560E+01
15	.80760E-01	.13220E+04	.63040E+01
16	.86350E-01	.11040E+04	.58690E+01
17	.91700E-01	.95180E+03	.51260E+01
18	.97180E-01	.85190E+03	.48100E+01
19	.10281E+00	.81330E+03	.43920E+01
20	.10857E+00	.76540E+03	.42310E+01
21	.11398E+00	.72880E+03	.41290E+01
22	.11932E+00	.69840E+03	.39090E+01
23	.12494E+00	.67200E+03	.36280E+01
24	.13072E+00	.64270E+03	.35270E+01
25	.13616E+00	.62980E+03	.35120E+01
26	.14148E+00	.62440E+03	.34000E+01
27	.14713E+00	.60640E+03	.31490E+01
28	.15302E+00	.59430E+03	.31020E+01
29	.15848E+00	.58810E+03	.31790E+01
30	.16386E+00	.57470E+03	.29660E+01
31	.16945E+00	.57630E+03	.29440E+01
32	.17514E+00	.55870E+03	.28240E+01
33	.18062E+00	.56620E+03	.29050E+01
34	.18607E+00	.54790E+03	.27060E+01
35	.19157E+00	.55400E+03	.30390E+01
36	.19706E+00	.56110E+03	.29720E+01
37	.20266E+00	.54380E+03	.33420E+01
38	.20827E+00	.55140E+03	.35910E+01
39	.21387E+00	.53630E+03	.38480E+01
40	.21941E+00	.52850E+03	.40600E+01
41	.22498E+00	.53730E+03	.44350E+01
42	.23058E+00	.53710E+03	.46970E+01
43	.23630E+00	.53040E+03	.50520E+01
44	.24185E+00	.55720E+03	.58960E+01
45	.24709E+00	.55850E+03	.66930E+01
46	.25230E+00	.52610E+03	.72190E+01
47	.25812E+00	.52740E+03	.76950E+01

SAMPLE - SBd1-MT ORNL # - 1172
SDD = 1.8m Pinhole Diam. = 1.3cm Source A.= 3.2x3.6 cm
t =.043cm T =.820 time =25936sec beam cts-57567 scaled -YES

	Q (A*-1)	INTENSITY	ERROR
1	.36700E-02	.50720E+02	.35340E+01
2	.85000E-02	.35450E+02	.18690E+01
3	.13890E-01	.43220E+02	.15380E+01
4	.19470E-01	.80640E+02	.17480E+01
5	.24700E-01	.21600E+03	.26630E+01
6	.30360E-01	.29180E+04	.80820E+01
7	.36380E-01	.42960E+04	.91980E+01
8	.42000E-01	.68530E+04	.11180E+02
9	.47060E-01	.71610E+04	.11220E+02
10	.52680E-01	.49660E+04	.80220E+01
11	.58800E-01	.27160E+04	.55770E+01
12	.64440E-01	.15610E+04	.44980E+01
13	.69420E-01	.12140E+04	.37290E+01
14	.74870E-01	.10500E+04	.32160E+01
15	.80650E-01	.84620E+03	.27280E+01
16	.86160E-01	.69210E+03	.25360E+01
17	.91560E-01	.60530E+03	.22100E+01
18	.97250E-01	.51000E+03	.19360E+01
19	.10286E+00	.47230E+03	.18770E+01
20	.10834E+00	.43580E+03	.17390E+01
21	.11392E+00	.40850E+03	.16270E+01
22	.11948E+00	.38520E+03	.15500E+01
23	.12501E+00	.36940E+03	.14890E+01
24	.13069E+00	.36210E+03	.14150E+01
25	.13631E+00	.34710E+03	.13860E+01
26	.14161E+00	.33990E+03	.13790E+01
27	.14716E+00	.32480E+03	.12580E+01
28	.15293E+00	.31790E+03	.12330E+01
29	.15839E+00	.31510E+03	.12520E+01
30	.16373E+00	.31030E+03	.11950E+01
31	.16937E+00	.31000E+03	.11520E+01
32	.17511E+00	.29610E+03	.11070E+01
33	.18064E+00	.29350E+03	.11210E+01
34	.18606E+00	.29340E+03	.10930E+01
35	.19167E+00	.29280E+03	.11610E+01
36	.19725E+00	.29370E+03	.13530E+01
37	.20271E+00	.29190E+03	.14030E+01
38	.20842E+00	.28320E+03	.14880E+01
39	.21401E+00	.28750E+03	.16340E+01
40	.21942E+00	.28600E+03	.17690E+01
41	.22477E+00	.27100E+03	.18500E+01
42	.23025E+00	.27980E+03	.19840E+01
43	.23595E+00	.27920E+03	.21410E+01
44	.24160E+00	.27440E+03	.24240E+01
45	.24698E+00	.27720E+03	.28340E+01
46	.25253E+00	.28350E+03	.31580E+01
47	.25867E+00	.26730E+03	.38240E+01
48	.26529E+00	.26320E+03	.80500E+01

SAMPLE - SBd2/S1-M ORNL # - 1167

SDD = 1.8m Pinhole Diam. = 1.3cm Source A.= 3.2x3.6 cm

t =.250cm T =.333 time = 3599sec beam cts- 7968 scaled -YES

	Q (A*-1)	INTENSITY	ERROR
1	.44100E-02	.29430E+02	.49750E+01
2	.87000E-02	.47760E+02	.40080E+01
3	.13260E-01	.39520E+02	.28820E+01
4	.19350E-01	.77920E+02	.29560E+01
5	.25630E-01	.48760E+03	.67500E+01
6	.30950E-01	.39570E+04	.19780E+02
7	.35750E-01	.54120E+04	.19890E+02
8	.41450E-01	.56040E+04	.18030E+02
9	.47550E-01	.49470E+04	.15640E+02
10	.53140E-01	.31780E+04	.12920E+02
11	.58040E-01	.21740E+04	.10220E+02
12	.63580E-01	.16360E+04	.78200E+01
13	.69460E-01	.12250E+04	.66930E+01
14	.75250E-01	.99800E+03	.56270E+01
15	.80710E-01	.83290E+03	.52930E+01
16	.86110E-01	.73490E+03	.46160E+01
17	.91900E-01	.68720E+03	.42830E+01
18	.97640E-01	.64990E+03	.41320E+01
19	.10298E+00	.59240E+03	.39150E+01
20	.10812E+00	.55610E+03	.37640E+01
21	.11382E+00	.55250E+03	.33660E+01
22	.11966E+00	.53010E+03	.33810E+01
23	.12505E+00	.52330E+03	.33380E+01
24	.13025E+00	.50800E+03	.32280E+01
25	.13590E+00	.50390E+03	.29870E+01
26	.14183E+00	.49010E+03	.29000E+01
27	.14737E+00	.48880E+03	.29890E+01
28	.15261E+00	.47460E+03	.28540E+01
29	.15826E+00	.48650E+03	.27150E+01
30	.16416E+00	.47270E+03	.26640E+01
31	.16977E+00	.47820E+03	.27160E+01
32	.17499E+00	.47310E+03	.27140E+01
33	.18038E+00	.46580E+03	.25550E+01
34	.18608E+00	.46200E+03	.25340E+01
35	.19164E+00	.45600E+03	.27560E+01
36	.19707E+00	.46430E+03	.30490E+01
37	.20263E+00	.46750E+03	.33050E+01
38	.20821E+00	.45810E+03	.34970E+01
39	.21391E+00	.46180E+03	.37240E+01
40	.21957E+00	.47600E+03	.41270E+01
41	.22511E+00	.45310E+03	.43640E+01
42	.23077E+00	.44530E+03	.45640E+01
43	.23654E+00	.46450E+03	.51900E+01
44	.24204E+00	.44320E+03	.59570E+01
45	.24711E+00	.45710E+03	.69320E+01
46	.25205E+00	.46840E+03	.81020E+01
47	.25743E+00	.44550E+03	.91240E+01

SAMPLE - SBd3-T ORNL # - 1171

SDD = 1.8m Pinhole Diam. = 1.3cm Source A.= 3.2x3.6 cm

t =.186cm T =.402 time = 3599sec beam cts- 7996 scaled -YES

	Q (A*-1)	INTENSITY	ERROR
1	.36700E-02	.87020E+02	.85330E+01
2	.85000E-02	.48860E+02	.40440E+01
3	.13890E-01	.57830E+02	.32790E+01
4	.19470E-01	.96550E+02	.35250E+01
5	.24700E-01	.27680E+03	.55570E+01
6	.30360E-01	.36580E+04	.16680E+02
7	.36380E-01	.44700E+04	.17300E+02
8	.42000E-01	.51690E+04	.17900E+02
9	.47060E-01	.44570E+04	.16320E+02
10	.52680E-01	.29570E+04	.11410E+02
11	.58800E-01	.19390E+04	.86870E+01
12	.64440E-01	.14660E+04	.80350E+01
13	.69420E-01	.11720E+04	.67530E+01
14	.74870E-01	.95000E+03	.56390E+01
15	.80650E-01	.83420E+03	.49930E+01
16	.86160E-01	.74140E+03	.48380E+01
17	.91560E-01	.70200E+03	.43880E+01
18	.97250E-01	.63540E+03	.39840E+01
19	.10286E+00	.61940E+03	.39630E+01
20	.10834E+00	.59040E+03	.37300E+01
21	.11392E+00	.57710E+03	.35650E+01
22	.11948E+00	.56600E+03	.34630E+01
23	.12501E+00	.56450E+03	.33940E+01
24	.13069E+00	.54510E+03	.32020E+01
25	.13631E+00	.54430E+03	.31990E+01
26	.14161E+00	.53560E+03	.31910E+01
27	.14716E+00	.52230E+03	.29420E+01
28	.15293E+00	.51750E+03	.29000E+01
29	.15839E+00	.52050E+03	.29660E+01
30	.16373E+00	.52250E+03	.28590E+01
31	.16937E+00	.50680E+03	.27160E+01
32	.17511E+00	.50770E+03	.26720E+01
33	.18064E+00	.51210E+03	.27300E+01
34	.18606E+00	.51690E+03	.26740E+01
35	.19167E+00	.50890E+03	.28210E+01
36	.19725E+00	.51990E+03	.33190E+01
37	.20271E+00	.51070E+03	.34220E+01
38	.20842E+00	.50830E+03	.36740E+01
39	.21401E+00	.50720E+03	.40020E+01
40	.21942E+00	.51000E+03	.43550E+01
41	.22477E+00	.49540E+03	.46100E+01
42	.23025E+00	.48800E+03	.48300E+01
43	.23595E+00	.50670E+03	.53170E+01
44	.24160E+00	.49960E+03	.60290E+01
45	.24698E+00	.50700E+03	.70640E+01
46	.25253E+00	.48220E+03	.75920E+01
47	.25867E+00	.50110E+03	.96530E+01

SAMPLE - SBd3-B ORNL # - 1170

SDD = 1.8m Pinhole Diam. = 1.3cm Source A.= 3.2x3.6 cm

t =.210cm T =.361 time = 3599sec beam cts- 7993 scaled -YES

	Q (A*-1)	INTENSITY	ERROR
1	.36700E-02	.61130E+02	.71070E+01
2	.85000E-02	.53200E+02	.41930E+01
3	.13890E-01	.53970E+02	.31480E+01
4	.19470E-01	.87060E+02	.33260E+01
5	.24700E-01	.26090E+03	.53610E+01
6	.30360E-01	.36530E+04	.16560E+02
7	.36380E-01	.46980E+04	.17620E+02
8	.42000E-01	.55910E+04	.18500E+02
9	.47060E-01	.46630E+04	.16590E+02
10	.52680E-01	.30840E+04	.11580E+02
11	.58800E-01	.20280E+04	.88260E+01
12	.64440E-01	.15380E+04	.81770E+01
13	.69420E-01	.12150E+04	.68330E+01
14	.74870E-01	.10270E+04	.58260E+01
15	.80650E-01	.88620E+03	.51130E+01
16	.86160E-01	.79310E+03	.49720E+01
17	.91560E-01	.73160E+03	.44510E+01
18	.97250E-01	.68460E+03	.41090E+01
19	.10286E+00	.66770E+03	.40880E+01
20	.10834E+00	.62890E+03	.38260E+01
21	.11392E+00	.62850E+03	.36970E+01
22	.11948E+00	.60120E+03	.35460E+01
23	.12501E+00	.59830E+03	.34720E+01
24	.13069E+00	.58470E+03	.32950E+01
25	.13631E+00	.57930E+03	.32800E+01
26	.14161E+00	.57040E+03	.32730E+01
27	.14716E+00	.55540E+03	.30140E+01
28	.15293E+00	.56070E+03	.29990E+01
29	.15839E+00	.56390E+03	.30680E+01
30	.16373E+00	.55920E+03	.29380E+01
31	.16937E+00	.54810E+03	.28060E+01
32	.17511E+00	.55430E+03	.27740E+01
33	.18064E+00	.54750E+03	.28050E+01
34	.18606E+00	.56110E+03	.27680E+01
35	.19167E+00	.54770E+03	.29080E+01
36	.19725E+00	.54260E+03	.33690E+01
37	.20270E+00	.54840E+03	.35230E+01
38	.20842E+00	.53940E+03	.37610E+01
39	.21401E+00	.54440E+03	.41190E+01
40	.21942E+00	.53780E+03	.44440E+01
41	.22477E+00	.53520E+03	.47620E+01
42	.23025E+00	.54080E+03	.50520E+01
43	.23595E+00	.54170E+03	.54620E+01
44	.24160E+00	.54040E+03	.62300E+01
45	.24698E+00	.54460E+03	.72750E+01
46	.25253E+00	.53210E+03	.79250E+01
47	.25867E+00	.53550E+03	.99150E+01
48	.26529E+00	.56340E+03	.21570E+02

SAMPLE - SBd3-M ORNL # - 1169

SDD = 1.8m Pinhole Diam. = 1.3cm Source A.= 3.2x3.6 cm

t =.240cm T =.373 time = 3599sec beam cts- 7991 scaled -YES

	Q (A*-1)	INTENSITY	ERROR
1	.41000E-02	.56690E+02	.68250E+01
2	.89800E-02	.45190E+02	.35180E+01
3	.14160E-01	.58540E+02	.34680E+01
4	.19540E-01	.10880E+03	.35740E+01
5	.25490E-01	.54280E+03	.72440E+01
6	.30690E-01	.47530E+04	.20830E+02
7	.35990E-01	.51660E+04	.18810E+02
8	.41670E-01	.59630E+04	.18380E+02
9	.47540E-01	.45320E+04	.15250E+02
10	.52880E-01	.30700E+04	.12560E+02
11	.58160E-01	.22170E+04	.97920E+01
12	.63800E-01	.15850E+04	.76940E+01
13	.69670E-01	.12430E+04	.65240E+01
14	.75160E-01	.10440E+04	.61060E+01
15	.80550E-01	.86320E+03	.50780E+01
16	.86130E-01	.80060E+03	.48910E+01
17	.91690E-01	.74010E+03	.44290E+01
18	.97300E-01	.69530E+03	.42590E+01
19	.10284E+00	.65430E+03	.39190E+01
20	.10845E+00	.61000E+03	.37840E+01
21	.11398E+00	.61320E+03	.36170E+01
22	.11960E+00	.59990E+03	.35780E+01
23	.12499E+00	.59120E+03	.34630E+01
24	.13052E+00	.57300E+03	.33090E+01
25	.13608E+00	.57570E+03	.32240E+01
26	.14181E+00	.55930E+03	.30940E+01
27	.14726E+00	.54550E+03	.31210E+01
28	.15270E+00	.55170E+03	.29810E+01
29	.15831E+00	.55780E+03	.29410E+01
30	.16401E+00	.54590E+03	.28560E+01
31	.16946E+00	.54420E+03	.29040E+01
32	.17499E+00	.54510E+03	.27210E+01
33	.18060E+00	.55100E+03	.27940E+01
34	.18607E+00	.53940E+03	.27290E+01
35	.19158E+00	.53910E+03	.29470E+01
36	.19710E+00	.53930E+03	.32290E+01
37	.20282E+00	.53550E+03	.34480E+01
38	.20839E+00	.52070E+03	.37776E+01
39	.21378E+00	.52170E+03	.40220E+01
40	.21933E+00	.53870E+03	.42940E+01
41	.22499E+00	.53220E+03	.46180E+01
42	.23050E+00	.53120E+03	.51430E+01
43	.23585E+00	.53900E+03	.56240E+01
44	.24140E+00	.51880E+03	.59600E+01
45	.24703E+00	.54150E+03	.70310E+01
46	.25274E+00	.54710E+03	.80130E+01
47	.25839E+00	.51390E+03	.10980E+02
48	.26317E+00	.54770E+03	.17320E+02

SAMPLE - S3-T ORNL # - 1166

SDD = 1.8m Pinhole Diam. = 1.3cm Source A.= 3.2x3.6 cm

t =.165cm T =.450 time = 3599sec beam cts- 8001 scaled -YES

	Q (A*-1)	INTENSITY	ERROR
1	.79900E-02	.16340E+02	.20270E+01
2	.14450E-01	.12750E+02	.13220E+01
3	.20180E-01	.33060E+02	.20380E+01
4	.24980E-01	.33280E+02	.18290E+01
5	.30450E-01	.60120E+02	.20780E+01
6	.36500E-01	.37440E+03	.46610E+01
7	.42040E-01	.57570E+03	.58940E+01
8	.46980E-01	.55260E+03	.53610E+01
9	.52560E-01	.58610E+03	.48880E+01
10	.58590E-01	.57170E+03	.45860E+01
11	.64180E-01	.56000E+03	.45950E+01
12	.69290E-01	.56430E+03	.44490E+01
13	.74840E-01	.56500E+03	.40480E+01
14	.80710E-01	.55890E+03	.39150E+01
15	.86310E-01	.56290E+03	.39290E+01
16	.91710E-01	.57630E+03	.37750E+01
17	.97200E-01	.57660E+03	.37160E+01
18	.10280E+00	.57490E+03	.35450E+01
19	.10853E+00	.57420E+03	.34440E+01
20	.11400E+00	.56220E+03	.34320E+01
21	.11927E+00	.56550E+03	.33500E+01
22	.12484E+00	.57110E+03	.31840E+01
23	.13072E+00	.57570E+03	.30890E+01
24	.13637E+00	.56440E+03	.31100E+01
25	.14154E+00	.58090E+03	.31920E+01
26	.14700E+00	.56150E+03	.29100E+01
27	.15288E+00	.56740E+03	.28280E+01
28	.15857E+00	.56920E+03	.28870E+01
29	.16389E+00	.56490E+03	.28620E+01
30	.16942E+00	.57250E+03	.27400E+01
31	.17521E+00	.56690E+03	.26810E+01
32	.18071E+00	.57890E+03	.27920E+01
33	.18598E+00	.56530E+03	.26660E+01
34	.19155E+00	.57410E+03	.28720E+01
35	.19714E+00	.56750E+03	.32110E+01
36	.20278E+00	.57570E+03	.34260E+01
37	.20846E+00	.56820E+03	.37480E+01
38	.21376E+00	.56720E+03	.41360E+01
39	.21927E+00	.56710E+03	.41360E+01
40	.22499E+00	.57690E+03	.46640E+01
41	.23057E+00	.56910E+03	.49520E+01
42	.23629E+00	.57480E+03	.53760E+01
43	.24185E+00	.57300E+03	.64150E+01
44	.24701E+00	.57810E+03	.71620E+01
45	.25215E+00	.57250E+03	.84830E+01
46	.25757E+00	.57480E+03	.98150E+01

SAMPLE - SBd1-T ORNL # - 421

SDD = 4.2m Pinhole Diam. = 1.0cm Source A.= 2.5x2.5 cm

t =.203cm T =.375 time = 1800sec beam cts- 5117 scaled -NO

	Q (A*-1)	INTENSITY	ERROR
1	.20900E-02	.16160E+04	.32810E+02
2	.62200E-02	.14180E+04	.13420E+02
3	.10410E-01	.19310E+04	.13100E+02
4	.14710E-01	.33270E+05	.43430E+02
5	.18920E-01	.66430E+05	.55250E+02
6	.22960E-01	.18060E+05	.27870E+02
7	.27040E-01	.39600E+04	.10950E+02
8	.31170E-01	.21180E+04	.81010E+01
9	.35370E-01	.14230E+04	.57430E+01
10	.39570E-01	.75240E+03	.41580E+01
11	.43730E-01	.53140E+03	.32760E+01
12	.47900E-01	.45780E+03	.28620E+01
13	.51990E-01	.28340E+03	.22830E+01
14	.56120E-01	.16600E+03	.15760E+01
15	.60335E-01	.11180E+03	.12940E+01
16	.64870E-01	.10010E+03	.11640E+01
17	.69451E-01	.92900E+02	.10830E+01
18	.74056E-01	.81370E+02	.10090E+01
19	.78706E-01	.69240E+02	.87510E+00
20	.83310E-01	.62070E+02	.89400E+00
21	.87924E-01	.57400E+02	.94860E+00
22	.92686E-01	.53700E+02	.10570E+01
23	.97527E-01	.54480E+02	.11930E+01
24	.10243E+00	.50020E+02	.13160E+01
25	.10733E+00	.48890E+02	.14990E+01
26	.11217E+00	.49990E+02	.18980E+01
27	.11677E+00	.48230E+02	.24740E+01
28	.12131E+00	.49640E+02	.40670E+01

SAMPLE - SBd1-T ORNL # - 393

SDD = 7.0m Pinhole Diam. = .6cm Source A.= 1.0 (D) cm

t =.203cm T =.375 time = 3599sec beam cts-10147 scaled -NO

	Q (A*-1)	INTENSITY	ERROR
1	.22600E-02	.35410E+02	.36720E+01
2	.37800E-02	.29560E+02	.26760E+01
3	.51900E-02	.24560E+02	.21620E+01
4	.65400E-02	.42940E+02	.25220E+01
5	.79300E-02	.11660E+03	.36750E+01
6	.93600E-02	.15350E+03	.38930E+01
7	.10920E-01	.12230E+03	.30090E+01
8	.12430E-01	.11500E+03	.30020E+01
9	.13790E-01	.13790E+03	.31100E+01
10	.15190E-01	.34330E+03	.45600E+01
11	.16650E-01	.15520E+04	.90940E+01
12	.18130E-01	.39290E+04	.14060E+02
13	.19620E-01	.33580E+04	.12320E+02
14	.21100E-01	.92750E+03	.63140E+01
15	.22510E-01	.21040E+03	.30070E+01
16	.23920E-01	.15540E+03	.24330E+01
17	.25350E-01	.17600E+03	.25520E+01
18	.26820E-01	.16060E+03	.22850E+01
19	.28360E-01	.10510E+03	.17940E+01
20	.29800E-01	.82430E+02	.16470E+01
21	.31170E-01	.79600E+02	.15440E+01
22	.32590E-01	.68980E+02	.14060E+01
23	.34060E-01	.62520E+02	.12720E+01
24	.35627E-01	.53010E+02	.11390E+01
25	.37254E-01	.37760E+02	.96530E+00
26	.38815E-01	.27040E+02	.80940E+00
27	.40331E-01	.21760E+02	.72610E+00
28	.41888E-01	.22050E+02	.69990E+00
29	.43532E-01	.23680E+02	.69940E+00
30	.45220E-01	.21820E+02	.65880E+00
31	.46861E-01	.21430E+02	.66530E+00
32	.48376E-01	.18720E+02	.63690E+00
33	.50036E-01	.16090E+02	.55740E+00
34	.51741E-01	.12350E+02	.52830E+00
35	.53420E-01	.10240E+02	.51980E+00
36	.55051E-01	.91290E+01	.52880E+00
37	.56761E-01	.65580E+01	.47960E+00
38	.58458E-01	.70650E+01	.54670E+00
39	.60175E-01	.79500E+01	.60440E+00
40	.61915E-01	.72590E+01	.64160E+00
41	.63592E-01	.72440E+01	.70360E+00
42	.65302E-01	.72340E+01	.74220E+00
43	.67058E-01	.76150E+01	.85140E+00
44	.68824E-01	.61790E+01	.86520E+00
45	.70599E-01	.66630E+01	.10540E+01

SAMPLE - SBd1-B ORNL # - 392

SDD = 7.0m Pinhole Diam. = .6cm Source A.= 1.0 (D) cm

t =.238cm T =.336 time = 3599sec beam cts-10143 scaled -NO

	Q (A*-1)	INTENSITY	ERROR
1	.20800E-02	.12520E+02	.27320E+01
2	.33600E-02	.33780E+02	.33450E+01
3	.48800E-02	.18630E+02	.18630E+01
4	.63500E-02	.45240E+02	.28160E+01
5	.77700E-02	.10020E+03	.35280E+01
6	.92200E-02	.19610E+03	.48360E+01
7	.10540E-01	.14940E+03	.39870E+01
8	.11950E-01	.12420E+03	.32530E+01
9	.13320E-01	.15140E+03	.35910E+01
10	.14680E-01	.27280E+03	.44530E+01
11	.16070E-01	.94350E+03	.79050E+01
12	.17470E-01	.30990E+04	.13730E+02
13	.18930E-01	.40540E+04	.14430E+02
14	.20350E-01	.22130E+04	.10950E+02
15	.21740E-01	.47590E+03	.47830E+01
16	.23150E-01	.17400E+03	.28250E+01
17	.24560E-01	.16610E+03	.26600E+01
18	.25940E-01	.17150E+03	.27220E+01
19	.27260E-01	.15080E+03	.24650E+01
20	.28660E-01	.10160E+03	.19210E+01
21	.30110E-01	.83830E+02	.16760E+01
22	.31560E-01	.81850E+02	.16370E+01
23	.32940E-01	.78380E+02	.16290E+01
24	.34320E-01	.68290E+02	.14270E+01
25	.35791E-01	.57950E+02	.13340E+01
26	.37282E-01	.39620E+02	.10710E+01
27	.38804E-01	.28340E+02	.88440E+00
28	.40335E-01	.26990E+02	.85520E+00
29	.41897E-01	.26110E+02	.80200E+00
30	.43514E-01	.26680E+02	.80080E+00
31	.45095E-01	.25900E+02	.79230E+00
32	.46685E-01	.25890E+02	.77040E+00
33	.48217E-01	.22370E+02	.76810E+00
34	.49802E-01	.18690E+02	.69590E+00
35	.51409E-01	.14580E+02	.64970E+00
36	.52978E-01	.10700E+02	.61990E+00
37	.54591E-01	.11720E+02	.68710E+00
38	.56283E-01	.96540E+01	.65530E+00
39	.58008E-01	.92030E+01	.69370E+00
40	.59708E-01	.88780E+01	.75040E+00
41	.61322E-01	.76870E+01	.77650E+00
42	.62909E-01	.67060E+01	.79040E+00
43	.64481E-01	.83900E+01	.96240E+00
44	.66109E-01	.74520E+01	.10050E+01
45	.67733E-01	.91170E+01	.12640E+01
46	.69475E-01	.55030E+01	.11230E+01

SAMPLE - SBd1-M ORNL # - 1182

SDD = 7.0m Pinhole Diam. = .6cm Source A.= 1.0 (D) cm

t =.200cm T =.388 time = 3599sec beam cts- 8099 scaled -YES

	Q (A*-1)	INTENSITY	ERROR
1	.39800E-02	.23910E+01	.61720E+00
2	.51100E-02	.77690E+01	.12440E+01
3	.62700E-02	.34530E+01	.55290E+00
4	.79300E-02	.26890E+02	.13360E+01
5	.94700E-02	.11070E+03	.28320E+01
6	.10780E-01	.12290E+03	.27450E+01
7	.12030E-01	.10010E+03	.23860E+01
8	.13460E-01	.19000E+03	.29000E+01
9	.14990E-01	.43310E+03	.41030E+01
10	.16500E-01	.11860E+04	.66290E+01
11	.17780E-01	.26290E+04	.10360E+02
12	.19160E-01	.35240E+04	.10290E+02
13	.20760E-01	.22330E+04	.77010E+01
14	.22310E-01	.70780E+03	.44100E+01
15	.23650E-01	.28620E+03	.29060E+01
16	.24960E-01	.18470E+03	.21450E+01
17	.26490E-01	.13380E+03	.16970E+01
18	.28010E-01	.11620E+03	.16040E+01
19	.29270E-01	.92090E+02	.15640E+01
20	.30570E-01	.72590E+02	.11880E+01
21	.32120E-01	.59590E+02	.10270E+01
22	.33610E-01	.48460E+02	.96470E+00
23	.35000E-01	.39250E+02	.83840E+00
24	.36370E-01	.36950E+02	.80450E+00
25	.37850E-01	.28030E+02	.65230E+00
26	.39340E-01	.18180E+02	.53830E+00
27	.40800E-01	.15750E+02	.48200E+00
28	.42170E-01	.14530E+02	.48130E+00
29	.43530E-01	.13810E+02	.44730E+00
30	.45030E-01	.14240E+02	.42440E+00
31	.46520E-01	.13000E+02	.42260E+00
32	.47790E-01	.11170E+02	.41380E+00
33	.49180E-01	.10680E+02	.39710E+00
34	.50630E-01	.71900E+01	.36500E+00
35	.52050E-01	.76910E+01	.42150E+00
36	.53460E-01	.35310E+01	.29420E+00
37	.54990E-01	.35660E+01	.31030E+00
38	.56450E-01	.44620E+01	.39750E+00
39	.57870E-01	.26560E+01	.31750E+00
40	.59360E-01	.38070E+01	.41050E+00
41	.60850E-01	.38700E+01	.46940E+00
42	.62250E-01	.15940E+01	.33980E+00
43	.63610E-01	.28890E+01	.53640E+00
44	.64900E-01	.31870E+01	.65060E+00

SAMPLE - SBd2/S1 -M ORNL # - 397
SDD = 7.0m Pinhole Diam. = .6cm Source A.= 1.0 (D) cm
t =.169cm T =.437 time = 3599sec beam cts-10166 scaled -NO

	Q (A*-1)	INTENSITY	ERROR
1	.89000E-03	.40030E+02	.67660E+01
2	.22000E-02	.40030E+02	.39060E+01
3	.34200E-02	.70050E+02	.44750E+01
4	.47900E-02	.17890E+03	.54060E+01
5	.62300E-02	.17520E+04	.14920E+02
6	.77600E-02	.52640E+04	.21520E+02
7	.92100E-02	.74480E+04	.27830E+02
8	.10530E-01	.64290E+04	.21440E+02
9	.11960E-01	.35630E+04	.16210E+02
10	.13280E-01	.19380E+04	.10950E+02
11	.14670E-01	.99230E+03	.75330E+01
12	.16010E-01	.64420E+03	.58540E+01
13	.17460E-01	.40180E+03	.41260E+01
14	.18950E-01	.25900E+03	.32520E+01
15	.20360E-01	.17710E+03	.27140E+01
16	.21760E-01	.12800E+03	.21390E+01
17	.23150E-01	.11010E+03	.20490E+01
18	.24510E-01	.96190E+02	.17480E+01
19	.25930E-01	.84960E+02	.16660E+01
20	.27260E-01	.75630E+02	.15290E+01
21	.28690E-01	.59820E+02	.12760E+01
22	.30110E-01	.48190E+02	.11320E+01
23	.31560E-01	.32920E+02	.89500E+00
24	.32970E-01	.23310E+02	.77850E+00
25	.34350E-01	.16730E+02	.62170E+00
26	.35830E-01	.14160E+02	.56910E+00
27	.37303E-01	.14710E+02	.58000E+00
28	.38806E-01	.14710E+02	.55560E+00
29	.40296E-01	.13240E+02	.53710E+00
30	.41870E-01	.11880E+02	.46080E+00
31	.43498E-01	.10750E+02	.45270E+00
32	.45047E-01	.74660E+01	.36960E+00
33	.46614E-01	.71750E+01	.36380E+00
34	.48168E-01	.61210E+01	.36000E+00
35	.49685E-01	.59190E+01	.37360E+00
36	.51267E-01	.51780E+01	.36080E+00
37	.52834E-01	.55810E+01	.41260E+00
38	.54444E-01	.46430E+01	.39810E+00
39	.56109E-01	.64430E+01	.49560E+00
40	.57854E-01	.50140E+01	.46960E+00
41	.59572E-01	.34030E+01	.43570E+00
42	.61525E-01	.45030E+01	.56730E+00
43	.62683E-01	.37830E+01	.57690E+00
44	.64214E-01	.44710E+01	.68180E+00
45	.65705E-01	.47180E+01	.82120E+00
46	.67442E-01	.42700E+01	.80690E+00
47	.69407E-01	.38880E+01	.94310E+00
48	.71626E-01	.38120E+01	.17050E+01

SAMPLE - SBd3-T ORNL # - 396

SDD = 7.0m Pinhole Diam. = .6cm Source A.= 1.0 (D) cm

t =.230cm T =.353 time = 3599sec beam cts-10162 scaled -NO

	Q (A*-1)	INTENSITY	ERROR
1	.21900E-02	.75050E+02	.59520E+01
2	.36500E-02	.68480E+02	.41990E+01
3	.50800E-02	.12870E+03	.51020E+01
4	.65300E-02	.23630E+04	.18290E+02
5	.79900E-02	.56010E+04	.26260E+02
6	.94200E-02	.86360E+04	.30100E+02
7	.10880E-01	.79350E+04	.26500E+02
8	.12380E-01	.36680E+04	.16530E+02
9	.13810E-01	.16330E+04	.11180E+02
10	.15210E-01	.10690E+04	.82020E+01
11	.16680E-01	.82820E+03	.68490E+01
12	.18140E-01	.59730E+03	.57040E+01
13	.19640E-01	.37130E+03	.41520E+01
14	.21080E-01	.21860E+03	.33250E+01
15	.22450E-01	.12760E+03	.23580E+01
16	.23890E-01	.87960E+02	.19000E+01
17	.25370E-01	.82310E+02	.17290E+01
18	.26870E-01	.82920E+02	.17240E+01
19	.28330E-01	.71700E+02	.15740E+01
20	.29760E-01	.66840E+02	.14920E+01
21	.31170E-01	.53680E+02	.13140E+01
22	.32610E-01	.39770E+02	.10780E+01
23	.34090E-01	.30280E+02	.92150E+00
24	.35620E-01	.22280E+02	.77160E+00
25	.37239E-01	.16650E+02	.65780E+00
26	.38802E-01	.12610E+02	.58050E+00
27	.40353E-01	.12570E+02	.55400E+00
28	.41970E-01	.10900E+02	.50730E+00
29	.43619E-01	.11960E+02	.51250E+00
30	.45303E-01	.12050E+02	.51230E+00
31	.46928E-01	.10320E+02	.48560E+00
32	.48530E-01	.86400E+01	.45540E+00
33	.50187E-01	.72620E+01	.41930E+00
34	.51855E-01	.70530E+01	.43410E+00
35	.53615E-01	.66370E+01	.43570E+00
36	.55350E-01	.54940E+01	.43290E+00
37	.57050E-01	.65780E+01	.54810E+00
38	.58700E-01	.66410E+01	.56940E+00
39	.60432E-01	.56070E+01	.56360E+00
40	.62174E-01	.71130E+01	.68450E+00
41	.63963E-01	.43630E+01	.57790E+00
42	.65763E-01	.71290E+01	.83440E+00
43	.67549E-01	.22160E+01	.52240E+00

SAMPLE - SBd3-B ORNL # - 395

SDD = 7.0m Pinhole Diam. = .6cm Source A.= 1.0 (D) cm

t =.210cm T =.357 time = 3599sec beam cts-10163 scaled -NO

	Q (A*-1)	INTENSITY	ERROR
1	.22100E-02	.74310E+02	.58930E+01
2	.36500E-02	.73680E+02	.43340E+01
3	.50800E-02	.13020E+03	.51070E+01
4	.65600E-02	.20680E+04	.16620E+02
5	.80200E-02	.50380E+04	.25340E+02
6	.94800E-02	.81850E+04	.28130E+02
7	.10900E-01	.66110E+04	.25280E+02
8	.12260E-01	.36680E+04	.17140E+02
9	.13790E-01	.16580E+04	.10280E+02
10	.15270E-01	.10870E+04	.84200E+01
11	.16710E-01	.87170E+03	.69920E+01
12	.18210E-01	.58060E+03	.54410E+01
13	.19620E-01	.36690E+03	.44910E+01
14	.21000E-01	.20900E+03	.30750E+01
15	.22490E-01	.11700E+03	.21960E+01
16	.23930E-01	.88060E+02	.19200E+01
17	.25420E-01	.79240E+02	.16460E+01
18	.26910E-01	.79750E+02	.17500E+01
19	.28300E-01	.73740E+02	.15980E+01
20	.29730E-01	.65670E+02	.14630E+01
21	.31180E-01	.53370E+02	.12900E+01
22	.32630E-01	.43550E+02	.11160E+01
23	.34120E-01	.31145E+02	.92990E+00
24	.35653E-01	.22570E+02	.78010E+00
25	.37206E-01	.15290E+02	.64210E+00
26	.38758E-01	.13170E+02	.58210E+00
27	.40319E-01	.11140E+02	.52590E+00
28	.41947E-01	.11960E+02	.51790E+00
29	.43619E-01	.11530E+02	.50450E+00
30	.45301E-01	.10900E+02	.47940E+00
31	.46950E-01	.10130E+02	.46930E+00
32	.48540E-01	.97070E+01	.45760E+00
33	.50220E-01	.89010E+01	.43490E+00
34	.51853E-01	.91140E+01	.46940E+00
35	.53636E-01	.68740E+01	.41300E+00
36	.55383E-01	.68770E+01	.47920E+00
37	.57059E-01	.66350E+01	.51190E+00
38	.58733E-01	.54280E+01	.49550E+00
39	.60416E-01	.55570E+01	.53720E+00
40	.62134E-01	.63530E+01	.60300E+00
41	.63995E-01	.46940E+01	.53490E+00
42	.65844E-01	.84980E+01	.84980E+00
43	.67581E-01	.38830E+01	.64710E+00

SAMPLE - SBd3-M ORNL # - 1180

SDD = 7.0m Pinhole Diam. = .6cm Source A.= 1.0 (D) cm

t =.204cm T =.373 time = 3599sec beam cts- 8091 scaled -YES

	Q (A*-1)	INTENSITY	ERROR
1	.22600E-02	.97380E+01	.14060E+01
2	.39800E-02	.34080E+01	.74380E+00
3	.51100E-02	.15420E+02	.17690E+01
4	.62700E-02	.55720E+02	.22420E+01
5	.79300E-02	.61030E+03	.64240E+01
6	.94700E-02	.55300E+04	.20200E+02
7	.10780E-01	.85930E+04	.23160E+02
8	.12030E-01	.60390E+04	.18710E+02
9	.13460E-01	.27590E+04	.11150E+02
10	.14990E-01	.13590E+04	.73350E+01
11	.16500E-01	.97900E+03	.60790E+01
12	.17780E-01	.85140E+03	.59530E+01
13	.19160E-01	.62340E+03	.43690E+01
14	.20760E-01	.40760E+03	.33210E+01
15	.22310E-01	.22780E+03	.25250E+01
16	.23650E-01	.13470E+03	.20120E+01
17	.24960E-01	.84520E+02	.14640E+01
18	.26490E-01	.59900E+02	.11460E+01
19	.28010E-01	.49610E+02	.10580E+01
20	.29270E-01	.57670E+02	.12490E+01
21	.30570E-01	.56370E+02	.10560E+01
22	.32120E-01	.48110E+02	.93150E+00
23	.33610E-01	.40500E+02	.88990E+00
24	.35000E-01	.31330E+02	.75590E+00
25	.36370E-01	.24170E+02	.65650E+00
26	.37850E-01	.19010E+02	.54210E+00
27	.39340E-01	.11540E+02	.43280E+00
28	.40800E-01	.70930E+01	.32650E+00
29	.42170E-01	.47390E+01	.27730E+00
30	.43530E-01	.50610E+01	.27330E+00
31	.45030E-01	.68140E+01	.29630E+00
32	.46520E-01	.59600E+01	.28880E+00
33	.47790E-01	.46350E+01	.26890E+00
34	.49180E-01	.57260E+01	.29330E+00
35	.50630E-01	.42460E+01	.28310E+00
36	.52050E-01	.44690E+01	.32420E+00
37	.53460E-01	.34460E+01	.29330E+00
38	.54990E-01	.33560E+01	.30380E+00
39	.56450E-01	.24170E+01	.29520E+00
40	.57870E-01	.30530E+01	.34350E+00
41	.59360E-01	.26150E+01	.34330E+00
42	.60850E-01	.49850E+01	.53750E+00
43	.62250E-01	.12540E+01	.30420E+00
44	.63610E-01	.27390E+01	.52710E+00
45	.64900E-01	.22990E+01	.55770E+00

SAMPLE - SB7-T ORNL # - 1183
SDD = 7.0m Pinhole Diam. = 1.0cm Source A.= 3.2x3.6 cm
t =.230cm T =.356 time = 3599sec beam cts- 8096 scaled -YES

	Q (A*-1)	INTENSITY	ERROR
1	.22600E-02	.21000E+02	.67820E+00
2	.39800E-02	.44550E+02	.88340E+00
3	.51100E-02	.99290E+02	.14750E+01
4	.62700E-02	.45900E+03	.21140E+01
5	.79300E-02	.28630E+04	.45710E+01
6	.94700E-02	.24540E+04	.44210E+01
7	.10780E-01	.52120E+04	.59260E+01
8	.12030E-01	.40730E+04	.50480E+01
9	.13460E-01	.24150E+04	.34280E+01
10	.14990E-01	.13920E+04	.24390E+01
11	.16500E-01	.77140E+03	.17730E+01
12	.17730E-01	.44430E+03	.14130E+01
13	.19160E-01	.21910E+03	.85100E+00
14	.20760E-01	.14610E+03	.65320E+00
15	.22310E-01	.13720E+03	.64370E+00
16	.23650E-01	.15260E+03	.70360E+00
17	.24960E-01	.15160E+03	.64430E+00
18	.26490E-01	.13790E+03	.57140E+00
19	.28010E-01	.11640E+03	.53220E+00
20	.29270E-01	.98370E+02	.53590E+00
21	.30570E-01	.81040E+02	.41610E+00
22	.32120E-01	.62730E+02	.34940E+00
23	.33610E-01	.57250E+02	.34760E+00
24	.35000E-01	.53860E+02	.32560E+00
25	.36370E-01	.51900E+02	.31610E+00
26	.37850E-01	.54640E+02	.30190E+00
27	.39340E-01	.50530E+02	.29750E+00
28	.40800E-01	.49940E+02	.28460E+00
29	.42170E-01	.47140E+02	.28740E+00
30	.43530E-01	.46450E+02	.27200E+00
31	.45030E-01	.42990E+02	.24450E+00
32	.46520E-01	.46550E+02	.26510E+00
33	.47790E-01	.42080E+02	.26620E+00
34	.49180E-01	.44730E+02	.26940E+00
35	.50630E-01	.43300E+02	.29700E+00
36	.52050E-01	.39620E+02	.31720E+00
37	.53460E-01	.40940E+02	.33220E+00
38	.53499E-01	.44250E+02	.36250E+00
39	.56450E-01	.43230E+02	.41030E+00
40	.57870E-01	.43360E+02	.42530E+00
41	.59360E-01	.42140E+02	.45280E+00
42	.60850E-01	.43970E+02	.52450E+00
43	.62250E-01	.40540E+02	.56820E+00
44	.63610E-01	.39140E+02	.65470E+00
45	.64900E-01	.41780E+02	.78100E+00
46	.66220E-01	.38630E+02	.91970E+00

SAMPLE - SBd1-T ORNL # - 384

SDD = 15.3m Pinhole Diam. = .6cm Source A.= 1.Ø (D) cm

t =.2Ø3cm T =.375 time = 3599sec beam cts-1Ø12Ø scaled -NO

	Q (A*-1)	INTENSITY	ERROR
1	.17500E-02	.82180E+01	.13510E+01
2	.24800E-02	.23360E+02	.19140E+01
3	.31500E-02	.27490E+02	.19640E+01
4	.37700E-02	.45080E+02	.22860E+01
5	.44400E-02	.31090E+02	.16620E+01
6	.51200E-02	.32630E+02	.16230E+01
7	.58300E-02	.29320E+02	.13810E+01
8	.65500E-02	.20350E+02	.11100E+01
9	.72600E-02	.23450E+02	.11180E+01
10	.79400E-02	.23440E+02	.11290E+01
11	.85900E-02	.28540E+02	.11760E+01
12	.92400E-02	.29970E+02	.11840E+01
13	.99100E-02	.23740E+02	.97920E+00
14	.10620E-01	.22260E+02	.89540E+00
15	.11340E-01	.23020E+02	.89260E+00
16	.12040E-01	.22220E+02	.86040E+00
17	.12710E-01	.25070E+02	.91960E+00
18	.13380E-01	.28700E+02	.92180E+00
19	.14070E-01	.35340E+02	.10120E+01
20	.14760E-01	.60440E+02	.12760E+01
21	.15470E-01	.14640E+03	.19280E+01
22	.16160E-01	.32990E+03	.29080E+01
23	.16830E-01	.55830E+03	.37120E+01
24	.17490E-01	.84620E+03	.44870E+01
25	.18196E-01	.93510E+03	.45010E+01
26	.18941E-01	.75510E+03	.40780E+01
27	.19713E-01	.41690E+03	.28800E+01
28	.20489E-01	.16130E+03	.17840E+01
29	.21271E-01	.60060E+02	.10690E+01
30	.22034E-01	.40540E+02	.88480E+00
31	.22791E-01	.36590E+02	.88330E+00
32	.23553E-01	.41550E+02	.97290E+00
33	.24319E-01	.45680E+02	.10670E+01
34	.25124E-01	.49970E+02	.11600E+01
35	.25934E-01	.49910E+02	.12580E+01
36	.26738E-01	.46040E+02	.13630E+01
37	.27534E-01	.37880E+02	.12870E+01
38	.28335E-01	.25890E+02	.11870E+01
39	.29152E-01	.23570E+02	.11820E+01
40	.29998E-01	.24360E+02	.13430E+01
41	.30826E-01	.28650E+02	.16510E+01
42	.31633E-01	.27860E+02	.18370E+01
43	.32409E-01	.22080E+02	.20500E+01
44	.33287E-01	.20090E+02	.20300E+01
45	.34219E-01	.26650E+02	.34410E+01

SAMPLE - SBd1-B ORNL # - 381
SDD = 15.3m Pinhole Diam. = .6cm Source A.= 1.0 (D) cm
t =.238cm T =.336 time = 3599sec beam cts-10115 scaled -NO

	Q (A*-1)	INTENSITY	ERROR
1	.17500E-02	.10180E+02	.15900E+01
2	.24700E-02	.16830E+02	.17180E+01
3	.31500E-02	.36400E+02	.23890E+01
4	.37800E-02	.34530E+02	.20710E+01
5	.44800E-02	.46150E+02	.21070E+01
6	.51300E-02	.33880E+02	.18350E+01
7	.58100E-02	.28790E+02	.14470E+01
8	.65400E-02	.27890E+02	.13590E+01
9	.72500E-02	.23600E+02	.12100E+01
10	.79100E-02	.24220E+02	.12260E+01
11	.85700E-02	.26930E+02	.11760E+01
12	.92600E-02	.30500E+02	.12310E+01
13	.99100E-02	.30690E+02	.12240E+01
14	.10620E-01	.25770E+02	.10050E+01
15	.11340E-01	.21570E+02	.91980E+00
16	.12030E-01	.25510E+02	.98100E+00
17	.12710E-01	.26030E+02	.97260E+00
18	.13390E-01	.30140E+02	.10050E+01
19	.14080E-01	.37400E+02	.10950E+01
20	.14760E-01	.53530E+02	.12760E+01
21	.15460E-01	.92570E+02	.16290E+01
22	.16160E-01	.23530E+03	.25720E+01
23	.16830E-01	.55990E+03	.39490E+01
24	.17510E-01	.97420E+03	.49820E+01
25	.18207E-01	.11210E+04	.53210E+01
26	.18941E-01	.78240E+03	.43900E+01
27	.19713E-01	.35840E+03	.28130E+01
28	.20501E-01	.12180E+03	.16460E+01
29	.21272E-01	.52810E+02	.10640E+01
30	.22024E-01	.36750E+02	.89750E+00
31	.22782E-01	.36650E+02	.85920E+00
32	.23555E-01	.38510E+02	.92200E+00
33	.24332E-01	.40530E+02	.97530E+00
34	.25126E-01	.49160E+02	.11140E+01
35	.25937E-01	.46870E+02	.12390E+01
36	.26729E-01	.41540E+02	.12440E+01
37	.27549E-01	.32230E+02	.11720E+01
38	.28350E-01	.25340E+02	.11410E+01
39	.29168E-01	.24010E+02	.11510E+01
40	.30003E-01	.19980E+02	.11630E+01
41	.30818E-01	.25720E+02	.14800E+01
42	.31614E-01	.26530E+02	.16230E+01
43	.32463E-01	.26950E+02	.18290E+01
44	.33317E-01	.28320E+02	.21650E+01
45	.34176E-01	.13410E+02	.19990E+01

SAMPLE - SBd1-M ORNL # - 1175

SDD = 15.3m Pinhole Diam. = .6cm Source A.= 1.0 (D) cm

t =.200cm T =.388 time = 3599sec beam cts- 8082 scaled -YES

	Q (A*-1)	INTENSITY	ERROR
1	.10400E-02	.23950E+01	.69130E+00
2	.18200E-02	.83020E+01	.11510E+01
3	.23400E-02	.37920E+01	.86990E+00
4	.28700E-02	.61200E+01	.73680E+00
5	.36300E-02	.11910E+02	.89000E+00
6	.43400E-02	.26850E+02	.13960E+01
7	.49400E-02	.22970E+02	.11880E+01
8	.55100E-02	.25940E+02	.12160E+01
9	.61700E-02	.21380E+02	.97370E+00
10	.68700E-02	.27410E+02	.10330E+01
11	.75600E-02	.20720E+02	.87710E+00
12	.81500E-02	.20140E+02	.90810E+00
13	.87800E-02	.25880E+02	.88290E+00
14	.95100E-02	.27860E+02	.86100E+00
15	.10202E-01	.23450E+02	.80350E+00
16	.10840E-01	.23390E+02	.83150E+00
17	.11430E-01	.23870E+02	.77170E+00
18	.12140E-01	.24230E+02	.72300E+00
19	.12830E-01	.33770E+02	.86540E+00
20	.13410E-01	.37040E+02	.99280E+00
21	.14000E-01	.49400E+02	.98070E+00
22	.14720E-01	.79720E+02	.11890E+01
23	.15400E-01	.13600E+03	.16170E+01
24	.16030E-01	.22900E+03	.20270E+01
25	.16660E-01	.34600E+03	.24640E+01
26	.17340E-01	.57880E+03	.29670E+01
27	.18020E-01	.77530E+03	.35180E+01
28	.18690E-01	.85290E+03	.35510E+01
29	.19320E-01	.73470E+03	.34250E+01
30	.19940E-01	.42190E+03	.24750E+01
31	.20630E-01	.21000E+03	.16310E+01
32	.21310E-01	.10610E+03	.12090E+01
33	.21900E-01	.68610E+02	.10260E+01
34	.22530E-01	.53740E+02	.89130E+00
35	.23200E-01	.43550E+02	.89920E+00
36	.23850E-01	.40840E+02	.97210E+00
37	.24490E-01	.33900E+02	.91250E+00
38	.25190E-01	.35370E+02	.97830E+00
39	.25860E-01	.30480E+02	.10400E+01
40	.26510E-01	.28130E+02	.10340E+01
41	.27190E-01	.25990E+02	.10740E+01
42	.27870E-01	.19040E+02	.10420E+01
43	.28520E-01	.18430E+02	.11570E+01
44	.29140E-01	.16860E+02	.12970E+01
45	.29730E-01	.19030E+02	.15910E+01
46	.30340E-01	.16960E+02	.18400E+01

SAMPLE - SB1-T ORNL # - 389

SDD = 15.3m Pinhole Diam. = .6cm Source A.= 1.0 (D) cm

t =.173cm T =.458 time =28793sec beam cts-80901 scaled -NO

	Q (A*-1)	INTENSITY	ERROR
1	.14900E-02	.14210E+02	.19700E+01
2	.21300E-02	.40280E+02	.25080E+01
3	.28300E-02	.69370E+02	.28250E+01
4	.34700E-02	.88350E+02	.31880E+01
5	.40000E-02	.57250E+02	.24410E+01
6	.46000E-02	.46530E+02	.19060E+01
7	.52600E-02	.28220E+02	.13670E+01
8	.58900E-02	.30230E+02	.13740E+01
9	.64900E-02	.18900E+02	.10570E+01
10	.71100E-02	.20120E+02	.99970E+00
11	.77700E-02	.15480E+02	.83100E+00
12	.83700E-02	.16340E+02	.90110E+00
13	.89300E-02	.18840E+02	.90760E+00
14	.95400E-02	.17030E+02	.80120E+00
15	.10190E-01	.20970E+02	.84630E+00
16	.10830E-01	.18600E+02	.79080E+00
17	.11450E-01	.14850E+02	.69090E+00
18	.12050E-01	.14350E+02	.67420E+00
19	.12650E-01	.22710E+02	.81910E+00
20	.13290E-01	.16350E+02	.65630E+00
21	.13920E-01	.16060E+02	.65820E+00
22	.14510E-01	.20580E+02	.73180E+00
23	.15130E-01	.19190E+02	.67900E+00
24	.15770E-01	.20430E+02	.67500E+00
25	.16400E-01	.25340E+02	.77170E+00
26	.16970E-01	.35290E+02	.90120E+00
27	.17646E-01	.82560E+02	.12870E+01
28	.18361E-01	.17120E+03	.18120E+01
29	.19048E-01	.23540E+03	.21930E+01
30	.19706E-01	.23640E+03	.21480E+01
31	.20401E-01	.14900E+03	.16410E+01
32	.21111E-01	.64690E+02	.10720E+01
33	.21814E-01	.28710E+02	.70290E+00
34	.22499E-01	.15160E+02	.51290E+00
35	.23222E-01	.12540E+02	.52620E+00
36	.23926E-01	.12740E+02	.58630E+00
37	.24645E-01	.13170E+02	.62380E+00
38	.25381E-01	.14450E+02	.71390E+00
39	.26074E-01	.16060E+02	.82160E+00
40	.26806E-01	.13450E+02	.75190E+00
41	.27565E-01	.17430E+02	.95250E+00
42	.28306E-01	.18340E+02	.10550E+01
43	.29050E-01	.16900E+02	.11100E+01
44	.29750E-01	.11300E+02	.10510E+01
45	.30466E-01	.13990E+02	.12360E+01
46	.31284E-01	.17360E+02	.14520E+01
47	.32143E-01	.10380E+02	.16840E+01

SAMPLE - SBd2/S1-M ORNL # - 388

SDD = 15.3m Pinhole Diam. = .6cm Source A.= 1.0 (D) cm

t =.169cm T =.437 time = 3599sec beam cts-10117 scaled -NO

	Q (A*-1)	INTENSITY	ERROR
1	.16400E-02	.23790E+02	.23330E+01
2	.22800E-02	.24020E+02	.19810E+01
3	.29300E-02	.62840E+02	.27500E+01
4	.35600E-02	.46570E+03	.72980E+01
5	.41700E-02	.71820E+03	.79490E+01
6	.48300E-02	.70070E+03	.73090E+01
7	.54500E-02	.68850E+03	.70150E+01
8	.60900E-02	.77290E+03	.68210E+01
9	.67200E-02	.91830E+03	.72470E+01
10	.73600E-02	.11080E+04	.74230E+01
11	.80100E-02	.12780E+04	.76460E+01
12	.86400E-02	.14670E+04	.81110E+01
13	.92700E-02	.15460E+04	.78760E+01
14	.99100E-02	.14340E+04	.73330E+01
15	.10570E-01	.11790E+04	.62070E+01
16	.11240E-01	.86870E+03	.54460E+01
17	.11860E-01	.62390E+03	.44520E+01
18	.12480E-01	.44160E+03	.36950E+01
19	.13120E-01	.31380E+03	.29410E+01
20	.13790E-01	.23830E+03	.24890E+01
21	.14440E-01	.18860E+03	.22010E+01
22	.15070E-01	.15360E+03	.19650E+01
23	.15700E-01	.11870E+03	.16900E+01
24	.16340E-01	.10070E+03	.15020E+01
25	.16990E-01	.80920E+02	.13210E+01
26	.17702E-01	.65710E+02	.11850E+01
27	.18386E-01	.57180E+02	.10900E+01
28	.19097E-01	.44900E+02	.94090E+00
29	.19824E-01	.38640E+02	.84430E+00
30	.20566E-01	.32680E+02	.76420E+00
31	.21280E-01	.29870E+02	.75450E+00
32	.21986E-01	.28440E+02	.73020E+00
33	.22708E-01	.25720E+02	.70310E+00
34	.23446E-01	.25740E+02	.71550E+00
35	.24188E-01	.25920E+02	.82550E+00
36	.24935E-01	.24120E+02	.83560E+00
37	.25698E-01	.23280E+02	.89150E+00
38	.26454E-01	.22630E+02	.95300E+00
39	.27202E-01	.20500E+02	.95880E+00
40	.27967E-01	.20150E+02	.10480E+01
41	.28724E-01	.18730E+02	.10760E+01
42	.29522E-01	.13310E+02	.96040E+00
43	.30289E-01	.14760E+02	.12390E+01
44	.31035E-01	.12690E+02	.12050E+01
45	.31822E-01	.94760E+01	.12440E+01

SAMPLE - SBd3-T ORNL # - 387

SDD = 15.3m Pinhole Diam. = .6cm Source A.= 1.Ø (D) cm

t =.23Øcm T =.353 time = 3599sec beam cts-1Ø121 scaled -NO

	Q (A*-1)	INTENSITY	ERROR
1	.16400E-02	.27190E+02	.27750E+01
2	.22800E-02	.21850E+02	.21020E+01
3	.29000E-02	.29650E+02	.22230E+01
4	.35100E-02	.98450E+02	.36440E+01
5	.41400E-02	.15600E+03	.42040E+01
6	.48200E-02	.15400E+03	.36350E+01
7	.54800E-02	.14030E+03	.35230E+01
8	.60900E-02	.11720E+03	.29950E+01
9	.67000E-02	.13240E+03	.31420E+01
1Ø	.73600E-02	.23490E+03	.36120E+01
11	.80600E-02	.55060E+03	.55300E+01
12	.86800E-02	.11800E+04	.82580E+01
13	.92700E-02	.19500E+04	.10210E+02
14	.98900E-02	.22670E+04	.10100E+02
15	.10580E-01	.18040E+04	.85440E+01
16	.11250E-01	.10090E+04	.64350E+01
17	.11870E-01	.56350E+03	.47750E+01
18	.12470E-01	.37050E+03	.37910E+01
19	.13110E-01	.30390E+03	.31950E+01
2Ø	.13780E-01	.26060E+03	.29130E+01
21	.14440E-01	.23470E+03	.27330E+01
22	.15060E-01	.21250E+03	.26000E+01
23	.15680E-01	.19470E+03	.23960E+01
24	.16330E-01	.18110E+03	.22210E+01
25	.17011E-01	.15330E+03	.19870E+01
26	.17710E-01	.12960E+03	.18970E+01
27	.18369E-01	.10120E+03	.16220E+01
28	.19066E-01	.74560E+02	.13490E+01
29	.19800E-01	.55170E+02	.11090E+01
3Ø	.20549E-01	.36480E+02	.90200E+00
31	.21247E-01	.29060E+02	.84600E+00
32	.21949E-01	.25750E+02	.81420E+00
33	.22667E-01	.21210E+02	.76000E+00
34	.23411E-01	.21270E+02	.80920E+00
35	.24172E-01	.19860E+02	.80870E+00
36	.24902E-01	.20640E+02	.89480E+00
37	.25660E-01	.20800E+02	.98270E+00
38	.26410E-01	.21160E+02	.10630E+01
39	.27153E-01	.20470E+02	.11480E+01
4Ø	.27900E-01	.20720E+02	.12430E+01
41	.28675E-01	.19650E+02	.12990E+01
42	.29455E-01	.17650E+02	.13860E+01
43	.30227E-01	.17280E+02	.15640E+01
44	.30954E-01	.17650E+02	.19610E+01
45	.31673E-01	.17560E+02	.22300E+01
46	.32507E-01	.13100E+02	.21530E+01

SAMPLE - SBd3-B ORNL # - 386
SDD = 15.3m Pinhole Diam. = .6cm Source A.= 1.0 (D) cm
t =.210cm T =.357 time = 3599sec beam cts-10120 scaled -NO

	Q (A*-1)	INTENSITY	ERROR
1	.16300E-02	.18790E+02	.22950E+01
2	.22500E-02	.30420E+02	.25610E+01
3	.29000E-02	.30400E+02	.21180E+01
4	.35500E-02	.10630E+03	.37680E+01
5	.48300E-02	.14020E+03	.38160E+01
6	.54300E-02	.11290E+03	.31450E+01
7	.60700E-02	.11330E+03	.28910E+01
8	.67400E-02	.13390E+03	.29210E+01
9	.73800E-02	.24310E+03	.39820E+01
10	.80000E-02	.51180E+03	.54120E+01
11	.86300E-02	.10550E+04	.75440E+01
12	.93000E-02	.17400E+04	.88700E+01
13	.99700E-02	.19250E+04	.94060E+01
14	.10580E-01	.15300E+04	.84570E+01
15	.11190E-01	.99630E+03	.63630E+01
16	.11840E-01	.58350E+03	.46710E+01
17	.12510E-01	.40360E+03	.37610E+01
18	.13160E-01	.31520E+03	.33450E+01
19	.13760E-01	.27600E+03	.31500E+01
20	.14380E-01	.24850E+03	.27670E+01
21	.15060E-01	.22950E+03	.25240E+01
22	.15740E-01	.20850E+03	.24550E+01
23	.16360E-01	.18240E+03	.23320E+01
24	.16960E-01	.15460E+03	.20820E+01
25	.17655E-01	.12260E+03	.17450E+01
26	.18391E-01	.94850E+02	.15010E+01
27	.19110E-01	.71880E+02	.13600E+01
28	.19788E-01	.53160E+02	.11150E+01
29	.20504E-01	.39420E+02	.93660E+00
30	.21247E-01	.29280E+02	.79180E+00
31	.21983E-01	.23400E+02	.70250E+00
32	.22678E-01	.20030E+02	.71140E+00
33	.23388E-01	.21050E+02	.76440E+00
34	.24148E-01	.22530E+02	.86220E+00
35	.24913E-01	.21450E+02	.92040E+00
36	.25636E-01	.19920E+02	.97290E+00
37	.26398E-01	.21810E+02	.10270E+01
38	.27164E-01	.20250E+02	.11230E+01
39	.27899E-01	.20120E+02	.11880E+01
40	.28662E-01	.19370E+02	.12830E+01
41	.29394E-01	.16500E+02	.13340E+01
42	.30189E-01	.17260E+02	.13640E+01
43	.31014E-01	.20680E+02	.19040E+01
44	.31757E-01	.15420E+02	.20800E+01
45	.32517E-01	.14820E+02	.24370E+01

SAMPLE - SBd3-M ORNL # - 1176

SDD = 15.3m Pinhole Diam. = .6cm Source A.= 1.0 (D) cm

t =.204cm T =.373 time = 3599sec beam cts- 8075 scaled -YES

	Q (A*-1)	INTENSITY	ERROR
1	.10400E-02	.15650E+02	.17840E+01
2	.18200E-02	.16260E+02	.16260E+01
3	.23400E-02	.12400E+02	.15880E+01
4	.28700E-02	.20330E+02	.13550E+01
5	.36300E-02	.46950E+02	.17840E+01
6	.43400E-02	.12600E+03	.30520E+01
7	.49400E-02	.13100E+03	.28620E+01
8	.55100E-02	.11280E+03	.25590E+01
9	.61700E-02	.12000E+03	.23280E+01
10	.68700E-02	.12660E+03	.22410E+01
11	.75600E-02	.16360E+03	.24870E+01
12	.81500E-02	.25580E+03	.32660E+01
13	.87800E-02	.46950E+03	.37960E+01
14	.95100E-02	.10520E+04	.53400E+01
15	.10220E-01	.17170E+04	.69370E+01
16	.10840E-01	.19560E+04	.76750E+01
17	.11430E-01	.17650E+04	.66970E+01
18	.12140E-01	.10650E+04	.48380E+01
19	.12830E-01	.61980E+03	.37410E+01
20	.13410E-01	.46030E+03	.35320E+01
21	.14000E-01	.34510E+03	.26160E+01
22	.14720E-01	.28600E+03	.22730E+01
23	.15400E-01	.25490E+03	.22350E+01
24	.16030E-01	.23090E+03	.20540E+01
25	.16660E-01	.21360E+03	.19540E+01
26	.17340E-01	.19330E+03	.17300E+01
27	.18020E-01	.17320E+03	.16780E+01
28	.18690E-01	.15000E+03	.15030E+01
29	.19320E-01	.13020E+03	.14550E+01
30	.19940E-01	.11110E+03	.12820E+01
31	.20630E-01	.86560E+02	.10570E+01
32	.21310E-01	.69800E+02	.98910E+00
33	.21900E-01	.57510E+02	.94820E+00
34	.22530E-01	.48740E+02	.85660E+00
35	.23200E-01	.43790E+02	.90990E+00
36	.23850E-01	.38200E+02	.94880E+00
37	.24490E-01	.38050E+02	.97570E+00
38	.25190E-01	.39080E+02	.10380E+01
39	.25860E-01	.36100E+02	.11420E+01
40	.26510E-01	.38760E+02	.12250E+01
41	.27190E-01	.35370E+02	.12640E+01
42	.27870E-01	.37520E+02	.14760E+01
43	.28520E-01	.34150E+02	.15890E+01
44	.29140E-01	.38620E+02	.19810E+01
45	.29730E-01	.37260E+02	.22470E+01
46	.30340E-01	.33740E+02	.26190E+01

SAMPLE - 16% SBdl in SBl ORNL # - 1944
SDD = 2.74m Pinhole Diam. = 1.0cm Source A.= 3.2x3.6 cm
t =.163cm T =.498 time = sec beam cts- scaled -YES

	Q (A*-1)	INTENSITY	ERROR
1	.10600E-01	.20360E+03	.41660E+01
2	.14660E-01	.24070E+03	.38790E+01
3	.18750E-01	.27840E+03	.36130E+01
4	.23190E-01	.33040E+03	.33870E+01
5	.27820E-01	.31780E+03	.30050E+01
6	.32130E-01	.34290E+03	.32200E+01
7	.35960E-01	.36530E+03	.30850E+01
8	.40040E-01	.36130E+03	.28070E+01
9	.44220E-01	.35200E+03	.26500E+01
10	.48500E-01	.33790E+03	.24220E+01
11	.52920E-01	.31280E+03	.22300E+01
12	.57260E-01	.29260E+03	.21210E+01
13	.61450E-01	.28240E+03	.20180E+01
14	.65540E-01	.27220E+03	.19370E+01
15	.69720E-01	.26080E+03	.17940E+01
16	.73810E-01	.25220E+03	.17880E+01
17	.78080E-01	.24290E+03	.16000E+01
18	.82450E-01	.23700E+03	.15890E+01
19	.86710E-01	.23620E+03	.15270E+01
20	.90910E-01	.22660E+03	.15030E+01
21	.95020E-01	.22230E+03	.14370E+01
22	.99160E-01	.21940E+03	.14130E+01
23	.10335E+00	.21630E+03	.13400E+01
24	.10776E+00	.21420E+03	.12830E+01
25	.11208E+00	.21270E+03	.13000E+01
26	.11629E+00	.21040E+03	.12510E+01
27	.12042E+00	.20980E+03	.12700E+01
28	.12447E+00	.20790E+03	.12200E+01
29	.12865E+00	.20950E+03	.11930E+01
30	.13302E+00	.20730E+03	.13170E+01
31	.13727E+00	.20610E+03	.14570E+01
32	.14148E+00	.20580E+03	.16260E+01
33	.14557E+00	.20280E+03	.17240E+01
34	.14980E+00	.20760E+03	.18320E+01
35	.15411E+00	.20060E+03	.19790E+01
36	.15827E+00	.20360E+03	.22120E+01
37	.16241E+00	.20880E+03	.24740E+01
38	.16660E+00	.20190E+03	.26480E+01
39	.17097E+00	.19940E+03	.29840E+01
40	.17544E+00	.20060E+03	.36650E+01
41	.17966E+00	.20640E+03	.56800E+01
42	.18342E+00	.19550E+03	.95740E+01

SAMPLE - S3-T ORNL # - 1947

SDD = 2.74m Pinhole Diam. = 1.0cm Source A.= 3.2x3.6 cm

t =.137cm T =.562 time = sec beam cts- scaled -YES

	Q (A*-1)	INTENSITY	ERROR
1	.32800E-02	.12440E+02	.47020E+01
2	.69200E-02	.52420E+02	.68250E+01
3	.10600E-01	.66880E+02	.56930E+01
4	.14660E-01	.77130E+02	.52360E+01
5	.18750E-01	.85030E+02	.47610E+01
6	.23190E-01	.10330E+03	.45160E+01
7	.27820E-01	.10920E+03	.42000E+01
8	.32130E-01	.11940E+03	.45310E+01
9	.35960E-01	.14420E+03	.46220E+01
10	.40040E-01	.15050E+03	.43200E+01
11	.44220E-01	.16350E+03	.43060E+01
12	.48500E-01	.15420E+03	.39020E+01
13	.52920E-01	.15390E+03	.37290E+01
14	.57260E-01	.16120E+03	.37540E+01
15	.61450E-01	.16120E+03	.36360E+01
16	.65540E-01	.16000E+03	.35420E+01
17	.69720E-01	.16080E+03	.33580E+01
18	.73810E-01	.16050E+03	.34010E+01
19	.78080E-01	.16170E+03	.31120E+01
20	.82450E-01	.16630E+03	.31740E+01
21	.86710E-01	.16350E+03	.30290E+01
22	.90910E-01	.17000E+03	.31050E+01
23	.95020E-01	.15290E+03	.28410E+01
24	.99160E-01	.16660E+03	.29360E+01
25	.10335E+00	.16660E+03	.28040E+01
26	.10776E+00	.16460E+03	.26820E+01
27	.11208E+00	.16780E+03	.27530E+01
28	.11629E+00	.16590E+03	.26490E+01
29	.12042E+00	.16900E+03	.27180E+01
30	.12447E+00	.16550E+03	.25950E+01
31	.12865E+00	.16820E+03	.25490E+01
32	.13302E+00	.16200E+03	.27770E+01
33	.13727E+00	.16560E+03	.31140E+01
34	.14148E+00	.16900E+03	.35130E+01
35	.14557E+00	.16590E+03	.37170E+01
36	.14980E+00	.17720E+03	.40360E+01
37	.15411E+00	.16620E+03	.42960E+01
38	.15827E+00	.17180E+03	.48470E+01
39	.16241E+00	.16660E+03	.52680E+01
40	.16660E+00	.17120E+03	.58140E+01
41	.17097E+00	.17030E+03	.65760E+01
42	.17544E+00	.17440E+03	.81500E+01
43	.17966E+00	.18480E+03	.12810E+02
44	.18342E+00	.18130E+03	.21980E+02

SAMPLE - 16% SBd3 in SB7 ORNL # - 1742
SDD = 6.00m Pinhole Diam. = 1.3cm Source A.= 3.2x3.6 cm
t =.169cm T =.480 time = sec beam cts- scaled -YES

	Q (A*-1)	INTENSITY	ERROR
1	.12060E-01	.65389E+03	.63000E+01
2	.13680E-01	.61336E+03	.60250E+01
3	.15340E-01	.55355E+03	.52050E+01
4	.16940E-01	.49709E+03	.49490E+01
5	.18570E-01	.44665E+03	.43750E+01
6	.20210E-01	.41432E+03	.41580E+01
7	.21750E-01	.36623E+03	.39190E+01
8	.23370E-01	.32488E+03	.34040E+01
9	.24960E-01	.29549E+03	.33590E+01
10	.26550E-01	.26830E+03	.29910E+01
11	.28140E-01	.23826E+03	.28500E+01
12	.29750E-01	.21603E+03	.26400E+01
13	.31400E-01	.20109E+03	.24910E+01
14	.32970E-01	.17920E+03	.24340E+01
15	.34560E-01	.17176E+03	.22540E+01
16	.36180E-01	.16188E+03	.21840E+01
17	.37790E-01	.15256E+03	.21160E+01
18	.39410E-01	.14663E+03	.19920E+01
19	.41020E-01	.13763E+03	.20170E+01
20	.42630E-01	.13210E+03	.18620E+01
21	.44230E-01	.12610E+03	.18590E+01
22	.45870E-01	.12112E+03	.17640E+01
23	.47490E-01	.11632E+03	.17590E+01
24	.49030E-01	.11437E+03	.17620E+01
25	.50630E-01	.11285E+03	.16400E+01
26	.52250E-01	.10682E+03	.16750E+01
27	.53860E-01	.10682E+03	.15850E+01
28	.55490E-01	.10449E+03	.15650E+01
29	.57100E-01	.10166E+03	.15510E+01
30	.58690E-01	.97344E+02	.15140E+01
31	.60280E-01	.99704E+02	.17360E+01
32	.61880E-01	.91510E+02	.17220E+01
33	.63490E-01	.93544E+02	.19730E+01
34	.65120E-01	.92073E+02	.20010E+01
35	.66780E-01	.94030E+02	.22770E+01
36	.68350E-01	.90921E+02	.24060E+01
37	.69960E-01	.90172E+02	.25450E+01
38	.71570E-01	.91462E+02	.26990E+01
39	.73220E-01	.90641E+02	.29840E+01
40	.74850E-01	.89498E+02	.32740E+01
41	.76470E-01	.86345E+02	.36310E+01
42	.78060E-01	.84206E+02	.41210E+01
43	.79620E-01	.89103E+02	.48330E+01
44	.81190E-01	.85580E+02	.56940E+01
45	.82770E-01	.96599E+02	.87750E+01
46	.84360E-01	.86993E+02	.11796E+02

SAMPLE - S3-T ORNL # - 1746

SDD = 6.00m Pinhole Diam. = 1.3cm Source A.= 3.2x3.6 cm

t =.137cm T =.562 time = sec beam cts- scaled -YES

	Q (A*-1)	INTENSITY	ERROR
1	.12060E-01	.49759E+02	.32030E+01
2	.13680E-01	.57181E+02	.32310E+01
3	.15340E-01	.52312E+02	.28360E+01
4	.16940E-01	.49599E+02	.27780E+01
5	.18570E-01	.51037E+02	.25910E+01
6	.20210E-01	.57542E+02	.25970E+01
7	.21750E-01	.52538E+02	.25150E+01
8	.23370E-01	.54204E+02	.23070E+01
9	.24960E-01	.51344E+02	.23270E+01
10	.26550E-01	.51052E+02	.21450E+01
11	.28140E-01	.51725E+02	.21410E+01
12	.29750E-01	.52182E+02	.20730E+01
13	.31400E-01	.53488E+02	.20060E+01
14	.32970E-01	.53631E+02	.20410E+01
15	.34560E-01	.51348E+02	.18970E+01
16	.36180E-01	.51717E+02	.18800E+01
17	.37790E-01	.54958E+02	.18800E+01
18	.39410E-01	.54111E+02	.17840E+01
19	.41020E-01	.53643E+02	.18480E+01
20	.42630E-01	.54082E+02	.17270E+01
21	.44230E-01	.54371E+02	.17480E+01
22	.45870E-01	.52535E+02	.16700E+01
23	.47490E-01	.52882E+02	.16840E+01
24	.49030E-01	.52449E+02	.16930E+01
25	.50630E-01	.56938E+02	.16140E+01
26	.52250E-01	.55022E+02	.16600E+01
27	.53860E-01	.54855E+02	.15660E+01
28	.55490E-01	.55308E+02	.15560E+01
29	.57100E-01	.55824E+02	.15580E+01
30	.58690E-01	.54985E+02	.15350E+01
31	.60280E-01	.54845E+02	.17480E+01
32	.61880E-01	.56986E+02	.17970E+01
33	.63490E-01	.58414E+02	.20550E+01
34	.65120E-01	.56872E+02	.20850E+01
35	.66780E-01	.57738E+02	.23570E+01
36	.68350E-01	.58739E+02	.25330E+01
37	.69960E-01	.56165E+02	.26440E+01
38	.71570E-01	.57491E+02	.28110E+01
39	.73220E-01	.59783E+02	.31540E+01
40	.74850E-01	.58512E+02	.34560E+01
41	.78060E-01	.59362E+02	.44380E+01
42	.79620E-01	.61226E+02	.51470E+01
43	.81190E-01	.57112E+02	.60310E+01
44	.82770E-01	.59031E+02	.90430E+01